Technical Report
TR-19-22
December 2019

Exploring alternative models for the formation of conspicuously flat basement surfaces in southern Sweden

Bradley W Goodfellow
Arjen P Stroeven
Stephen J Martel
Jakob Heyman
Matteo Rossi
Marc W Caffee

SVENSK KÄRNBRÄNSLEHANTERING AB

SWEDISH NUCLEAR FUEL
AND WASTE MANAGEMENT CO

Box 3091, SE-169 03 Solna
Phone +46 8 459 84 00
skb.se

SVENSK KÄRNBRÄNSLEHANTERING

ISSN 1404-0344
SKB TR-19-22
ID 1872114

December 2019

Exploring alternative models for the formation of conspicuously flat basement surfaces in southern Sweden

Bradley W Goodfellow
Swedish Geological Survey (SGU)

Arjen P Stroeven
Department of Physical Geography, Stockholm University

Stephen J Martel
Department of Earth Sciences, University of Hawai'i at Mānoa

Jakob Heyman
Department of Earth Sciences, University of Gothenburg

Matteo Rossi
Department of Biomedical Engineering, Lund University

Marc W Caffee
Department of Physics and Astronomy, Purdue University

Preface

A comprehensive study on glacial erosion, denudation and long-term development of bedrock morphology/stability was conducted between 2015 and 2019 at the Forsmark site and in the surrounding Uppland province, Sweden (Hall et al. 2019a). The present report describes a study that emanated from that work, investigating key conceptualizations of the morphology of the basement surface at Forsmark prior to Quaternary glacial erosion.

A series of bedrock surfaces developed in Precambrian gneissic granite in the Trollhättan area and the nearby village of Nordkroken, on the southern shores of Lake Vänern, in Västra Götaland County, Sweden. These surfaces are renowned for displaying exceptionally low relief. The aim of the present study is to explore possible formation mechanisms for these conspicuously flat elements within the overall low-relief landscape, and to help frame their importance for general models of landscape evolution, with specific application to Forsmark. Two hypotheses are compared for the conspicuously flat surfaces: i) that these surfaces are remnants of a regional near-planar unconformity formed through peneplanation processes related to chemical weathering and granular-scale erosion through surface wash, with final planation during Cambrian marine transgressions, and ii) that these surfaces have formed through ice sheet erosion that includes exploitation of subhorizontal bedrock joints.

In addition to the present report, another supporting report (Hall et al. 2019b), with a similar overall objective and using the same study area as the present study, but using a different scientific starting point regarding the view of the genesis of the sub-Cambrian unconformity, also emerged from the main study. Preferably, the main report of the glacial erosion and denudation study (Hall et al. 2019a) should be read in light of both supporting reports. The present study was written independently of, and without reading or referring to, the Hall et al. (2019b) report of the same study area.

Bradley Goodfellow led the study and writing and participated in the GPR profiling and sampling for cosmogenic nuclides. Arjen Stroeven contributed to the scientific development of the project and report, report writing and editing, especially of the chapter on cosmogenic exposure dating, and sampling for cosmogenic nuclides. Stephen Martel proposed the GPR study, participated in GPR profiling, led the development of conceptual modelling of bedrock fracturing, and contributed to report editing. Jakob Heyman participated in sampling for cosmogenic nuclides and modelled cosmogenic nuclide data for bedrock apparent exposure ages and erosion rates. Matteo Rossi provided GPR training, analysed the GPR data, and produced the GPR profiles. Marc Caffee participated in sampling for cosmogenic nuclides and produced the cosmogenic nuclide data. All authors reviewed the report.

The results of the present report will be used, together with results of Hall et al. (2019a,b) and other published scientific information, for constructing future scenarios of climate and climate-related processes in SKB's work on assessing long-term safety of nuclear waste repositories in Sweden. The safety assessments performed for the planned repository for spent nuclear fuel in Forsmark, Sweden, cover a total time span of one million years. Since this time span covers the timescales relevant for glacial cycles, the effect of future glacial erosion needs to be analysed in the safety assessments. In this context, the three reports that emerged from the glacial erosion study provide important results on the potential amount of glacial erosion that may be expected in the topographical, geological, and glaciological setting of the Forsmark site.

The glacial erosion study was initiated by Jens-Ove Näslund (SKB) and jointly designed by Jens-Ove Näslund, Adrian Hall (Stockholm University), Karin Ebert (Södertörn University), Bradley Goodfellow (Stockholm University, Swedish Geological Survey), Clas Hättestrand (Stockholm University), Jakob Heyman (University of Gothenburg), and Arjen Stroeven (Stockholm University).

The report was externally reviewed by Prof. Paul Bishop (School of Geographical and Earth Sciences, University of Glasgow), Assoc. Prof. Henriette Linge (Dept. of Earth Science, University of Bergen), Assoc. Prof. Mats Olvmo (Dept. of Earth Sciences, University of Gothenburg), and Assoc. Prof. Jens-Ove Näslund. Input to an earlier version of the manuscript was provided by Christina Truedsson (Tintra consult).

Stockholm, December 2019

Jens-Ove Näslund
Coordinator Climate Research Programme SKB

Abstract

A series of near-planar subhorizontal bedrock surfaces are developed in Precambrian gneissic granite in Trollhättan and Nordkroken, Västra Götaland County, Sweden. They have traditionally been interpreted as exhumed remnants of the Subcambrian peneplain but processes by which they may have formed have not been explored. This study therefore explores processes of formation by comparing two hypotheses: 1) that these surfaces have formed through marine erosion during the Cambrian transgression of rock previously weathered to base level; 2) that these surfaces formed through exploitation of subhorizontal sheeting joints by the Fennoscandian ice sheet. We evaluated these hypotheses through a combination of landscape analyses in a GIS, field observations of landforms and bedrock jointing, ground penetrating radar imaging of subsurface jointing, and erosion rate inferences from cosmogenic nuclides. We conclude that marine erosion of weathered rock was likely important to the formation of the regional Subcambrian peneplain but that the extreme flatness of the surfaces at Trollhättan and Nordkroken is attributable to Quaternary glacial erosion, with sheeting joints providing a first order structural control on their flatness.

Sammanfattning

En serie exceptionellt flacka ytor finns bildade i prekambrisk gneissisk granit vid Trollhättan och Nordkroken i Västra Götaland, Sverige. De har traditionellt blivit tolkade som exhumerade rester av det subkambriska peneplanet men processerna som varit med och format dem har inte undersökts. Denna studie undersöker därför processer som kan ha format ytorna genom att jämföra två hypoteser: 1) att ytorna har formats under den kambriska transgressionen genom marin erosion av berggrund som vittrats till basnivån; 2) att ytorna har formats genom glacial erosion då subhorisontella sprickor utnyttjats av det fennoskandiska inlandsisen. Vi utvärderar dessa hypoteser genom en kombination av landskapsanalys i GIS, fältobservationer av landformer och sprickbildning i berget, visualisering av underjordiska sprickor med georadar och simulerad erosionshastighet baserad på kosmogena nuklider. Vi drar slutsatsen att marin erosion av vittrad berggrund sannolikt var viktig för bildningen av det regionala subkambriska peneplanet men att den extrema flackheten hos ytorna vid Trollhättan och Nordkroken är ett resultat av kvartär glacial erosion i kombination med den geologiska strukturalla kontrollen orsakad av subhorisontella sprickor.

Contents

1 Aims

A series of subhorizontal surfaces developed in Precambrian gneissic granite in the city of Trollhättan and the nearby village of Nordkroken, on the southern shores of Lake Vänern, in Västra Götaland County, Sweden, are renowned for being near planar (Rudberg et al. 1976, Johansson et al. 2001b). Because of their exceptional flatness (relief is tens of cm over 1 000s of square meters), their location in a low relief landscape that characterizes much of lowland Sweden (and well beyond), and also near two table mountains comprised of Cambro–Ordovician sedimentary rocks capped by dolerite sills, these surfaces have been interpreted as exhumed remnants of a Subcambrian 'peneplain' (SCP; Johansson et al. 2001b). They might also be considered as analogue surfaces for the former relief of the SCP across regional-to-continental scales and offer potentially key support to landscape evolution models that treat present-day relief as having evolved from surfaces that were initially almost entirely flat. Indeed, the exceptionally flat surfaces of Västra Götaland County are central to the education of students and the general public regarding the SCP and are a central feature of a proposed regional geopark (Geopark 2019). However, the processes by which these striking surfaces may have formed have not been explored in detail. Hence, the aim of this study is to explore possible formation mechanisms for these conspicuously flat elements within the overall low-relief landscape, and to help frame their importance for general models of landscape evolution, with specific application to Forsmark, which is the site of a planned undergone repository for spent nuclear fuel.

We compare two hypotheses for the conspicuously flat surfaces (CFSs): 1. That these surfaces are remnants of a regional near-planar unconformity formed through peneplanation processes related to chemical weathering, granular scale erosion through surface wash, with final planation during Cambrian marine transgressions. 2. That these surfaces have formed through Quaternary ice sheet erosion that includes exploitation of subhorizontal sheeting joints. Predictable, and testable, implications of these hypotheses include whether or not: (i) the Subcambrian unconformity preserved under cover rocks shows the same near-planar relief; (ii) the unconformity is undeformed and the near-planar surfaces are accordant; (iii) near-planar subhorizontal sheeting joints are located beneath, and closely parallel to, these near-planar surfaces; and (iv) these surfaces have undergone erosion below the Cambrian unconformity through Quaternary glacial processes. To test these hypotheses, we use a combination of field-, laboratory-, and GIS-based analyses of these surfaces and of basement that lies beneath, or near, Cambro–Ordovician cover rock remnants. These analyses include measurements of fracture spacing on exposed bedrock surfaces, imaging of the subsurface using ground-penetrating radar, and inferences of glacial erosion rates from measurements of cosmogenic nuclides accumulated in quartz in bedrock surface samples. We provide further context to these results with observations of bedrock landforms from other glacially eroded landscapes. We interpret our results as most likely supporting hypothesis 2 and therefore consider that the exceptional flatness of these surfaces reflects a first-order structural control, specifically erosion of bedrock beneath (or in front of) the Fennoscandian ice sheet along subhorizontal sheeting joints. These joints are known to form elsewhere inside hills (Jahns 1943) but may also be attributable to crack propagation by high water pressures below near-planar outcrops beneath ice sheets or in their forefields (Lönnqvist and Hökmark 2013). We recognize uncertainties in our interpretation and note ways in which our interpretation may converge with hypothesis 1. We place our interpretations of these surfaces within the context of landscape evolution in Sweden to reflect anew about previous interpretative models of this landscape, offer a hypothesis on how the SCP may have formed, and provide implications for glacial erosion at Forsmark.

2 Background

In this section we summarize key concepts that have driven interpretations of landscapes, especially those that support an enduring strong historical geomorphological tradition in Sweden. With process geomorphological investigation techniques, we now query components of historical geomorphology in Sweden in a search for explanations to the question of how extraordinarily extensive, and in places extraordinarily flat, surfaces – interpreted as a Subcambrian peneplain – were formed.

2.1 Historical geomorphology: landscape evolution models

Peneplains, i.e. surfaces that are 'almost a plain', form a key landscape element in the Fennoscandian geomorphic literature. The process, or processes, that create a peneplain are collectively, and non-specifically, referred to as peneplanation, which forms the ultimate stage of the Davisian model of landscape evolution. According to Davis (1899), an initial, relatively short-lived, pulse of land uplift is followed by rapid valley incision during which maximum relief is attained and then a gradual decay of the relief through summit lowering and decreasing slope gradients to create an almost entirely flat peneplain. Three contrasting classical models of landscape evolution were proposed by W. Penck, L.C. King, and J.T. Hack. In Penck's model, uplift takes place at a temporally varying rate over a longer period, is immediately accompanied by landscape incision, and slopes and summits decline to what he termed an endrumph, which displays almost-flat morphology analogous to Davis's peneplain (Penck 1924). A primary difference in King's model to either of the preceding two models is that the uplifted surface remains elevated and is consumed laterally by ever-widening valleys through parallel slope retreat to form low-angle pediplains (King 1953). Hack's model, finally, promotes the concept of dynamic equilibrium, in which a landscape responds to a moderate but constant rate of uplift (Hack 1975). Initially, rapid valley incision occurs until equal rates of summit and valley incision result in persistence of relief and even persistence of summit elevations by the ongoing uplift. Whereas Davis's and King's models are strongly time-dependent, Penck's model is less so and Hack's model is time-independent.

2.2 The onset and current dominance of process geomorphology

While these conceptual landscape evolution models played central roles in the development of geomorphology as a discipline, they largely fell out of vogue as process geomorphology, pioneered by G.K. Gilbert, rose to prominence during the quantitative revolution that occurred through the 1950s to 1970s. During this time, the study of landscape evolution came to be dominated by the study of geomorphic processes, in which quantitative measurement and principles of study derived from mathematics, physics, chemistry, biology, and geology became routinely applied.

Early technical limitations with this approach to landscape evolution inhibited the ability of geomorphologists to extrapolate small-scale, short-duration, measurements over both space and time. This led to the study of active processes that might be of secondary importance to landscape evolution across larger spatial and temporal scales, an associated focus on high frequency-low magnitude geomorphic events (Wolman and Miller 1960), and an implicit assumption of landscapes being in a state of dynamic equilibrium (cf. Hack 1975) over geologically short timescales of investigation, corresponding with the concept of steady time (Schumm and Lichty 1965). However, a new wave of technological advances, including the developments of digital elevation models (now frequently of meter-scale resolution, or better); remote imaging techniques (e.g., seismic, magnetic, visible light spectrum); desktop geographic information systems (GIS) to process spatial data; a variety of thermochronometers that permit assessment of long-term rock exhumation histories; cosmogenic nuclide dating techniques with nuclides that span a broad range of half-lives to calculate erosion rates over spatial scales and durations relevant to landscape evolution; and quantum leaps in numerical modelling have contributed to the present 'golden age' of geomorphic research. These advances have

helped reduce, but not eliminate, the dependence of geomorphic process research on active processes and short time scales. Geomorphologists can now, in favourable settings such as active orogenic belts, quantitatively assess large-scale landscape evolution over cyclic and graded time (Schumm and Lichty 1965), including also low frequency-high magnitude geomorphic events (Wolman and Miller 1960). Conversely, applying process-based research to landscapes that have been post-orogenic for up to 10^8–10^9 years frequently remains much more challenging.

Using geomorphic process research, some key elements of classical landscape evolution models can be tested, and some have been verified. For example, a study of hillslopes during and after tectonic uplift on the Dragonsback pressure ridge along the San Andreas fault revealed a landscape evolving as in Penck's model (Hilley and Arrowsmith 2008). Cosmogenic nuclide exposure studies show that summits in glaciated high-latitude ranges erode slowly both in absolute terms and relative to glacially-incised valleys (Small et al. 1997, Fabel et al. 2002, Stroeven et al. 2006, Andersen et al. 2018), findings in some ways compatible with the models of King (especially) but also those of Davis and Penck, where relief formation through valley incision greatly exceeds rates of summit erosion until late in the erosion cycles. Furthermore, research on dynamic topography has provided a mechanism for non-orogenic uplift, formerly termed epeirogenic uplift, which can produce doming of low-relief landscapes and consequent rejuvenation of erosion (McKenzie 1984). These latter advances support inferences for doming and renewed erosion of the Southern Swedish Dome (Lidmar-Bergström et al. 2013, Japsen et al. 2016) and provide for some recent uplift of southwestern Norway (Pedersen et al. 2016). We cast our study against these broad patterns of geomorphological inquiry in bringing a process approach towards the development of low-relief, low elevation surfaces in post-orogenic Sweden.

2.3 Geomorphological models of the SCP – The Swedish setting

The Swedish geomorphic community has made an important, perhaps unique, contribution to understanding the evolution of extremely old post-orogenic landscapes, which have histories constrained by sedimentary cover rocks. This contribution remains little known outside of Scandinavia. Whereas the trend to embrace process geomorphology was more-or-less complete in many countries by the 1980s, Sweden followed a different path. Notwithstanding important contributions in, amongst others, hydrology (e.g., Hjulström 1935, Sundborg 1956), glaciology (e.g., Hooke et al. 1989), and paleoglaciology (e.g., Kleman and Borgström 1996, Kleman and Hättestrand 1999), all of them relevant for Swedish landscape evolution studies, historical geomorphology remains forefront as the paradigm by which pre-Quaternary landscapes are interpreted (Bonow et al. 2003, Lidmar-Bergström et al. 2007, 2013, Ebert et al. 2011, 2012). This alternate pathway stems in part from the landscape itself in that much of it displays low relief, is post-orogenic, and cover rock remnants of various ages occur. Cambro–Ordovician cover rocks occur as particularly extensive bodies beneath the Caledonides and in offshore basins, especially in the Baltic Sea basin (Nielsen and Shovsbo 2011). Cambro–Ordovician cover rocks also onlap onshore in southeastern Sweden and occur as small remnants scattered through southern Sweden. Cover rock remnants add crucial constraints on landscape evolution of the underlying basement both prior to their deposition and after exhumation (Lidmar-Bergström 1995, 1996, Lidmar-Bergström et al. 2013), leading to a novel temporal understanding.

Historical geomorphology in Sweden most closely identifies with Davis, with respect to direct citation, frequent use of the term 'peneplain', and inferences of cyclical landscape evolution (Lidmar-Bergström 1996, Bonow et al. 2003, Lidmar-Bergström et al. 2013). However, it also borrows elements from the models of Penck and King in that inferred 'peneplains' are frequently thought to be preserved in summits and landscapes implicitly evolve by slope retreat during valley expansion. In contrast, direct references to Gilbert's work (Gilbert 1877), adoption of concepts he introduced, and acknowledgement of his crucial role as a founder of process geomorphology have, to our knowledge, been non-existent. Hence, there is little overlap between process and historical geomorphology in Sweden.

A crucial aspect of historical geomorphology as practiced in Scandinavia is the concept of an Eulerian fixed reference point, taken to describe high points in the landscape (Figure 2-1a). Where these high points can be considered accordant, they form an envelope surface, which may be promoted from a model surface to the status of a real surface by being referred to as a "reconstructed peneplain", the remnants of which have undergone only trivial, even zero, erosion (Lidmar-Bergström et al. 2007, Hall et al. 2019a). This 'peneplain' is then used as reference surface against which to infer subsequent

landscape change. Processes of peneplanation, including with respect to the SCP, are often considered in only general terms, such as 'fluvial, 'epigene', 'erosion surface', 'etch surface', 'weathering', and 'slope processes' (Bonow et al. 2003, Lidmar-Bergström et al. 2013), and are sometimes ignored (Lidmar-Bergström et al. 2007). Glacial erosion is rarely, if ever, considered as a possible mechanism for peneplanation (Bonow et al. 2003, Lidmar-Bergström et al. 2013), although Snowball Earth conditions have been inferred for the late Precambrian (Keller et al. 2019) and glacial erosion might therefore have contributed to the formation of the SCP. An Eulerian perspective implies that accordant summits, particularly those that display low local relief, can only represent peneplain remnants and that all relief below these summits has formed following exhumation from beneath cover rocks, including through Quaternary glacial erosion. It then follows that glacial erosion can only increase relief.

The Eulerian perspective of historical geomorphology differs fundamentally to the more broadly applied concepts of process geomorphology which take a Lagrangian approach (Figure 2-1b). Here, landscapes are recognized as evolving over time, albeit slowly in many low-relief post-orogenic locations, and fixed reference points are not required to interpret the evolution of the landscape. Although applying a Eulerian perspective to landscapes may be appealing because it offers a simple approach to understanding landscape evolution, it is also highly restrictive. The Lagrangian approach is more complicated and uncertainties may be perceived to be larger, but it also offers flexibility and more potential to understand how diverse landscapes evolve. These opposing perspectives for interpreting landscape evolution also underlie the polarization that exists between process and historical geomorphology.

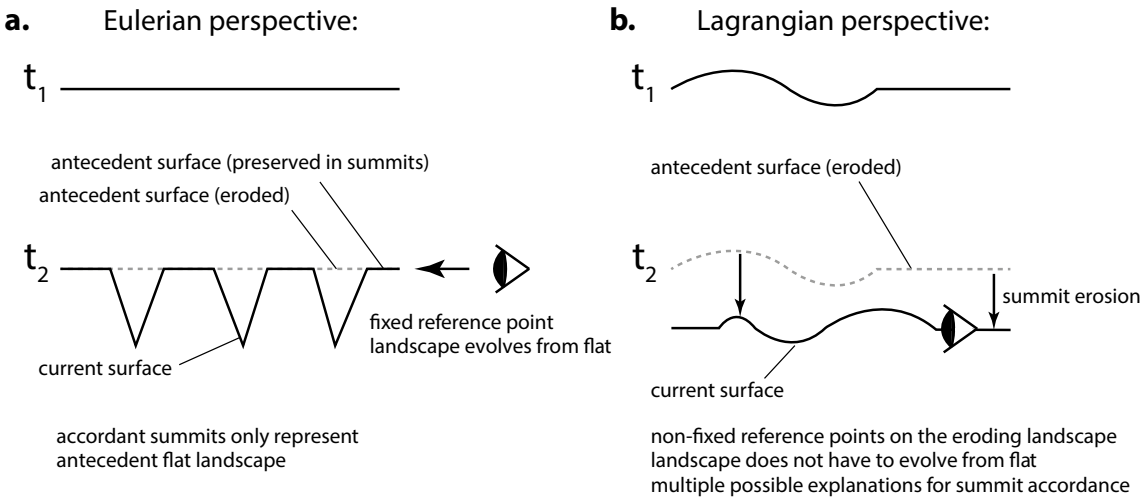

Figure 2-1. *(a) Eulerian and (b) Lagrangian perspectives for interpreting landscape evolution. The Eulerian perspective requires fixed reference points (summits) from which to assess landscape evolution. It is implicit that accordant summits represent slightly- or non-eroded remnants of an antecedent flat surface. Erosion into the inferred antecedent surface can then only increase relief. The Lagrangian perspective is fundamentally different in that the observation points are located on an evolving landscape. It requires neither non-eroding summits as fixed reference points nor antecedent surfaces. It offers much more flexibility and does not dictate that erosion can only increase relief. However, those potential benefits come with the price of increased complexity and acknowledged difficulty in reconstructing the former precise layout of antecedent surfaces.*

2.4 Topography on a peneplain

Low-relief and 'almost flat' are descriptive terms that can have varying meanings across spatial scales and their application is frequently qualitative to semi-quantitative. For example, how many hills, and of what amplitude, are permissible in the definition of 'almost flat'? It is the type of question for which a broad consensus is unlikely to be achieved because whatever definition is adopted is likely to be arbitrarily defined, except for the ultimate end-member of an entirely even surface graded to sea level. Adapting this end-member definition might hold some appeal as a simplifying argument. However, rather than attempting to generally define 'almost flat', it is perhaps more productive to quantitatively characterize relief within an area of interest.

In assessing regional to continental histories of rock uplift, erosion, subsidence, and sedimentation, representing the SCP as everywhere being a low-relief unconformity appears reasonable. While absolute relief may be low, relative relief, expressed as the ratio of amplitude to wavelength may be high on short-wavelength landforms, with potentially important feedbacks and controls on bedrock fracturing, weathering, erosion, and therefore further topographic development (Martel 2017). Useful ways of characterizing low-relief topography quantifiably include spectral analyses, which reveal superimposed wavelengths and amplitudes of relief (Perron et al. 2008). Details of the different wavelengths and amplitudes of the relief may shed further light on the processes by which the SCP formed and has been modified following exhumation. These potentially important topographic aspects are easily overlooked if the landscape is assessed solely in terms of its absolute relief over macro scales, particularly where it is envisaged as an entirely flat (or domed or tilted) surface envelope based on present-day summits as its pinning points.

2.5 Peneplain – a cumbersome concept in landscape evolution

In addition to the difficulty in defining 'almost flat', a key issue with the term 'peneplain' is that its application to any low-relief erosional surface carries with it a genetic connotation of having formed at sea level. The implication of this is that elevated low-relief surfaces must have been uplifted from sea level and low-relief surfaces at different elevations must represent different generations of peneplains that have undergone step-wise uplift from sea level (Lidmar-Bergström et al. 2000, 2007, 2013, Bonow et al. 2003, Japsen et al. 2018). Where accordant summits are inferred, those summits must be remnants of a peneplain and indeed the same peneplain, even where they occur on opposing sides of mountain ranges (Lidmar-Bergström et al. 2000, 2007, 2013, Bonow et al. 2003, Japsen et al. 2018). In addition, the flattest surface elements in a landscape interpreted as peneplain must best represent the original form of the peneplain or perhaps even be recently exposed uneroded remnants of it (Rudberg et al. 1976, Johansson et al. 2001b, Lidmar-Bergström et al. 2013). The assignment of a genetic label to a surface is cumbersome because it doesn't require the exploration of processes by which that surface may have formed, thus increasing the likelihood of erroneous interpretations and limiting further theoretical development. Genetic connotations should be avoided. Our preference is to dispose of the term 'peneplain' and replace it with 'unconformity' to entertain the possibility that the Subcambrian surface had sufficient relief to warrant its further evolution as that of a Lagrangian surface and to emphasize that not all low relief erosional surfaces are peneplains. Our use of 'peneplain' in this report reflects the traditional noun 'Subcambrian peneplain' for this landscape and no genetic connotation is implied.

The conceptual elevation of peneplains to the status of paradigm by which to interpret the landscape is also problematic because it can inhibit testing through falsification. As highlighted previously by Rhoads and Thorn (1996), study methods can be employed that confirm what is already common knowledge within the paradigm and expected conclusions can guide the interpretations. In either of these cases, circular argumentation is established.

Important nuances could be missed by focusing on flatness and embedding 'flatness as synonymous with peneplain' in the Eulerian perspective. For example, higher-relief parts of the current Swedish landscape inferred to have evolved from an initially flat SCP may, in some locations, have evolved from higher relief parts of the 'peneplain'. Conversely, very low relief parts of the present landscape may not be uneroded remnants of the SCP.

Figure 2-2a illustrates some difficulties in applying traditional peneplain models to landscape evolution. One interpretation of the relief and cover rock distribution shown in this map is that Quaternary glacial erosion has progressively roughened the landscape from an initially flat peneplain after it was progressively exposed from beneath cover rocks. Because of the glacial erosion, the southern part of the mapped area now constitutes a relatively high relief part of the landscape (in which Lake Mälaren resides). However, the increased roughness of the landscape towards the south also reflects antecedent topography, including the illustrated faults. Notably, Cambrian sandstone outliers also occur in Lake Mälaren. These are not shown in this map but are described in Hagenfeldt and Söderberg (1994) and the presence of these outliers in topographic lows indicates that the relief is not all glacial but is at least partly antecedent.

Furthermore, the preferential preservation of cover rocks in basins and in grabens, combined with their absence from relatively high, and convex, parts of the landscape (Figure 2-2a–c) also calls into question assumptions that glacial erosion always preferentially erodes valleys, that it does not erode summits (or not to the same extent), and that it only increases relief. Cover rock preservation in topographic lows might reflect their increased thicknesses in these locations, and therefore topographic relief at the time of deposition. They might also be located in grabens that are shielded from glacial erosion, such as in troughs trending transverse to ice flow. The striking dichotomy of cover preservation in topographic lows and cover rock erosion from topographic highs is the inverse of what is frequently implied for exhumed basement, namely glacial erosion of topographic lows and preservation of topographic highs. A key question is then why might this inferred inversion occur? There are glaciological reasons for enhanced erosion of topographic lows versus topographic highs (Stroeven and Kleman 1999, Cuffey and Paterson 2010). Also, cover rocks are softer than crystalline rocks, in part because bedding planes increase their vulnerability to erosion. However, the low relief and accordant summits of the exhumed and glacially eroded basement landscape might be somewhat misleading with respect to how much glacial erosion has occurred and where it has occurred. One possibility might be that relief is further lowered in some locations concurrently with it increasing in others (Egholm et al. 2017). For example, relief reduction across the uplifted margins of tilted basement blocks has been affected by glacial erosion ‘because of the greater prominence of higher scarps’ (Hall et al. 2019a, p 137) at Forsmark, Uppland, and Närke, (Figures 4-42 to 4-44 in Hall et al. 2019a). Another possibility is that there might be negative feedbacks on relief development through, for example, the glacial erosion of sheeting joints, which lie subparallel to ground surfaces, and which preferentially form under convex landscape elements (Martel 2011). If, for example, glacial erosion dissects the landscape by eroding concavities, the curvatures of the coevolving adjacent convexities might increase, which in turn increases the likelihood of sheet jointing under those convexities, making them potentially vulnerable to subsequent glacial erosion. A resulting negative feedback on glacial erosion could even ultimately establish a dynamic equilibrium, whereby relief does not change much over time while the landscape continues to lower. We do not advocate for a particular model of relief development in the Swedish lowlands through glacial erosion but highlight that assessing each of the above possibilities can be accommodated using a Lagrangian perspective, whereas only the first possibility (glacial erosion everywhere increases relief) can be assessed using a Eulerian perspective.

Finally, the Swedish lowland landscape (Figure 2-2a) had a spatially varying Cambro–Ordovician history. The area of lowest-relief in Uppland did not maintain a Cambrian cover prior to deposition of alum shale and limestone during the late Cambrian and Ordovician. Rather, it is thought that this part of the landscape experienced a regression (Nielsen and Schovsbo 2011), during which there was erosion of Cambrian sediments and renewed basement erosion with associated minor clastic deposition. Nearby Cambrian glaciation has also been inferred from sedimentary deposits (Westergård 1939). Consequently, this area is actually an eroded Subordovician unconformity, rather than a Subcambrian unconformity, and it is questionable that relative relief was necessarily everywhere entirely flat in this mapped area during the Cambro–Ordovician, or entirely comparable to other parts of the SCP, given also that the Cambrian regression inferred for this area apparently did not impact the broader region.

a. Rudberg (1954)

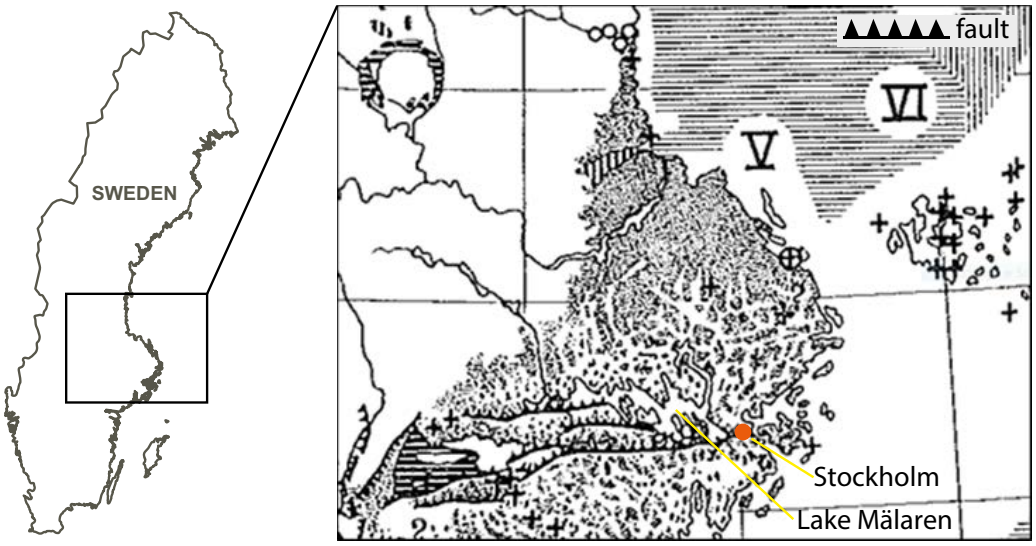

b. Lidmar-Bergström et al. (2013)

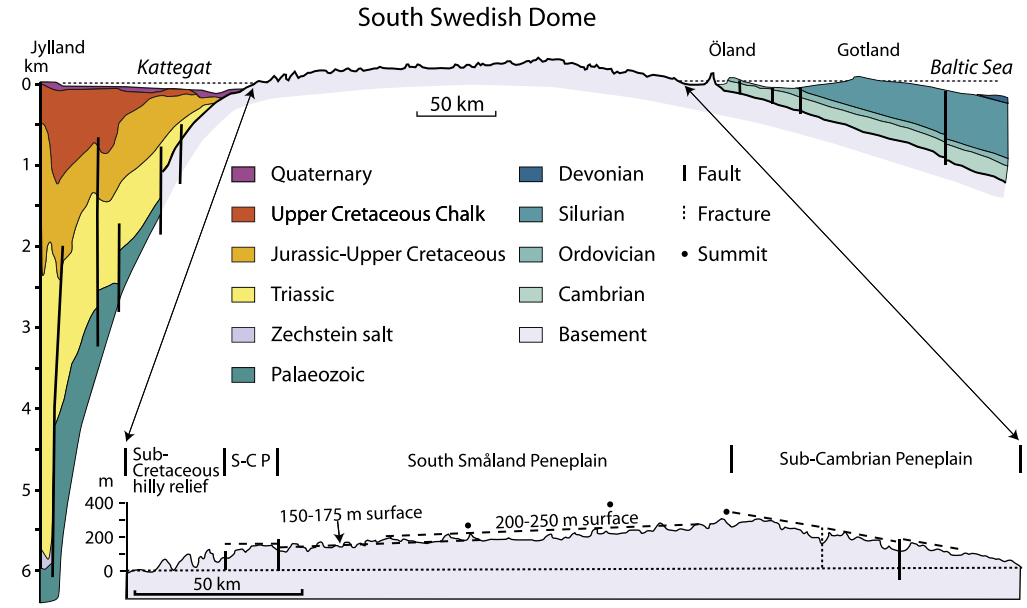

c. Lidmar-Bergström et al. (2017)

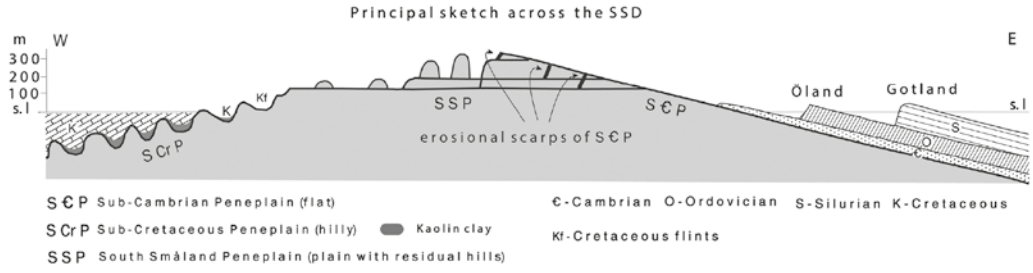

Figure 2-2. *(a) A hand-drawn relief map of Uppland and Lake Mälaren, adapted from Rudberg (1954). Albeit crude, this map shows some important information. The area South of Lake Mälaren is faulted and Ordovician (circles), Cambrian (horizontal lines), and older sedimentary rocks (vertical lines) remain preserved in topographic depressions (basins and grabens). Cambrian sandstone has also been observed in subvertical fractures (crosses). (b) An east–west profile across the South Swedish Dome, adapted from Lidmar-Bergström et al. (2013), showing its relation to sedimentary cover rocks. (c) A more stylized east–west profile of the South Swedish Dome from Lidmar-Bergström et al. (2017) detailing the evidence for three peneplain generations. Figure 2-2b and c reproduced with permission from Elsevier and Taylor & Francis respectively.*

Treating ‘summit accordance as synonymous with dissected peneplain’ can also be problematic. Firstly, several competing mechanisms can account for summit accordance (Phillips 2002, Mitchell and Montgomery 2006, Bishop 2011, Egholm et al. 2017). Hence, the grounds on which any one of those mechanisms is inferred, including the dissected peneplain inference, need to be justified on a case by case basis. Secondly, the formation of a peneplain demands the removal of all topography and therefore requires that most erosion occurs across summits, regardless of which erosional process is invoked. But how can peneplanation ever be achieved if antecedent peneplains are endlessly preserved, through non-erosion, in accordant summits (e.g., Tarr 1898, Bishop 2011)? Given the ubiquity of summit accordance, can the assignment of summit accordance to peneplain remnants be done with any certainty in the absence of cover rock constraint? A crucial issue that follows from these questions is whether this Eulerian interpretation of summit accordance is falsifiable. Bishop (1980) argues it is not whereas Rhoads and Thorn (1996) argue it can be if temporal data can be used rather than maintaining a reliance on the existing morphology, It would be extremely important to attempt to falsify this Eulerian perspective of landscape evolution by demonstrating landscapes where peneplains cannot be inferred from summit accordance.

This last point is illustrated in Figure 2-2b, c. The key interpretation from these two panels, that a low relief SCP experienced subsequent doming and renewed erosion to form the South Småland Peneplain (SSP), appears robust. However, these figures also lead to at least two important questions. How can it be known when the summits represent a peneplain or when they represent an evolving component of the landscape? How much summit lowering can occur for the ‘peneplain’ to still be considered a peneplain? The domed SCP underwent most erosion beneath the apex of the dome to produce the SSP but yet remnants of two younger peneplains, including the SSP, are inferred to be preserved in summits that are interpreted to be accordant on the 2-dimensional profiles. On the one hand, most erosion occurred under the dome summit, whereas trivial (even zero) erosion is inferred for the summits on the SSP. While an elevated ‘peneplain’ can indeed undergo subsequent incision, summits must ultimately be eroded to create a new ‘peneplain’ at a lower elevation in the landscape. An alternative view of these two inferred peneplains is that the hills and valleys are co-evolving, also through Quaternary glacial erosion. The mechanisms that might drive stepwise peneplanation shown in Figure 2-2c are also unclear. Do the inferred steps necessarily indicate step-wise uplift or might low relief surfaces evolve at different elevations through some other control, including lithological and valley network organization?

The international geomorphic community can be skeptical of the existence of peneplains (Phillips 2002). However, parts of the landscape that have been identified as SCP may provide some of the best examples on Earth of Davisian-style peneplain remnants. The SCP is developed in metamorphosed crystalline rocks, which frequently have a granitoid composition, and is part of a globally distributed feature that has elsewhere been labelled “The Great Unconformity” (Peters and Gaines 2012, Keller et al. 2019). It has traditionally been interpreted as an inert platform displaying either subaerially-exposed bedrock or a thin regolith, upon which relief varies from 0–20 m at broad regional-to-continental scales (Rudberg 1960, Rudberg et al. 1976, Calner et al. 2013, Gabrielsen et al. 2015). Vast tracts were graded close to sea level (i.e. within a range of meters to hundreds of meters) prior to the onset of transgression in the early Cambrian. Hills higher than 20 m appear to be rare. Crucially, there are cover rock remnants that locally constrain SCP history, both prior to deposition and following exhumation. The inference that the SCP was an inert, exposed, bedrock platform or mantled only by a thin regolith is made because the formation of this landscape predated the evolution of vascular plants, which in modern landscapes stabilize sediments, slow erosion, and maintain, often thick (tens of meters), regolith covers. Without vascular plants, regolith is more easily eroded, and bedrock surfaces become subaerially exposed, as also observed today in many arid (but not hyper-arid) environments.

In summary, we agree with observations and interpretations of the SCP being characterized by “low relief” over large areas. As we further explore the details of the relief on, or subsequently developed from, the SCP we question (i) assertions that regolith was thin to non-existent, (ii) the genetic connection to a Davisian model of peneplanation, (iii) whether some near-planar bedrock surfaces are indeed original SCP, and (iv) if so whether these were typical of the SCP in general and therefore the appropriate analogue to justify an Eulerian-style assessment of post-exhumation landscape evolution. Ultimately, we present hypotheses that might help to explain how the SCP formed and was reshaped by Quaternary glacial erosion.

2.6 SCP relief

The basement rock on which the SCP has formed has been subjected to multiple episodes of uplift and subsidence. For example, in Forsmark, some 400 km northeast of Trollhättan, a complex 1.89 billion-year history has involved orogeny accompanying crustal shortening, followed by multiple periods of rifting and associated sediment loading, interspersed with periods of exhumation related to far-field orogenic events (Stephens et al. 2007). The amplitudes of these tectonically-driven oscillatory loading and unloading cycles have decayed through time. However, the landscape has also undergone repeated loading and unloading by Quaternary ice sheets and the Baltic Sea, with the effects of the most recent ice sheet unloading and marine loading continuing up to the present-day (Kleman et al. 2008, Stroeven et al. 2016). Multiple periods of uplift and associated renewal of erosion has likely contributed to the development of low relief on the SCP (Stephens 2010; for example, the Cambro–Ordovician unconformity appears to coincide with an approximately 1.5 Ga unconformity). However, the removal of sediments from the landscape to offshore depocenters during the Cambrian transgression produced sediment thicknesses up to kilometers (Nielsen and Schovsbo 2011, Lassen and Thybo 2012). This redistribution of mass is expected to have induced flexural isostasy, as has occurred elsewhere (e.g., Bishop and Brown 1992), which would increase long wave-length relief and drive further erosion of uplifted parts of the landscape. It furthermore seems likely that a landscape developed on crystalline basement that was already saturated in fractures that had formed over multiple orogenic and subsidence events, faulted, and undergoing regional extension (e.g. Munier and Talbot 1993, Cocks and Torsvik 2005) and subsidence, would not be everywhere entirely flat. We expect residual relief on the SCP over long flexural wavelengths as a result of regional erosion but also at smaller wavelengths as a result of local erosion and deposition.

As a complement to the previously inferred history of cyclic uplift, cover rock and basement erosion, subsidence, and burial of the SCP, we highlight here a potential causal relationship between the decaying series of uplift amplitudes (Stephens 2010) and the evolving crust of the East European Craton. Over time, the crust of the craton has increased in thickness and density through underplating by eclogite formed through garnet-producing metamorphic reactions (Alinaghi et al. 2003, Grad et al. 2009, Blackburn et al. 2018, Mansour et al. 2018). The maintenance of thick crust by underplating beneath ancient cratons has previously escaped attention as a potentially key component to the formation of the SCP through helping to maintain positive elevations on the landscape for exceedingly long periods. The underplating may help maintain positive elevations because the density of the added rock, while high, remains lower than the mantle. However, because thick crust is being maintained by the addition of high density rock during and after surface erosion of low density rock, positive elevations are modest (i.e., limited to a few hundred meters), and may even by negative in the absence of another mechanism that can also drive uplift, such as dynamic topography (Blackburn et al. 2018). Such a model of underplating overprinted with dynamic topography is consistent with a history of repeated subsidence to below sea level and uplift in southern Sweden (Stephens 2010, Nielsen and Schovsbo 2011, Lidmar-Bergstrom et al. 2013, Japsen et al. 2016). The resulting positive elevations help to maintain weathering and erosion on the landscape for much longer than would otherwise be expected from the erosion of lower density crustal roots that formed during orogenesis. The inferred importance of underplating on SCP formation may also help to explain why true Davisian-style peneplains appear to be absent from younger continental landscapes (Phillips et al. 2002). Where landscapes are young, less mafic underplating would have occurred.

However, while mafic underplating may partly assist peneplanation, it also poses a challenge. This is because reduced amplitudes of uplift over time also reduce the potential energy stored in the landscape (stream gradients are lower). The erosional power of a stream displays a power-law relationship to its gradient, and so erosion rates decline rapidly over time in conjunction with decreasing amplitudes of uplift and declining river long profiles. Entirely removing topography from the landscape through fluvial erosion, particularly at a continental scale, therefore becomes increasingly difficult. The closer the landscape becomes to a Davisian-style peneplain, the harder it is to ever get there. Residual relief may therefore be expected, even on the SCP where relief is low over vast areas (Rudberg 1960, Lidmar-Bergström et al. 2013). Here we briefly summarize observations related to estimates of former relief on exhumed parts of the SCP and from parts of the SCP that remain beneath Cambro–Ordovician cover rocks (Hall et al. 2019a). From these, we make inferences on landscape relief prior to the Cambrian transgression.

Relief observations. Some observations of relief point to exemplary planar surface elements, including at Nordkroken, Trollhättan, and Fågelmara (Figures 2-3 and 2-4; Johansson et al. 2001b, Lidmar-Bergström et al. 2013). Other observations point to short wavelength relief of tens of meters (Figure 2-5; e.g. at Finse in Norway, Kinnekulle, and Rockneby). While the relief at Kinnekulle along the eastern shore of Lake Vänern varies according to rock structure, it appears superimposed on a longer wavelength relief that is revealed at times of lower lake levels (Högbom and Ahlström 1924, Nielsen and Schovsbo 2011). Yet other observations of the 'almost flat' SCP adjacent to the cover rock margin in southeastern Sweden (Figure 2-6a; Kalmar region) point to short wavelength (10^1–10^2 meter), low amplitude, relief superimposed on tens of meters of relief over longer wavelengths (Figures 2-5a and 2-6b–d). The Åland island group collectively provides another, but much more extensive, residual upland on the SCP (Figure 2-7). Both the persistence of Precambrian Jotnian rocks in the Bothnian Sea (Flodén 1977) and the late Cambrian erosion of early Cambrian marine sediments in Uppland (Nielsen and Schovsbo 2011) indicate long wavelength topography on the SCP (Figure 2-7).

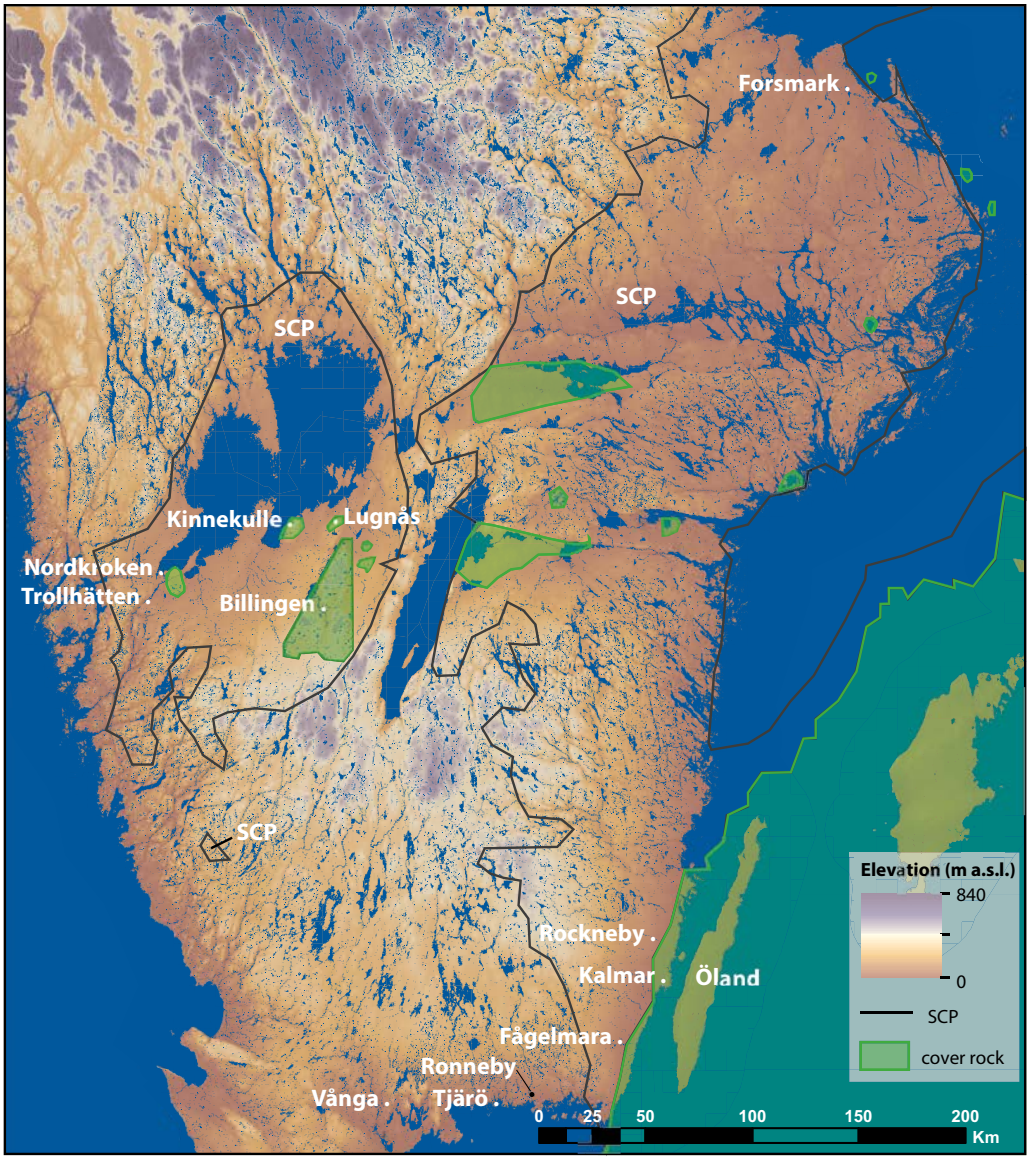

Figure 2-3. *Digital elevation model of southern Sweden showing the extents of the inferred Subcambrian Peneplain (SCP; enclosed by the black line), from Lidmar-Bergström and Olvmo (2015), and the current Lower Paleozoic cover rock extents. Outliers of Cambro–Ordovician cover rocks at Halleberg and Hunneberg (near Nordkroken), at Kinnekulle, and at Billingen are preserved beneath Permo-Carboniferous dolerite sills (Lundqvist et al. 2011). The protective sill has been eroded at Lugnås, exposing Ordovician limestone. Billingen and all other Lower Paleozoic outliers are located on downfaulted blocks. Other place names indicate locations referred to in the text. DEM with 2 m resolution, from LiDAR data, Lantmäteriet.*

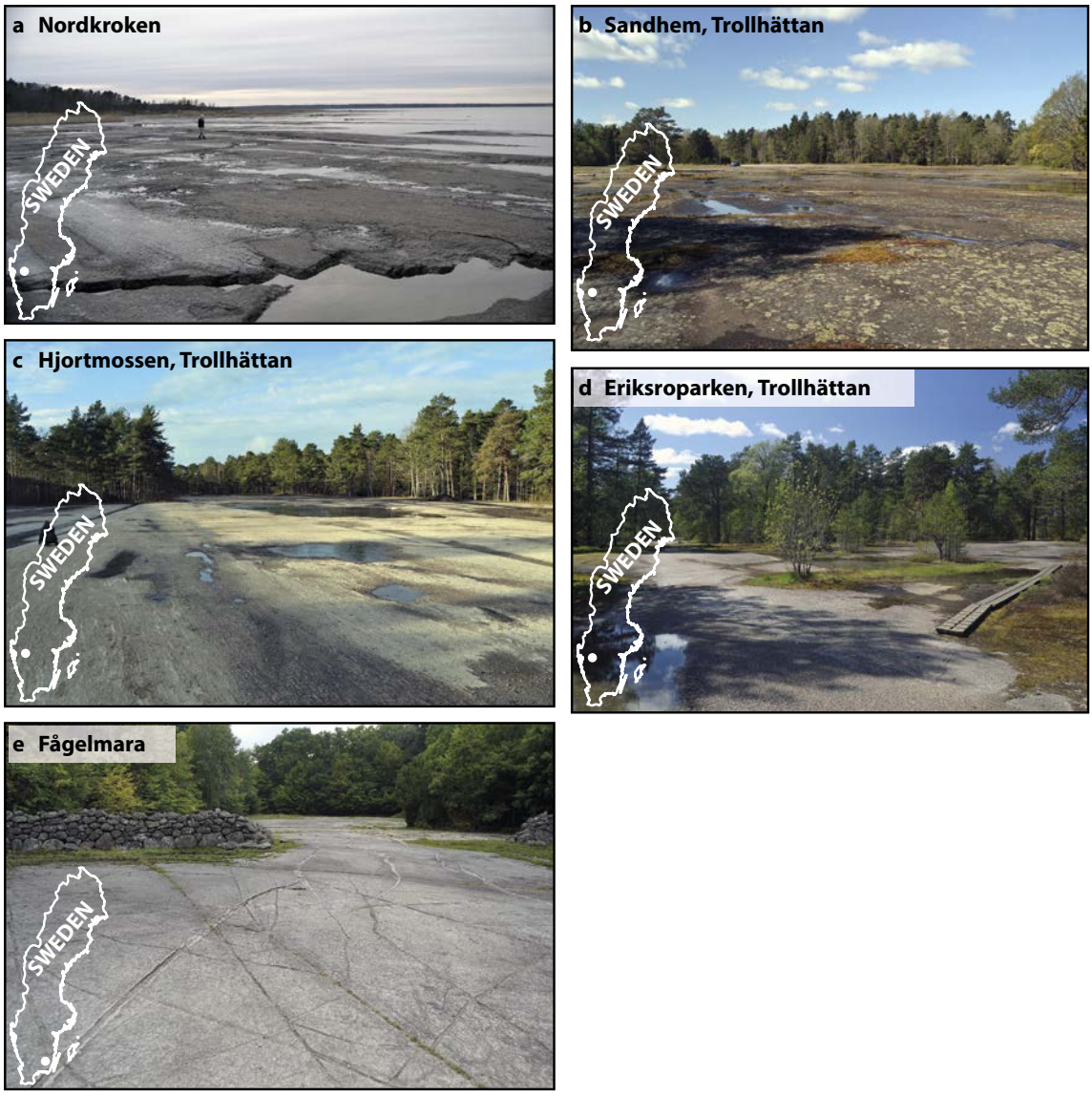

Figure 2-4. *Exceptionally low-relief outcrop surfaces at (a) Nordkroken, (b) Sandhem (c) Hjortmossen, (d) Eriksroparken, and (e) Fågelmara. Locations are shown on the inset maps and in Figure 2-3. The outcrops each occur on porphyritic gneissic granite where meters-scale spacing of vertical joints is common. These exceptionally low relief surfaces cover hundreds to even thousands of* m^2.

Figure 2-5. *Examples of meters-scale relief on the Subcambrian Peneplain. (a) Rockneby quarry, located a few hundred meters from the Cambrian sandstone margin (Figure 2-3). The basement is partly weathered and reveals convex–concave topography with an amplitude of a few meters. Glacial erosion has removed partly weathered basement, further flattening basement relief, and has lowered the basement surface by a few meters. These changes are visible in the basement surface surrounding the quarry wall (background). (b) Meter-scale bumps at Råbäcks Hamn with Cambrian rock patches illustrating the Subcambrian origin of the topography (Mattsson 1962, panel c). The site is located within 100 m of Kinnekulle, a table mountain comprised of a Cambrian–Ordovician sedimentary sequence preserved beneath a dolerite sill. (c) Cambrian sandstone preserved in basement concavities at Råbäcks Hamn. The outline of the Subcambrian Peneplain at (d) Finse and (e) Ustaoset on the Hardangervidda plateau of Southern Norway (Øvretveit 2016, Fig. 68). (d) The dotted white line shows the peneplain margin above a glacial trough. Cambrian phyllites form the higher ground above the unconformity. Convexities with amplitudes of a few meters (some arrowed) are superimposed on hundreds of m-long wavelength topography, which also has an amplitude of a few meters. (e) A low relief unconformity, with two valleys only meters deep, is illustrated by the white dotted line.*

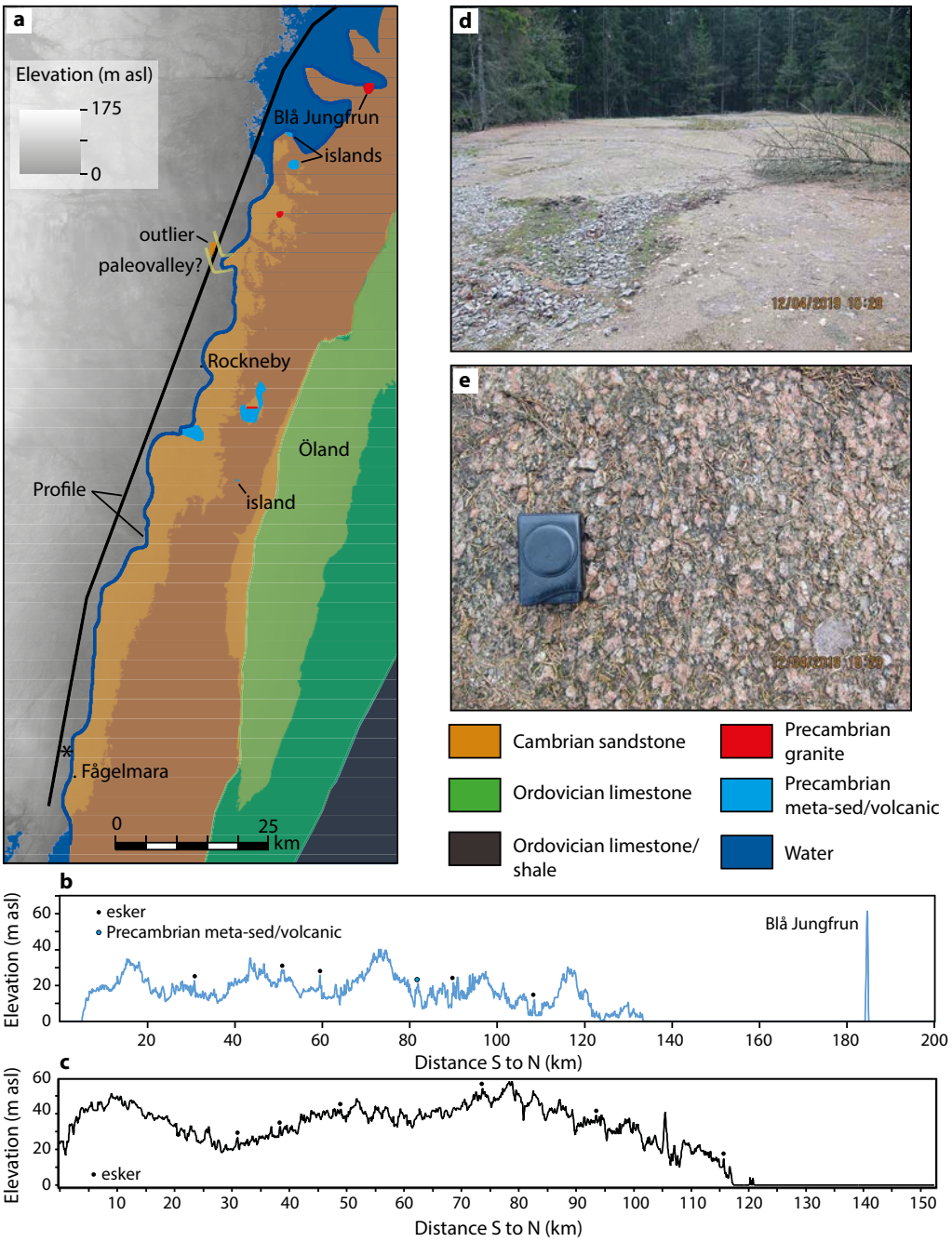

Figure 2-6. *Topographic and geologic characteristics of SE Sweden. (a) Precambrian basement exposed west of Cambrian sedimentary units is shown in grey scale whereas the Cambrian sedimentary units are shown in colours, which are semi-transparent to allow visualization of the landscape. Cambrian sandstone extends onto the mainland in SE Sweden. Its margin is irregular and an outlier occurs in what might have been a valley on the SCP. Precambrian rocks protrude through the Cambrian sandstone in seven locations, indicating hills on the SCP. Locations of two coast-parallel topographic profiles are indicated in blue (cf. panel b) and black (cf. panel c). The location of Figure 6-5a–b is shown by the asterisk. (b) A topographic profile across the SCP adjacent to the cover rock margin reveals low relief, with the exception of Blå Jungfrun, which protrudes over 100 m above the surrounding Cambrian sandstone surface. Summits tend to be granite-gneiss basement, but some are eskers, and concavities contain glacial sediments. Bedrock relief is therefore generally underestimated. Hills up to about 15 m are superimposed on a long wavelength topography, where convexities partly reflect cover rock excursions further inland, in particular at the relatively high area located about 70 km along the transect. (c) A profile constructed on the SCP from straight line segments subparallel to the coastline and inland of the cover rock margin. Two low domes are revealed at 0–30 km and 30–115 km, with amplitudes of 30–60 m. Short wavelength hills are superimposed on these domes, with amplitudes of meters to about 15 m. It appears that hills and valleys relate to fault blocks between about 80 and 110 km along the transect, but otherwise short wavelength topography appears more subdued than on the profile that mirrors the cover rock margin (panel b). (d) An inspection of the SCP along the cover rock margin reveals numerous domes, such as the one illustrated here (starred in panel a), which protrude some meters above their surroundings. (e) These domes occur in porphyritic gneissic granite, commonly with meters-scale spacing of subvertical joints.*

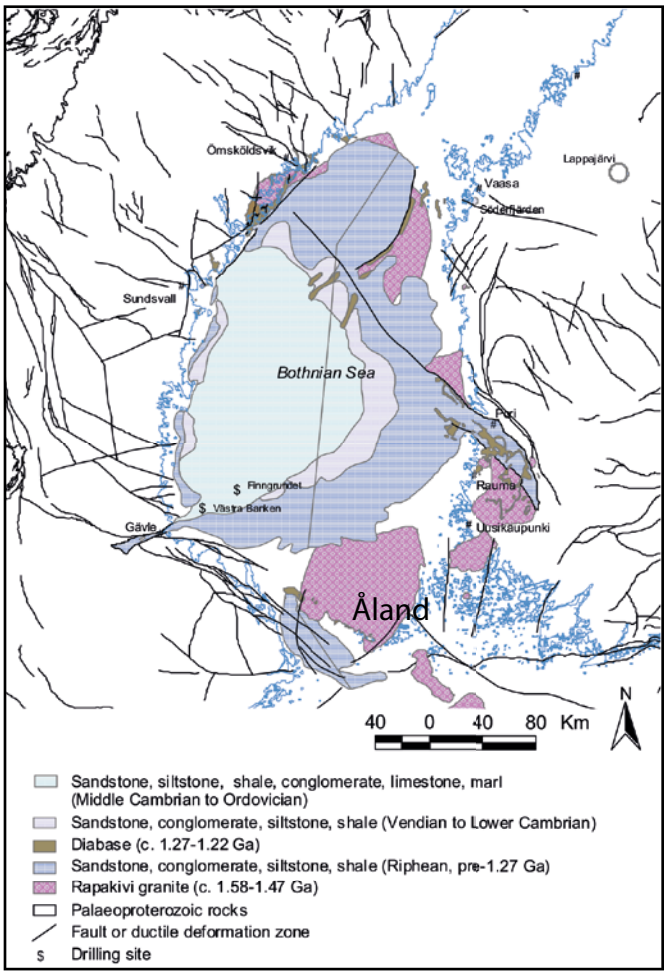

Figure 2-7. *Precambrian to Ordovician sedimentary rocks are preserved in the Bothnian Sea (Korja et al. 2001). This Mesoproterozoic basin is an example of persistent long wavelength basement topography (adapted from Korja et al. 2001). Preservation of sedimentary rocks in basins is part of a general trend observed in Sweden. This probably reflects that deposits were thicker in basins and perhaps that they have been shielded from erosion processes, including those attributable to Quaternary glaciations, for example where they are located on grabens oriented transverse to ice flow. The Åland islands form high points, perhaps formed during the inferred Cambrian uplift of this area, with which erosion of Cambrian sedimentary units has been associated (Söderberg and Hagenfeldt 1995, Nielsen and Shovsbo 2011). Figure reproduced with permission from Elsevier.*

Hills and depressions. The geological map over southeastern Sweden reveals seven hills, the largest over 100 m high, protruding through the cover rocks (Figure 2-6a). It also indicates an outlier of Cambrian sandstone deposited in a depression in the SCP, likely similar to nearby buried outliers that are inferred to have sourced sandstone rocks and clasts in Quaternary tills and diamictites (Olvmo et al. 1996). A further three hills, tens of meters high, are located under the island of Öland (Figure 2-3; Bastani et al. 2018). This region appears to offer one answer to the question of how many hills are required for them to no longer be considered exceptional but rather that they can be a feature of 'almost flat' surfaces. In the Kalmar–Öland area, we suspect that the ten, or more, "exceptions" are accompanied by smaller hills that do not protrude through the present onshore cover rock. The presence of Precambrian rocks such as arenites and rhyolites that formed in the near-surface to surface (SGU Geokartan) points to the SCP in southeastern Sweden roughly coinciding with an even older unconformity, such as occurs in other parts of the SCP including Forsmark (Hall et al. 2019a).

Weathering profile estimates of Precambrian relief. Along the Caledonian front and in Estonia, remnants of oxidized weathering profiles are preserved, or likely preserved, on downfaulted basement blocks and display thicknesses up to meters (Gabrielsen et al. 2015), tens of meters (Angerer and Greiling 2012), and even exceeding a hundred meters (Liivamägi et al. 2015). Those in Estonia also contain abundant kaolinite (Liivamägi et al. 2015). These weathering profiles are interpreted to be Precambrian remnants because they are overlain by Cambrian sedimentary rocks. Because these remnants likely represent minimum thicknesses of former vadose zone weathering profiles, and because weathering profile thickness scales up to 1:1 with relief in positive water balance locations, minimum estimates for relief in the landscape prior to Cambrian marine transgression are up to tens of meters in the Swedish and Norwegian locations and over 100 meters in Estonia.

Transgression durations indicate Precambrian relief. The Cambro–Ordovician transgression of the Precambrian landscape occurred over tens of millions of years and was likely the sum of a series of transgressions (Nielsen and Schovsbo 2011, Lassen and Thybo 2012). This duration qualitatively appears to be a function of regional landscape gradients. This interpretation is based on the expectation that an entirely flat horizontal surface would seemingly have been transgressed over much shorter timescales. The relief may have been higher on the Precambrian landscape than that which characterized the transgressed basement surface that was ultimately covered by marine sedimentary units across vast tracts during the Cambro–Ordovician.

Topography from offshore seismic profiles. Offshore seismic profiles show a range of topographies and wavelengths similar to the onshore evidence, from essentially planar to hills of a few tens of meters and larger (Tuuling et al. 1997, Tuuling and Flodén 2001, Lassen and Thybo 2012). However, even where offshore seismic reflection profiles of the buried basement indicate planar surfaces (i.e. straight lines), interpreted as relief as low as meter-scale (Lassen and Thybo 2012), the resolution of the of the data is such that they may represent short wavelength convexities and concavities up to some tens-of-meter-scale amplitudes. Finally, where seismic reflections of the buried offshore basement surface are dipping straight lines but overlying sedimentary strata display lower dip angles, a landscape gradient on the basement is indicated at the time of cover rock deposition (Lassen and Thybo 2012).

Summary. These different lines of evidence converge towards the paradigm that relief was generally low on the post-transgression basement surface to an extent that this SCP appears to be exceptional in the geologic record. However, we also highlight that some relief was maintained on the parts of the landscape identified as SCP, of varying amplitudes, and over different wavelengths. Secondly, higher relief and higher elevation surfaces may have been maintained on other parts of the post-transgression landscape that are not interpreted as remnants of the SCP (because the SCP is identified on the basis of low relief). Finally, the Precambrian landscape may have had higher relief than the post-transgression basement surface. Therefore, the Precambrian landscape and the SCP may be better conceptualized as distinct landforms separated in time by up to tens of millions of years.

In this study we test two hypotheses for the formation of exceptionally flat surfaces in the Trollhättan area from a mixture of observations, both local and from other locations, and measurements. These surfaces are set in a landscape which has previously been interpreted using an historical geomorphology perspective. We use our observations and measurements to query some aspects of historical geomorphology, particularly as they apply to these specific surfaces, but also to the wider SCP. We test whether exceptionally flat surfaces are necessarily SCP and whether the SCP, in the absence of cover rocks, is best modelled as a flat surface from accordant summits. Our study has implications for the formation of the SCP and also for how Quaternary glacial erosion has modified the landscape. We also highlight implications for the Forsmark area, because of its future use for permanent underground storage for spent nuclear fuel rods. Our study illustrates how different conclusions can be drawn depending upon whether a Eulerian or Lagrangian perspective is being applied.

3 Study site

This study focuses on some remarkable bedrock outcrops in Trollhättan and at Nordkroken, on the southern shore of Lake Vänern (Figure 3-1). Most outcrops are of porphyritic gneissic granite, with K-feldspar phenocrysts as long as a few centimeters (Figures 2-6e and 3-2). The summits of these outcrops display exceptionally low relief of tens of centimeters and low surface curvatures. The outcrops appear to the naked eye to be near-planar, with curvatures increasing on their flanks (Figure 2-4). The long axes of the exposures extend as much as a few hundreds of meters in Trollhättan. At Nordkroken, these outcrops are even larger (Figure 3-3). Their low-relief surfaces extend over hundreds of meters to over a kilometer in plan-view and they are cut by subvertical fracture networks. Similar outcrops located as far as 1 km to the southwest of Nordkroken have long axes of only tens of meters and clearly convex surfaces.

Cambrian sandstone fissure fills, millimeters to centimeters wide, occur in outcrops at Trollhättan and at Nordkroken (Mattsson 1962, Rudberg et al. 1976.) They usually extend horizontally for a few meters to tens of meters, but some reach lengths of ~100 m. Rare vertical exposures indicate that the fissure fills only extend tens of cm to a few meters vertically into the host rock.

The Nordkroken surfaces are located as close as 300 m to the twin table mountains of Halleberg and Hunneberg. Those mountains are remnants of Cambro–Ordovician sedimentary units preserved beneath a Carboniferous dolerite sill. A contact apparently strikes along the northwestern flank of Hunneberg-Halleberg, separating porphyritic gneissic granite outcrops on which the CFSs have developed from the gneissic granite underlying the table mountain (Figure 3-2). The porphyritic gneissic granite unit appears to abut the southwestern flank of the Hunneberg and might continue beneath it. Other similar table mountains also occur in the region, at Kinnekulle, Lugnås (where the dolerite cap has been eroded away), Billingen (downfaulted along its western and southern flanks), and near Falköping. This wider region extending away from the southeastern shore of Lake Vänern is of generally low relief. The Nordkroken and Trollhättan outcrop summits have been traditionally interpreted as original remnants of the SCP, because of their remarkably low relief, the presence of Cambrian sandstone fissure fills, their location near the table mountains, and the low regional relief (Johansson et al. 2001b). Also, because they are massive and have widely spaced vertical joints, they are reasonably considered to be resistant to erosion, displaying only granular-scale lowering through Quaternary glacial erosion and non-glacial weathering and erosion (Rudberg et al. 1976). They may therefore essentially represent the unconformity surface that was covered in Cambrian sediments.

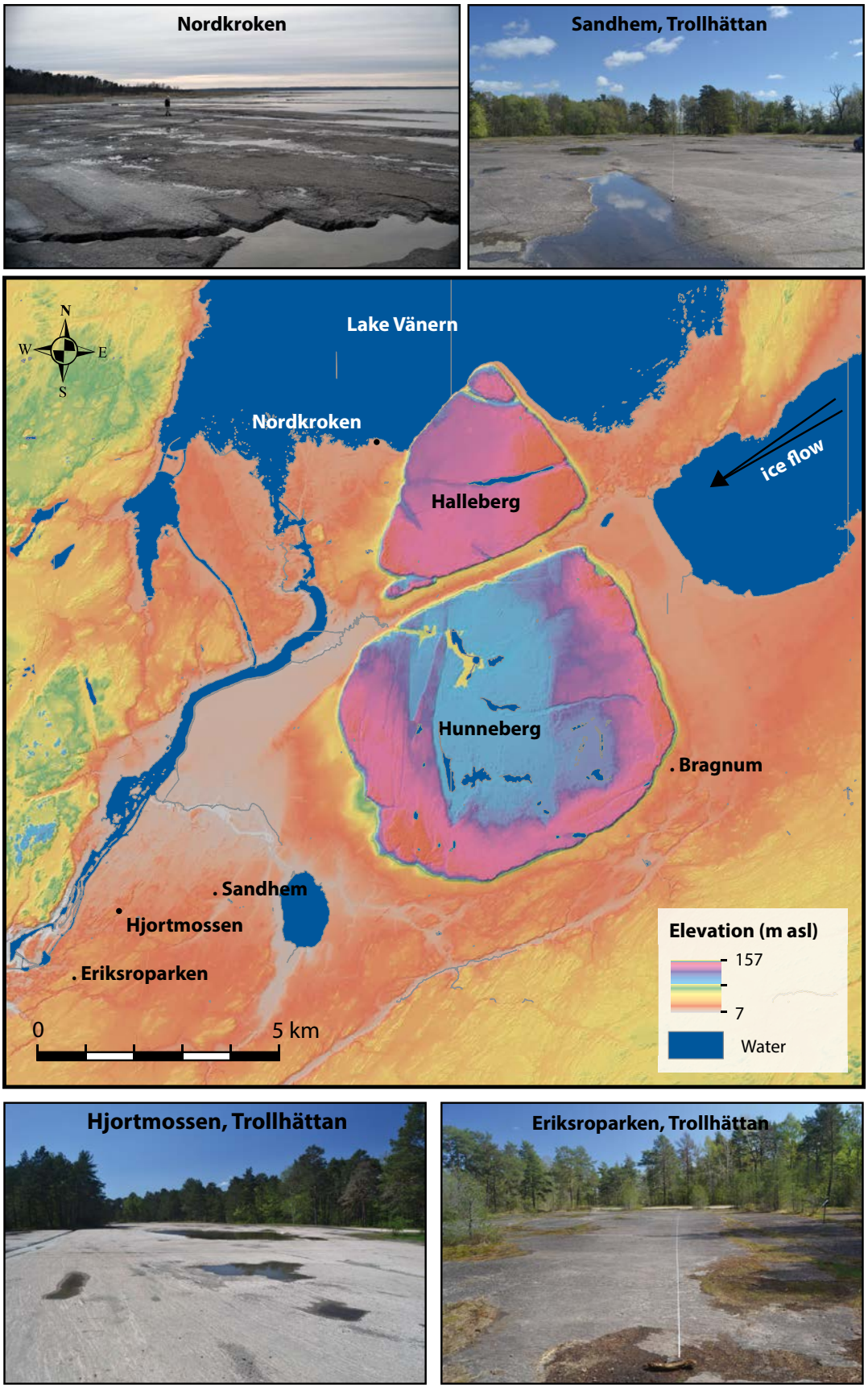

Figure 3-1. *Topographic map of area around the table mountains of Halleberg and Hunneberg and study sites mentioned in the text. Sandhem, Hjortmossen, and Eriksroparken are locations in the city of Trollhättan. Striae and glacially-sculpted bedrock forms indicate ice flow over this area from the northeast (arrow). DEM is based on LiDAR data with 2 m resolution (Lantmäteriet).*

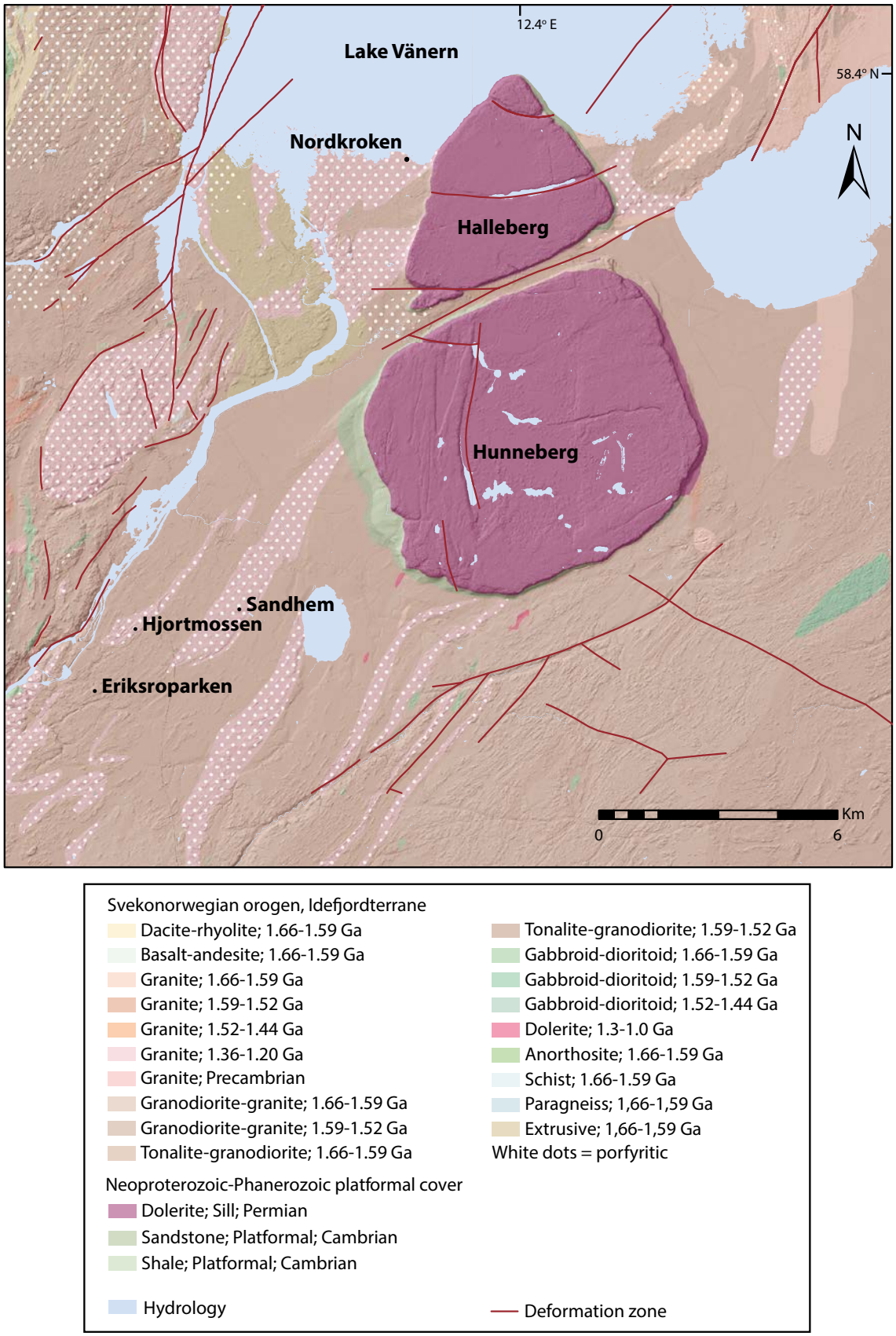

Figure 3-2. *Geologic map of the area around Halleberg and Hunneberg (data from Geological Survey of Sweden). Cambro–Ordovician sedimentary rocks are preserved beneath the dolerite sill that caps Halleberg and Hunneberg. The exceptionally-low relief surfaces at Hjortmossen, Sandhem, and Nordkroken are all located on kernels of porphyritic, coarse-grained gneissic granite. The low relief summit surface developed at Eriksroparken is also located on coarse-grained rock.*

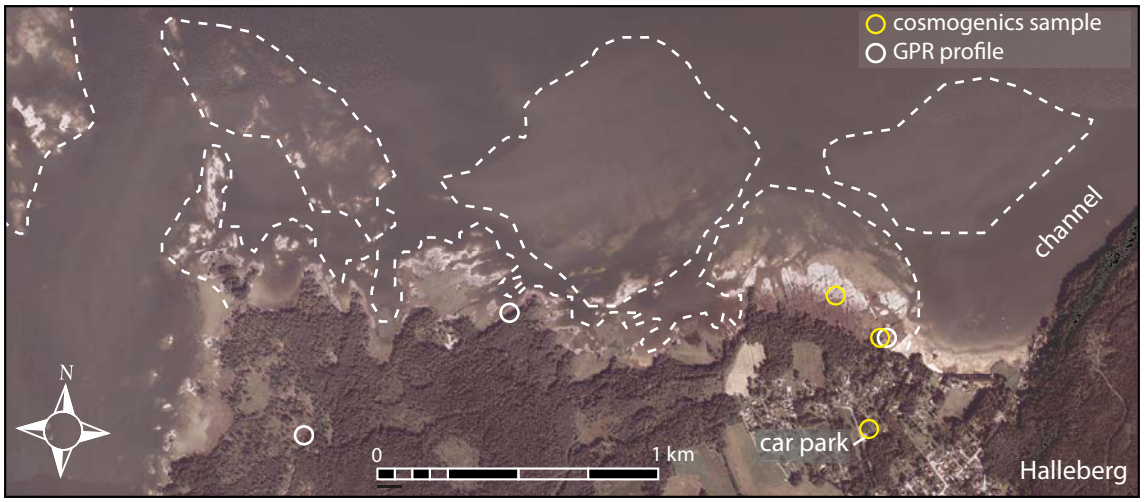

Figure 3-3. *Aerial photograph showing the distribution of exceptionally-low relief surfaces (white dotted lines) at Nordkroken. Locations of cosmogenic nuclide sample sites and the ground penetrating radar (GPR) profiles are shown in yellow circles and white circles, respectively. The nature of the topography on the blocks offshore is unclear in this image but has been inspected in recent Google Earth imagery with lower water levels in Lake Vänern. The inland borders of the exceptionally low relief surface are uncertain because of sediment covers. However, low domes, rather than these exceptionally low relief surfaces, are exposed in the area around the study site indicated by the white circle to the SW of the image. Halleberg is located a few hundred meters to the east of these blocks and is separated from them by a channel that appears to have been subglacially eroded along a pre-existing fracture or fault. The presence of this channel might indicate that the western flank of Halleberg has been stable since before the last glacial.*

4 Methods

To investigate processes by which these remarkable outcrops may have formed, we selected several for detailed study, including three in Trollhättan ("Slättbergen" at Sandhem, Hjortmossen, and Eriksroparken), the shoreline area at Nordkroken, and two outcrops about 1 km inland of, and to the southwest of, Nordkroken (Figure 3-1). We describe outcrop characteristics including their topography (size, relief, aspect) and fracture distributions (spacing, orientation). We also collected data on subsurface fracturing using ground penetrating radar (GPR). We collected samples for dating the exposure ages of the surface from concentrations of two *in situ*-produced cosmogenic nuclides, ^{10}Be and ^{26}Al, from surface quartz samples. We also conducted simulations of glacial erosion over multiple glacial and interglacial cycles, with timing and durations of glaciation inferred from benthic δ^{18}O records.

To provide context to the Västra Götaland sites, we have also initiated the study of granitic outcrops located within 1 km of the Cambrian sandstone margin, about 315 km to the southeast of Trollhättan near Fågelmara (Figure 2-3). These outcrops occur as domes with horizontal dimensions of up to about 100 m and with amplitudes < 10 meters. We compare qualitative observations of crystal sizes and joint characteristics from these outcrops with the studied outcrops in Västra Götaland. We also used GPR to detect bedrock fractures beneath the flattest example of these that we have observed in the Fågelmara area. These outcrops help to provide context because they have also been previously identified as remnants of the SCP (Neubeck 2000), where it is further implicit that glacial erosion has been trivial, they display bedrock and relief characteristics similar to the outcrops studied in Västra Götaland, and they are located within 1 km of Cambrian sandstone.

4.1 Jointing from GPR

4.1.1 GPR equipment and data processing

We used GPR to detect subsurface bedrock fracturing at Nordkroken and at three Trollhättan sites, including Sandhem, Hjortmossen, and Eriksroparken (Figure 3-1), to assess whether these low-relief bedrock surfaces are underlain by sheeting joints. GPR utilizes electromagnetic (EM) waves that propagate in the shallow subsurface according to its electromagnetic properties. GPR consists of a transmitting antenna that sends a signal within a specific frequency range and a receiving antenna that records the timing and amplitude of the signal that is reflected from discontinuities in physical properties of the material (Figure 4-1). Contrast in the dielectric permittivity is the main factor that generates reflections of EM waves.

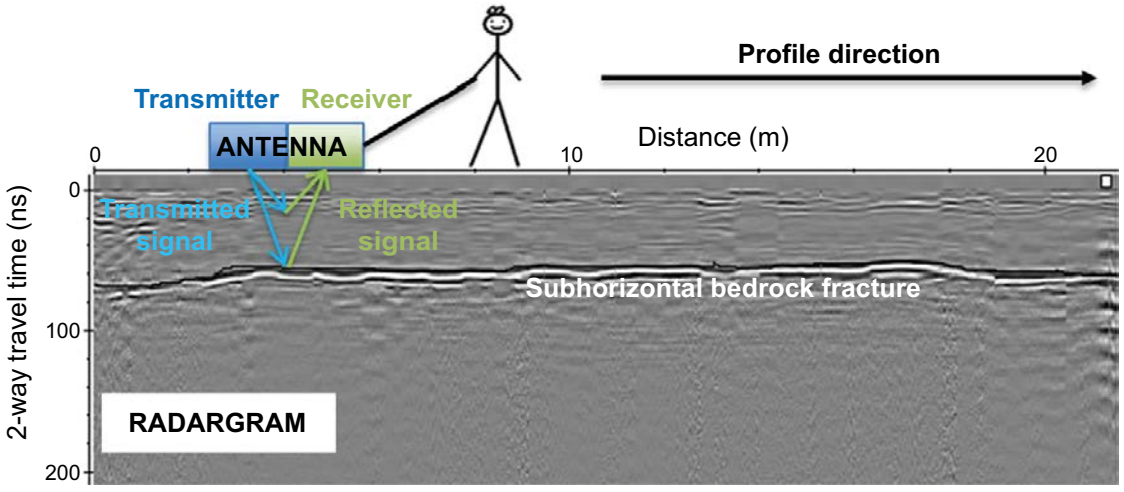

Figure 4-1. *Schematic figure showing the principle and the acquisition of GPR data.*

The velocity of EM waves does not depend on the frequency of the transmitted signal (non-dispersive technique), which can vary from 20 MHz to 2 GHz, but essentially only on the contrast of the dielectric permittivity. Because EM wave velocity varies with material properties, the receiving antenna records reflected waves at different times depending on distance from the reflector and the electrical properties of the media above the discontinuity (Figure 4-1).

The GPR is a CrossOver® CO1760 (ImpulseRadar Sweden AB). It is a dual-channel antenna which simultaneously transmits two different central frequencies, 170 MHz and 600 MHz. The data acquisition was done at a minim rate of 800 scans/s and the recorded trace is an average of all the scans acquired at travel distance intervals of 5 cm measured by an odometer. The GPR unit has a differential GPS (an external global navigation satellite system; GNSS) with real-time kinematic (RTK) correction to locate the unit with cm vertical and horizontal resolution.

Raw GPR radargrams have been processed with a Matlab code developed by M. Rossi consisting of: (1) A Finite-Impulse-Response Passband filter for removing noise at high and low frequencies (according to the central frequency processed); (2) Time Zero Correction for placing the starting point of the traces at the first reflection coming from the topographic surface; (3) Background Removal filter for removing horizontal stripes due to ringing of the signal (very weak in the data); (4) Gain Function for enhancing the signal at latent times (we used a gaining function obtained from fitting the Instantaneous Power curve of the mean trace of the profile); (5) Hyperbolae Fitting for estimating the mean velocity of EM waves along the profile; (6) Migration of the radargram using Stolt's algorithm and the previously estimated velocity (velocities have been further calibrated in an iterative process that uses the results of the migration); (7) Static Correction for incorporating the topography (elevation from GNSS coordinates); (8) Depth transformation for displaying the vertical axis of the radargram with a space unit dimension instead of time (the previously estimated velocity has been used for this transformation); and (9) Hilbert Transform for showing the envelope of the signal, where the reflected waves, with their characteristic positive and negative amplitudes, are transformed in the instantaneous amplitude (only positive).

4.1.2 GPR data acquisition

The presence of surface-parallel sheeting joints below the bedrock surface would provide key evidence that the bedrock surface itself could have formed by erosive exploitation of sheeting joints. GPR identifies fractures based on their dielectric contrast with the host rock. The GPR unit emits a radar signal and detects the time of the return signal to determine the depth of the fractures below the ground surface. GPR data were processed to produce accurate and precise locations of subsurface reflectors (e.g., sheeting joints) with respect to the ground surface geometry. Where GPR transects intersected rough bedrock surfaces and highly convex outcrops, or extended beneath tree cover, spatial resolutions were lower, which in some places required interpolation of transect segments of the ground surfaces and subsequent vertical re-positioning of the GPR unit. High quality spatial positioning was achieved over all of the Nordkroken transects, and across most of the transects elsewhere.

The resolution and depth to which the GPR can detect bedrock fractures depends upon antennae frequency. Higher frequencies (and shorter wavelengths) permit higher resolution reflections but at the cost of decreased depth penetration. We therefore used two antennas, with frequencies of 170 MHz and 600 MHz to optimize depth penetration and resolution.

GPR offers an efficient means of detecting subsurface bedrock fractures parallel, or oblique, to the ground surface, but does not directly image fractures perpendicular to the ground surface. Locally, however, subvertical fractures are indicated where they intersect the ground surface either by a break in the subsurface reflectors (represented by a vertical white streak in a GPR image) or an intense subhorizonal reflector in the immediate subsurface. These vertical fractures have apertures of centimeters to tens of centimeters at the ground surface and may contain sediments and vegetation.

The GPR unit we used detects only fractures with an aperture of a centimeter or more. A fracture can be filled with air, water, transported sediments, or in situ weathering products, and in each case produce a reflection because the density of the fill is less than that of the host bedrock. Fractures with hairline or mm-scale apertures, however, are unlikely to be visible on GPR images. Consequently, false negatives are to be expected, where fractures are present but undetected. Conversely, the likelihood of a false positive attributable, for example, to the surface of the groundwater table is low in the massive bedrock outcrops that we imaged.

To provide context to the Västra Götaland sites, we also used GPR to detect fractures beneath a bedrock outcrop of similar low relief near Fågelmara (Figure 2-3). This outcrop of porphyritic gneissic granite is located ~1 km from the mapped contact of Cambrian sandstone and contains a distinctive pegmatite dyke that is in places more than 2 m wide. The surface of the outcrop is even, including where it intersects the broad pegmatite vein. The outcrop displays subvertical fractures that typically are spaced more than a meter apart. Owing to time and weather constraints, this is the only outcrop we investigated near Fågelmara. It is, however, the most planar outcrop with an area of hundreds of m^2 that we are aware of in this region, following an extensive survey of tens of km along the Cambrian sandstone margin.

To ground-truth our interpretations at the Västra Götaland and Fågelmara sites, we also examined a quarry near Vånga in northeastern Skåne (Figure 2-3). This quarry is excavated into a hill trending NNW and is underlain by gneissic granite (Figure 4-2). This quarry was examined because it displays well-developed subhorizontal fractures at different depths and with different apertures in its walls. It was also easily accessible for GPR use. Profile 1 (Figure 4-2a) is located on a native (non-quarried) bedrock surface. The maximum elevation of the profile is 138.5 m a.s.l. Profile 2 (Figure 4-2a) is on a sub-horizontal quarried bench. This profile has a maximum elevation of 130.5 m a.s.l. We ran both GPR transects about 1.5 m away from the tops of vertical quarry faces (Figure 4-3). We also photographed fractures visible in the quarry faces (Figures 4-4 and 4-5) and surveyed the fracture locations, so we could compare the presence and locations of reflectors in the images with visible fractures in the quarry walls. Perfect matches between fractures in the photographs and GPR images cannot be expected. For example, the GPR transects are not exactly along the quarry faces, so the reflectors may show differences to the jointing exposed on those faces. Also, unless the sheeting joints were perfectly horizontal, and they are not, the dips apparent on the photographs and GPR images will differ if the directions of the profiles are not perpendicular to the viewing directions of the photographs.

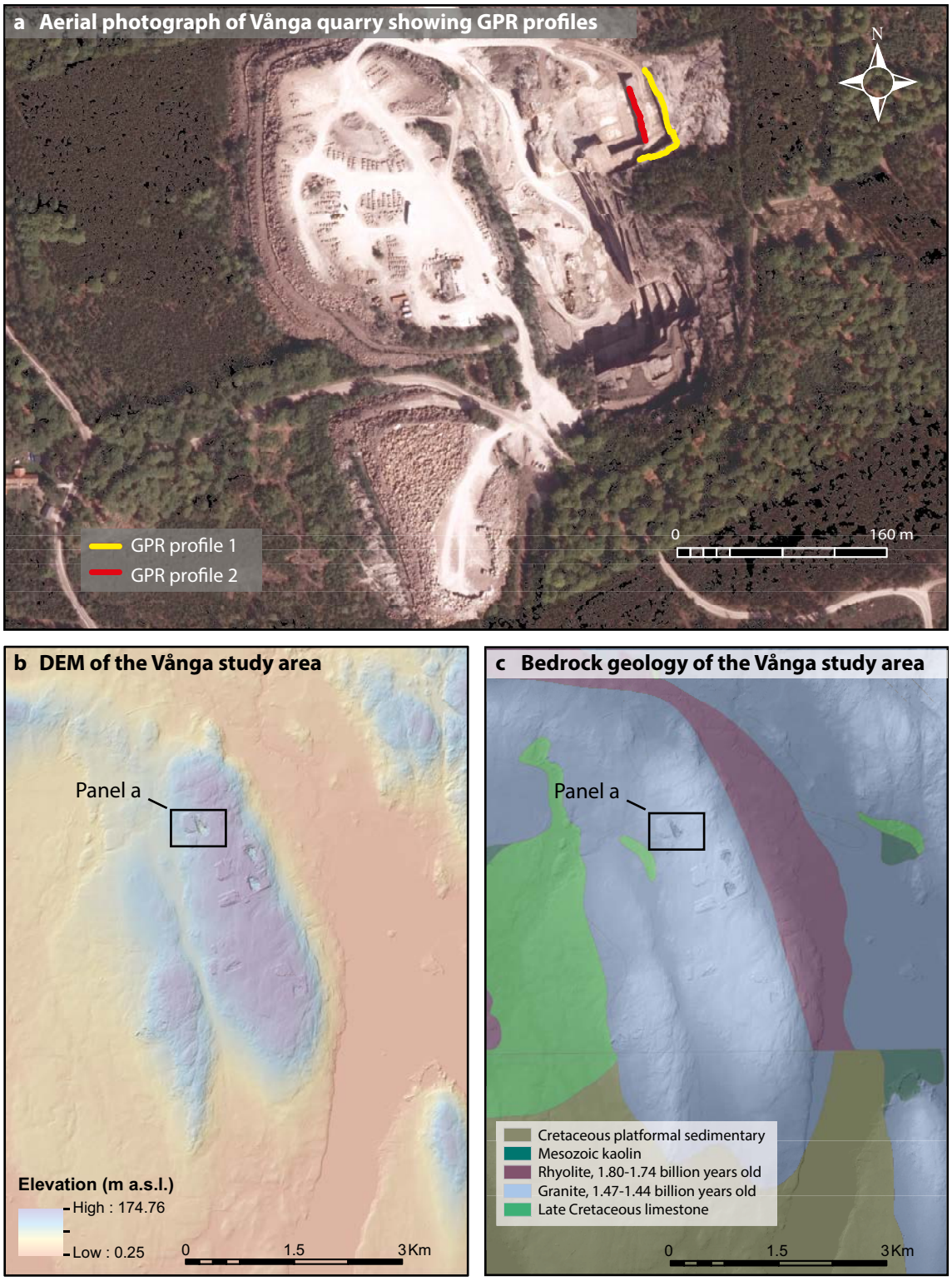

Figure 4-2. *Study site location at Vånga quarry (Figure 2-3). (a) Orthorectified aerial photograph showing the locations of the two GPR profiles used to ground-truth our GPR interpretations at sites in the Trollhättan area and at Fågelmara. Note the sharp bend in GPR profile 1 (yellow line). (b) DEM of the Vånga study area with 2 m resolution, from LiDAR data. The study site, indicated with a rectangle, is only one of three quarries on this 175 m-high hill. It is located on the stoss-side of the hill with respect to former ice flow, which was from the north. The location of the photograph in (a) is shown by the black rectangle. (c) Local bedrock geology showing the study site located on granite. Nearby, at lower elevations, Late Cretaceous limestones overlie kaolinized granite, which has also been quarried. The location of the photograph in (a) is shown by the black rectangle.*

Figure 4-3. *Locations of the two GPR profiles at Vånga quarry (cf. Figure 5-1). Well-developed sheeting joints lie subparallel to the ground surface, which is original. The quarry walls to the left in the picture face west, whereas those to the right face North. Both quarry faces are 6 m high. Note the presence of saprolite in a sheeting joint.*

4.2 Cosmogenic nuclide sampling and laboratory preparation

Cosmogenic nuclides have been used frequently to study the dynamics and history of former ice sheets, including the Fennoscandian (Brook et al. 1996, Fabel et al. 2002, Stroeven et al. 2002a, b, Anjar et al. 2014, Blomdin et al. 2015, Jansen et al. 2019). Here, we measure cosmogenic nuclide concentrations to infer bedrock glacial erosion rates in the Trollhättan area, during late Quaternary time. Our methodology builds on the production of cosmogenic nuclides in quartz in rock surfaces that are exposed to cosmic rays (Lal 1991, Gosse and Phillips 2001). Cosmic ray interactions with the Earth's atmosphere yield a cascade of secondary particles, primarily neutrons but also muons, that bombard the Earth's surface, and which are capable of inducing nuclear reactions in bedrock. Cosmic ray particles penetrating a rock surface are rapidly attenuated, so the production of cosmogenic nuclides is almost entirely constrained to the uppermost 3 m. When these secondary cosmic rays interact with rock minerals, such as quartz, daughter isotopes are produced with half-lives relevant to the timescales of geologic processes, i.e. ^{10}Be has a half-life of 1.39 Ma (Chmeleff et al. 2010, Korschinek et al. 2010), and ^{26}Al a half-life of 705 ka (Nishiizumi 2004). Production rates vary spatially and temporally because of differences in atmospheric pressure and the strength of the Earth's magnetic field (production rates increase with both latitude and altitude; Lal 1991, Gosse and Phillips 2001). The production rates of these nuclides in quartz (especially ^{10}Be) are well-constrained (e.g., Nishiizumi et al. 1989, Stroeven et al. 2015). Hence, a measured nuclide concentration indicates the total duration of exposure to cosmic rays.

In formerly glaciated regions, a nuclide concentration in quartz at the Earth's surface may be interpreted as a deglaciation age provided the last ice sheet removed >3 m of rock so that the new surface started with a nuclide concentration near zero. Where apparent exposure ages exceed the local deglaciation age, the incomplete removal of previously accumulated nuclides results in an inheritance signal from one, or more, preceding ice-free exposure periods. While we must always account for geologic-, nuclide production rate-, laboratory-, and measurement uncertainties (Gosse and Phillips 2001, Putkonen and Swanson 2003, Balco 2011, Heyman et al. 2011), the concentration of cosmogenic nuclides in surface rock minerals offers a powerful tool for inferring glacial erosion rates from samples with inheritance. This is because such concentrations are fundamentally the integrated result of depth-dependent production rates and the surface erosion rate (Lal 1991).

Our sampling strategy was designed to evaluate erosion by the Fennoscandian ice sheet over the flattest landscape elements in the investigation area, all of which have traditionally been regarded as examples of intact SCP. In addition, we sampled the summits of two convex surfaces at the southeastern base of Hunneberg at Bragnum, in an area where extensive flat surfaces are non-existent (Figure 3-1). Given the results of sampling two of the flat surfaces in 2000 (Hjortmossen and Sandhem; Stroeven et al. 2016), the expectation was that our new results would yield concentrations higher than those expected for postglacial exposure duration. If so, the presence of inheritance would allow us to calculate glacial erosion depths and rates over recent glaciations, based on reconstructed durations of ice cover. Were the Fennoscandian ice sheet to have removed rock sufficiently thick to essentially reset the surface cosmogenic nuclide inventory, no further insight on glacial erosion rate can be gleaned using this technique.

Thirteen bedrock samples have been measured from four different geographic locations; Nordkroken (n = 3) along the southern shore of Vänern, Hjortmossen (n = 4) and Sandhem (n = 4) in Trollhättan, and Bragnum (n = 2) at the southeastern base of Hunneberg. Two samples at Nordkroken were located on the flat exposed to Lake Vänern and one sample was located south of a string of dunes at the flat that is used as a car park (Figure 3-3). Two samples from Hjortmossen come from its top surface (sampled in 2000, now below a sports arena) and two from its flank. Three samples from Sandhem were taken from within a fenced-in area used as a dump for soil and gravel and one sample was collected from the adjacent Slättbergen in year 2000. The two samples from Bragnum are on bedrock surfaces that protrude through fine-grained sediments that fill the depression aligning the southeastern base of Hunneberg.

Samples were collected during the summers of 2000, 2016 and 2017 with a rock saw, hammer, and chisel. We recorded coordinates using handheld GPS and subsequently determined the sample elevation based on a 2 m resolution LiDAR elevation model (Lantmäteriet). We measured geometric shielding (Dunne et al. 1999) for sample locations where the topographic horizon was more than 10° above a horizontal plane. Measurements of topographic shielding are used to correct local nuclide production rates.

To calculate erosion based on inheritance, it is imperative that we know the duration of exposure following deglaciation. The timing of deglaciation is well-constrained through the Fennoscandian ice sheet retreat reconstruction by Stroeven et al. (2016), with the timing of ice retreat from the Trollhättan moraine around 13.6 cal ka BP. We assign individual deglaciation ages for our sample sites based on the Stroeven et al. (2016) reconstruction, yielding ages of 13.45–13.70 ka before sampling. At the time of deglaciation, the Trollhättan region was covered by water and the sea level was then lowered due to glacial isostatic rebound. To accurately calculate the production of cosmogenic nuclides we therefore need to consider the water depth following the deglaciation and the timing of emergence from the sea. We use a single shoreline displacement curve from Hunneberg for all samples, parameterised by Påsse and Daniels (2015) and constrained by radiocarbon data from a study by Björck and Digerfeldt (1982).

The nuclide ^{10}Be was analyzed because it is the most widely used, and best understood, nuclide in the study of Earth-surface processes (Dunai 2010, p 46). Additionally, ^{26}Al was selected because it has a shorter half-life than ^{10}Be, a known production rate, and can be measured with equal precision. Hence, apart from providing an independent constraint upon erosion rates inferred from ^{10}Be concentrations, the ^{26}Al/^{10}Be ratio may provide additional information on how long rock surfaces may have been buried by glacial ice or sediments after first exposure. In using ^{26}Al we also take advantage of significant recent advances in the accelerator mass spectrometry (AMS) measurement of this nuclide resulting from the use of a gas-filled magnet at PRIME lab (Granger et al. 2014), which allows the efficient separation of ^{26}Al from Mg, resulting in highly accurate ^{26}Al measurements.

Sample preparation and measurement of ^{10}Be and ^{26}Al was completed at PRIME Lab, Purdue University, using standard methods (Kohl and Nishiizumi 1992). This includes separation of quartz, addition of ^{9}Be and ^{27}Al carrier, extraction of ^{10}Be and ^{26}Al, and AMS measurements of ^{10}Be/^{9}Be and ^{26}Al/ ^{27}Al ratios. Total Al concentrations were determined by ICP measurements. Isotope measurements were standardized against the 07KNSTD standard for ^{10}Be (Nishiizumi et al. 2007), and the KNSTD standard for ^{26}Al (Nishiizumi 2004).

4.3 Exposure age calculations

This section is modified from Section 5.2.2 of Hall et al. (2019a) to account for site specifics in this report. We calculate simple apparent exposure ages from the measured ^{10}Be and ^{26}Al concentrations using the expage calculator (http://expage.github.io/calculator v. 201902). This calculator is based on the original CRONUS calculator of Balco et al. (2008) but adopts the nuclide-specific LSD production rate computations (Lifton et al. 2014). Production rate from spallation varies over time and is calibrated against a global set of ^{10}Be and ^{26}Al production rate calibration sites. Production rates of ^{10}Be and ^{26}Al from muons is constant over time (Marrero et al. 2016). In our study, this production rate is adjusted to reduce a potential near-surface artefact (Balco 2017) and is calibrated against the Beacon Heights ^{10}Be and ^{26}Al sandstone bedrock core data (Borchers et al. 2016, Marrero et al. 2016, Phillips et al. 2016, Balco 2017).

We followed the approach of Stroeven et al. (2015) in also accounting for shielding during glacial isostatic uplift through the water column in the expage calculator (expage_sealevel.m). We calculate the mismatch in time (yr) between a simple exposure age and an expected exposure age given a reconstructed deglaciation age and the shoreline displacement curve. The deglaciation age is based on the Stroeven et al. (2016) deglaciation reconstruction. Deglaciation occurs between 13 424 and 13 703 years before our sampling, depending on location.

The attenuation length of spallogenic production of ^{10}Be and ^{26}Al is calculated from atmospheric pressure and a time-dependent geomagnetic rigidity cut-off, similar to the CRONUScalc calculator (Marrero et al. 2016). For the Trollhättan region, this results in an average attenuation length of 152 g cm^{-2}. We use a rock density of 2.65 g cm^{-3} and a water density of 1.0 g cm^{-3} in our calculations. We assume that there has been no post-emergence shielding by vegetation, snow, or sediments. While that assumption appears generally reasonable, samples taken from the car park at Nordkroken and from the dump at Sandhem may have maintained a sediment cover up to tens of centimeters thick up to recent decades.

The code used for cosmogenic nuclide exposure age calculations, erosion simulations, and interquartile range calculations are found in a supplementary file (1900553_supplementary_information_cosmogenic-nuclide-code_tr-19-22.zip[1]).

4.4 Glacial erosion simulations

This section is modified from Section 5.2.3 of Hall et al. (2019a) to also account for site specifics in this report. To simulate site-specific glacial erosion based on ^{10}Be and ^{26}Al concentrations, we use a modified version of the expage glacial erosion calculator by also including shielding by sea water after deglaciation (glacialE_sealevel.m). In this calculator, a glaciation history is defined by a cut-off value for the benthic δ^{18}O record from the LR04 stack of Lisiecki and Raymo (2005). We assume that the growth and decay of the Fennoscandian ice sheet tracks this proxy for global ice volume (cf. Stroeven et al. 2002b). Because the duration of cosmic ray exposure since the last glaciation is of major importance for the erosion rate estimate, local last deglaciation is set independently by the Stroeven et al. (2016) reconstruction. During periods of ice coverage, the ^{10}Be and ^{26}Al production rates are assumed to be zero. During ice-free periods the production rates are computed from a sample shielding depth, which is a function of glacial erosion, non-glacial subaerial erosion, submergence, and the densities of rock and water.

Glacial erosion simulations are run in two modes: (1) constant erosion rate and (2) constant erosion depth. In the first case, the glacial erosion at a constant rate means erosion depth of each ice cover period scales with the duration of ice coverage. In the second case, the glacial erosion depth of each ice cover period is constant, independent of the duration of ice coverage, and the total glacial erosion instead scales with the number of ice coverage periods. Whereas the former may mimic the effect of wet-bed glaciation, the latter may mimic glaciations dominated by dry-bed conditions but experiencing erosion during wet-bed deglaciation (Kleman 1992, Harbor et al. 2006, Cowton et al. 2012, Sugden et al. 2019). We acknowledge that this is a simplification of natural conditions under ice sheets. For

[1] Can be downloaded from www.skb.se/publications. Direct link: http://www.skb.com/publication/2495089/

example, conditions conducive for either mode of operation may have co-occurred or have switched-on or switched-off within any single glaciation. We anticipate that these two situations establish end-member glacial erosion scenarios.

Subaerial erosion is assumed to operate at a constant rate for all ice-free periods. Again, this is a necessary simplification of a complex reality, but one which appears reasonable for an area which has most likely maintained low-relief over the course of Quaternary glaciation. Inundation by sea water occurs following each ice cover period because of glacial isostatic depression. While submerged, the samples undergo neither glacial nor subaerial erosion. To calculate emergence through the water column during isostatic rebound, we use the shoreline displacement curve for the last deglaciation and a filtering approach-derived displacement curve following previous ice cover periods. For the latter, the ice cover history of the preceding 30 ka determines the sea level displacement curve. This filtering approach (subfunction uplift_preLGM) is calibrated against the shoreline displacement curve for Forsmark for the last deglaciation and modelled sea level displacement in Forsmark following the MIS 4 glaciation (SKB 2010).

Erosion rates have been calculated in two ways. First, in a simple calculation for single nuclides (^{10}Be or ^{26}Al), glacial erosion is computed for a specific ice cover (δ^{18}O cut-off value) and subaerial erosion rate couple, based on an interpolation of 50 simulated nuclide concentrations derived from a suite of glacial erosion rates or suite of glacial erosion depths (cf. Fu et al. 2019). We use this method to investigate the sensitivity of glacial erosion to perturbations of specific model parameters. Second, following a more sophisticated approach, predefined minimum and maximum values for glacial erosion, subaerial erosion, and δ^{18}O cut-off values are all imposed to allow for a search of the parameter space yielding the target nuclide concentration within measurement uncertainties plus propagated production rate uncertainties. This is done iteratively to approach the minimum and maximum parameter values that yield the target nuclide concentrations. The iterative search for the parameter space yielding the measured cosmogenic nuclide concentrations is done with repeat computations of cosmogenic nuclide production for a range of scenarios, with the minimum and maximum values for each of the three parameters searched with decreasing step size down to a maximum of 0.01 mm/ka or 0.01 cm/ice cover period for glacial erosion, 0.01 mm/ka for subaerial erosion, and 0.01 ‰ for the δ^{18}O cut-off value. Because the relation between the input parameters values and the resulting cosmogenic nuclide concentration is potentially non-linear and discontinuous, we use a guided Monte Carlo approach to search for the full range of parameter limits and potential erosion depths over time. This is done first focused around the interatively determined minimum and maximum parameter values searching actively for lower minimum values and higher maximum values for each of the three parameters using five Monte Carlo runs with 150 scenarios each for each of the six parameter limits. Finally, Monte Carlo runs with 150 random scenarios using parameters drawn from ranges defined by the determined minimum and maximum parameter limits each decreased and increased, respectively, by 10 %, are run iteratively to generate at least 1 000 cosmogenic nuclide concentration solutions or for a maximum of 100 runs. For full details of the erosion simulations, we refer to the function glacialE_sealevel.m in a supplementary file (1900553_supplementary_information_cosmogenic-nuclide-code_tr-19-22.zip[2]). With this method, we can find the range of glacial erosion rates that satisfies the measurements for assumed subaerial erosion rates and reasonable ice cover histories (see below). This method also enables the calculation of erosion histories for ^{26}Al/^{10}Be pairs. Specifically, only certain scenarios will yield a match with both measured nuclide concentrations, and we use this method to simulate the erosion history of the Trollhättan surfaces.

4.5 Input parameter constraints

This section is modified from Section 5.2.4 of Hall et al. (2019a) to also account for site specifics in this report. To constrain the potential ice cover history of the Trollhättan region, we use a minimum δ^{18}O cut-off value of 4.4 ‰ and a maximum value of 4.7 ‰. For the last glacial cycle, this yields glaciation during MIS 2 and potentially most but not all of the period from MIS 4 to MIS 2. These two cut-off values allow for a range of possible glaciation histories. Through the last glacial cycle (from ~115 ka) and the Quaternary (from 2.588 Ma) the total duration of ice cover becomes 18–49 ka and

[2] Can be downloaded from www.skb.se/publications. Direct link: http://www.skb.com/publication/2495089/

104–340 ka, respectively. This corresponds well with previous interpretations of average Quaternary ice sheet extent and indicates that the Trollhättan region has remained ice free for most of Quaternary time (Porter 1989, Kleman et al. 1997, 2008).

Subaerial erosion is assumed to operate at a constant rate for all ice-free periods. For the subaerial erosion rate, we set the minimum and maximum values to 0 and 5 mm/ka, respectively. The upper limit of 5 mm/ka is somewhat higher than estimated Holocene erosion rates (André 1996, 2002) to account for higher average subaerial erosion rates if weathering accelerates under longer ice-free periods.

We run the simulations starting from various points back in time with the cosmogenic nuclide samples starting at zero nuclide concentration. For a case where the sample starts at great depth with a minimal cosmogenic nuclide production rate, this zero-nuclide assumption is appropriate. For a case where the sample starts a shallow depth with a notable cosmogenic nuclide production rate, the zero-nuclide assumption implies that the bedrock must have been shielded from cosmic rays prior to the point in time when the simulation starts. In such a situation, we can mentally equate the start of our simulation to follow a sudden and instantaneous erosion of the sedimentary cover rocks that completely shielded the underlying basement rock surface from cosmic rays. Because it is difficult to determine the timing of cover rock removal with certainty, we ran the simulations starting from 130 ka, 0.5 Ma, 1.0 Ma, 2.588 Ma, and 10 Ma. These starting points cover a wide range of scenarios, including likely end-members where cover rock removal occurred as recently as the penultimate glaciation (130 ka) or as long as 10 Ma ago, through non-glacial processes.

Because the constant glacial erosion scenarios are crude simplifications of a much more complex reality, we considered two end-member scenarios starting at 10 Ma which assume no glacial erosion (1) between 10 Ma and 130 ka and (2) after 55 ka. We do not consider these end-members to be particularly likely, but they are chosen simply to explore the boundaries of our model space. In the first scenario, all glaciations prior to the last glacial cycle are non-erosive and the only glacial erosion is that which occurs in the last glacial cycle. This scenario requires intense glacial erosion during the last glacial cycle up to the late Weichselian to account for measured concentrations. In the second scenario there is no glacial erosion in the ice cover period(s) after MIS 4. Because the samples will be exposed at or close to the surface for the full subaerial period after MIS 4, glacial erosion in MIS 4 and earlier ice cover periods will be higher than in the constant glacial erosion scenarios. Similar to the other simulations, we ran these extreme scenarios with both constant glacial erosion rate and constant glacial erosion depth. Table 4-1 specifies simulation specific parameters for all 14 simulation scenarios.

Table 4-1. Glacial erosion simulations. All simulations have the same predetermined parameter boundaries for the $\delta^{18}O$ cut-off value (4.4–4.7 ‰) and the subaerial erosion rate (0–5 mm/ka).

Simulation	Starting point	Glacial erosion
1	130 ka	Constant glacial erosion rate
2	130 ka	Constant glacial erosion depth
3	0.5 Ma	Constant glacial erosion rate
4	0.5 Ma	Constant glacial erosion depth
5	1.0 Ma	Constant glacial erosion rate
6	1.0 Ma	Constant glacial erosion depth
7	2.588 Ma	Constant glacial erosion rate
8	2.588 Ma	Constant glacial erosion depth
9	10 Ma	Constant glacial erosion rate
10	10 Ma	Constant glacial erosion depth
11	10 Ma	10 Ma–130 ka: no glacial erosion; 130–0 ka: constant glacial erosion rate
12	10 Ma	10 Ma–130 ka: no glacial erosion; 130–0 ka: constant glacial erosion depth
13	10 Ma	10 Ma–55 ka: constant glacial erosion rate; 55–0 ka: no glacial erosion
14	10 Ma	10 Ma–55 ka: constant glacial erosion depth; 55–0 ka: no glacial erosion

4.6 Sensitivity tests of the glacial erosion simulations

This section is modified from Section 5.2.5 of Hall et al. (2019a) to also account for site specifics in this report. To test the sensitivity of the glacial erosion simulations to specific scenario parameters, we ran a set of ^{10}Be simulations for four particular samples (TROLL-16-07, 16-09, 17-01, and 17-03) in which we varied one parameter at a time. The four samples were chosen to cover a range of cosmogenic nuclide inheritance and to include the samples that have potentially been covered by sediments. For a reference scenario, we use a δ^{18}O cut-off value of 4.55 ‰, a subaerial erosion rate of 2.5 mm/ka, and we start the simulation from 1 Ma. We varied the δ^{18}O cut-off value, the subaerial erosion rate, the simulation starting point, and also the sediment cover, and we ran simulations in the constant erosion rate and the constant erosion depth modes. These tests help us to evaluate the reliability of derived glacial erosion rates.

5 Results

5.1 Subsurface fracture imaging using GPR

5.1.1 Vånga quarry

Profile 1 (Figure 5-1) reveals a series of reflectors that correspond to fractures visible in the quarry wall (for example, those marked ‘c’, ‘d’, ‘e’, ‘f’, ‘g’, and ‘j’ in Figure 5-1) that are subparallel to the native topographic surface. The subhorizontal fractures visible in the GPR images (Figure 5-1c, d) are either open (e.g. fractures ‘c’ and ‘e’), and/or represent fracture zones formed by two subhorizontal fractures that display overlapping sinusoidal traces with wavelength of tens of centimeters (Figure 5-2), e.g., fractures ‘f’, ‘e’, ‘g’ and ‘j’ (Figure 5-1). Strong reflections, in purple, correspond to relatively wide joint apertures, whereas weaker reflections, in yellow, correspond to relatively narrow joint apertures. A surface step and a fracture-bound cavity (marked ‘a’ and ‘b’, respectively, in Figure 5-1) assist with matching the subsurface fractures in the GPR images to the photographs. The qualitative match of the major fractures in the photograph and GPR images is striking. Some smaller fractures also appear in both the photograph and GPR images. For example, two obliquely dipping fractures (marked ‘h’ and ‘i’) and two subvertical fractures (marked ‘l’ and ‘m’) are visible in the photographs and GPR images.

In contrast to the abundant subhorizontal fractures, obliquely-dipping and subvertical fractures are rare. Some do occur (e.g., fracture ‘i’ in Figure 5-1b), but they are barely discernible in the GPR images (Figure 5-1c, d). The GPR image shows a few inclined reflectors that have no apparent counterparts in the photographs, such as weak reflector that extends from the terminus of fracture ‘h’ and dips to the right (west) to a depth of 7 m (Figure 5-1c, d). Notably, none of the obliquely-dipping and subvertical fractures are strong reflectors.

Some other fracture details also differ between the photographs and the GPR images. For example, the photograph of Figure 5-1b clearly shows that fractures ‘g’ and ‘h’ project up dip to coincide with the bedrock surface. This relationship, however, is not readily apparent on the GPR images (Figure 5-1c, d). Also, as seen in the photograph of Figure 5-1b, fractures ‘e’, ‘j’, and ‘k’ are intersected by the inclined fracture ‘i’, but this relationship is not apparent in the GPR images (Figure 5-1c, d). Similarly, as seen in the photograph of Figure 5-1a, some subhorizontal fractures (e.g., ‘f’) are intersected by subvertical fracture ‘m’. Despite these differences in details, the GPR images for profile 1 reproduce the major fractures subparallel to the surface quite well. Near parallelism of the convex topography and the subhorizontal fractures is also apparent.

The Vånga GPR profile 2 (Figure 5-3) has an excavated bench as a top surface and is located about 6 m below the native ground surface. Again, fractures subparallel to the ground surface are visible on the GPR image and can be identified on the photograph of Figure 5-3a (e.g., fractures a–f). Fracture ‘a’ displays a strong reflection and has a wide aperture (>10 cm) filled with saprolite. Fractures ‘b’ and ‘e’ display mineral staining, indicative of water flow. Three obliquely dipping fractures are visible in the photograph (fractures g–i) but are invisible on the GPR image. Fracture ‘e’ is invisible in the GPR images where it is located below the strongly-reflecting fracture ‘b’. Neither subvertical fractures nor hairline fractures are visible in the GPR images, although fractures with hairline apertures were visible in the field below fracture ‘b’ and in the vicinity of ‘f’.

a GPR profile 1 at Vånga quarry, West-facing wall

b GPR profile 1 at Vånga quarry, South-facing wall

c GPR profile 1 at Vånga quarry

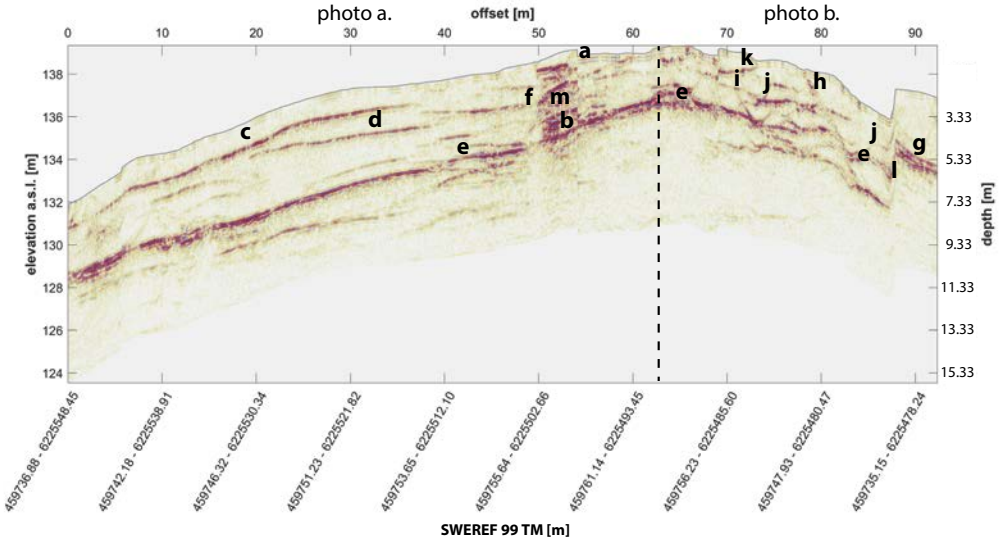

d GPR profile 1 at Vånga quarry; equal horizontal and vertical scales

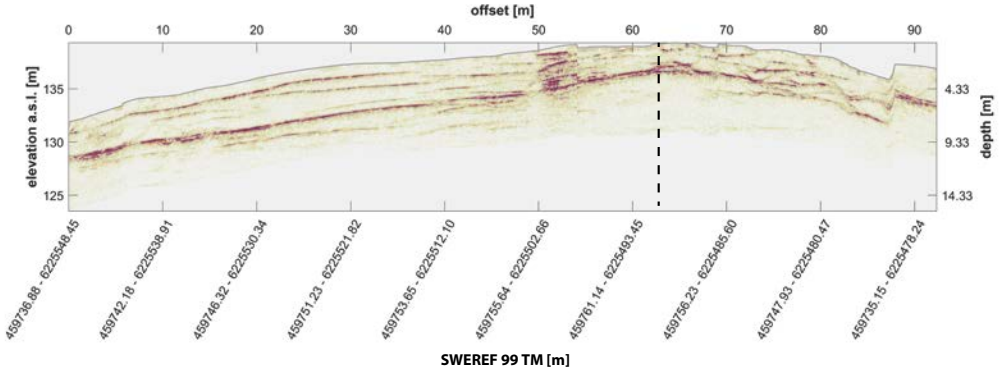

Figure 5-1. *GPR profile 1 at Vånga quarry. (a) The fractured west-facing quarry wall imaged on GPR Profile 1. The letters mark individual fractures shown in the ensuing panels. (b) The fractured north-facing quarry wall imaged as a continuation of GPR profile 1. The white box shows the location of Figure 5-1. The horizontal scales of panels a and b differ. (c) 600 MHz GPR image showing strong reflections in purple and weak reflections in yellow. The black dashed line indicates where the profile makes a right angle turn and the letters indicate features discussed in the text. (d) 600 MHz GPR image shown with equal vertical and horizontal scales.*

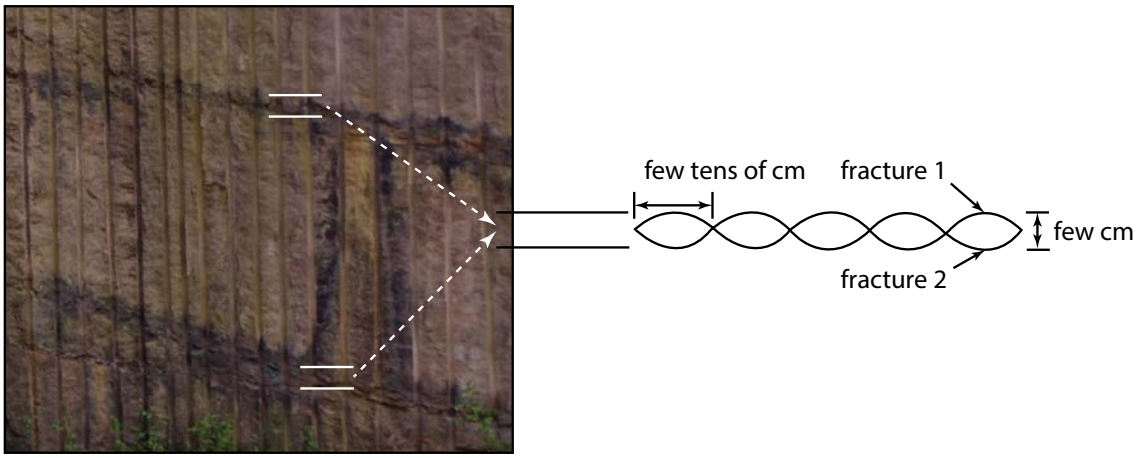

Figure 5-2. *Sheeting joints subparallel to the ground surface with superimposed sinusoidal traces at Vånga quarry. The photograph location is shown in Figure 5-1b. The line drawing represents a segment of the sinusoidal fracture traces shown in the photograph.*

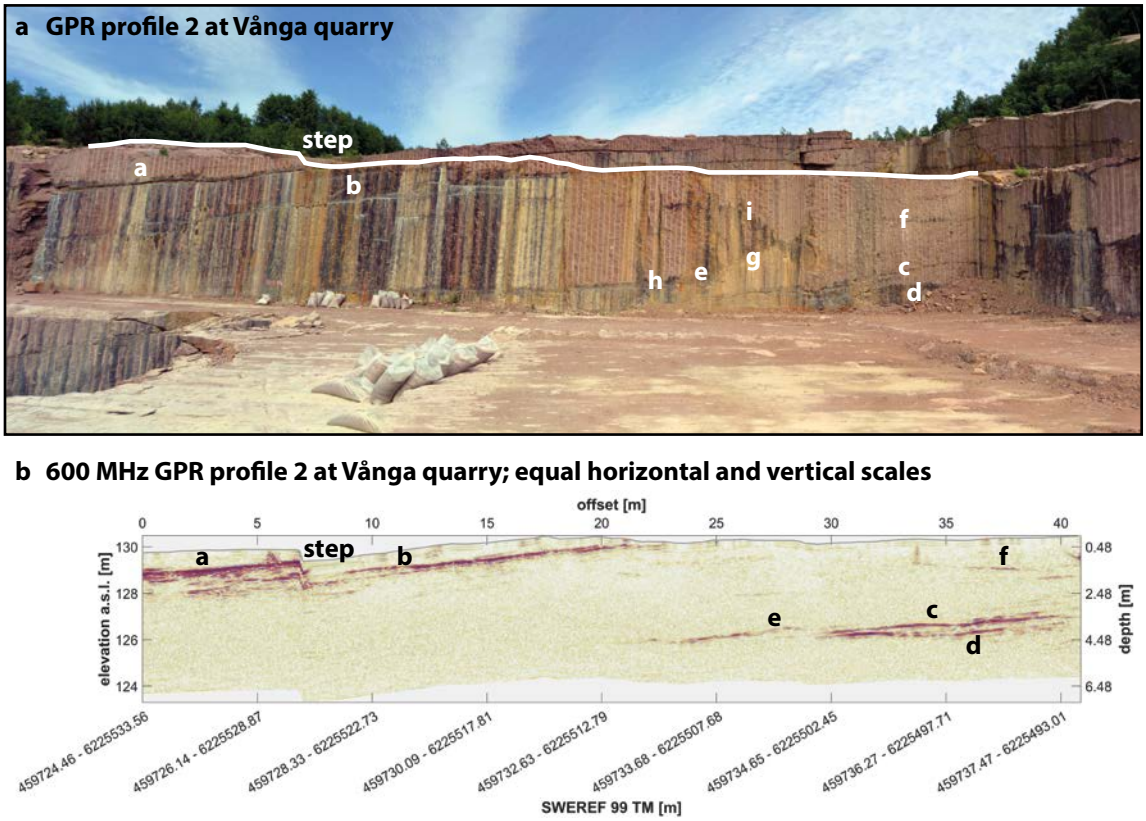

Figure 5-3. *GPR profile 2 at Vånga quarry. (a) The fractured west-facing quarry wall imaged on GPR Profile 2. The white line indicates the quarried bench that forms the ground surface of this profile. (b) 600 MHz GPR image showing strong reflections in purple and weak reflections in yellow. The letters indicate features discussed in the text. (c) 600 MHz GPR image shown with equal vertical and horizontal scales.*

5.1.2 Nordkroken 1

At Nordkroken, profile 1 (Figure 5-4a) trends northwest, approximately normal to the southern shoreline of Lake Vänern. The bedrock surface there dips towards the shoreline by about 40 cm over a horizontal distance of 20 m, and then forms a 50 cm deep concavity in the 1.5 m span adjacent to the shoreline, giving a total relief of 90 cm along the transect (Figure 5-4b). The GPR image indicates a prominent reflector (labelled 'a') parallel to the bedrock surface at a depth of 2.69–2.74 m. This reflector extends ~20 m from the left edge of Figure 5-4b and appears partly underlain by another reflector (labelled 'b') that extends about 5.5 m horizontally from ~17.5 m to the right edge of the transect. The vertical spacing between these two reflectors is only a few centimeters. We interpret these two reflectors as marking overlapped sheeting joints that might merge out of the plane of the profile. The lower two reflections (labelled 'c' and 'd' in Figure 5-4b) are multiples ('echoes') of the uppermost reflection and do not represent additional fractures. The vertical spacing between the surface and the uppermost (real) reflector equals the spacing between successively lower reflectors along the transect, demonstrating that features 'c' and 'd' are artifacts. Their presence may indicate that reflector 'a' represents an open subhorizontal fracture with an aperture of at least centimeters.

a Aerial photograph showing the locations of the four GPR transects at Nordkroken

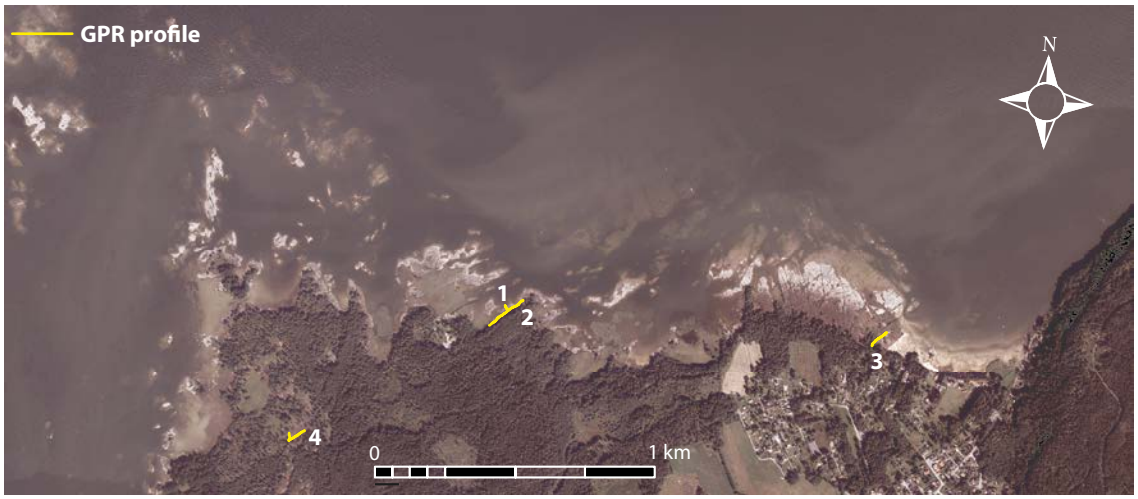

b 600 MHz GPR profile 1: Shore-normal at Nordkroken

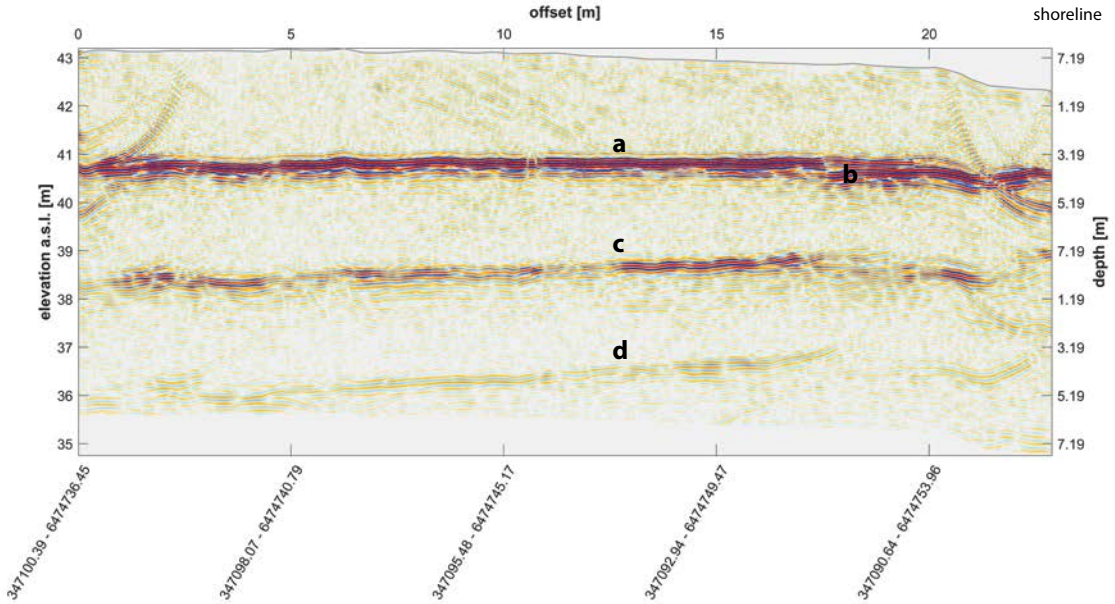

Figure 5-4. *(a) Orthorectified aerial photograph showing the locations of GPR profiles 1–4 at Nordkroken. (b) 600 MHz GPR image of Nordkroken profile 1, which is oriented normal to the southern shoreline of Lake Vänern. Strong reflections are shown in purple and weak reflections are shown in yellow. The letters indicate features discussed in the text.*

5.1.3 Nordkroken 2

Profile 2 at Nordkroken (Figure 5-5) sub-parallels the shoreline (Figure 5-4a). The total relief along the bedrock surface is 50 cm over the 151 m length of this GPR transect. Most of that relief develops along the segment from 75 m to 86 m along the transect, marked by the grey horizontal line labelled 'a' in Figure 5-5a. A long subhorizontal reflector 'b' extends about 115 m horizontally and descends to maximum depth of about 5 m below the ground surface near the left (SW) end of the profile. The reflector bends upwards by about 1.5 m from its lowest point to terminate against an overlying subhorizontal reflector (labelled 'c' in Figure 5-5a). This latter reflector somewhat mirrors another subhorizontal reflector located 1 m above it (labelled 'd' in Figure 5-5a). Another subhorizontal reflector (labelled 'e' in Figure 5-5a) curves towards, and terminates on, the long subhorizontal reflector labelled 'g'. The traces of the three reflectors labeled 'd', 'e', and 'f' end where they terminate against another reflector or because the apertures of the causative fractures presumably narrow such that the fractures become undetectable on GPR. The GPR reflectors marked 'f', 'g', and 'h' in Figure 5-5a are multiples of the long subhorizontal reflector ('b'), based on their spacing and the argument in the previous paragraph. The lowest part of the bedrock surface is at a vertical fracture, which is indicated by a vertical band (labelled 'i' in Figure 5-5a) that disrupts the subhorizontal reflector labelled 'b'. Another vertical fracture indicated by a white streak (labelled 'j' in Figure 5-5a) marks the location where the saucer-shaped subsurface reflector 'b' terminates. The equal vertical and horizontal scales of Figure 5-5b emphasize that the subhorizontal reflectors are subparallel to the ground surface.

a 600 MHz GPR profile 2: Parallel to the shore (SW to NE) at Nordkroken

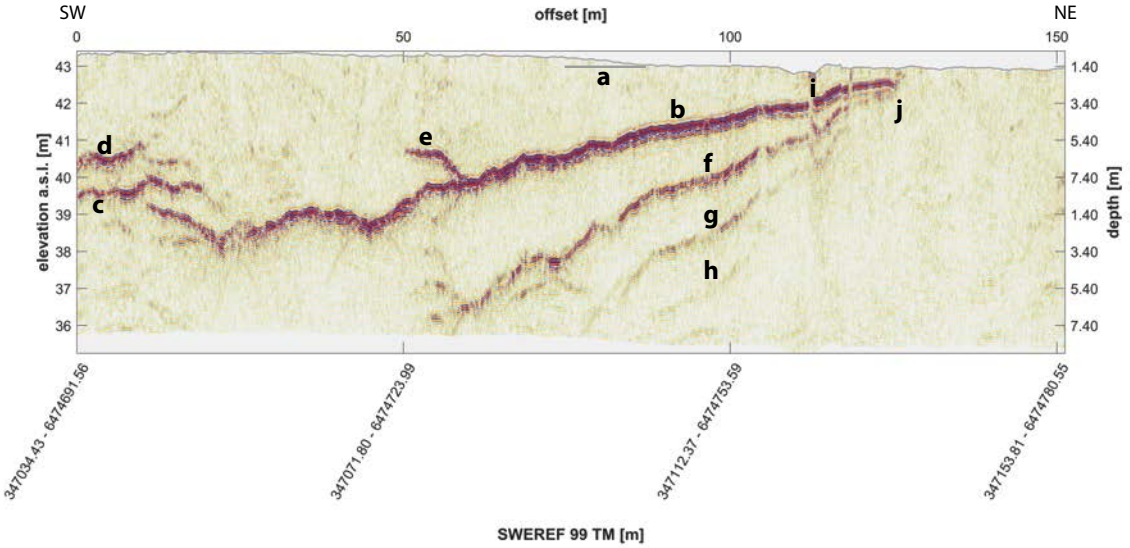

b 600 MHz GPR profile 2: Parallel to the shore (SW to NE) at Nordkroken, equal horizontal and vertical scales

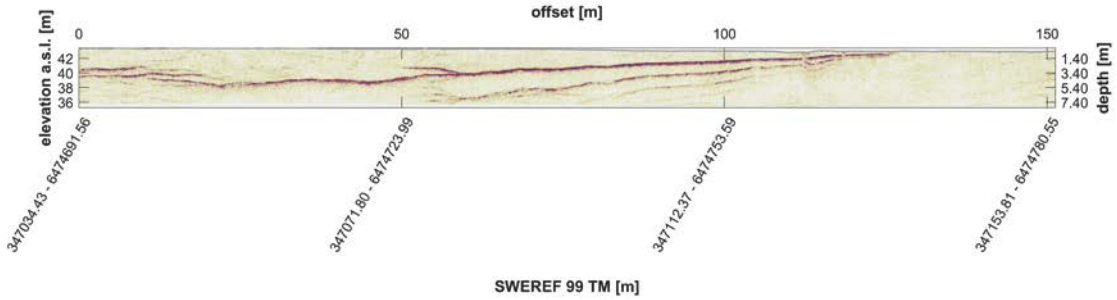

Figure 5-5. *(a) 600 MHz GPR image of Nordkroken profile 2. Strong reflections are shown in purple and weak reflections are shown in yellow. The letters indicate features discussed in the text. (b) 600 MHz GPR image of Nordkroken profile 2 shown with equal vertical and horizontal scales. Profile location is shown in Figure 5-4a.*

5.1.4 Nordkroken 3

Profile 3 at Nordkroken (Figure 5-6) trends northeast, approximately perpendicular to the coast (Figure 5-4a), and is 72.5 meters long. The bedrock surface is subhorizontal over a distance of 45 m from the left (SW) end of the profile. From 47 to 54 meters from its left end, the topography shows a 40 cm deep concavity. Over the 17 m stretch at the right (NE) part of the transect, the ground surface is convex and descends 60 cm. Five gently-dipping reflectors (labelled 'a', 'b', 'c', 'd', and 'e' in Figure 5-6a) occur, with trace lengths in the transect between 2 m and 26 m. Their depths below the surface range between 2.2 m and 6.2 m. Reflectors 'a', 'd', and part of 'b' nearly parallel the bedrock surface. Reflector 'a' additionally appears to be slightly convex. Fracture 'b' also curves towards fracture 'e', where it terminates. The hyperbolic reflectors (such as those labelled 'f') may not indicate the traces of real fractures. Visible traces of gently-dipping fractures underlie 50 m of the 72.5 m-long bedrock surface profile. The surface concavity at 50 m is bordered by two subvertical fractures (labelled 'g', and 'h' in Figure 5-6a). A further two subvertical fractures intersect the bedrock surface (labelled 'i' and 'j' in Figure 5-6a). The equal vertical and horizontal scales of Figure 5-6b again emphasize that the subhorizontal reflectors are subparallel to the ground surface.

a 600 MHz GPR profile 3: SW-NE oriented at Nordkroken

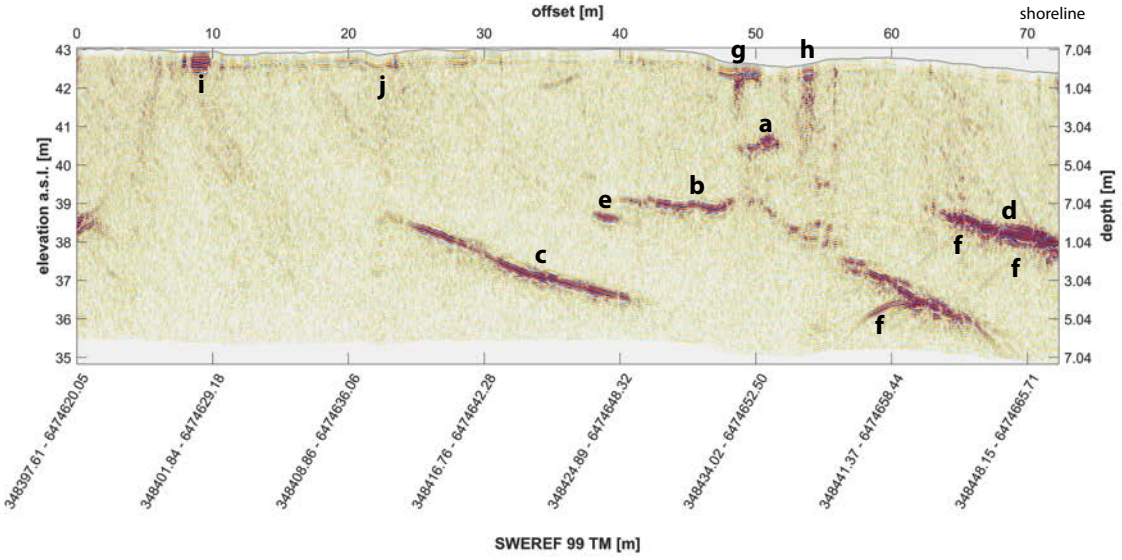

b 600 MHz GPR profile 3: SW-NE oriented at Nordkroken, equal horizontal and vertical scales

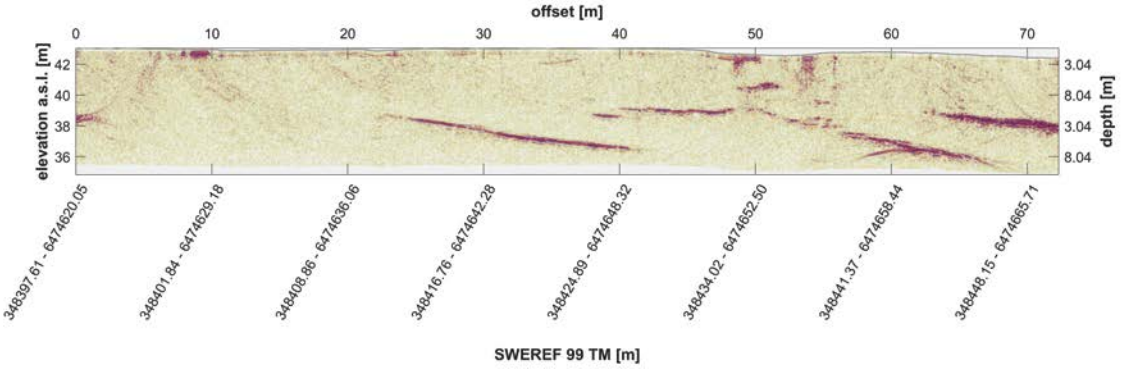

Figure 5-6. *(a) 600 MHz GPR image of Nordkroken profile 3. Strong reflections are shown in purple and weak reflections are shown in yellow. The letters indicate features discussed in the text. (b) 600 MHz GPR image of Nordkroken profile 3 shown with equal vertical and horizontal scales. Profile location is shown in Figure 5-4a.*

5.1.5 Nordkroken 4

Profile 4 at Nordkroken (Figure 5-7) is located about 800 m southwest of Nordkroken profile 2 (Figure 5-4a). The transect has the shape of a check mark and in contrast to the previous images (Figures 5-1 and 5-3 to 5-6), 170 MHz data is shown. The 27 m stretch of the transect at the right side of Figure 5-7 is where the transect trends south, and the remainder trends northeast; the vertical dashed black line marks the bend in the transect. The topographic surface along the transect is convex, with a ridgeline that trends northwest. At least 11 subhorizontal reflectors, labeled 'a' to 'k', are visible in the subsurface. These reflectors occur at depths up to ~16 m below the outcrop surface and their combined lengths underlie almost the entire horizontal transect. The longest subhorizontal reflector, 'd', extends for about 30 m and is located at ~15 m depth. Profile 4 indicates that subhorizontal reflectors can be imaged at 170 MHz to depths up to at least 16 m.

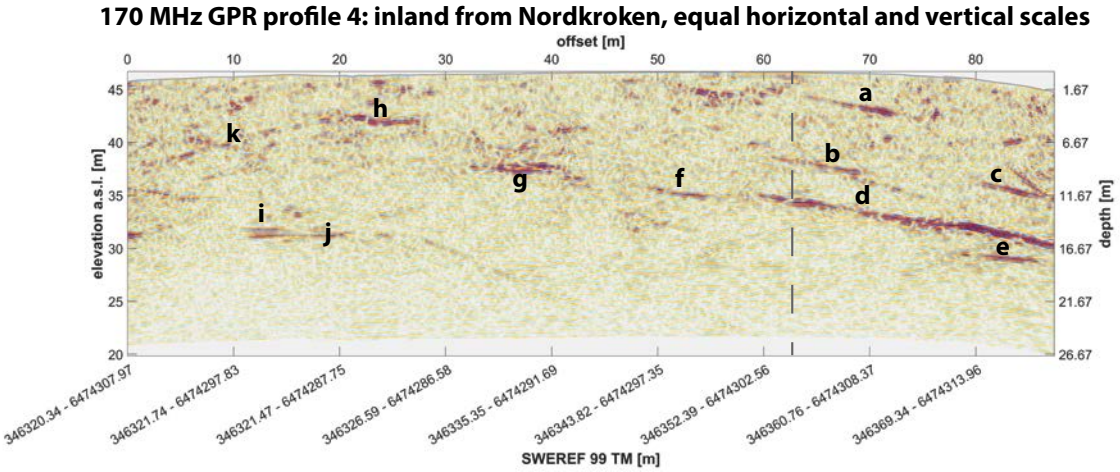

Figure 5-7. *170 MHz GPR image of Nordkroken profile 4, shown with equal vertical and horizontal scales. Strong reflections are shown in purple and weak reflections are shown in yellow. The letters indicate features discussed in the text. Profile location is shown in Figure 5-4a. The vertical dashed black line indicates the bend in the transect.*

5.1.6 Hjortmossen 1

The transect of GPR profile 1 at Hjortmossen (Figure 5-8) extends 75 m to the northeast down a gently convex surface and decreases in elevation by 75 cm over this distance. Horizontal and vertical positioning data were missing from the last 27 m of this transect, although the northeastern end of transect was correctly recorded, and so the surface topography and gradient are interpolated over this segment. The transect makes a dog-leg (marked 'b' in Figure 5-8a, b) across a 10s-of-centimeter wide, sediment- and vegetation-filled, subvertical fracture that strikes NNE–SSW. A series of subhorizontal reflectors (marked 'a' in Figure 5-8b) appear to nucleate at (or terminate against) the subvertical fracture marked 'b'. Other subhorizontal reflectors (including those marked 'c' to 'g') appear northeast of fracture 'b'. The depths of the subhorizontal reflectors range from ~1 m to ~13 m, with the dominant reflector located at about 5 m depth (seen extending to the left – southwest – of 'a'). We infer that the subhorizontal reflectors are subhorizontal fractures.

a Aerial photograph of Hjortmossen, Trollhättan, showing GPR transects

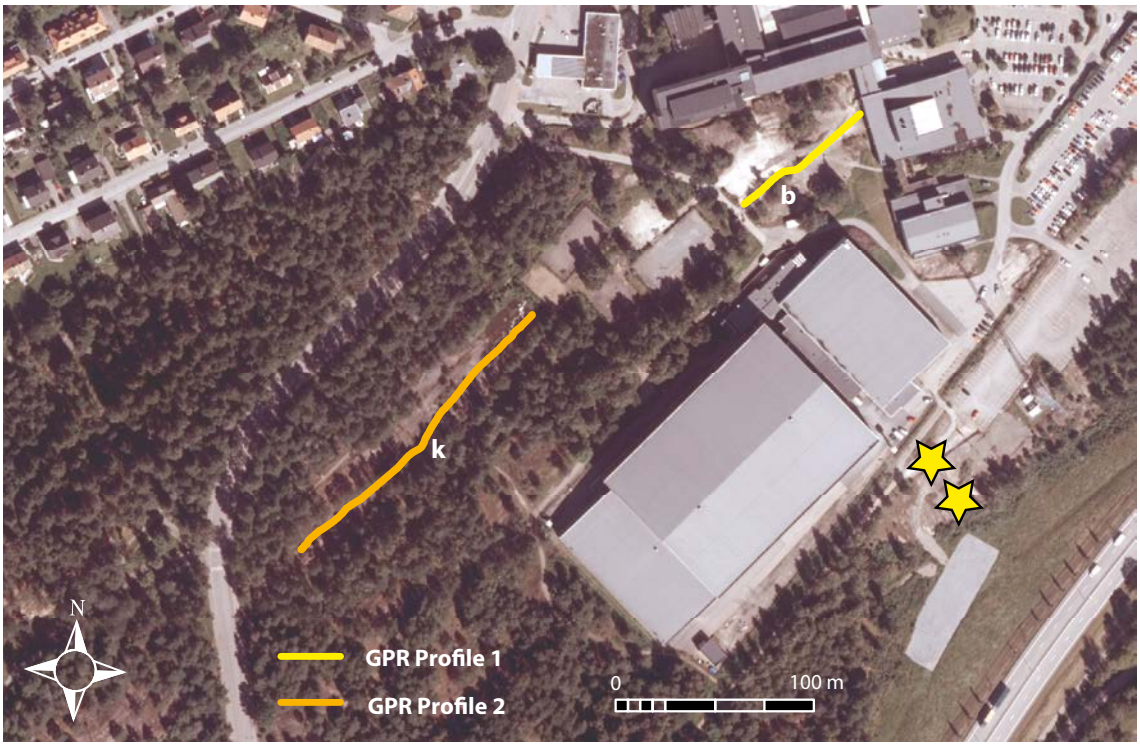

b 170 MHz GPR profile 1 at Hjortmossen, Trollhättan

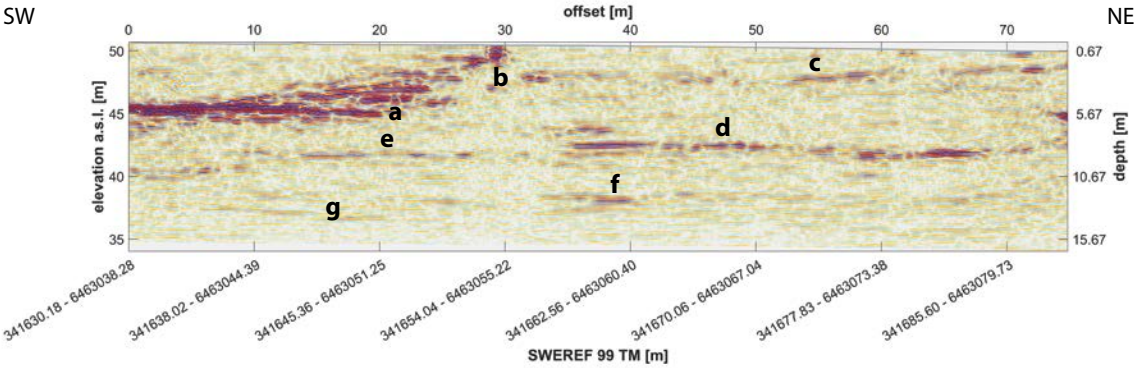

Figure 5-8. *(a) Orthorectified aerial photograph showing the locations of two GPR transects at Hjortmossen, Trollhättan. Yellow stars, southeast of the ice hockey hall, show cosmogenic nuclide sample locations. (b) 170 MHz GPR image of Hjortmossen profile 1 shown with equal vertical and horizontal scales. Strong reflections are shown in purple and weak reflections are shown in yellow. The location of fracture 'b' in plan view is shown in panel a.*

5.1.7 Hjortmossen 2

The transect of GPR profile 2 at Hjortmossen (Figures 5-8a and 5-9) extends 170 m from southwest to northeast. The bedrock surface declines about 50 cm over the length of the profile and displays a low amplitude (tens-of-cm scale) convexity over its southwestern half. The segment between 40 and 80 m had poor horizontal spatial resolution, and the topography there is interpolated from adjoining segments. The profile makes a small dogleg at location 'k' in Figure 5-9a across a wide (tens of cm), vegetated, subvertical fracture. Another subvertical fracture intersects the outcrop surface at 'l'. Subhorizontal reflectors located at 'a' to 'j' occur at depths between ~2.5 m and ~17 m. Additional short subhorizontal reflectors occur in the vicinity of 'j'. Reflector 'b' appears to terminate against (or nucleate at) the subvertical fracture marked 'l'. The strongest reflectors are located southwest of subvertical fracture 'l'. The 600 MHz profile shown in Figure 5-9b shows the strongest subhorizontal reflectors in the uppermost 6 m in higher resolution and further emphasizes the parallelism of the reflectors with the outcrop surface. We interpret al. the prominent subhorizontal reflectors as being subhorizontal fractures.

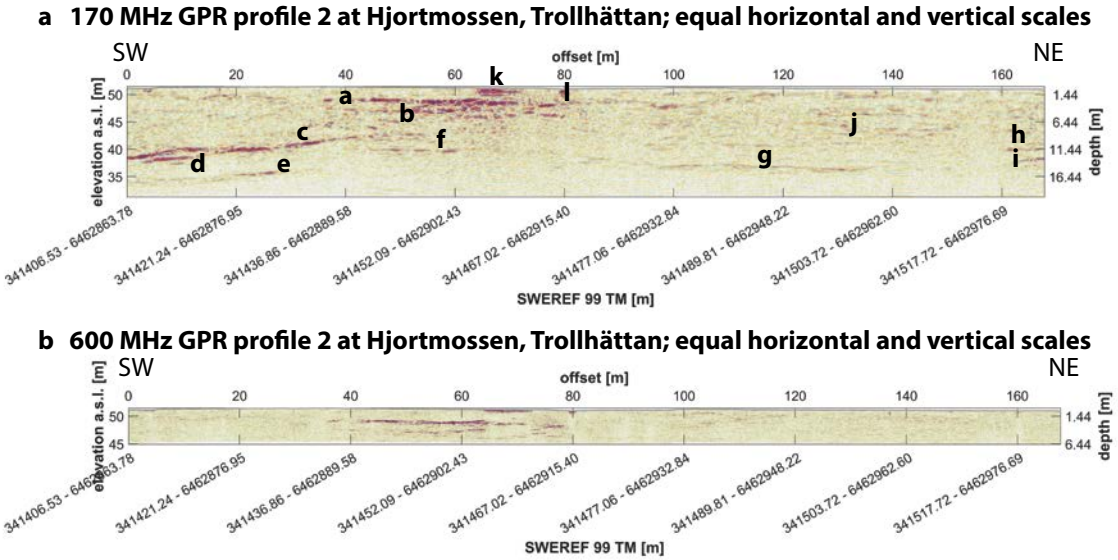

Figure 5-9. *(a) 170 MHz GPR image of Hjortmossen profile 2, shown with equal vertical and horizontal scales. Strong reflections are shown in purple and weak reflections are shown in yellow. The letters indicate features discussed in the text. (b) 600 MHz GPR image of Hjortmossen profile 2 shown with equal vertical and horizontal scales. Profile location and the plan view location of fracture k are shown in Figure 5-8a.*

5.1.8 Sandhem 1

The transect of GPR profile 1 at Sandhem (Figures 5-10 and 5-11) extends about 260 m from south-west to northeast. The topographic surface declines by about 80 cm over this distance and a road is located about half-way along the transect (Figure 5-11a). Numerous gently-dipping to subhorizontal reflectors occur (including those labelled 'a' to 'j'in Figure 5-11a), at a depth up to ~18 m and with lengths up to ~25 m. The subtle surface topography lies between the straight line (bottom) and curved line (top) in Figure 5-11b. This illustrates that the outcrop surface is gently convex along the transect.

Aerial photo of Sandhem, Trollhättan, showing GPR profiles

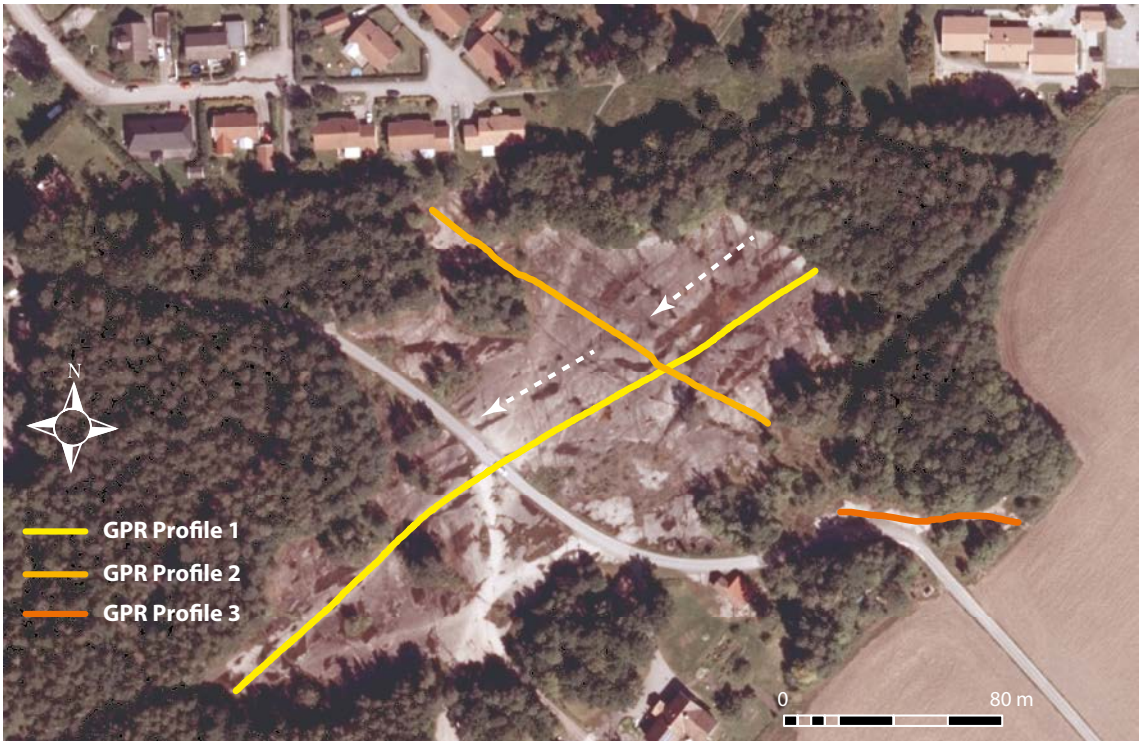

Figure 5-10. *Orthorectified aerial photograph showing the locations of three GPR profiles at Sandhem, Trollhättan. Former ice flow direction, inferred from water-filled linear depressions on the outcrop surface, is shown by the white dotted arrows.*

a 170 MHz GPR profile 1 at Sandhem, Trollhättan; equal horizontal and vertical scales

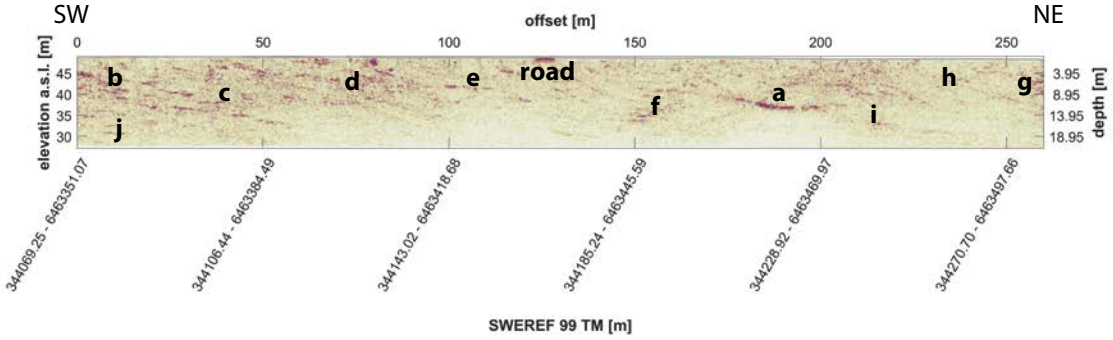

b 600 MHz GPR profile 1 at Sandhem, Trollhättan

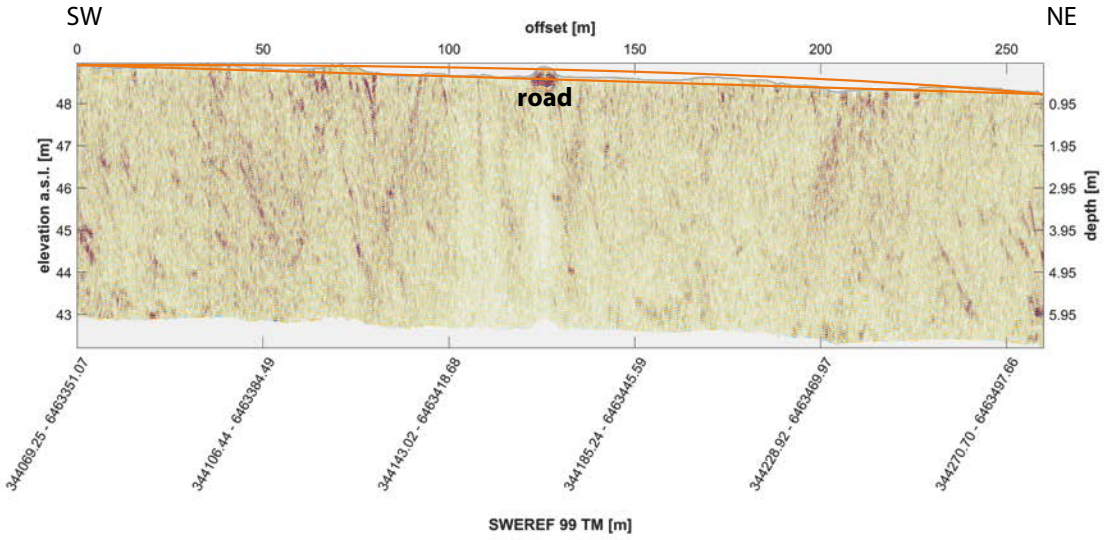

Figure 5-11. *(a) 170 MHz GPR image of Sandhem profile 1 shown with equal vertical and horizontal scales. Strong reflections are shown in purple and weak reflections are shown in yellow. The letters indicate features discussed in the text. (b) 600 MHz GPR image shown with unequal vertical and horizontal scales. The ends of the surface transect are shown connected by a straight line (bottom) and a curved line (top). Profile location is shown in Figure 5-10.*

5.1.9 Sandhem 2

The transect of GPR profile 2 at Sandhem extends approximately northwest to southeast and increases in elevation by about 30 cm over its 145 m length (Figures 5-10 and 5-12). Vertical positioning data are missing from the first 18 m from the NW end, so the vertical positioning of the profile was interpreted from a LiDAR DEM with a 2 m pixel size over this segment up to location 'a' in Figure 5-12. The dominant reflector, labelled 'b', extends ~40 m from the NW end of the transect and dips to the NW subparallel to the outcrop surface. It appears to bifurcate into two reflectors in the vicinity of label 'c'. Another reflector labelled 'd' lies parallel to reflector 'b' but is located 5 m higher and extends only ~4 m from the NW end of the transect. Numerous gently dipping to subhorizontal reflectors up to a few meters in length are also visible, such as those in the vicinity of labels 'e', 'f', and 'g'. Reflectors indicating subvertical fractures intersecting the surface occur at 'h' and 'i' and it appears that gently dipping reflector 'b' intersects with reflector 'h' at the outcrop surface.

5.1.10 Sandhem 3

The transect of GRP profile 3 at Sandhem runs approximately W to E down a convex slope (Figure 5-10 and 5-13). It decreases in elevation by ~1 m over its 65 m length. A series of reflectors are located subparallel to the ground surface to a depth up to 10 m over the last 25 m of the transect (labelled 'a' to 'e' in Figure 5-13a). The reflectors labelled 'a' and 'c' are either separate, closely spaced fractures, or perhaps represent opposing walls of an open fracture. Reflector 'f' appears to terminate on reflector 'a'. Fractures were observed in the field to intersect the ground surface at 'g', where they coincide with a relatively rough surface topography. The higher resolution 600 MHz data (Figure 5-13b) more clearly show the reflectors in the uppermost meters.

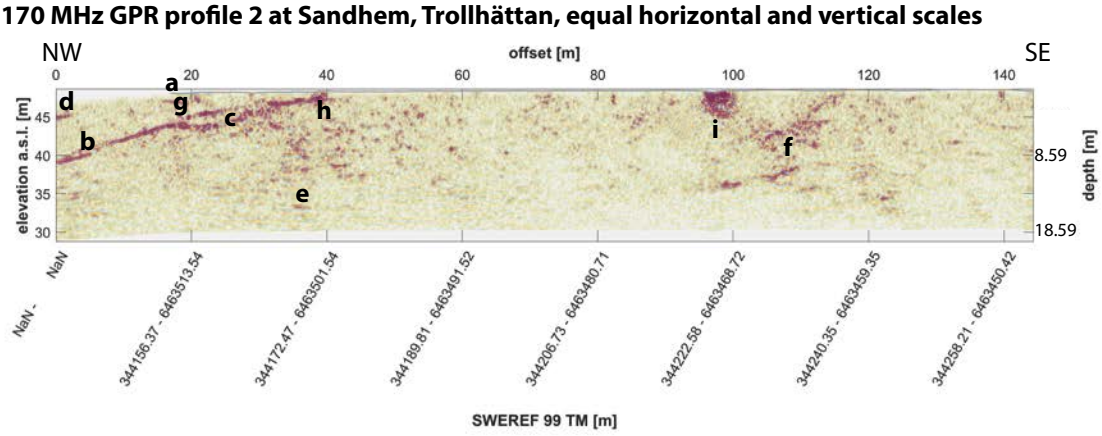

Figure 5-12. *170 MHz GPR image of Sandhem profile 2 shown with equal vertical and horizontal scales. Strong reflections are shown in purple and weak reflections are shown in yellow. The letters indicate features discussed in the text. Profile location is shown in Figure 5-10.*

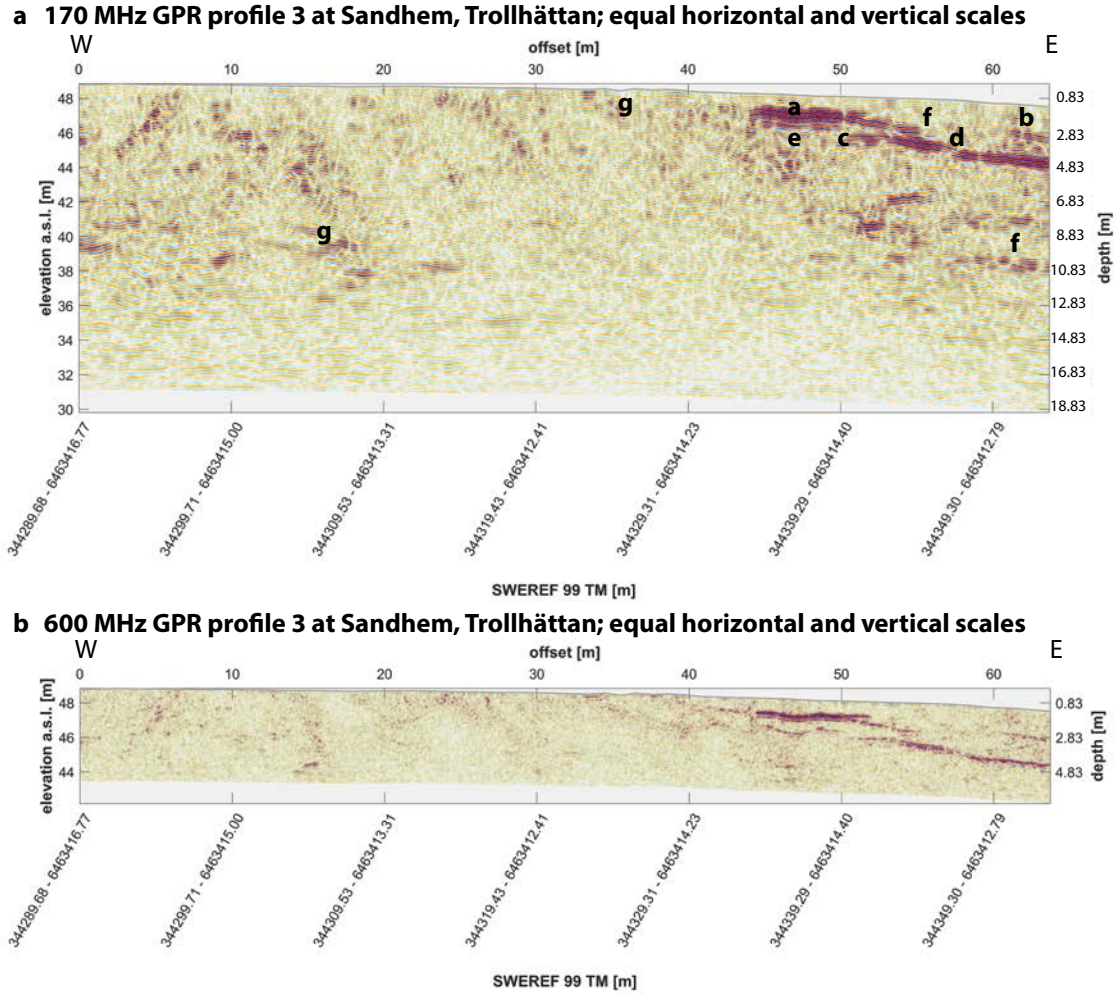

Figure 5-13. *(a) 170 MHz GPR image of Sandhem profile 3 shown with equal vertical and horizontal scales. Strong reflections are shown in purple and weak reflections are shown in yellow. The letters indicate features discussed in the text. (b) 600 MHz GPR image shown with equal vertical and horizontal scales. Profile location is shown in Figure 5-10.*

5.1.11 Eriksroparken 1

The transect for Eriksroparken GPR profile 1 is located on a part of a conspicuously low-relief summit surface (Figure 5-14a, b). Gently-dipping to subhorizontal reflectors are indicated by labels ‘a’ to ‘k’. Two subvertical reflectors intersect the outcrop surface at ‘l’ and ‘m’. In general contrast to the other transects located on conspicuously low relief bedrock surfaces (Figures 5-4 to 5-9 and 5-11 to 5-13) the gently-dipping to subhorizontal reflectors are short, with maximum lengths up to ~5 m.

a Aerial photo of Eriksroparken Trollhättan, showing GPR profile

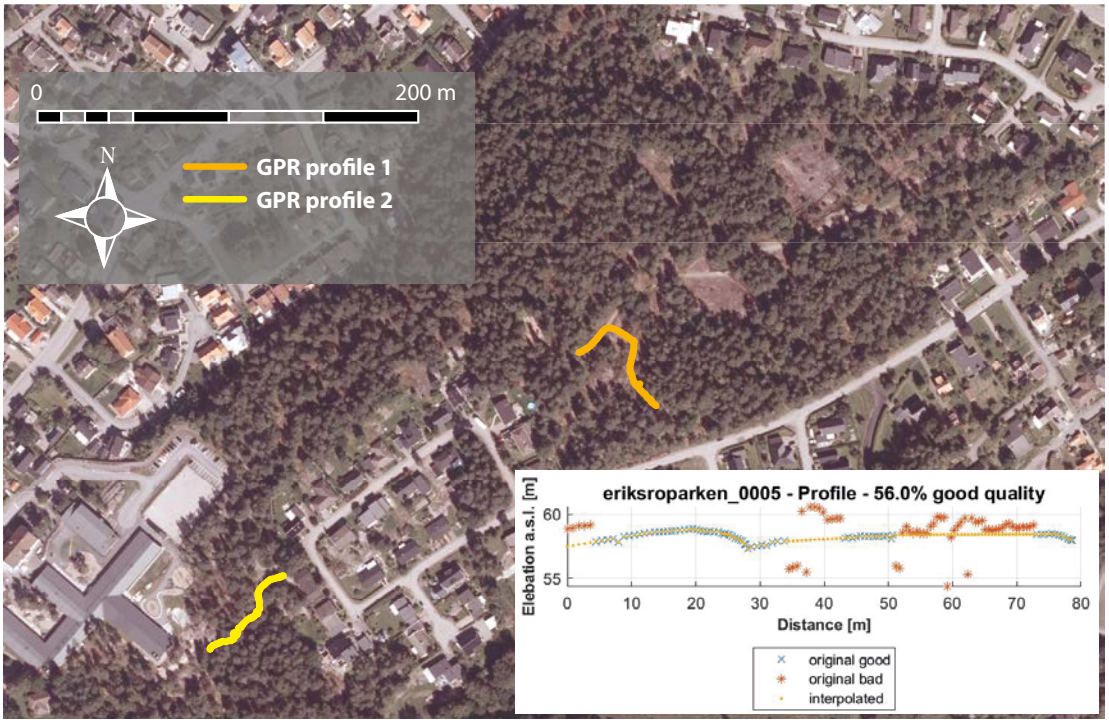

b 170 MHz GPR profile 1 at Eriksroparken, Trollhättan. equal horizontal and vertical scales

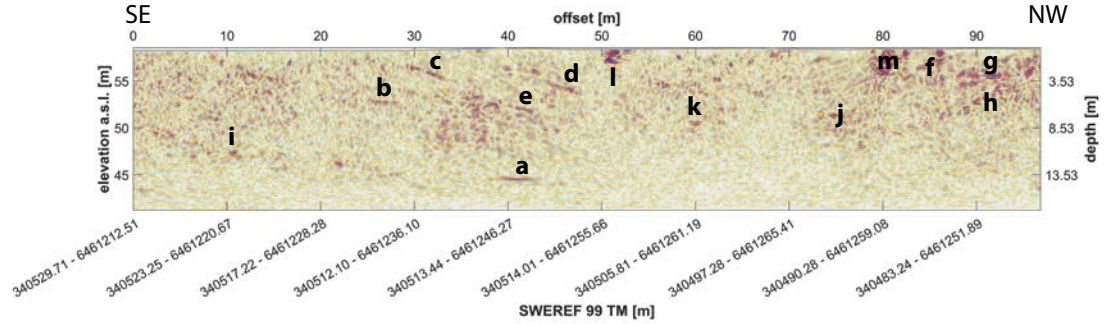

c 170 MHz GPR profile 2 at Eriksroparken, Trollhättan; equal horizontal and vertical scales

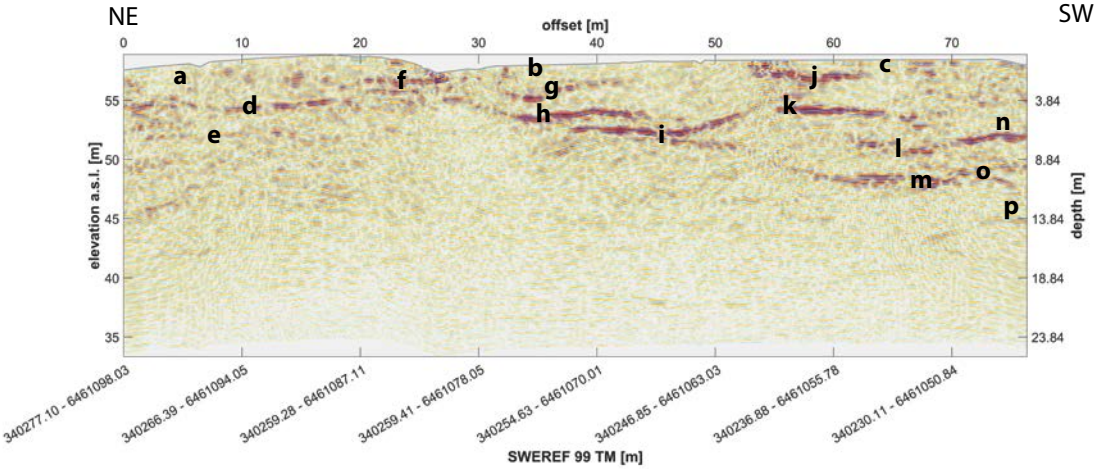

Figure 5-14. *(a) Orthorectified aerial photograph showing the location of a two GPR transects in Eriksroparken, Trollhättan. The inset shows the quality of the spatial positioning data from the differential GPS for GPR transect 2. Surface elevations had to be interpolated across sections of poor spatial positioning, which totaled 44 % of the profile length. (b) 170 MHz GPR image of Eriksroparken profile 1 shown with equal vertical and horizontal scales. c) 170 MHz GPR image of Eriksroparken profile 2 shown with equal vertical and horizontal scales. In both GPR images, strong reflections are shown in purple and weak reflections are shown in yellow. The letters indicate features discussed in the text.*

5.1.12 Eriksroparken 2

The transect for Eriksroparken GPR profile 2 (Figure 5-14c) is located southwest of the conspicuously low-relief summit surface on which GPR profile 1 is located (Figure 5-14a). GPR profile 2 meanders under a patchy tree cover over a bedrock surface with convex bumps of meter-scale amplitudes and with morphologies that conform with roches moutonnées. Consequently, the spatial positioning data received from the differential GPS was of low quality in three sections (labeled 'a', 'b', and 'c' in Figure 5-14c), totaling 44 % of the profile (Figure 5-14a). The bedrock surface at these three locations was interpolated as being flat, rather than convex, resulting in the images of the underlying GPR reflectors being processed as less convex than they are in reality. A series of undulating subhorizontal reflectors (labelled 'd' to 'p' in Figure 5-14c) occur at depths down to ~15 m. Reflector 'f' underlies a convex bedrock surface that forms a step to a lower bedrock surface, against which it terminates. The reflectors form hook shapes at 'h', 'i', 'j', 'k', 'm', and 'o'. The abundance of undulating subhorizontal reflectors along this transect contrasts with the frequently more linear subhorizontal reflectors located beneath the conspicuously low-relief summit surfaces (Figures 5-4 to 5-9 and 5-11 to 5-13a).

5.1.13 Fågelmara

The transect of the Fågelmara profile (Figure 5-15) extends 90 m from east to west across two gentle bumps with heights of ~0.5 m. The increase in elevation over the length of this transect is 1 m. Subhorizontal reflectors underlie the entire surface of the outcrop, with one series of reflectors located at about 4 m depth and a second at 8 m depth. The reflectors at 4 m depth appear to be comprised of 3 overlapped segments (labelled 'a', 'b', and 'c' in Figure 5-15e) and closely mirror the outcrop surface. Reflector 'b' bends downwards to the west and terminates against reflector 'c' at the location marked 'd'. Reflector 'b' might also terminate against reflector 'a'. Apparent bifurcations of reflectors are marked by 'e', 'f', 'g', and 'h' in Figure 5-15e. The bifurcating reflector marked 'e' appears to extend down to reflector 'i'. In addition to the long subhorizontal reflector series described above, shorter subhorizontal reflectors lie beneath reflector 'j' (reflector 'k'), beneath reflector 'c' (reflector 'i'), and within 3 m of the surface (reflectors 'l' 'm', and 'n'). Reflectors 'm' and 'l' appear to be linked by an inclined reflector. One prominent inclined reflector (reflector 'o') has a notably linear trace except near its right (west) end where it is convex. Reflector 'o' appears to terminate against reflector 'p' and perhaps also against reflector 'l' (or 'a')'. Reflector 'q' might terminate against reflector 'o' if reflector 'o" crosses reflector 'p'. In addition, a series of vertical fractures intersect the surface (marked as 'r'), including a pair that bound reflector 'n' and another pair that may bound inclined reflector 's' under the transect summit.

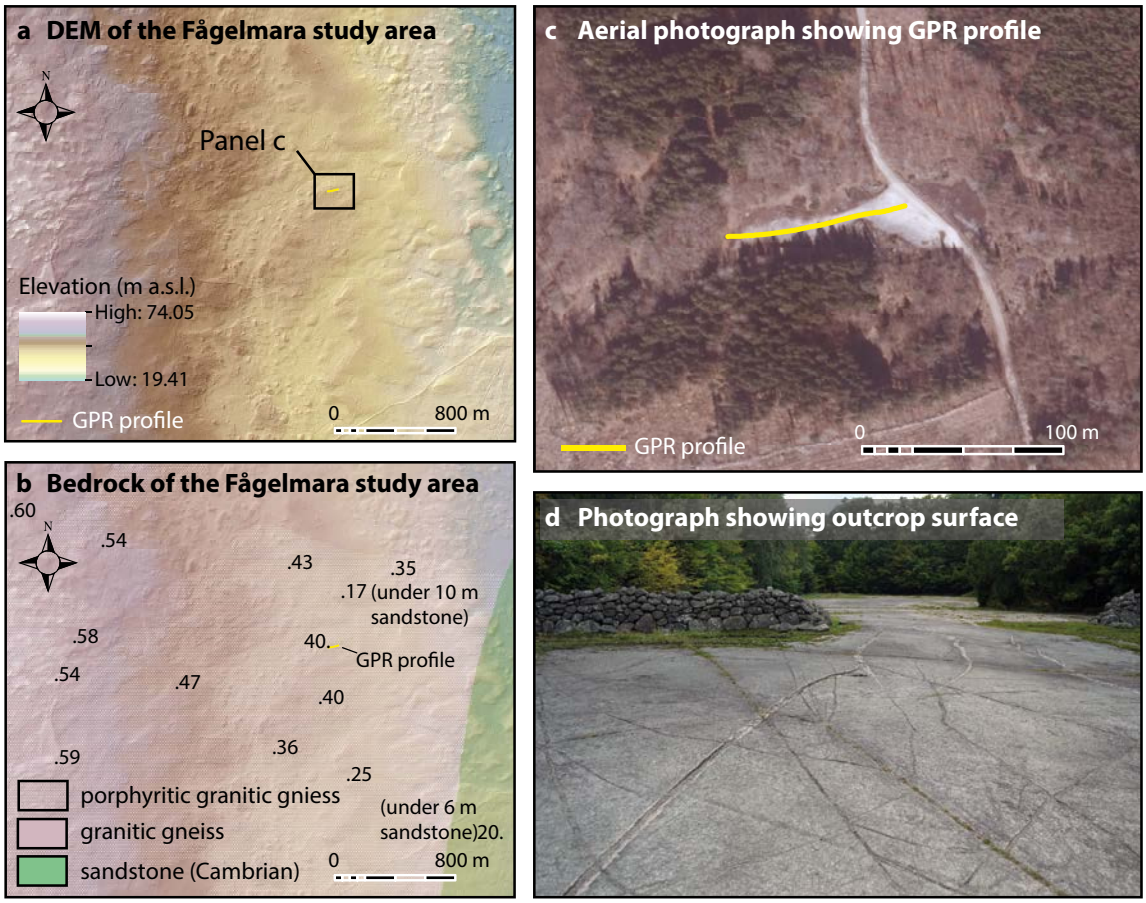

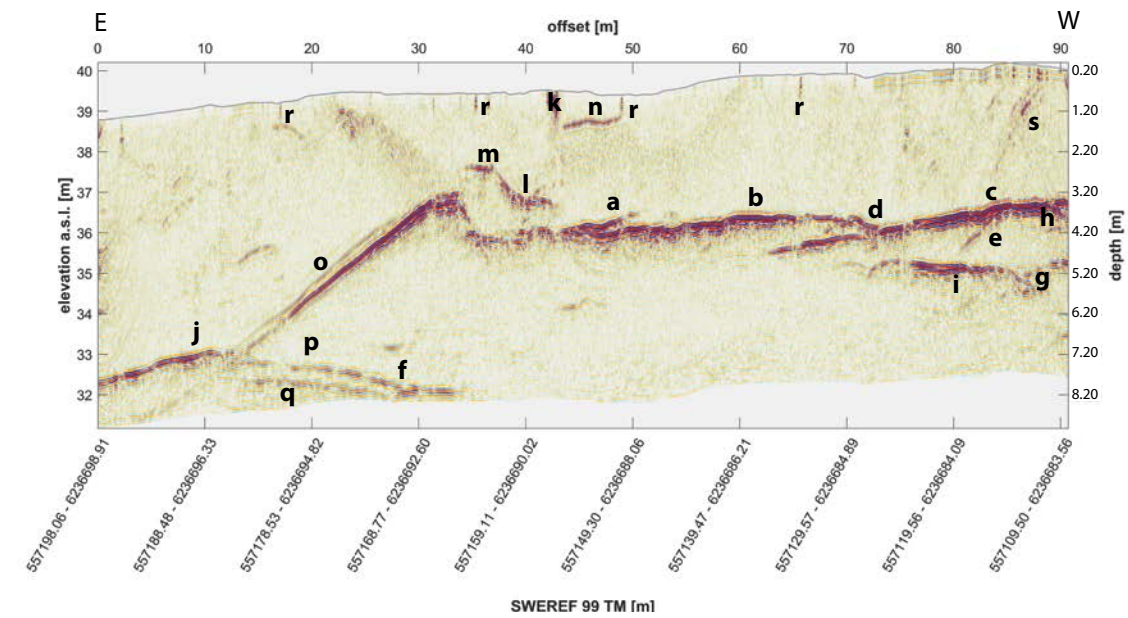

Figure 5-15. *Fågelmara study site. (a) DEM of Fågelmara with 2 m resolution, from LiDAR data. The rectangle shows the location of the aerial photograph and GPR profile in panel c. (b) Bedrock geology of the study area. The GPR profile is located on gneissic granite and the Cambrian sandstone margin is mapped as close as 1 100 m from the east end of the profile. Numbers indicate measured point elevations of the basement surface, frequently located beneath Quaternary sediments and in some places below Cambrian sandstone (indicated) Data are from well logs at the Geological Survey of Sweden. (c) Orthorectified aerial photograph showing the GPR profile in yellow. (d) Photograph of the outcrop surface, looking west. (e) 600 MHz GPR image of the Fågelmara profile. Strong reflections are shown in purple and weak reflections are shown in yellow. The letters indicate features discussed in the text.*

f 600 MHz GPR profile at Fågelmara, equal horizontal and vertical scales

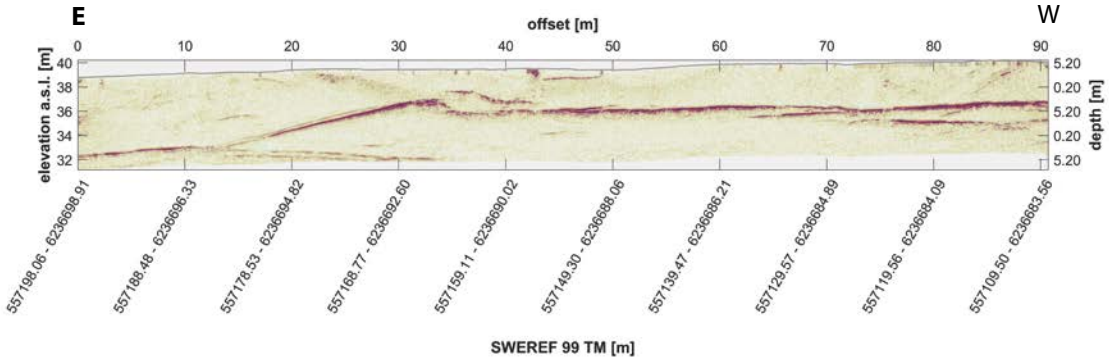

Figure 5-15 continued. *Fågelmara study site. (f) GPR profile shown with equal vertical and horizontal scales.*

5.2 Topography

In Trollhättan, the outcrops are elongated in the direction of the metamorphic fabric, which also coincides with former ice flow directions (Figures 2-4, 3-1 and 5-16a). The outcrop at Sandhem displays the largest exposed area and has an almost flat surface (Figures 2-4 and 3-1). It appears gently convex along its NE–SW long axis (coinciding with former ice flow direction; Figures 5-9 and 5-10) and is more convex transverse to former ice flow along its eastern flank (Figure 5-13). It also rises 60 cm from northeast to southwest along its long axis (Figure 5-10) and a subhorizontal joint is exposed along a part of its western flank (Figure 5-17e). Whether the Sandhem outcrop displays roche moutonnée topography is unclear because its stoss and lee sides are covered in sediment and vegetation. At Hjortmossen, the stoss-sides comprise broad slabs that are convex as they reach the summits (Figures 5-8a, 5-16b and 5-17c). In addition, adjacent stoss-side slabs display different slopes. The summit of the outcrop that remains accessible (one has a sports hall constructed on most of it) is planar along its long axis (Figures 2-4, 3-1 and 5-8a). A subvertical joint aligned parallel to former ice flow has been glacially eroded to form an elongated trough up to ~1 m deep (Figure 2-4c). The lateral flanks descend some meters to adjacent valleys, are highly convex where they intersect with the planar summits, and are in some locations underlain by exposed subhorizontal joints (Figure 5-17a, b). The lee-sides display plucking scarps in contrast to the convex stoss sides (Figure 5-17c, d). The Eriksroparken summit areas (Figures 2-4d, 3-1, 5-16a, d, e) appear planar along the outcrop long axis. The summit areas, however, display smaller areal extents than the other conspicuously flat surfaces at Hjortmossen, Sandhem, and Nordkroken. As observed at Hjortmossen, the stoss side is convex, whereas lee-side plucking by overriding glacial ice has occurred and numerous roches moutonnées, with lengths of a few meters, are observed (Figure 5-17f).

a Map showing profile locations

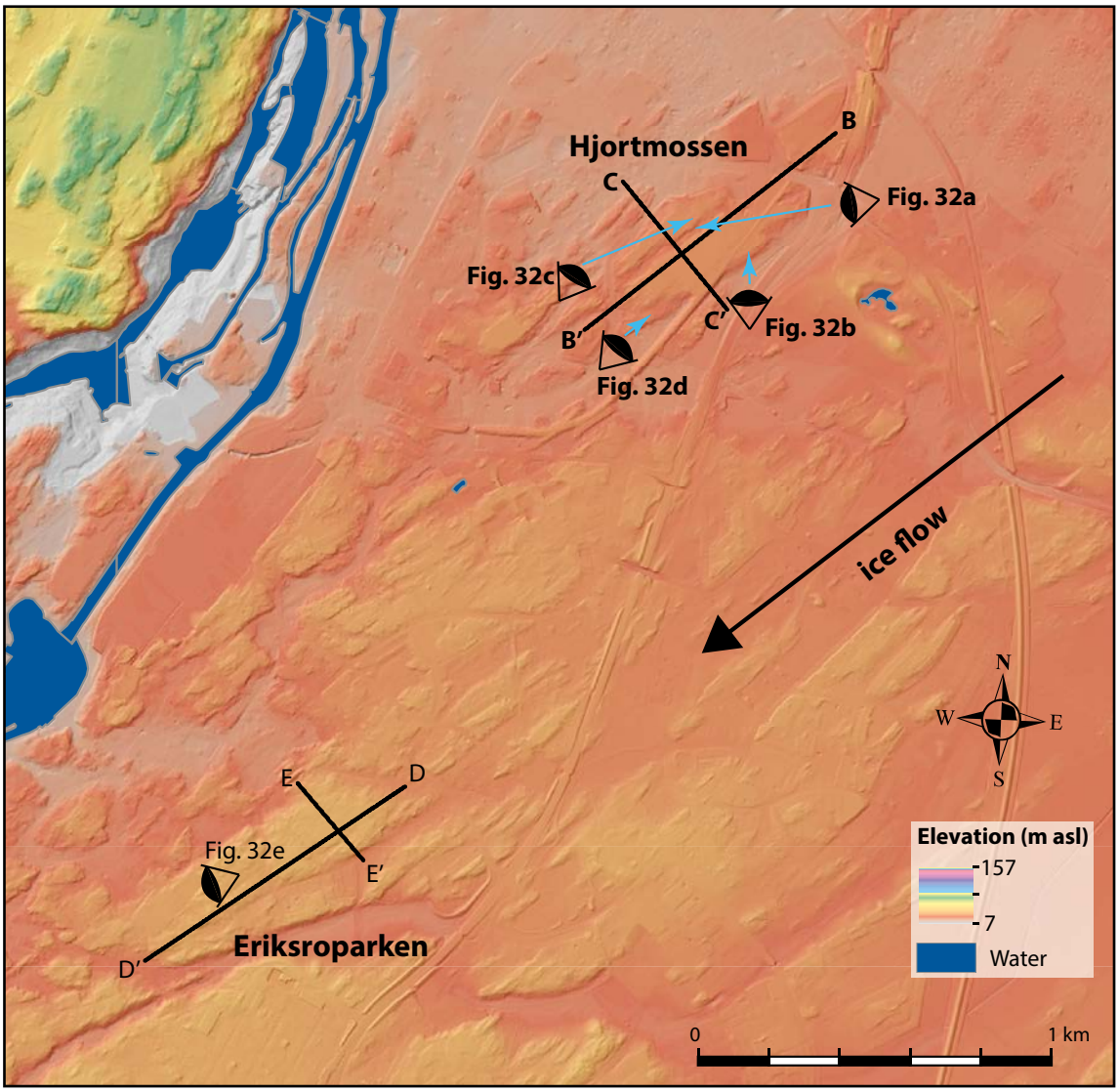

b Hjortmossen long profile

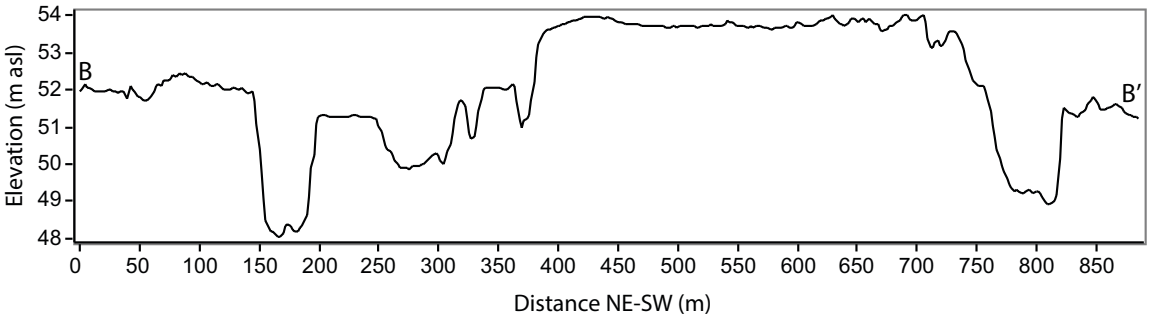

Figure 5-16. *Topographic map and topographic profiles through the Hjortmossen, and Eriksroparken outcrops, Trollhättan. (a) DEM of Trollhättan with 2 m resolution, from LiDAR data. The positions of the long- and cross profiles of panels b–e and photographs in Figure 5-19a–d are shown. Ice flow direction is also indicated. (b) A topographic profile of the Hjortmossen outcrop parallel to its long axis and to ice flow direction. (c) A topographic profile of Hjortmossen located transverse to the outcrop long axis and to former ice flow. (d) A topographic profile of the Eriksroparken outcrop parallel to its long axis and former ice flow direction. (e) A topographic profile of Eriksroparken located transverse to the outcrop long axis and to former ice flow.*

c Hjortmossen cross profile

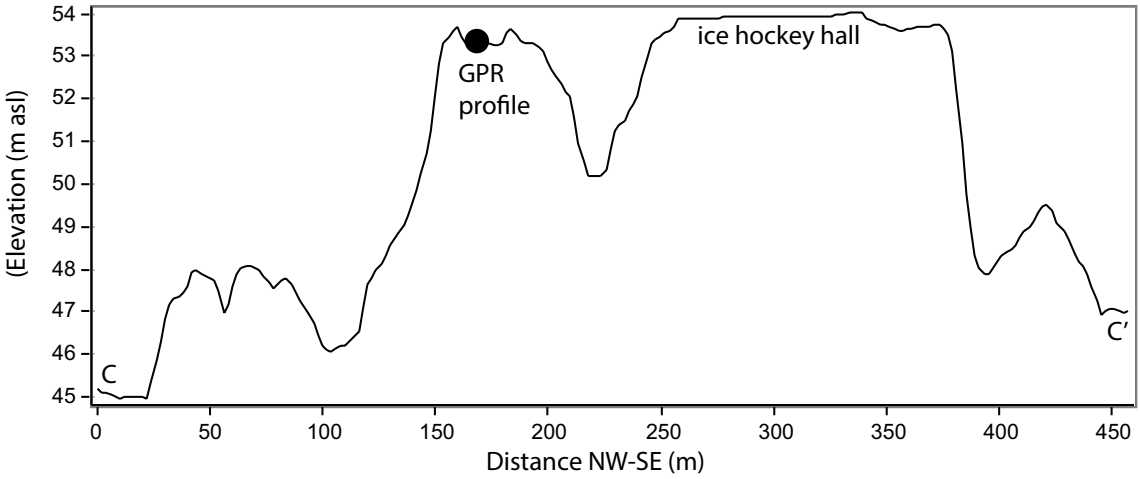

d Eriksroparken long profile

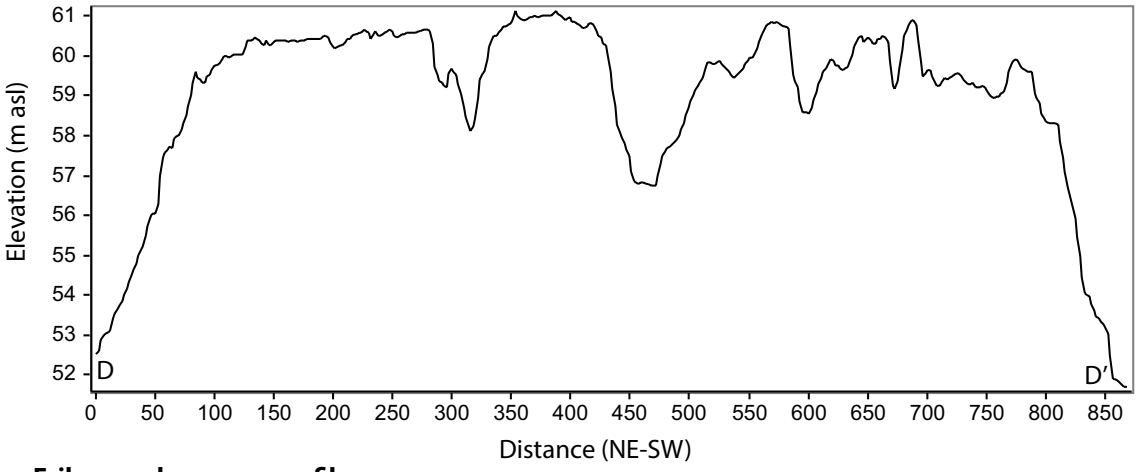

e Eriksroparken cross profile

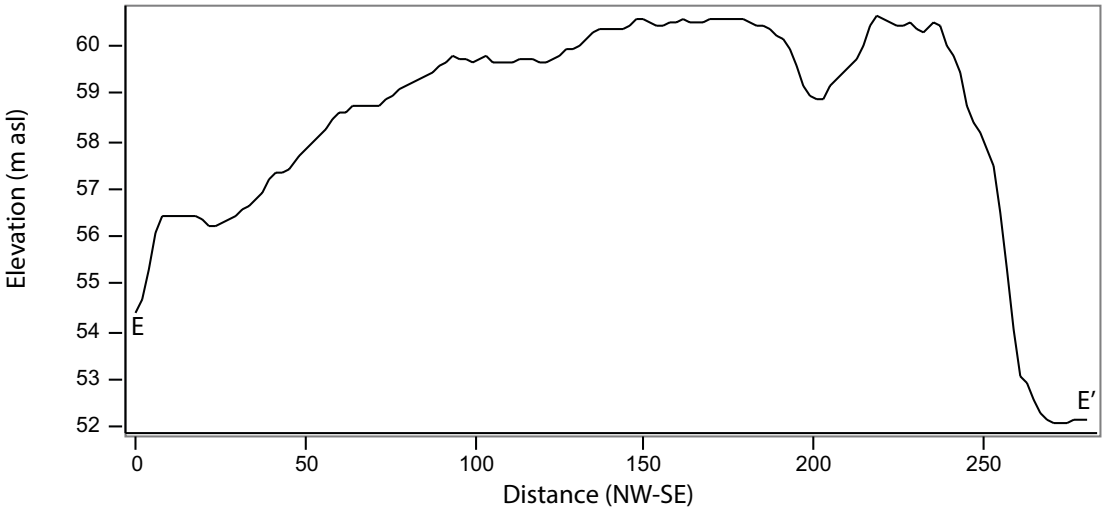

Figure 5-16. *Continuing.*

Figure 5-17. *Photographs of outcrop morphology, including sheeting joints and plucked subvertical joints at Hjortmossen and Sandhem, Trollhättan. (a) to (d) Hjortmossen, Trollhättan; see Figure 5-16a for locations of photographs. (e) Sandhem, Trollhättan. (f) Eriksroparken, Trollhättan.*

The Nordkroken shoreline outcrops display spatially varying surface features (Figure 5-18). The surface exposed along the shoreline is commonly flat and dips to the NNE (Figure 5-18c, h). However, low amplitude whalebacks with higher convexities transverse to former ice flow also occur (Figure 5-18a, b). In some cases, those whalebacks are being eroded along subhorizontal joints, which flattens the bedrock surface as the overlying blocks are transported away (Figure 5-18b, i). Other subtle components of the flat-looking Nordkroken bedrock topography include lee-side steps relative to former ice flow that have formed along subvertical fractures oriented transverse to former ice flow (Figure 5-18e, f). These steps can also be eroded along subhorizontal joints, which again flattens the surface topography (Figure 5-18c). Channels have also been eroded by ice along subvertical fractures oriented with ice flow (Figure 5-18b, c, h).

At the inland site at Nordkroken (Figure 5-3a), the long-axis and transverse curvatures of the outcrop measured with GPR are much higher than those generally apparent at the shoreline (Figure 5-6). Two other outcrops at the inland site located adjacent to the one measured with GPR are separated by a 2 m wide trench but the elevations of their almost-flat tops differ by 60 cm (Figure 5-18j). The long axes of these and other inland outcrops are aligned with former ice flow and with the metamorphic fabric.

Figure 5-18. *(a) to (d) Photographs of outcrop morphology, including jointing, at Nordkroken. (e) to (j) Photographs of outcrop morphology, including jointing, at Nordkroken.*

5.3 Field observations of grain size and joints

The Sandhem, Hjortmossen, and Nordkroken outcrops are developed in coarse-grained porphyritic gneissic granite containing K-feldspar phenocrysts. Crystal lengths are in the order of centimeters. The Eriksroparken outcrops are developed in a different gneissic granite of smaller, but still coarse, grains (Figure 3-2). Additional data on mapped joint spacings are found in a supplementary file (1900551_ suppementary_information_joint_spacing_tr-19-22.zip[3]).

All outcrops are notable for the wide spacing of subvertical joints, which is frequently on the scale of meters to tens of meters (Figures 2-4, 3-1 and 5-17 to 5-19). Notably, all of the studied outcrops display wider spacing of vertical joints oriented parallel to ice flow compared with vertical joints oriented transverse to ice flow (Figure 5-19). At Sandhem, towards the lee-side of the outcrop, one of these subvertical joints, oriented transverse to the long axis, displays a wedge-shape opening towards the west and has an aperture of tens of centimeters. Other subvertical joints are also open and are filled either with water or sediments and vegetation. Some water-filled surface pits, with long axes oriented in the direction of former ice flow are also visible on the surface (Figure 5-10). At Hjortmossen, a few of the subvertical joints striking parallel to the outcrop long axis are open, with apertures of some tens of centimeters, and are vegetated. Surface elevations vary by ~10 cm between opposing sides of these fractures.

Subhorizontal joints are visible in some locations on the flanks of the Sandhem and Hjortmossen outcrops (Figure 5-17). However, they are not observed to run along entire outcrops and do not appear in sets of multiple joints. At Nordkroken, 10s-of-centimeter thick sheets are visible at the surface of some shoreline locations. Tabular boulders with lithological characteristics consistent with the local bedrock are also observed at Nordkroken and have been locally sourced from subhorizontally-sheeted rock (Figure 5-18b, c).

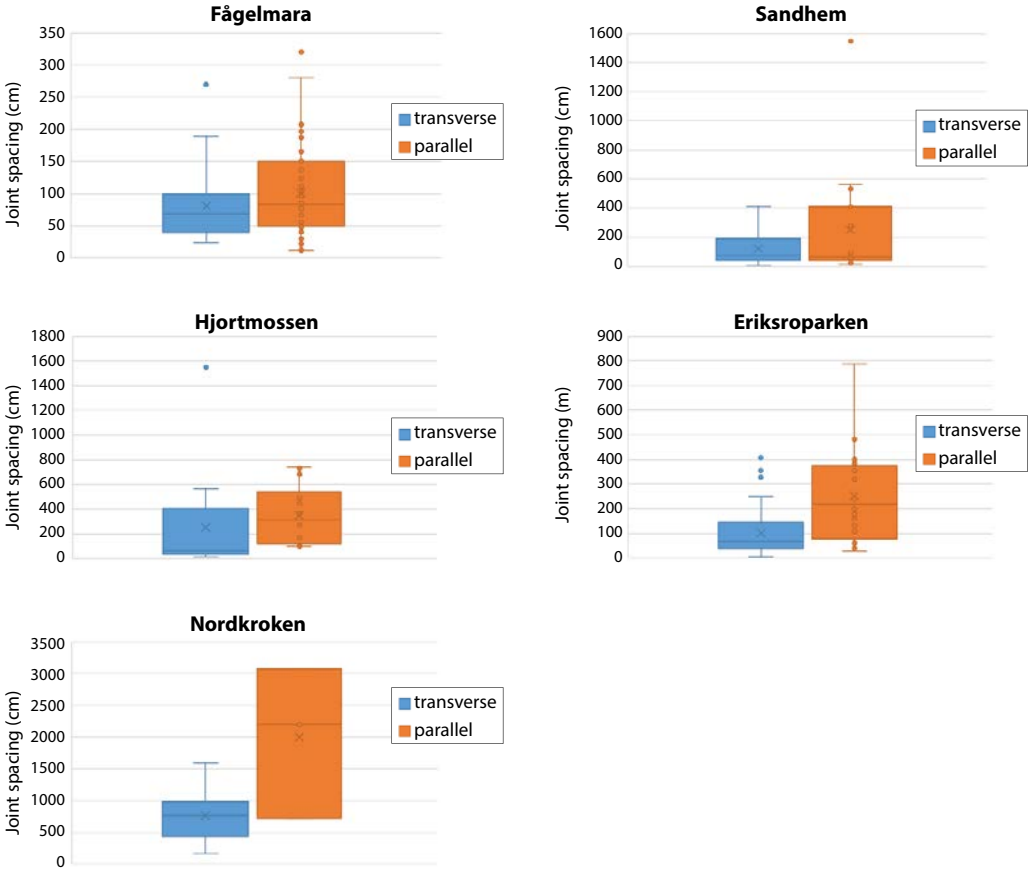

Figure 5-19. *Box and whisker plots of vertical joints spacings at Fågelmara, Sandhem, Hjortmossen, Eriksroparken, and Nordkroken. There are two box plots for each site. The blue box plots show the spacing of vertical joints oriented transverse ice flow, whereas the orange box plots show the spacing of vertical fractures oriented parallel to ice flow.*

[3] Can be downloaded from www.skb.se/publications. Direct link: http://www.skb.com/publication/2495089/

5.4 Spatial context of the conspicuously flat surfaces (CFSs)

We assess the spatial relationships of the CFSs in the context of the traditional model for these landscape elements as original, essentially uneroded, remnants of an almost entirely flat SCP. A key argument used for this model is that CSFs represent accordant summits, with accordance established through an analysis of topographic profiles (Johansson et al. 2001b). We test this accordance by constructing the topographic profiles shown in Figure 5-20. If each of the three Trollhättan CFSs represents a remnant of the same flat peneplain, the summit surfaces of any two of these should lie on the same plane when they are connected by topographic profiles. Because distances vary between the three CFSs, gradients also vary between connected pairs of CFSs, which invalidates the comparison of accordances using a single topographic profile connecting all three sites. Profiles drawn to cross and connect pairs of CFSs (Figure 5-20) show that: (i) each CFS forms a summit area located above the present regional surface; (ii) there is a gentle regional dip towards the north and a gentle dip to the west, and; (iii) there is a close accordance between the three CFSs. There are, however, some deviations within the accordances. Firstly, the Eriksroparken CFS may be interpreted as being horizontal (line 'a' in Figure 5-20b), which then projects on a plane different to the Sandhem CFS (line b in Figure 5-20b). Secondly, the summit surfaces of Eriksroparken and Hjortmossen lie on different planes (lines a to c in Figure 5-20d). Thirdly, the summit surfaces of Sandhem and Hjortmossen also project on different planes (lines a and b in Figure 5-20e). These findings might indicate a contribution by local, rather than entirely regional, controls on the present spatial characteristics of the CFSs. These local controls may include faulting, which might vertically displace and tilt remnants of a once contiguous flat surface, or some spatial variation in how these conspicuously flat surfaces formed, if they are not remnants of a once contiguous flat surface. In addition, by invoking other accordant summits on these profiles, either a stepped series of dissected horizontal peneplains (lines c and d in Figure 5-20b, lines b to d in Figure 5-20d and lines a and c in Figure 5-20e) or a peneplain lower in the landscape and dipping to the north could also be inferred ((line e in Figure 5-20b). Profiles adjoining CFSs at Sandhem (Figure 5-20f, g) also show that CFSs project on different planes and further indicate that there are local controls on their present spatial characteristics. We agree that there is a close summit accordance between the three CFSs but that there is also evidence of either local controls on their formation or displacement by faulting and that other 'peneplains' could also be invoked. We are also wary of drawing firm conclusions from summit accordance in plots where the vertical scale is exaggerated compared with the horizontal scale in such a low relief landscape (Figure 5-20c). We point to three-dimensional and landscape spectral analyses as being more helpful in future research.

The topographic and soil depth DEMs of the wider Nordkroken–Trollhättan area reveal a generally rough landscape, where local relief commonly is as much as 10 m, but locally is tens of meters (Figures 3-1 and 5-21). The bathymetry of Lake Vänern (up to 106 m deep) is excluded from the topographic DEM but adds further relief to this landscape (Drotz et al. 2014). Numerous low amplitude hills are observed, with the summits of many protruding through the Quaternary cover to elevations that vary by some meters (Figure 5-22). Bedrock hills up to 15 m high above the surrounding Quaternary sediment cover are located adjacent to the eastern and southeastern flanks of Halleberg and Hunneberg and a 37 m high hill is located 5 km to the northeast (Figures 3-1 and 5-21 to 5-25). A valley up to 61 m deep is located in the basement adjacent to the southwestern margin of Halleberg-Hunneberg (Figure 5-21). The exceptionally low-relief surfaces that characterize the Nordkroken shoreline are not observed to the east of Halleberg and Hunneberg and the Nordkroken shoreline relief is an exception to, rather than being typical of, the meters to tens of meters of local relief that otherwise characterizes this area (Figures 3-1 and 5-21 to 5-25).

a Map showing profile locations

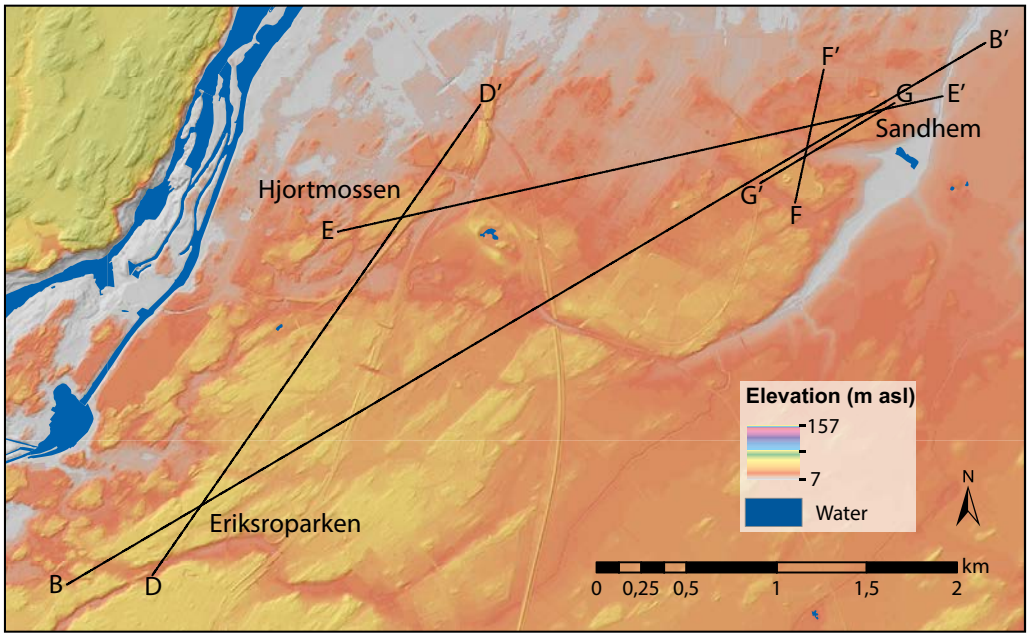

b Sandhem to Eriksroparken topographic profile

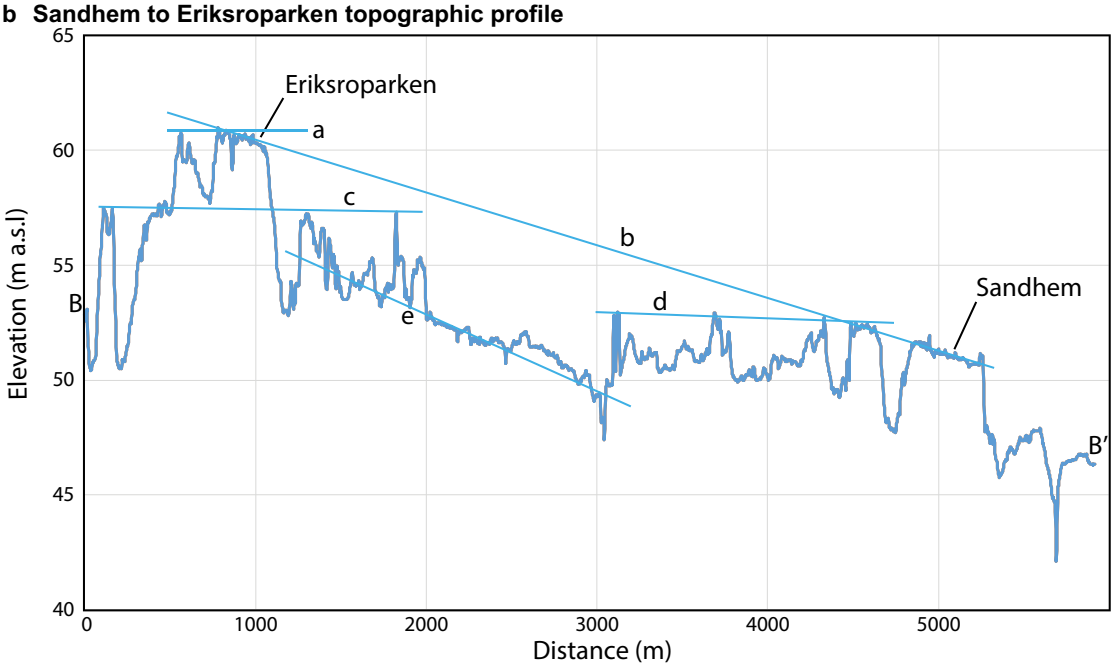

c Sandhem to Eriksroparken topographic profile- equal vertical and horizontal axes

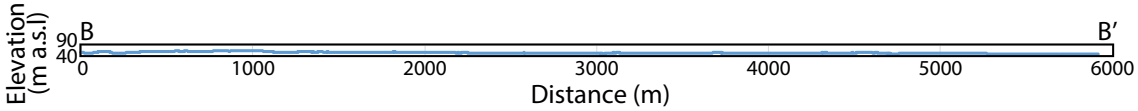

Figure 5-20. *Topographic map and topographic profiles through the Hjortmossen, Eriksroparken and Sandhem outcrops, Trollhättan. (a) DEM of Trollhättan with 2 m resolution, from LiDAR data. The positions of the profiles of panels b to f are shown. (b) A topographic profile joining the Eriksroparken and Sandhem outcrops (c) The topographic profile shown in panel 'b' joining the Eriksroparken and Sandhem outcrops, with equal vertical and horizontal scales. (d) A topographic profile joining the Eriksroparken and Hjortmossen outcrops (e) A topographic profile joining the Hjortmossen and Sandhem outcrops. (f) A SSW–NNE profile at Sandhem. (g) A NE–SW profile at Sandhem.*

d Eriksroparken to Hjortmossen topographic profile

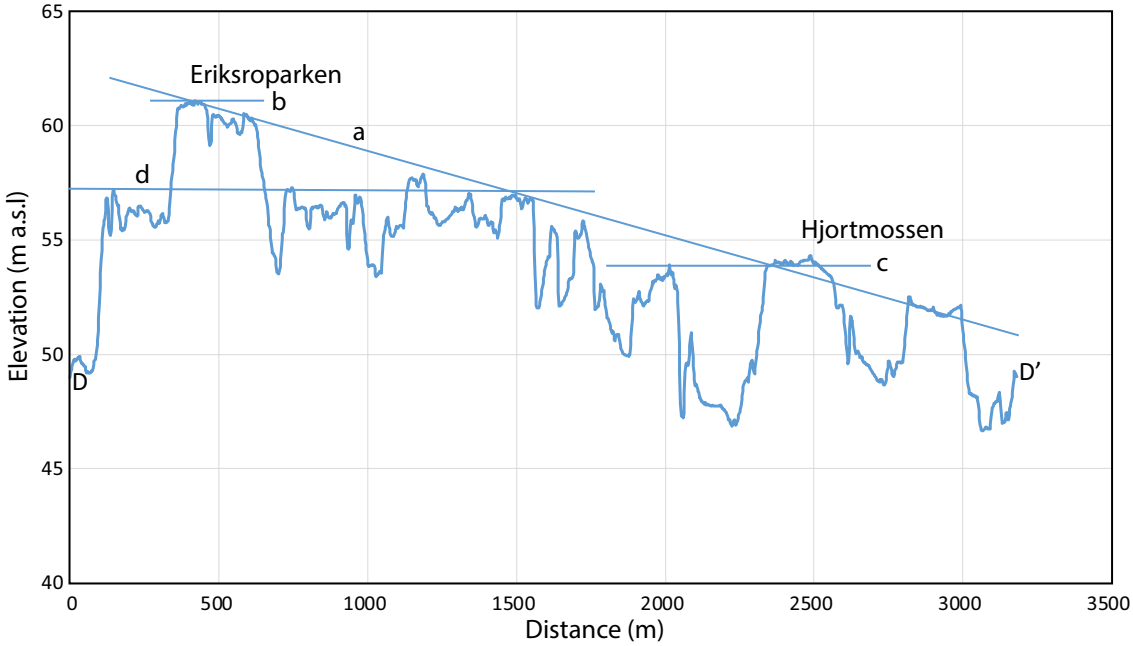

e Hjortmossen to Sandhem topographic profile

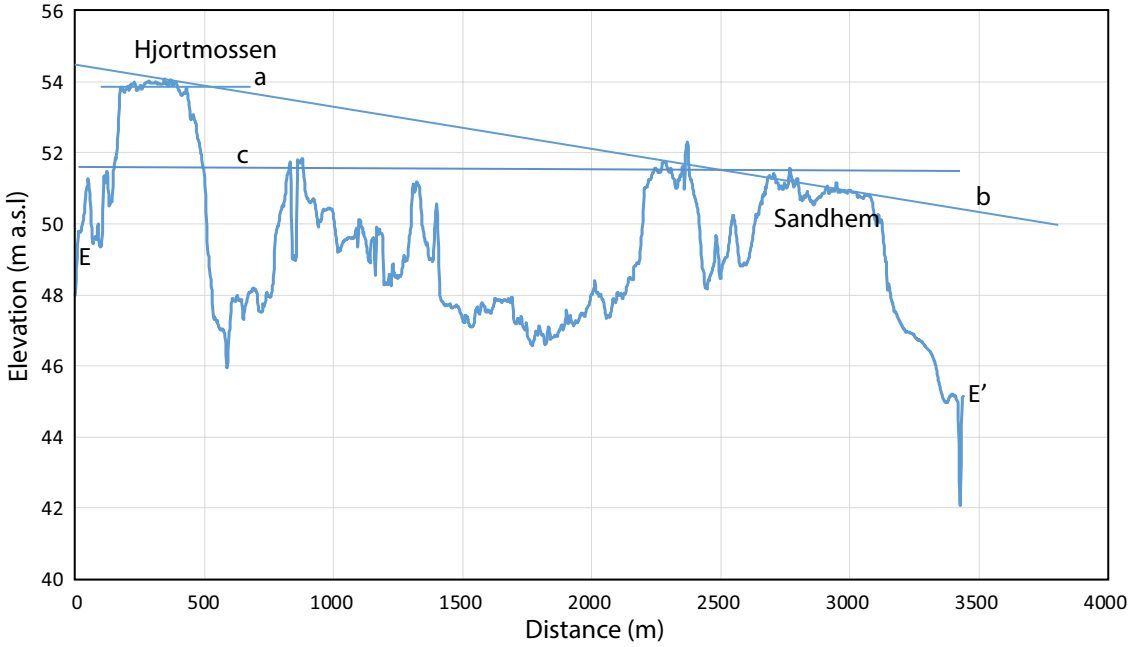

Figure 5-20. *Continuing.*

f Sandhem SSW-NNE topographic profile

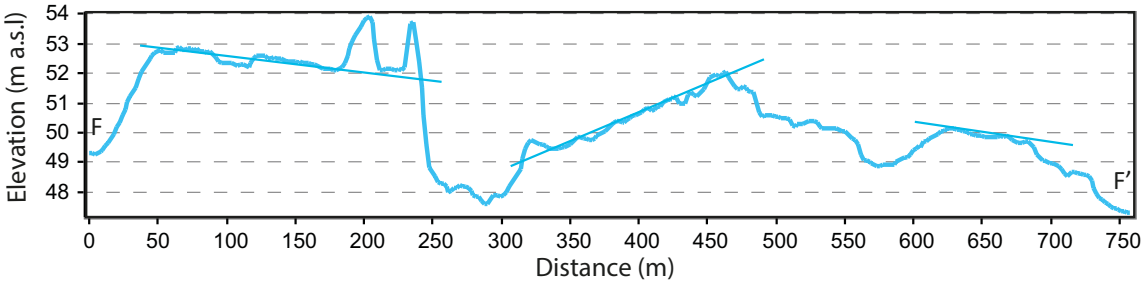

g Sandhem NE-SW topographic profile

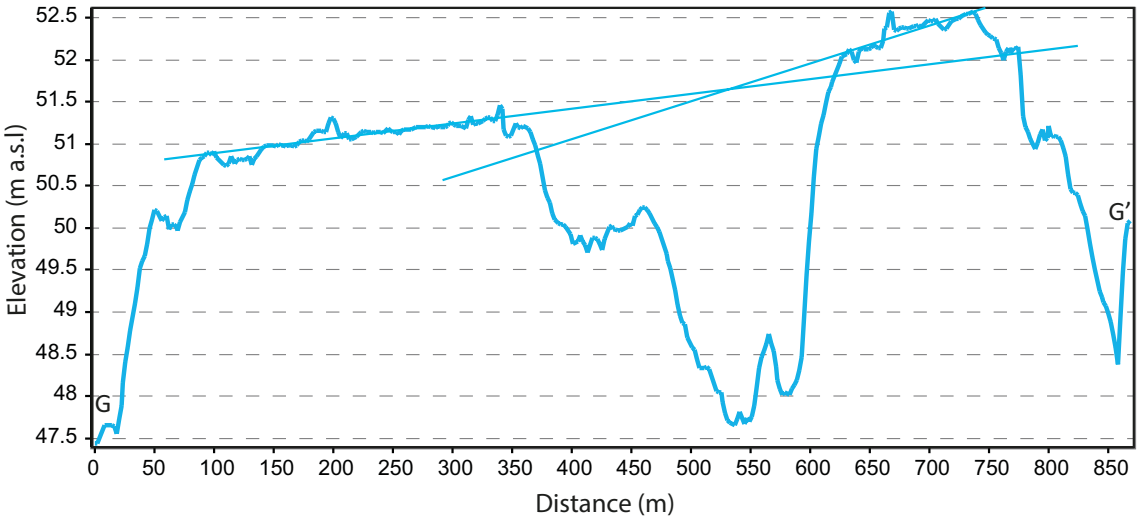

Figure 5-20. *Continuing.*

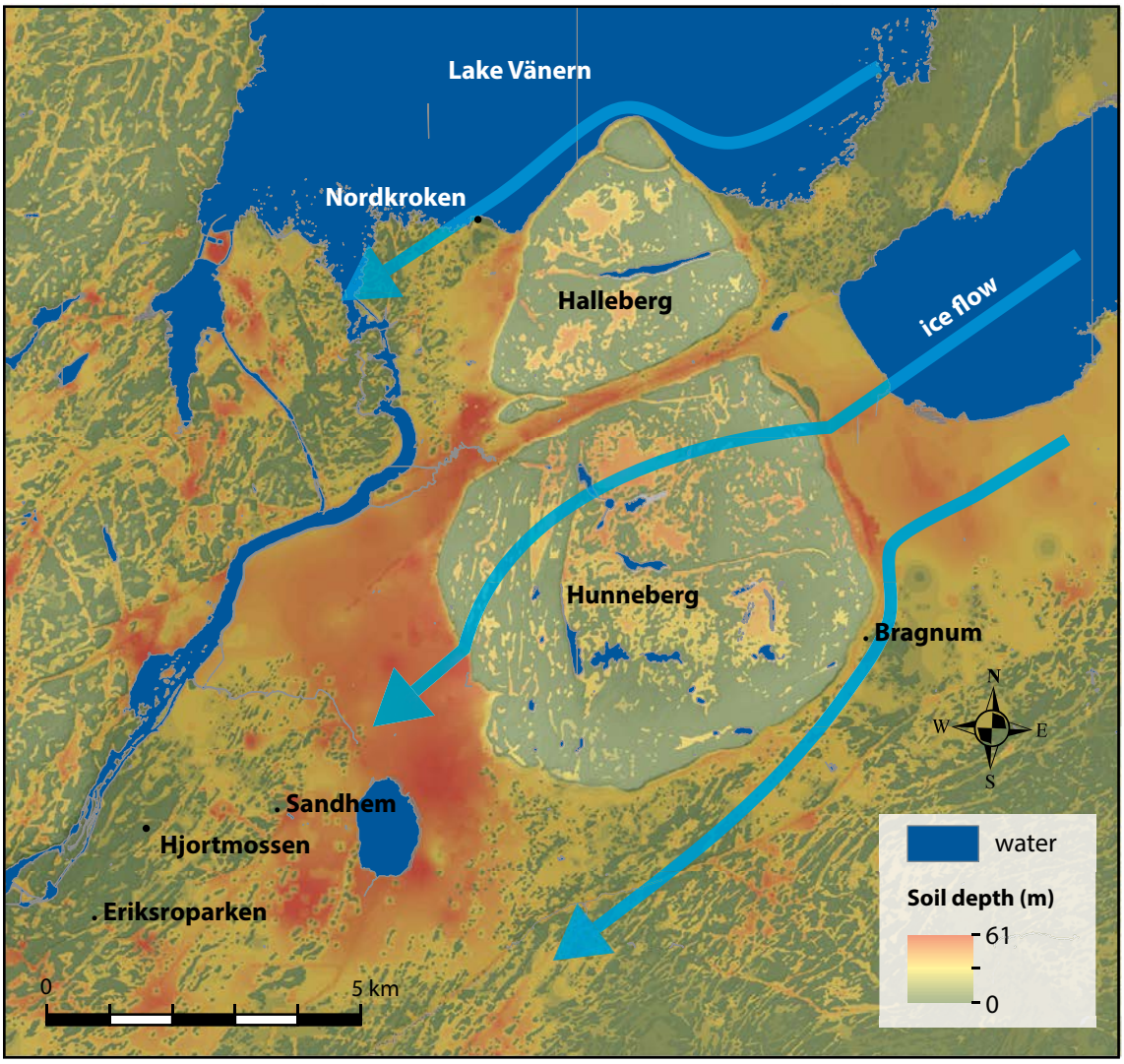

Figure 5-21. *Map of soil depths on and around Halleberg and Hunneberg, which is based on outcrop observations and well logs (Swedish Geological Survey). Most of the area is characterized by thin soils and abundant bedrock outcrops (shown in green). However, soil depths up to 61 m occur to the NE of Hunneberg, and especially to its SW. Soil depths are a proxy for depth to bedrock. Including also Lake Vänern, for which bathymetry is absent, bedrock relief on the granitic–gneissic basement is up to many tens of meters, without accounting for faulting, which increases relief to the west of the river Göta Älv. Sediments have infilled valleys, creating a ground surface topography that is of much lower relief than the basement surface topography. Ice flow from the NE across Hunneberg may have deepened the depression to the southwest. Study sites are labelled.*

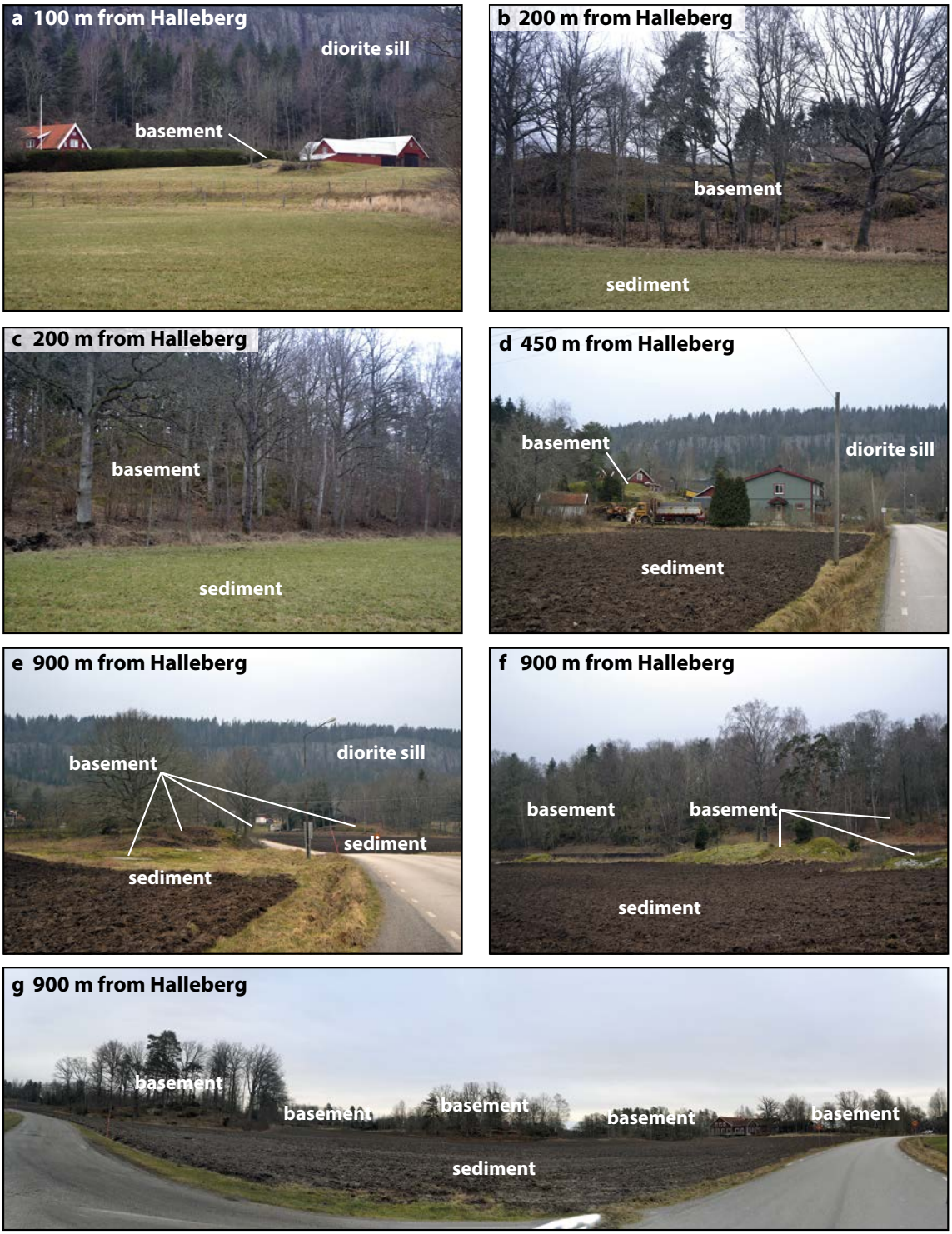

Figure 5-22. *Examples of the numerous basement convexities protruding through the sediment cover east of Halleberg. These convexities occur (a) within 100 m of the east flank of Halleberg, (b) to (c) within 200 m, (d) within 450 m, and (e) to (g) within 900 m of the east flank of Halleberg. Their heights above the sediment cover range between almost flush to 15 m.*

a Map of Halleberg area

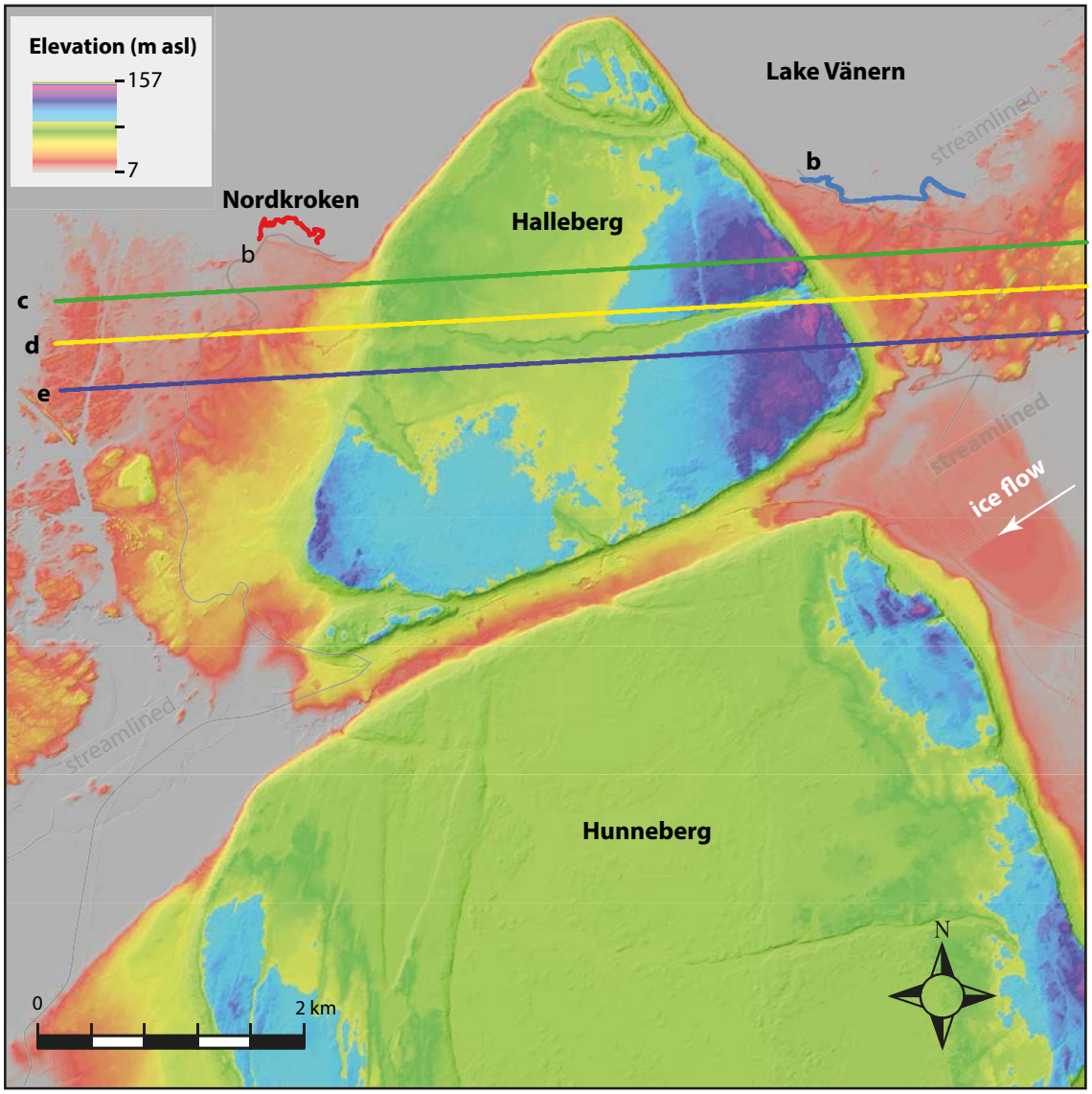

b Shoreline profiles

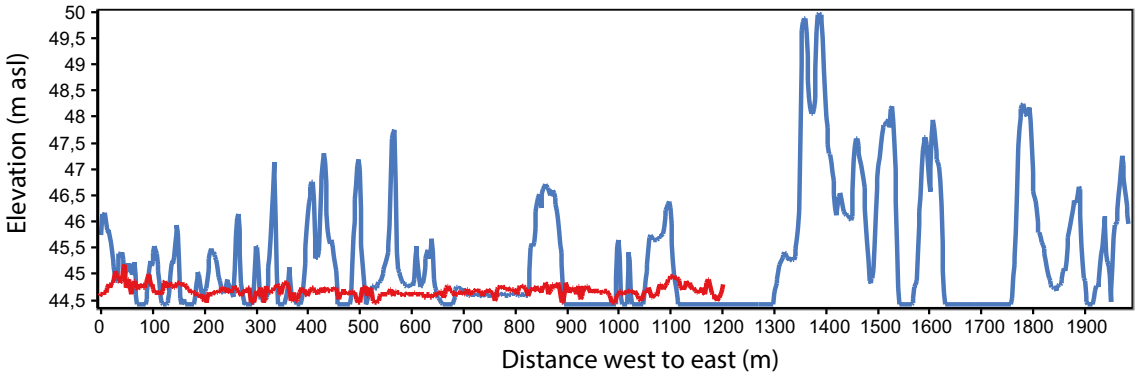

Figure 5-23. *Halleberg and its immediate surroundings. (a) DEM of Halleberg and the surrounding basement with 2 m resolution, from LiDAR data. The lettered transects b–e indicate the locations of topographic profiles shown in panels b–e. Area of streamlined bedrock is outlined in grey and the ice flow direction is shown by the white arrow. The colour gradient illustrating surface elevations above sea level has been stretched to highlight elevations between 50 and 60 m a.s.l. and between 130 and 150 m a.s.l. (b) Profiles along the shoreline of Lake Vänern at Nordkroken (red line) and to the east of Halleberg (blue line). (c) The northernmost topographic profile across Halleberg. (d) The central topographic profile across Halleberg. (e) The southernmost topographic profile across Halleberg.*

c Northernmost profile

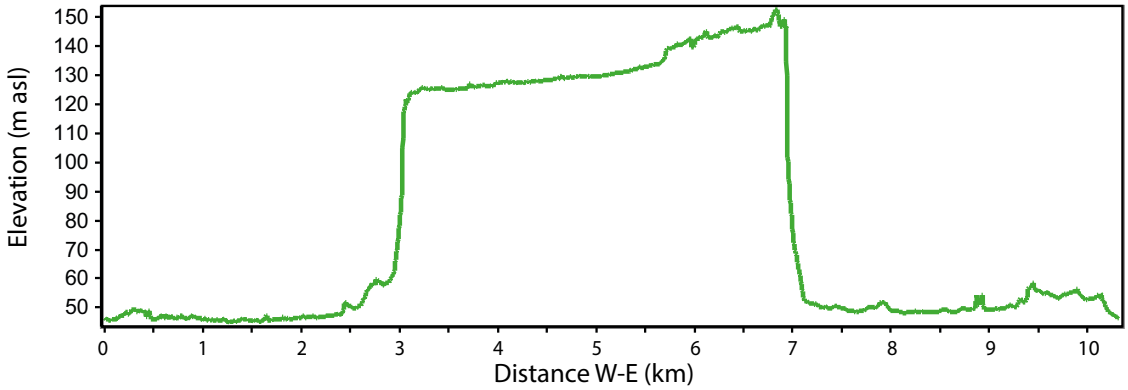

d Central profile

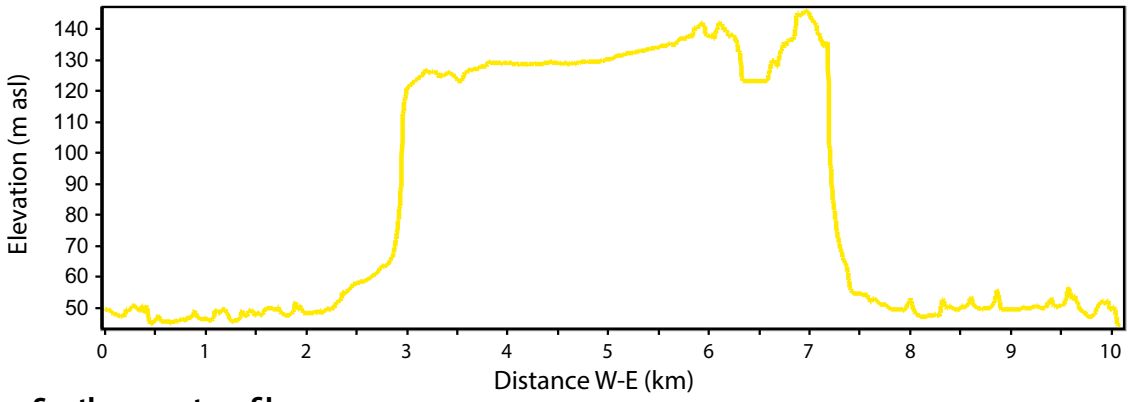

e Southernmost profile

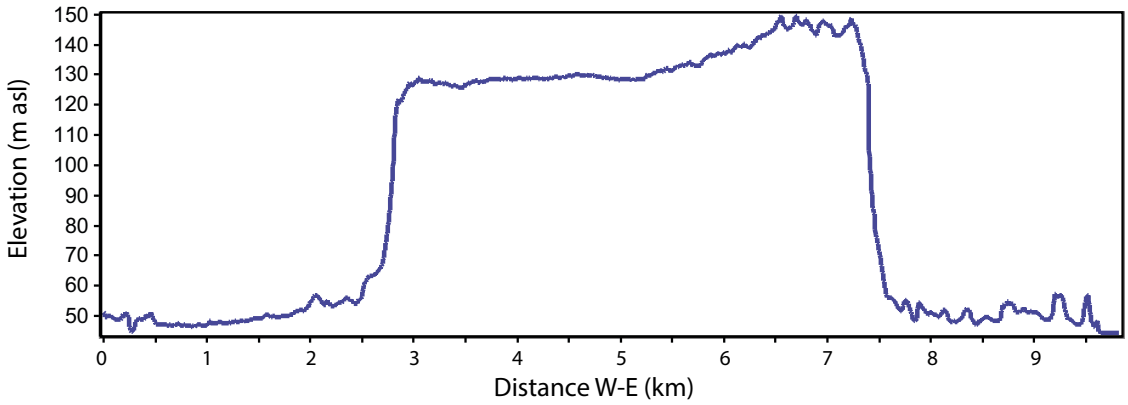

Figure 5-23. *Continuing.*

Figure 5-24. *(a) to (b) Bedrock outcrops at the coastline of Lake Vänern, 500 m to the east of Halleberg. Although these outcrops extend only meters above the lake surface, their morphology contrasts with the exceptionally-low relief surfaces at Nordkroken, on the west side of Halleberg.*

Figure 5-25. *(a) to (d) Bedrock outcrops with long axes aligned transverse to ice flow at Bragnum, adjacent to the SE corner of Hunneberg (Figures 3-1 and 5-22). Although each outcrop summit displays evidence of glacial erosion, none of them are represented by flat, horizontal surfaces.*

The elevation and local relief of the SCP beneath Hunneberg-Halleberg cannot be precisely determined. This is because it is buried by scree along the flanks of this table mountain and there are no data from well-logs that penetrate the dolerite cap through to the basement. However, well log data are available for basement areas immediately adjacent to this table mountain and also for the Kinnekulle and Lugnås table mountains from which elevations of the buried unconformity can be calculated. These data provide some constraint on SCP relief at the time of burial by Cambrian sediments (Figures 5-26 to 5-28). Relief can similarly be determined on the unconformity adjacent to and beneath the cover rock margin in the Fågelmara area (Figure 5-15). The well logs are derived from 14 cm wide boreholes drilled vertically into the bedrock, which at Kinnekulle (Figure 5-27), most sites at Lugnås (Figure 5-28), and some at Fågelmara (Figure 5-15) is sedimentary overlying crystalline basement. Errors in basement elevations may relate to deviations from vertical but these are likely to be minor (up to a few tens of cm) because the holes are drilled vertically to access water at minimum cost, the bore diameter is wide at 14 cm, sedimentary rocks are softer than crystalline basement, and most boreholes only extend downwards by up to a few tens of meters. Spatial positioning is cited in the well-log archive as having an error margin up to 100 m. Resulting errors in calculated basement elevations are expected to be < 1 m. However, larger errors might occur in selected locations where logging of depths to basement has been done incorrectly. The well-log data indicate bedrock amplitudes frequently up to 12 meters over wavelengths of tens to hundreds of meters. Larger amplitudes up to a few tens of meters over wavelengths of hundreds of meters also occur. A long wavelength dip to the west is also apparent on the SCP below the Kinnekulle and Lugnås table mountains. Similar amplitudes over wavelengths of tens to hundreds of meters might also be expected on the unconformity beneath the Hunneberg-Halleberg table mountains. In addition, the elevations of the Nordkroken surfaces and the elevation of the preserved unconformity beneath Halleberg and Hunneberg appear to differ by up to a few tens of meters (Figure 5-26). That difference may be attributable to vertical block movements along faults and/or glacial erosion.

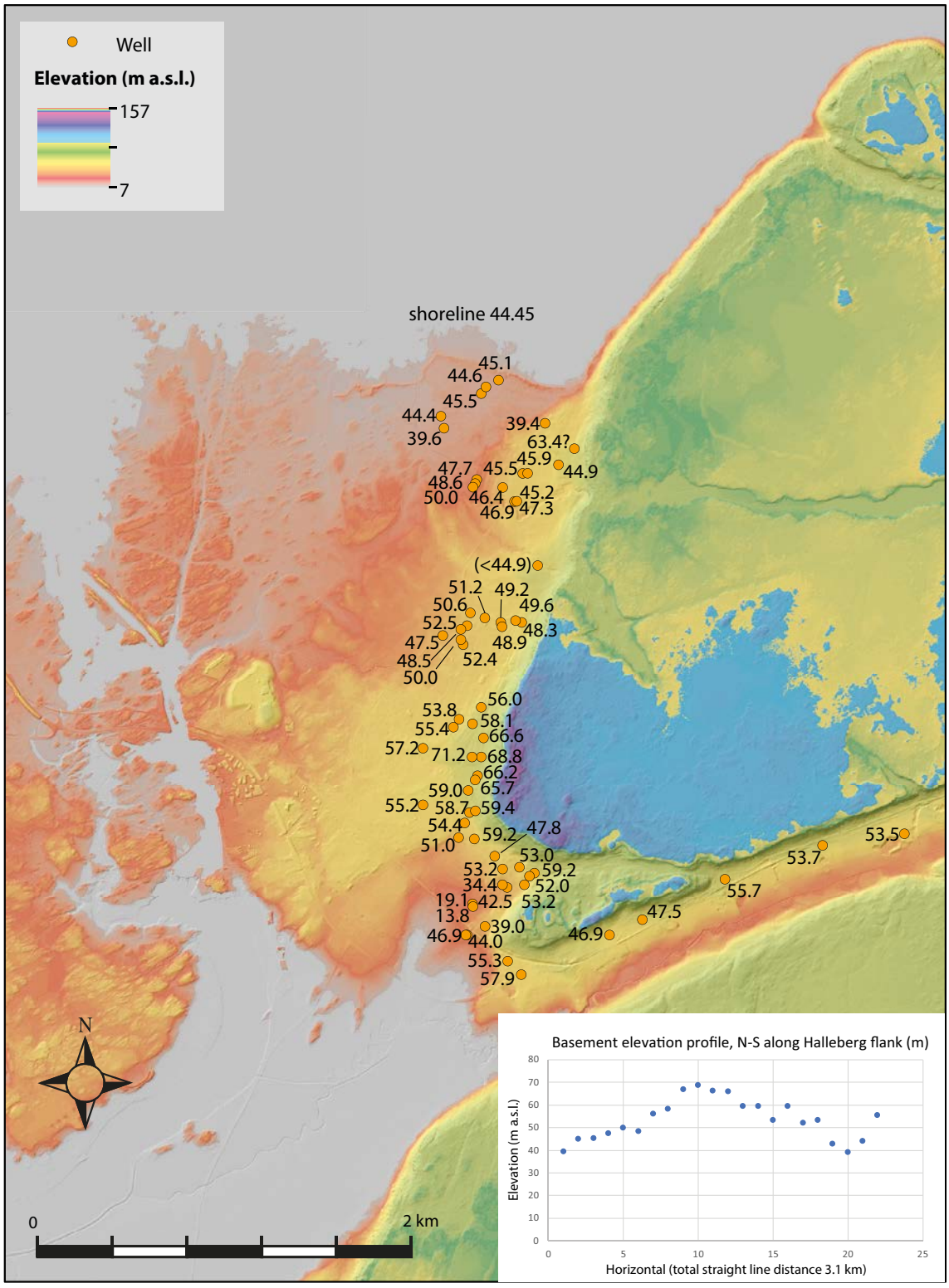

Figure 5-26. *Elevations of the basement buried by Quaternary sediments adjacent to the western flank of Halleberg. Values are derived from the well log archive at the Geological Survey of Sweden. Depths to bedrock are subtracted from surface elevations at each point. The colour gradient illustrating surface elevations above sea level has been stretched to highlight elevations between 50 and 60 m a.s.l. and between 130 and 150 m a.s.l. The inset shows a basement elevation profile over a total distance of 3.1 km along the western flank of Halleberg. Each point is horizontally separated by the same distance, rather than the actual distance.*

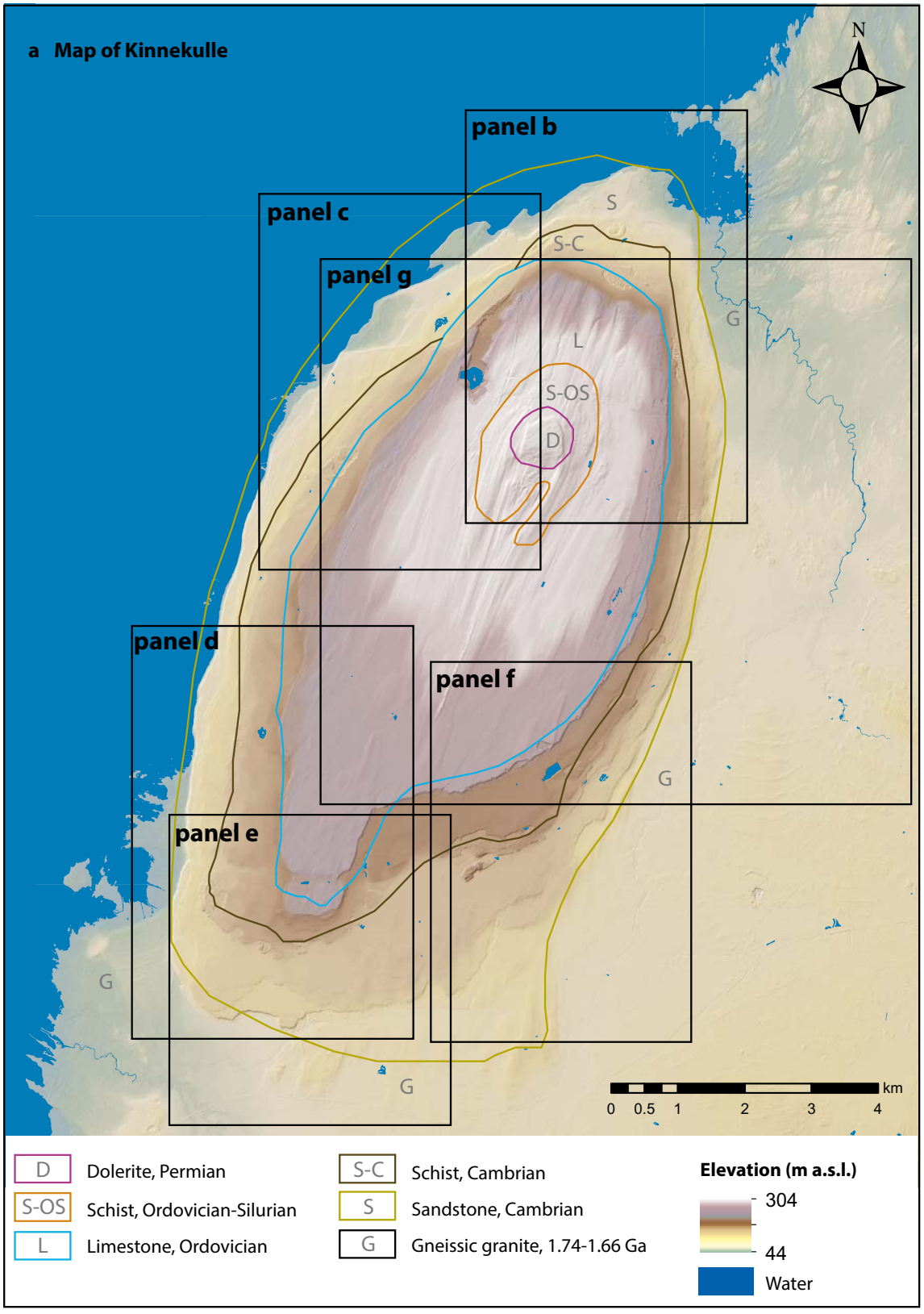

Figure 5-27. *Elevations of the SCP beneath the Kinnekulle table mountain. Elevations are derived from the well log archive at the Geological Survey of Sweden. Depths to basement are subtracted from surface elevations at each point. (a) Geological map of Kinnekulle showing its formation from Cambro–Ordovician cover rocks and a Permian dolerite sill (Geological map from the Geological Survey of Sweden) and the locations of panels b–g. (b) Elevations of the SCP below the (b) northeast (c) northwest (d) southwest (e) southern (f) southeast, and (g) eastern portions of Kinnekulle.*

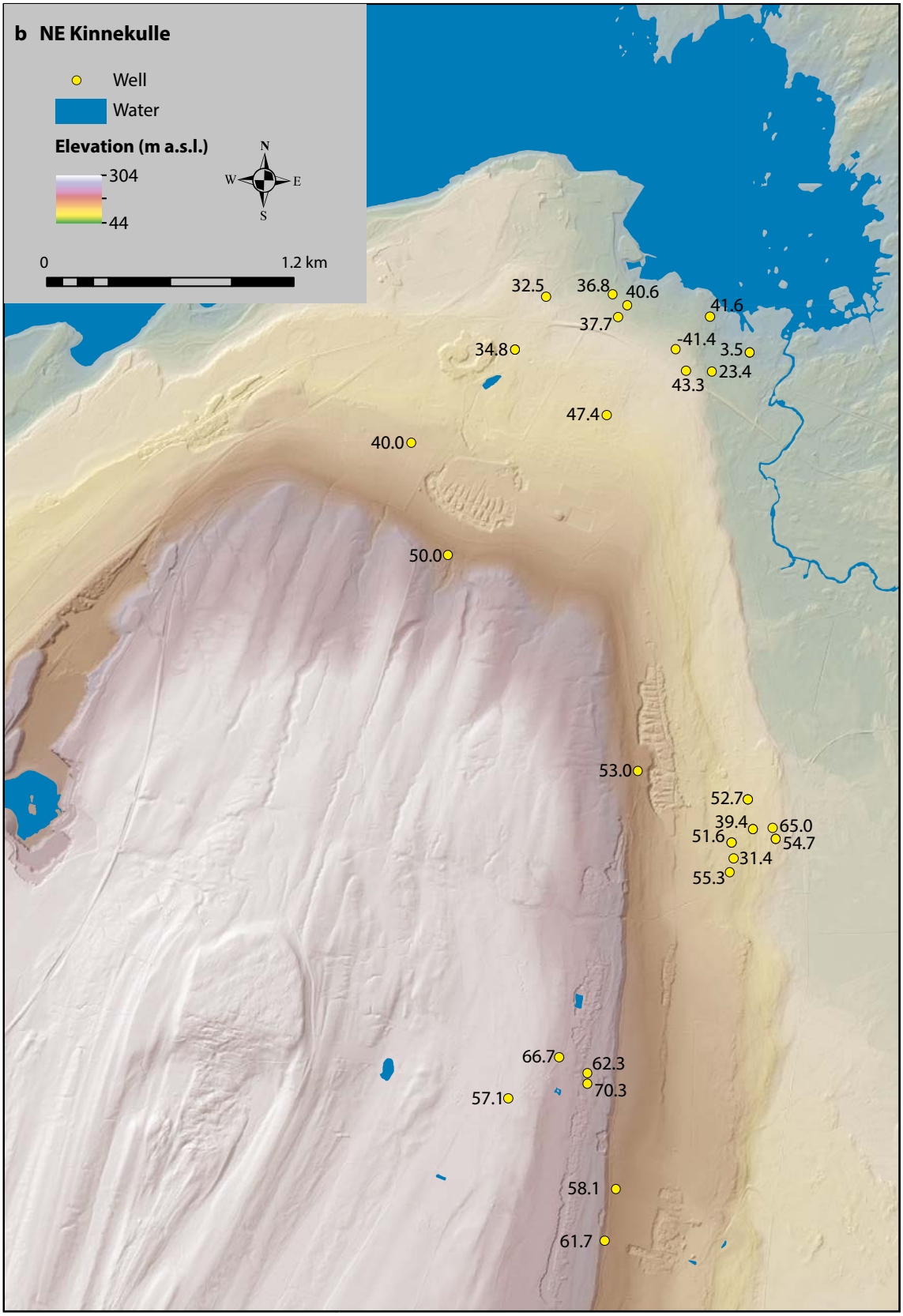

Figure 5-27. Continuing.

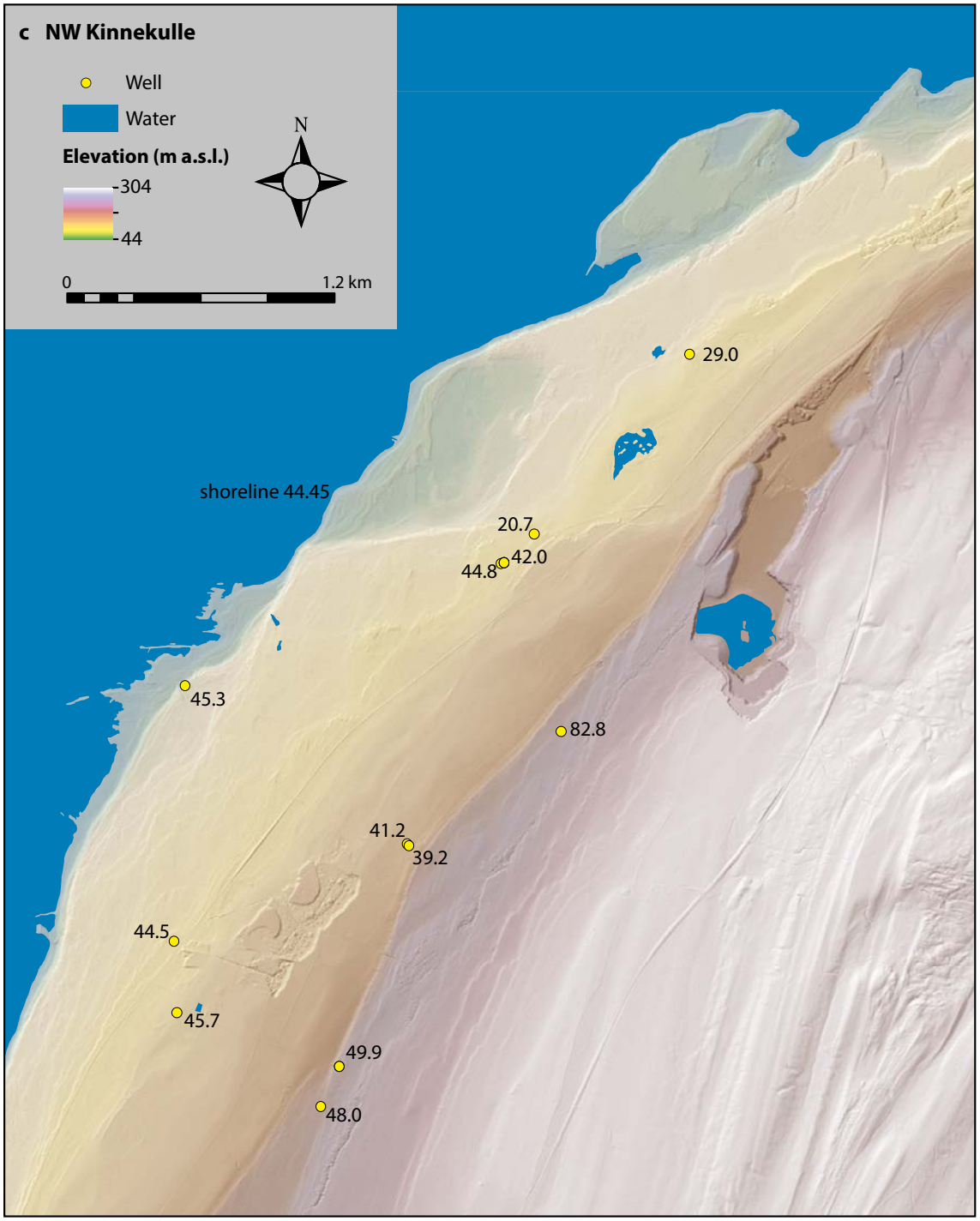

Figure 5-27. *Continuing.*

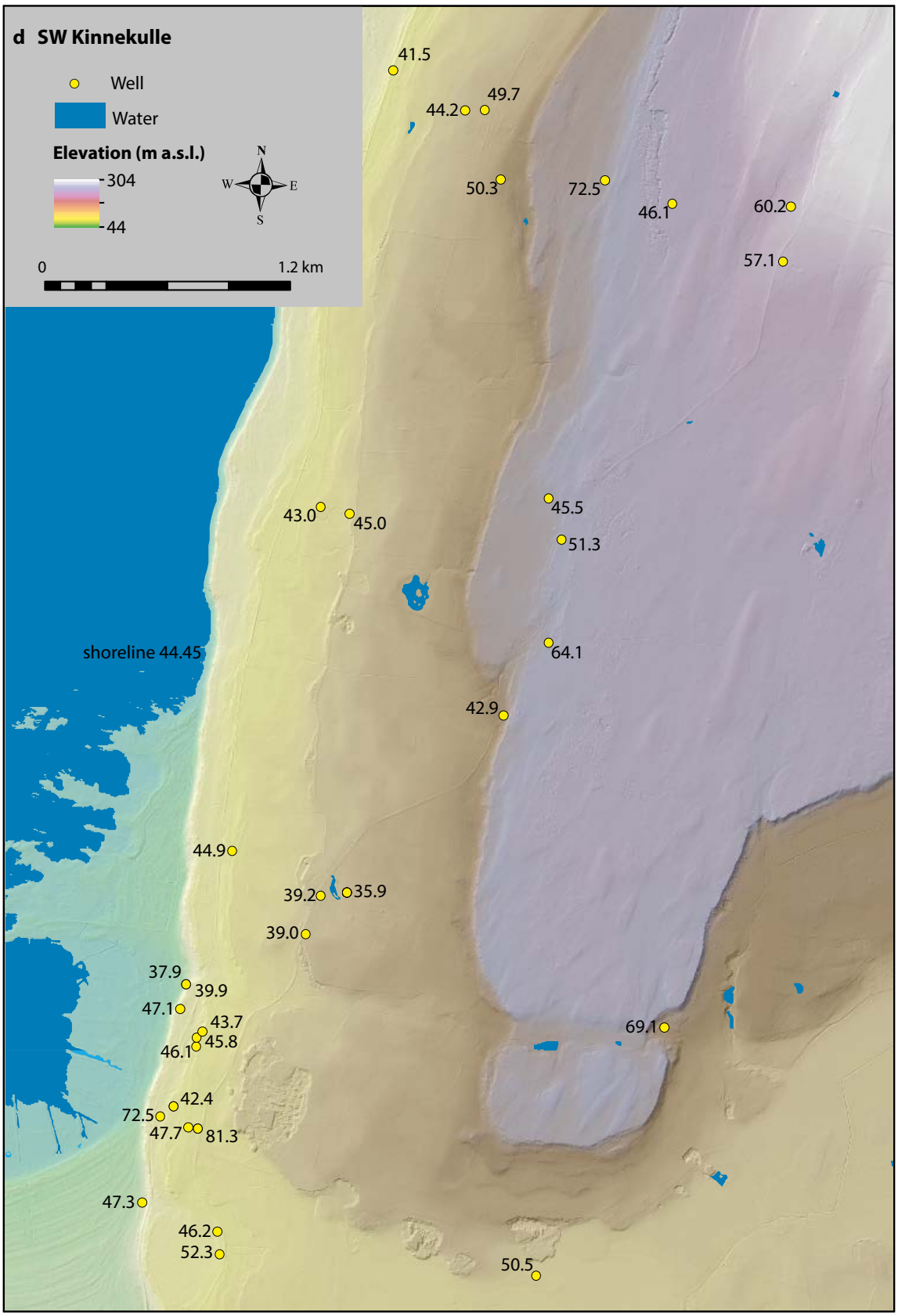

Figure 5-27. *Continuing.*

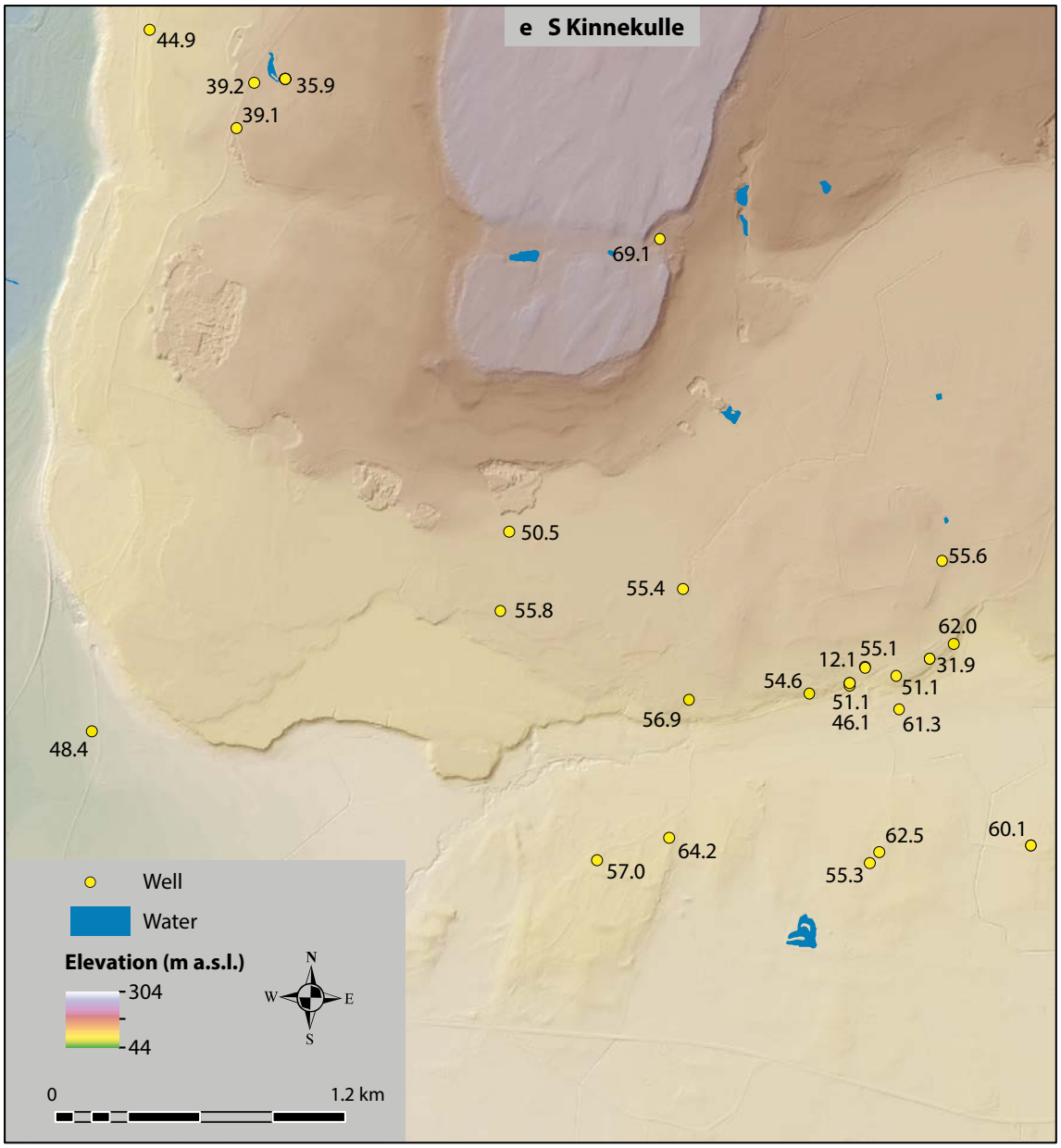

Figure 5-27. *Continuing.*

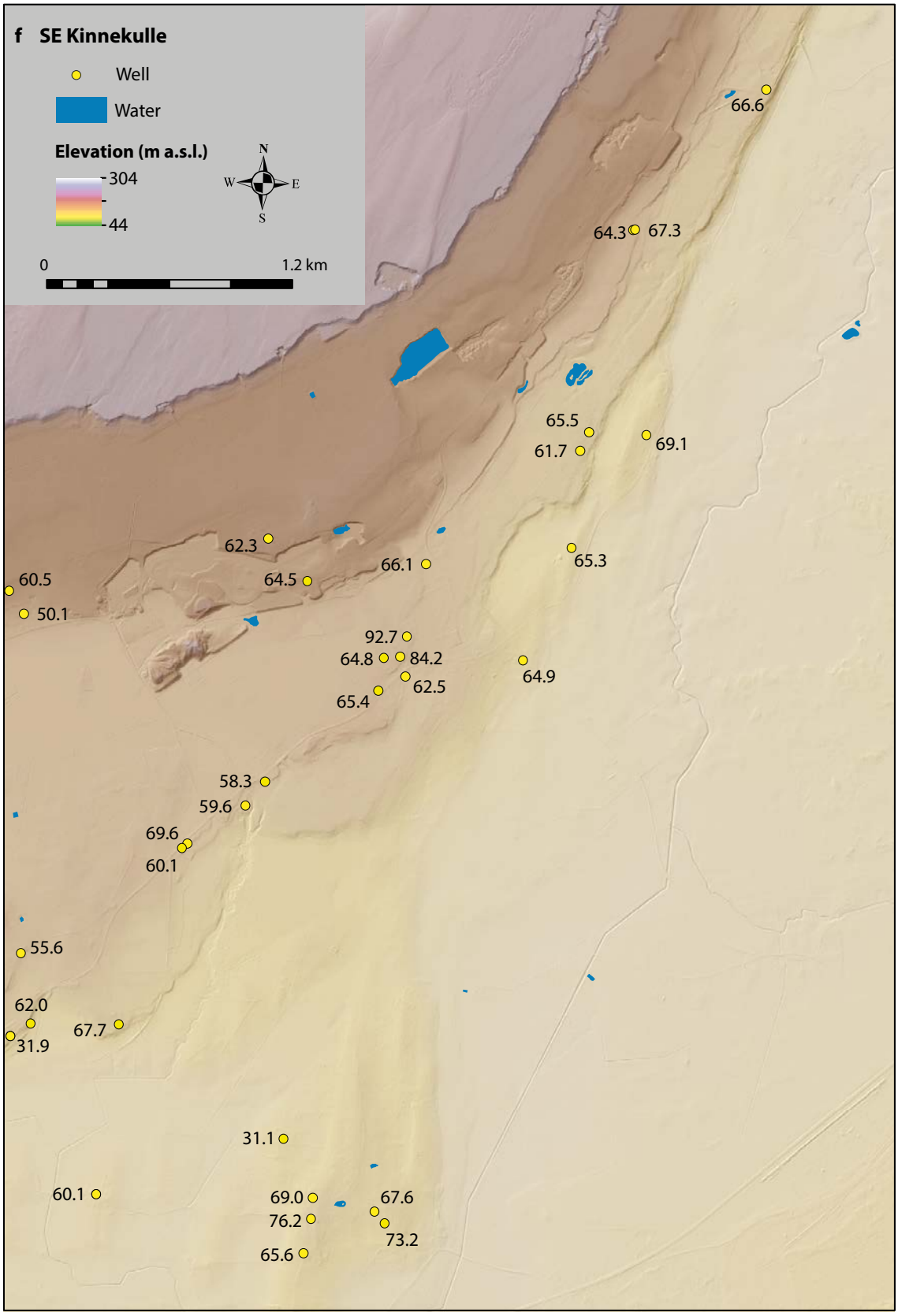

Figure 5-27. *Continuing.*

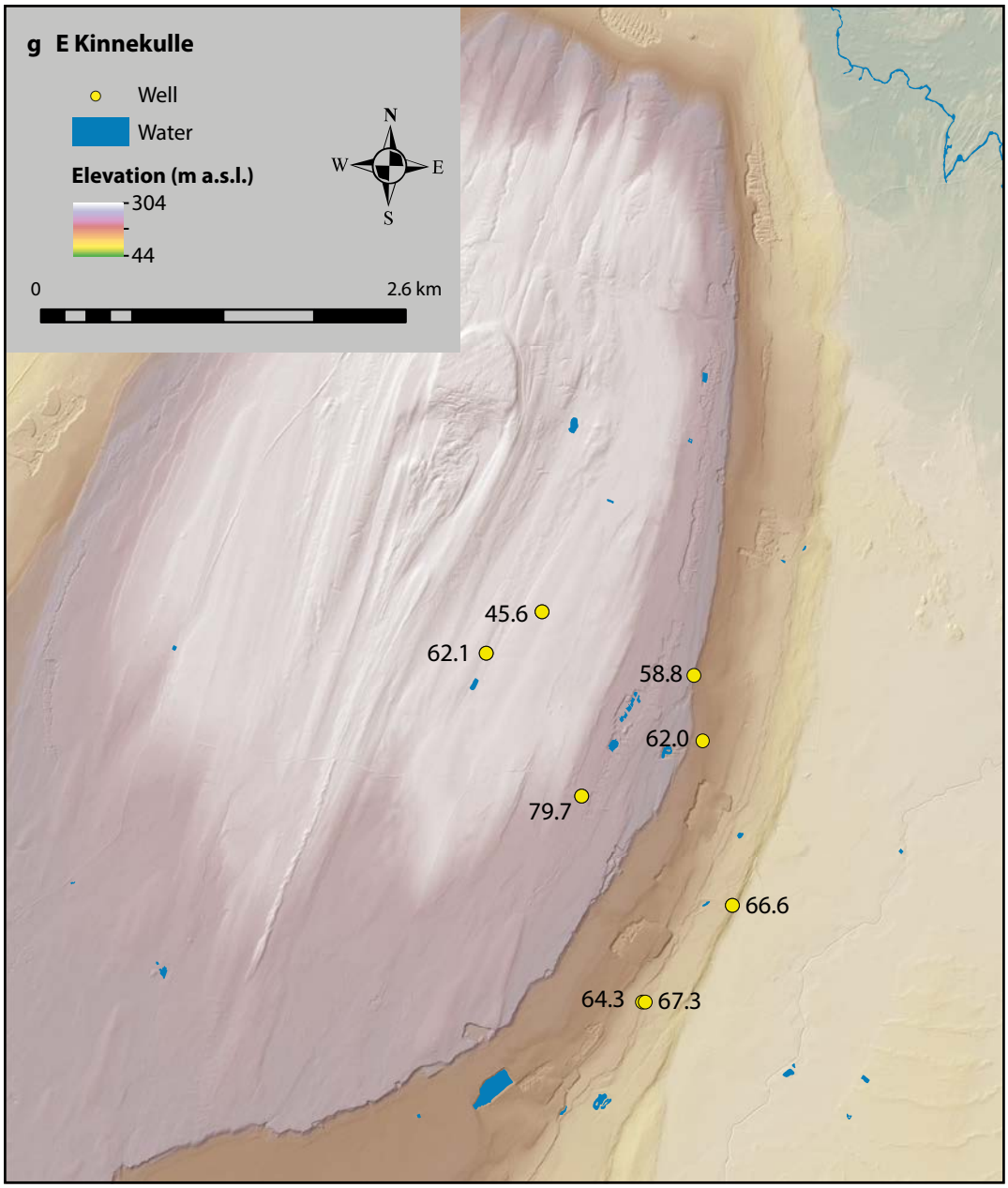

Figure 5-27. *Continuing.*

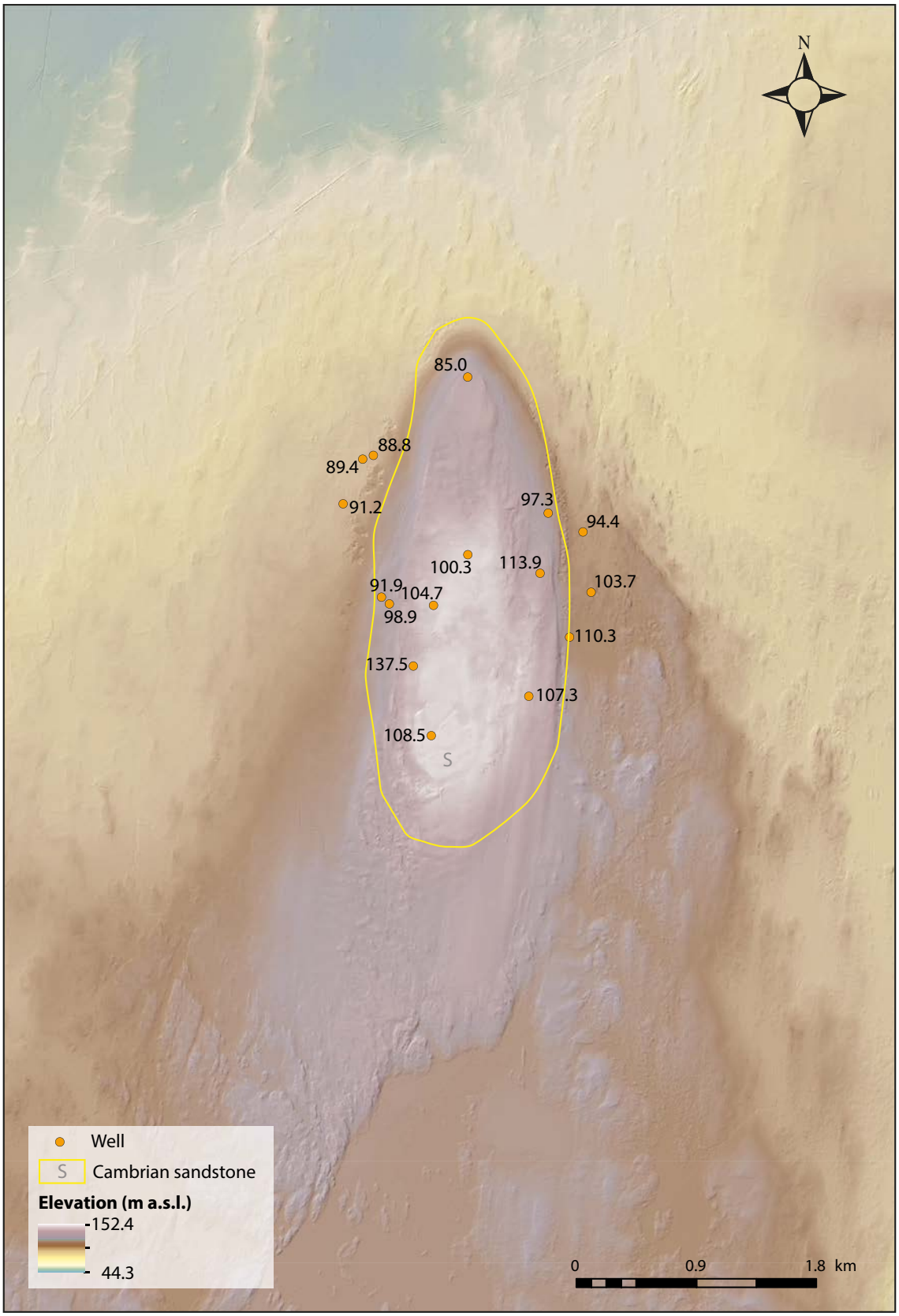

Figure 5-28. *Elevations of the SCP beneath the table mountain at Lugnås. Values are derived from the well log archive at the Geological Survey of Sweden. Depths to basement are subtracted from surface elevations at each point.*

5.5 Exposure ages

The dataset collected for the purpose of understanding the long-term erosional history of conspicuously flat bedrock outcrops in the Trollhättan area consists of 13 samples, three of which were sampled in 2000 (MJ-13 to MJ-15), and the results of which were listed but not discussed in Stroeven et al. (2016), and ten of which were sampled in 2016 (TROLL-16-04 to TROLL-16-10) and 2017 (TROLL-17-01 to TROLL-17-03). The samples derive from four different but closely-spaced geographical areas (Figure 5-29). Two of the areas flank the twin table mountains of Halleberg and Hunneberg.

Table 5-1 presents key exposure age data for the full set of samples. All sample details and exposure age calculations are found in a supplementary file (1900552_supplementary_information_cosmogenic_dating_tr-19-22.zip[4]). Simple ^{10}Be (^{26}Al) exposure ages range from 6.8 ± 1.4 ka (7.0 ± 1.4 ka) to 44.7 ± 2.8 ka (46.3 ± 3.5 ka), with nine samples being younger than 14 ka (15 ka) and the remaining four samples being older than 24 ka (19 ka). Compared to expected deglaciation exposure ages, taking into account post-glacial submergence, there are two ^{10}Be measurements and two ^{26}Al measurements that are too young, three ^{10}Be measurements and four ^{26}Al measurements that overlap within uncertainties with the expected deglaciation exposure age, and eight ^{10}Be measurements and seven ^{26}Al measurements that are too old due to prior exposure.

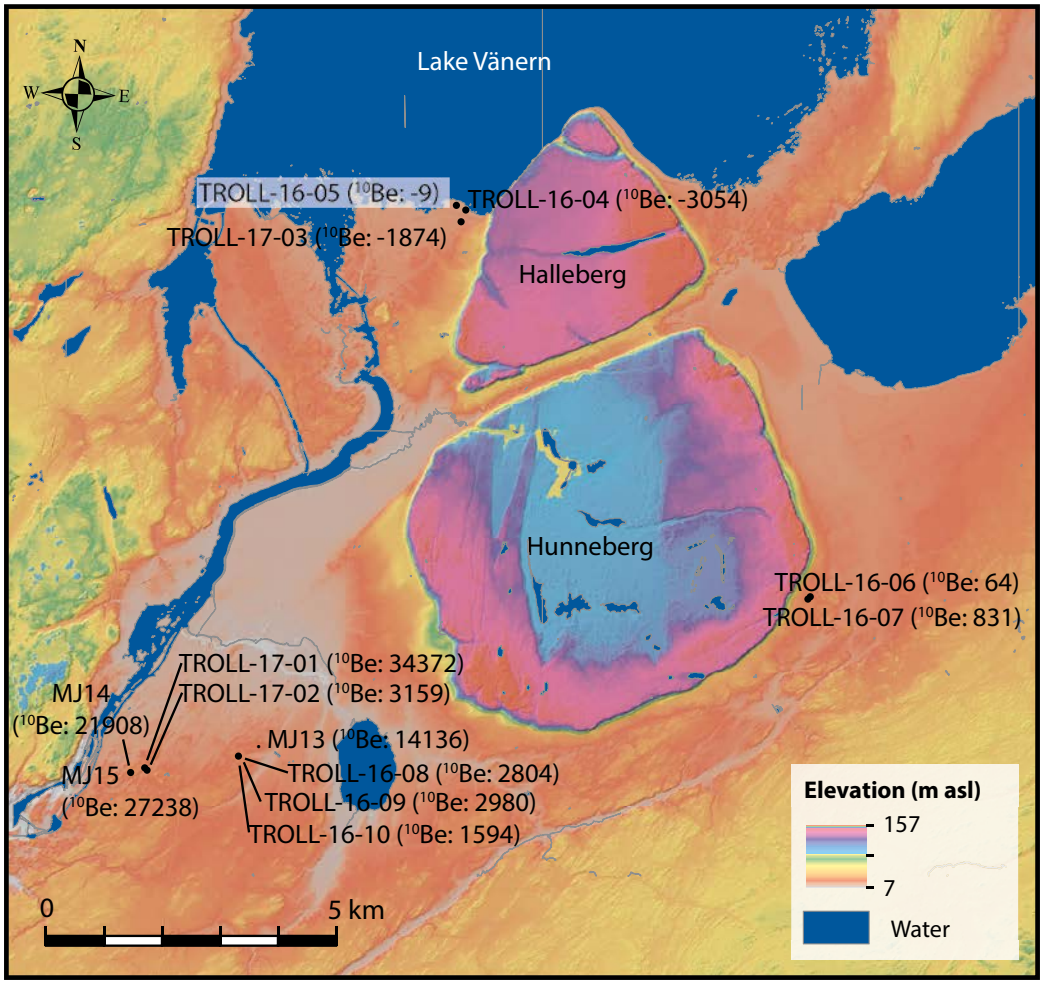

Figure 5-29. *Topographic map of the investigation area around Trollhättan, including the distribution of cosmogenic nuclide samples with sample names and ^{10}Be inheritance, defined as the difference between simple exposure age and expected exposure age based upon a reconstructed deglaciation age (Stroeven et al. 2016) and a reconstructed history of uplift through water from Björck and Digerfeldt (1982) (Figure 5-30). The topographic map is derived from the 2 m resolution LiDAR elevation model.*

[4] Can be downloaded from www.skb.se/publications. Direct link: http://www.skb.com/publication/2495089/

Table 5-1. Summary of ^{10}Be and ^{26}Al exposure age data for thirteen samples. The exposure ages are calculated assuming one single period of full exposure at the surface. ^{10}Be and ^{26}Al exposure age mismatches arise when they differ from theoretical simple exposure deglaciation ages, assuming no inheritance and considering the effect of post-glacial submergence. Deglaciation, emergence, and exposure ages are all related to the year of sampling (2000, 2016, 2017).

Sample	Elevation (m a.s.l.)	Deglaciation (yr)	Emergence (yr)	^{10}Be exposure age (yr)	^{10}Be exposure age mismatch (yr)	^{26}Al exposure age (yr)	^{26}Al exposure age mismatch (yr)
TROLL-16-04	45	13 452	9 615	6 771 ± 1 354	−3 054	10 273 ± 1 823	444
TROLL-16-05	45	13 452	9 615	9 817 ± 1 338	−9	7 021 ± 1 387	−2 809
TROLL-16-06	53	13 424	10 230	10 408 ± 911	64	10 078 ± 1 229	−270
TROLL-16-07	53	13 424	10 230	11 175 ± 855	831	10 238 ± 1 066	−110
TROLL-16-08	52	13 668	10 175	13 078 ± 1 132	2 804	14 242 ± 1 327	3 965
TROLL-16-09	52	13 668	10 175	13 254 ± 1 035	2 980	13 087 ± 1 277	2 810
TROLL-16-10	52	13 668	10 175	11 867 ± 945	1 594	13 719 ± 1 373	3 442
TROLL-17-01	53	13 703	10 231	44 707 ± 2 797	34 372	46 260 ± 3 507	35 922
TROLL-17-02	51	13 703	10 115	13 385 ± 1 003	3 159	11 841 ± 1 613	1 612
TROLL-17-03	47	13 453	9 823	8 123 ± 589	−1 874	8 891 ± 863	−1 110
MJ-13	51	13 635	10 101	24 371 ± 1 481	14 136	18 978 ± 1 819	8 741
MJ-14	54	13 686	10 270	32 283 ± 3 534	21 908	18 916 ± 2 269	8 538
MJ-15	54	13 686	10 270	37 612 ± 2 278	27 238	33 133 ± 2 713	22 755

West of Halleberg, on the southern shore of Lake Vänern, at Nordkroken, samples TROLL-16-04 and TROLL-16-05 were sampled from platforms at lake level (at 45 m a.s.l.), whereas sample TROLL-17-03 was derived from behind a sand dune on a platform that is currently used as a carpark (at 47 m a.s.l.). The latter sample appeared undisturbed from erosion by car traffic, but since the whole surface, at some point, also appears to have been cleared of a thin sediment cover to allow for the car park, cosmogenic nuclide results would potentially underestimate the time of postglacial exposure. The simple exposure ^{10}Be (^{26}Al) ages of these samples are 6.8 ± 1.4 ka (10.3 ± 1.8 ka), 9.8 ± 1.3 ka (7.0 ± 1.4 ka), and 8.1 ± 0.6 ka (8.9 ± 0.9 ka) for sites just above the current Lake Vänern water level. Interestingly, two of the sites (TROLL-16-04 and TROLL-17-03) underestimate our expectations for ^{10}Be by 2–3 ka, whereas one site (TROLL-16-05) is spot-on (Figure 5-30). The congruence between expected and measured age for the latter site yields some confidence to our ability to predict exposure ages using reconstructed deglaciation ages and a shoreline uplift curve.

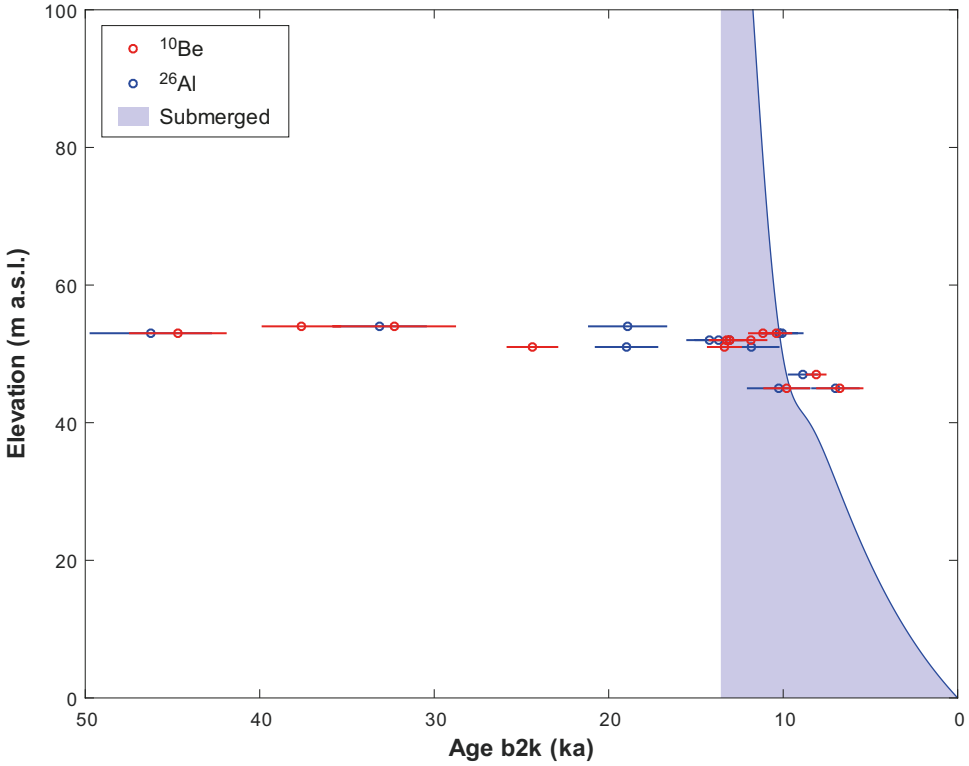

Figure 5-30. *Simple ^{10}Be and ^{26}Al exposure ages, assuming one period of full exposure to cosmic rays, against sample elevation. The blue line and area show the shoreline displacement of Björck and Digerfeldt (1982) and the post-glacial period of submergence, respectively. Surfaces that experienced glacial erosion deep enough to remove the inventory of cosmogenic nuclides overlap within uncertainty with the shoreline displacement curve. Data points that fall to the right of the shoreline displacement curve have cosmogenic nuclide concentrations lower than expected assuming full exposure to cosmic rays following emergence. Data points that fall to the left of the shoreline displacement curve have inherited cosmogenic nuclides from exposure to cosmic rays prior to the last glaciation.*

The second area, near Bragnum, is located 200 m southeast of the base of Hunneberg (Figure 5-29). Here we sampled two convex surfaces protruding above the surrounding farm fields at 53 m a.s.l. and located about 50 m from each other. These two samples, TROLL-16-06 and TROLL-16-07, yielded apparent full exposure ^{10}Be ages of 10.4 ± 0.9 ka, 11.2 ± 0.9 ka, respectively. These exposure ages are consistent with each other and overlap with the expected exposure age within uncertainties for both ^{10}Be and ^{26}Al (Figure 5-30).

The remaining two investigation areas are located within the city limits of Trollhättan (Figure 5-29). The area of Hjortmossen, nearest to the center of town was visited in 2000 and in 2017 for sampling. Sites of samples taken from the edge of the summit flat in 2000 (MJ-14 and MJ-15) are today covered by an indoor hockey rink and could not be inspected in 2017. Of these, MJ-15 was from the summit flat proper (54 m a.s.l.), and MJ-14 was taken from a pegmatite vein set 40 cm below the summit flat in what appeared to be a plucking scarp. To align these earlier measurements with samples from 2017, we re-sampled the summit flat on another side of the hockey rink (TROLL-17-01; 53 m a.s.l.), just above a pronounced slope, and the slope 2 m below the summit flat (TROLL-17-02). The results from 2000 and 2017 paint a consistent picture (Table 5-1). The two surface flat samples yielded simple exposure ^{10}Be (^{26}Al) ages of 37.6 ± 2.3 ka (33.1 ± 2.7 ka) and 44.7 ± 2.8 ka (46.3 ± 3.5 ka), whereas sample MJ-14, inset slightly below the surface flat, yielded 32.3 ± 3.5 ka (18.9 ± 2.3 ka). All three sites have concentrations well above those consistent with local deglaciation (including corrections for submergence; Figure 5-30). When inheritance concentrations are expressed as simple exposure ages (as if they were produced by continuous exposure at the locations studied), these three sites have 22–36 ka of inheritance for all nuclides apart from one ^{26}Al measurement with 8.5 ka of inheritance (Table 5-1; Figure 5-29). The fourth site, 2 m below the summit flats, has a simple exposure age much closer to deglaciation, with only 3 ka of ^{10}Be inheritance, and which almost overlaps within uncertainty with the expected ^{26}Al exposure age (Table 5-1).

The final investigation area is located at Sandhem and was sampled in 2000 and 2017. (Figure 5-29). The sampling of a thin layer of vein quartz at 51 m a.s.l. in 2000 (MJ-13) yielded a simple ^{10}Be (^{26}Al) exposure age of 24.4 ±1.5 ka (19.0 ±1.8 ka). The three samples (TROLL-16-08, TROLL-16-09, TROLL-16-10) from the fenced-in area used for storage of waste sediment have simple ^{10}Be (and ^{26}Al) exposure ages that all overlap with each other within uncertainty of 13.1 ±1.1 ka (14.2 ±1.3 ka), 13.3 ±1.0 ka (13.1 ±1.3 ka), and 11.9 ±0. 9 ka (13.7 ±1.4 ka); 52 m a.s.l.). Given identical expected exposure ages, inheritance varies by 1.6–3.0 ka (2.8–4.0 ka) between these samples (Figure 5-30). In contrast, these samples do not overlap with the simple exposure age of sample MJ-13, which displays a higher ^{10}Be (^{26}Al) inheritance of 14.1 ka (8.7 ka).

The ^{10}Be and ^{26}Al data show similar patterns for the investigated sites (Table 5-1; Figure 5-30). For the samples collected in 2016 and 2017, with ^{26}Al measurements improved by the use of a gas-filled magnet at PRIME Lab, the difference between the simple ^{10}Be and ^{26}Al exposure ages is less than 1 ka for all but one sample (TROLL-17-03), where only 3 g of clean quartz was dissolved. For the remaining four samples (TROLL-17-03 and MJ-13, MJ-14, and MJ-15, which were measured without a gas-filled magnet), the difference between the simple ^{10}Be and ^{26}Al exposure ages range from 1.6 ka to 13.3 ka.

In summary, sites on the summits or flanks of the CFSs, and at Bragnum, display exposure histories that range from requiring post-glacial shielding (n = 2; Nordkroken) through samples for which the full cosmogenic nuclide inventory can be explained by post-glacial exposure (n = 3–4; Nordkroken and Bragnum plus one ^{26}Al measurement for Sandhem), to samples with varying amounts of inheritance. In the latter category are those with minor amounts of inheritance (1.6–4.0 ka, n = 6; Bragnum, Hjortmossen flank, and Sandhem storage sites) to those with considerable amounts of inheritance at Hjortmossen summit flat and Slättbergen samples (n = 4; 8.5–36 ka). All five samples collected near the Halleberg-Hunneberg table mountains have cosmogenic nuclide concentrations that overlap with or are lower than expected for only post-glacial cosmogenic nuclide exposure, while all samples from Trollhättan some kilometers away from the table mountains (except for one ^{26}Al measurement) have inheritance from prior exposure.

5.6 Glacial erosion

The glacial erosion simulations yield output ranging from 0.3 m erosion over the last 100 ka to unlimited glacial erosion (>10 m). Figures 5-31 to 5-34 display the simulated erosion histories including sensitivity analyses for the erosion simulations (Figure 5-31) for the full set of samples that yield a solution, for all scenarios (Table 4-1), and for ^{10}Be only (Figure 5-32), ^{26}Al only (Figure 5-33), and combined ^{10}Be and ^{26}Al simulations (Figure 5-34). Calculation details are found in a supplementary file (1900552_supplementary_information_cosmogenic_dating_tr-19-22.zip[5]).

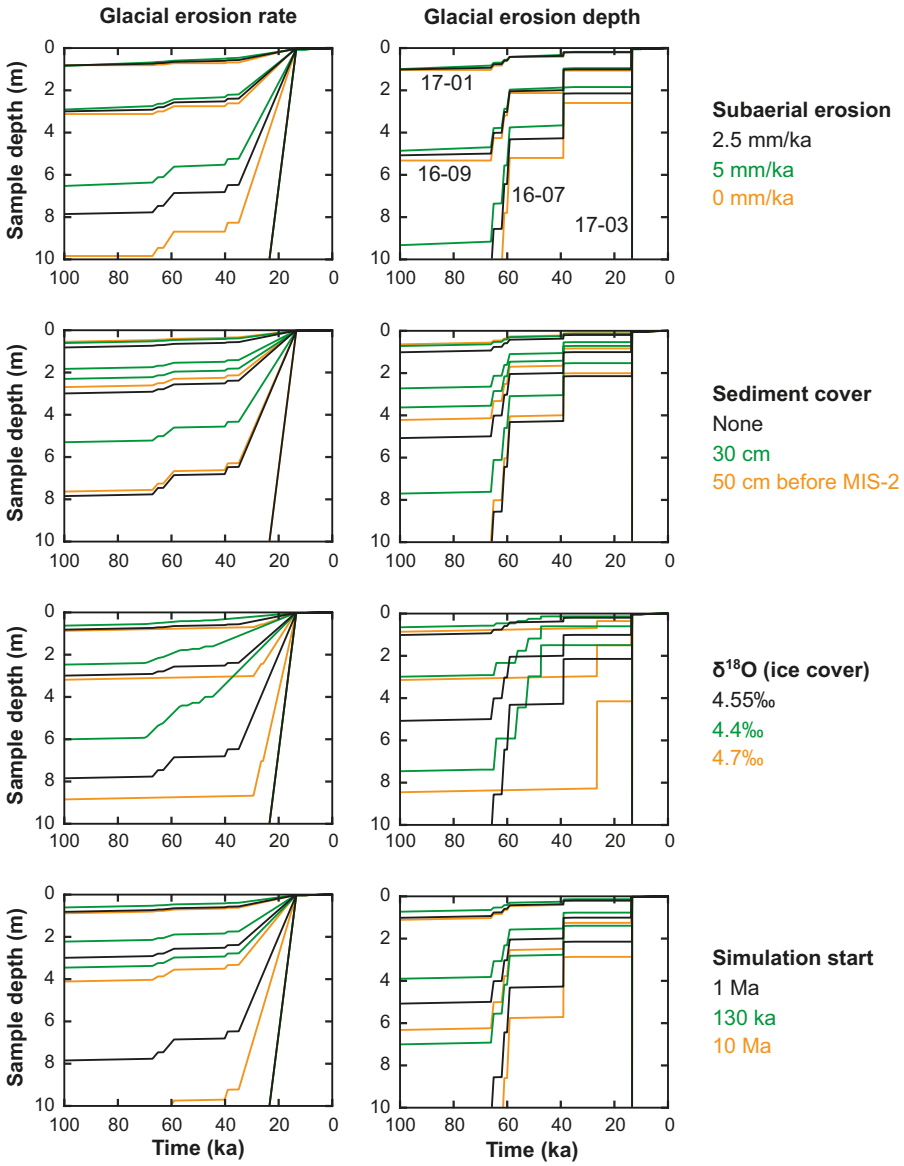

Figure 5-31. *Sensitivity tests of the erosion simulation. Each panel shows the simulated erosion (sample depth history) over the last 100 ka for four samples (TROLL-16-07, 16-09, 17-01, and 17-03) and three scenarios based on ^{10}Be concentration. The black lines show the erosion of the reference scenario, as defined by four reference parameters, with constant glacial erosion rate (left panels) and constant glacial erosion depth (right panels). The green and yellow lines show the erosion when perturbing one of the four parameters: subaerial erosion rate, sediment cover, $\delta^{18}O$ cut-off value, and simulation start. For the predetermined parameter space, the erosion is generally more sensitive to perturbations of the ice cover history and simulation start point than to perturbation of the subaerial erosion rate. Whereas 30 cm sediment cover (density: 2.0 g cm^{-3}) until just before sampling yields significant erosion difference, 50 cm sediment cover prior to the MIS-2 glaciation only has a limited effect on the erosion.*

[5] Can be downloaded from www.skb.se/publications. Direct link: http://www.skb.com/publication/2495089/

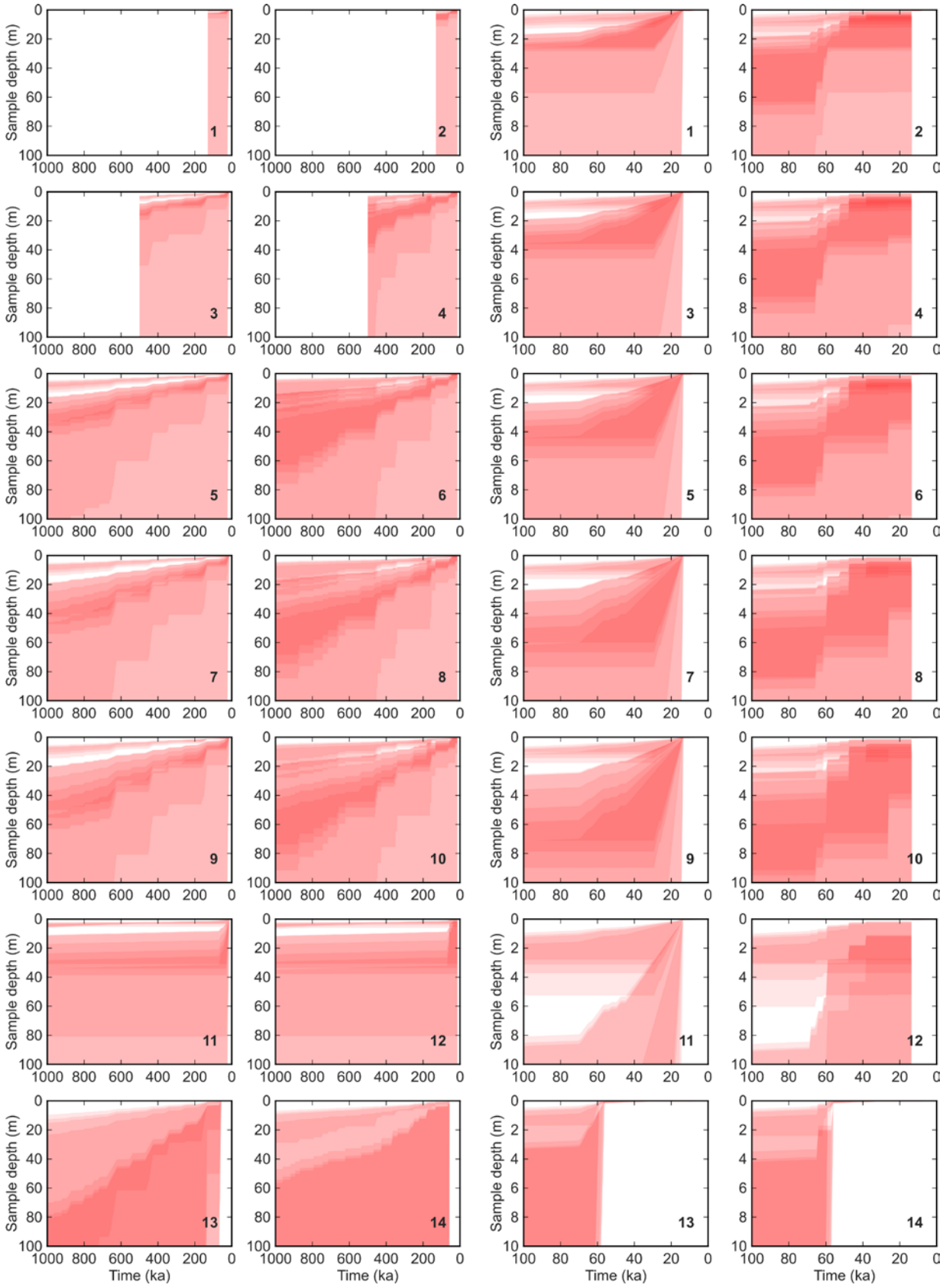

Figure 5-32. *Erosion simulation output for ^{10}Be simulations. Each simulated individual sample depth range is shown with 90 % transparency so that overlapping sample depths yield darker areas. The bold number in the lower right corner of each panel shows the simulation scenario number (Table 4-1). Odd number scenarios (columns one and three) involve constant erosion rate simulations and even number scenarios (columns two and four) involve constant erosion depth simulations. The two left panels show the sample depth history over the last 1 Ma and the two right panels show the sample depth history over the last 100 ka.*

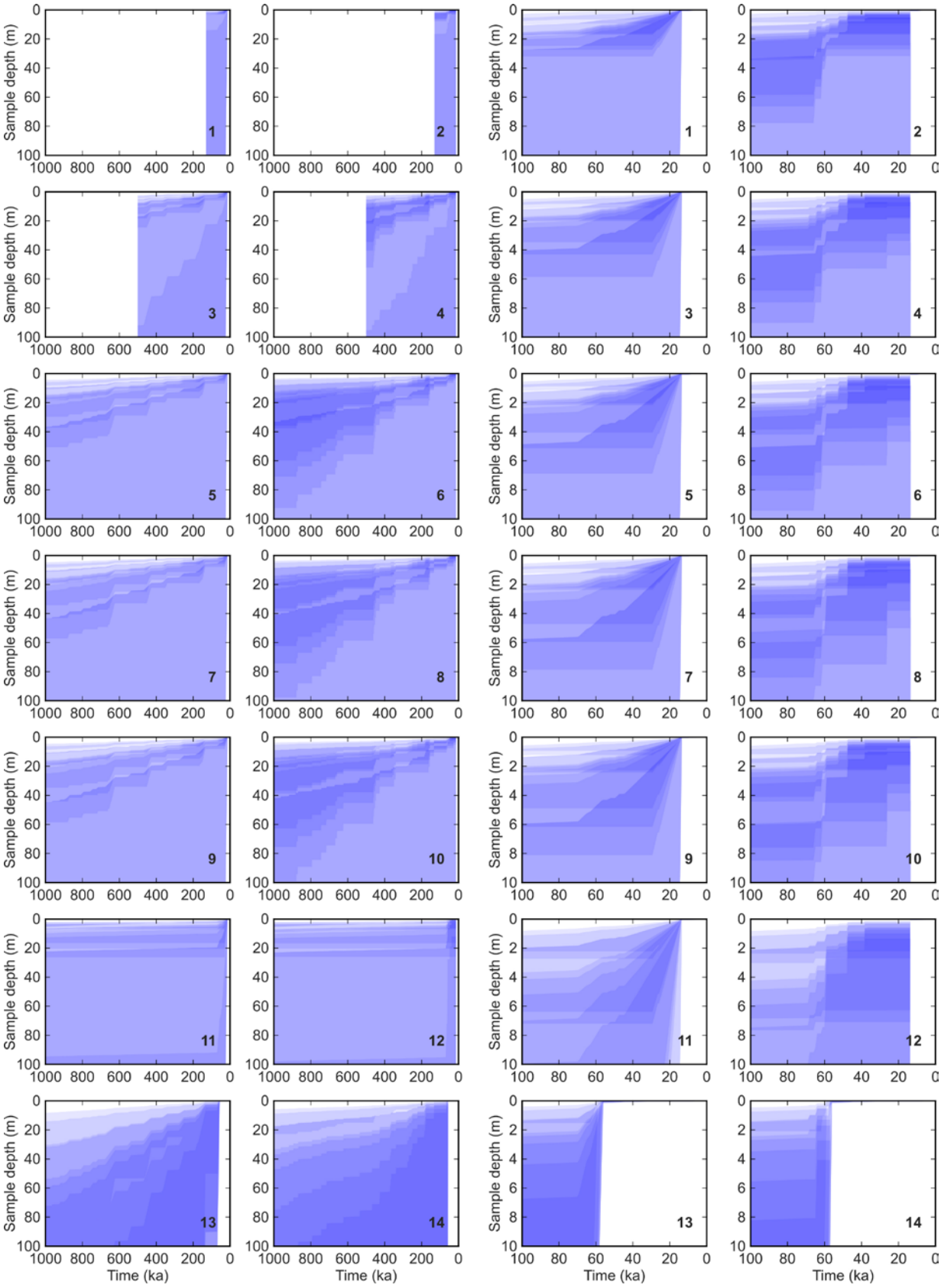

Figure 5-33. *Erosion simulation output for ^{26}Al simulations. Each simulated individual sample depth range is shown with 90 % transparency so that overlapping sample depths yield darker areas. The bold number in the lower right corner of each panel shows the simulation scenario number (Table 4-1). Odd number scenarios (columns one and three) involve constant erosion rate simulations and even number scenarios (columns two and four) involve constant erosion depth simulations. The two left panels show the sample depth history over the last 1 Ma and the two right panels show the sample depth history over the last 100 ka.*

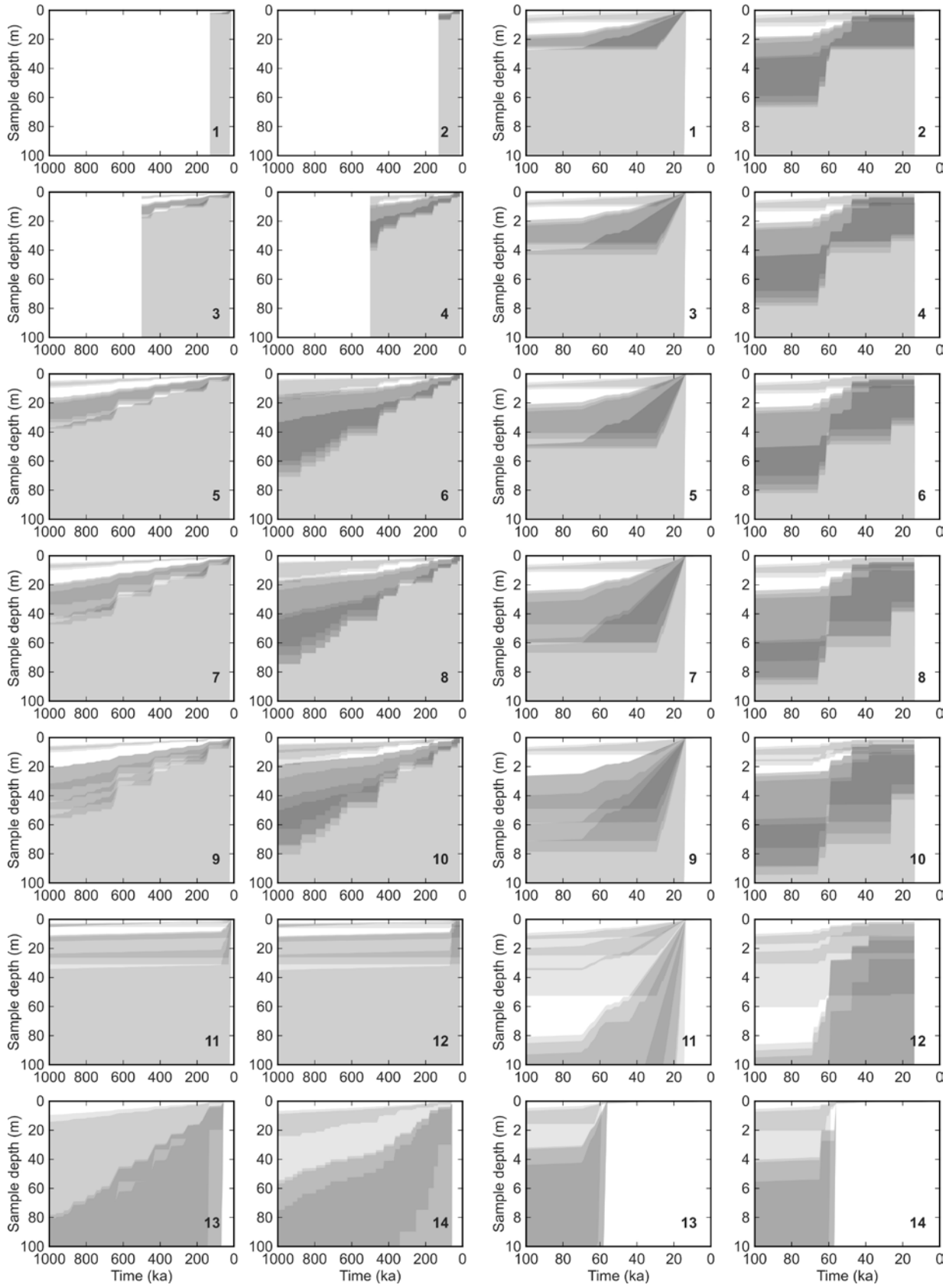

Figure 5-34. *Erosion simulation output for combined ^{10}Be and ^{26}Al simulations. Each simulated individual sample depth range is shown with 90 % transparency so that overlapping sample depths yield darker areas. The bold number in the lower right corner of each panel shows the simulation scenario number (Table 4-1). Odd number scenarios (columns one and three) involve constant erosion rate simulations and even number scenarios (columns two and four) involve constant erosion depth simulations. The two left panels show the sample depth history over the last 1 Ma and the two right panels show the sample depth history over the last 100 ka.*

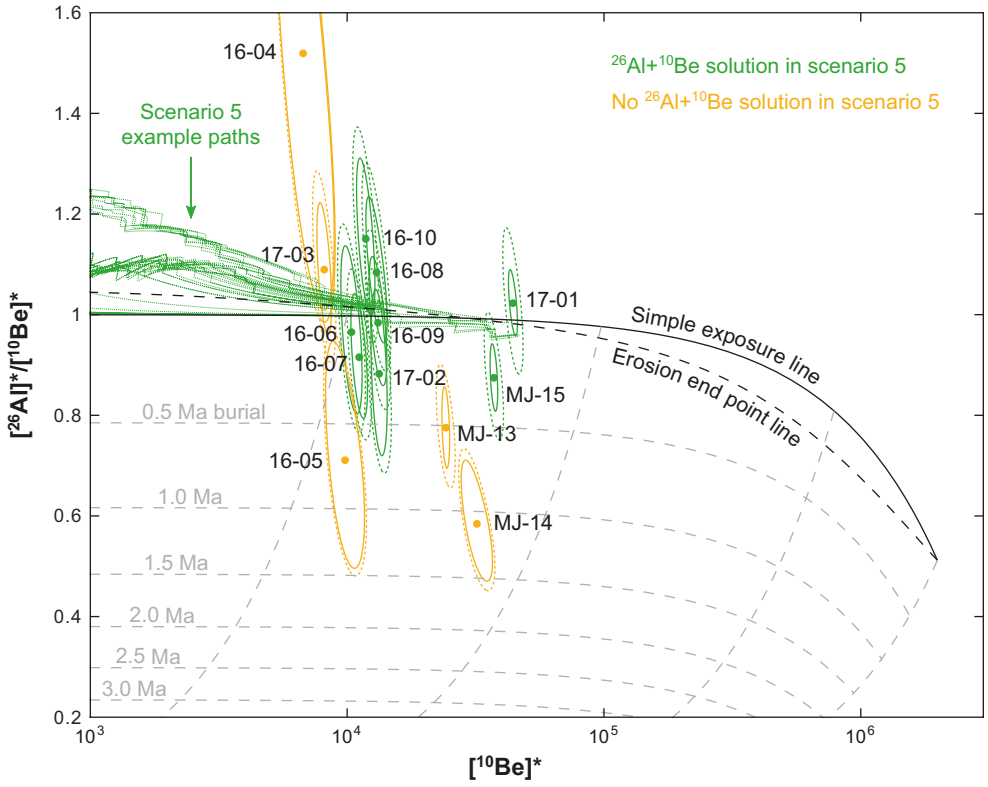

Figure 5-35. *Sample $^{26}Al/^{10}Be$ ratios with sample ^{10}Be and ^{26}Al concentrations normalized against long-term average surface ^{10}Be and ^{26}Al production rates. The simple exposure line shows the theoretical path under full exposure at the surface. The erosion end point line shows the theoretical surface ratios for various constant erosion rates. The sub-horizontal dashed curves show theoretical $^{26}Al/^{10}Be$ ratios after initial full exposure at the surface followed by burial (no cosmogenic nuclide production). The sub-vertical dashed curves show the path of $^{26}Al/^{10}Be$ ratios if buried after 10 ka, 100 ka, 1 Ma, and 10 Ma of exposure. The ellipses around the sample ratios show the uncertainty from measurement only (solid lines) and with production rate uncertainty added (dashed lines). The example paths coming in from the left edge show five examples of the $^{26}Al/^{10}Be$ ratio development for each sample that yield a solution for the combined ^{10}Be and ^{26}Al simulation with scenario 5, including the examples that yield the minimum and maximum end-point $^{26}Al/^{10}Be$ ratios. The elevated $^{26}Al/^{10}Be$ ratios at the left edge of the plot is caused by the elevated $^{26}Al/^{10}Be$ ratios due to increased importance of muogenic production at depth.*

For all five samples from Nordkroken and Bragnum, whose concentrations overlap with, or are lower than, concentrations expected from postglacial exposure, there is no upper limit of the potential glacial erosion in all erosion scenarios using either ^{10}Be or ^{26}Al (Figures 5-32 and 5-33). For the three ^{10}Be (^{26}Al) measurements with exposure ages overlapping with the expected post-glacial exposure age, the minimum total erosion over the last 100 ka ranges from 2.2 to 3.1 m (2.0–3.3 m) for scenarios 1–2 (simulation start at 130 ka) and from 4.0 to 7.1 m (3.2–6.0 m) for scenarios 9–10 (simulation start at 10 Ma). With the combined ^{10}Be and ^{26}Al simulations (Figures 5-34 and 5-35), only the two Bragnum samples yield a solution, with minimum total erosion over the last 100 ka ranging from 2.7 to 2.8 m for scenarios 1–2 and ranging from 5.5 to 7.1 m for scenarios 9–10.

For the three samples from the fenced-in area at Sandhem, the total erosion over the last 100 ka based on ^{10}Be (^{26}Al) measurements ranges from 1.7 to 11.2 m (1.5–7.7 m) for scenarios 1–2 and from 2.5 to 20.9 m (2.0–10.5 m) for scenarios 9–10 (Figures 5-32 and 5-33). Sample TROLL-17-02, from the slope below the summit flat at Hjortmossen, which has a similar amount of ^{10}Be inheritance as the three samples from the fenced-in area at Sandhem, yields a similar total erosion based on ^{10}Be ranging from 1.7 to 6.3 m for scenarios 1–2 and from 2.4 to 8.7 m for scenarios 9–10. With the combined ^{10}Be and ^{26}Al simulations (Figures 5-34 and 5-35), the three Sandhem samples yield total erosion over the last 100 ka ranging from 1.7 to 6.7 m for scenarios 1–2 and from 2.5 to 9.6 m for scenarios 9–10.

For the four samples from Hjortmossen and Sandhem with the highest cosmogenic nuclide inheritance, total erosion over the last 100 ka based on ^{10}Be (^{26}Al) measurements ranges from 0.3 to 2.1 m (0.3–3.5 m) for scenarios 1–2 and from 0.6 to 2.8 m (0.6–4.4 m) for scenarios 9–10 (Figures 5-32 and 5-33). With the combined ^{10}Be and ^{26}Al simulations (Figures 5-34 and 5-35), the samples that yield a solution have total erosion over the last 100 ka ranging from 0.3 to 1.1 m for scenarios 1–2 and 0.6 to 1.9 m for scenarios 9–10.

The end-member scenarios 11–14 generally yield more glacial erosion compared to the constant glacial erosion depth/rate scenarios 1–10 (Figures 5-32 to 5-34). For the simulations without glacial erosion between 10 Ma and 130 ka (scenarios 11–12), the four samples with most cosmogenic nuclide inheritance yield total erosion over the last 100 ka based on ^{10}Be (^{26}Al) ranging from 0.9 to 6.1 m (0.8–7.7 m). The remaining samples that yield a solution for these scenarios indicate minimum total erosion over the last 100 ka based on ^{10}Be (^{26}Al) ranging from 8.1 to 32.2 m (3.7–92.0 m). For the simulations without glacial erosion after 55 ka (scenarios 13–14), the four samples with most cosmogenic nuclide inheritance yield minimum total erosion over the last 100 ka based on ^{10}Be (^{26}Al) ranging from 0.5 to 1.1 m (0.4–1.5 m), and unlimited maximum total erosion. The remaining samples that yield a solution for these scenarios indicate minimum total erosion over the last 100 ka based on ^{10}Be (^{26}Al) ranging from 2.9 to 40.3 m (2.2–5.6 m).

Similar to the glacial erosion simulations for the Forsmark area (Hall et al. 2019a), the constant glacial erosion depth simulations commonly yield somewhat deeper glacial erosion compared to the constant glacial erosion rate simulations. This is an effect of the resulting erosion history with total glacial erosion either scaling directly against duration of ice cover (erosion rate) or against number of ice cover periods (erosion depth). To summarize, the glacial erosion of the Trollhättan samples based on cosmogenic ^{10}Be and ^{26}Al measurements indicate glacial erosion over the last glacial cycle ranging from decimeter-scale up to several meters, and potentially more than 10 m.

6 Discussion

We structure our discussion of the formation of CFSs around three key measurements: (1) GPR reflectors that are consistent with the widespread presence of sheeting joints beneath some but not all measured transects; (2) cosmogenic nuclide concentrations that are consistent with submeter to meters of bedrock erosion over the last glacial cycle and tens of meters of erosion over the Quaternary-to-last 10 Ma; and (3) measurements that indicate that relief is higher adjacent to, and beneath cover rock remnants, than on the CFSs. We also incorporate circumstantial evidence from other sites, which might provide partial analogues, and use all evidence to test our competing hypotheses.

6.1 Spatial relationships between grain sizes, jointing, and near planar bedrock surfaces

Groundtruthing at the Vånga quarry demonstrates that GPR accurately detects subsurface subhorizontal and obliquely-dipping fractures. The apertures of the fractures, identified by strong purple reflections on the GPR images, usually are about a centimeter. Fractures with narrower apertures in some places return faint, yellow, reflections. Not all fractures are detected by GPR, including those with hairline apertures and those located at depth beneath another, strongly reflecting, fracture. Significantly, no prominent reflectors were identified at Vånga that were unlikely to be fractures.

The GPR studies add significant detail to the outcrop observations of sheeting joints. Sheeting joints occur within ~15 m of the surface at many, but not all, of the low-relief outcrops we examined with GPR. The GPR reflectors illustrate sheeting joints commonly extend laterally for as much as many tens of meters, and multiple sheeting joints are also commonly imaged. The reflections observed at Nordkroken, Hjortmossen, and Fågelmara provide strong evidence that the erosional processes might have exploited subhorizontal sheeting joints to develop low-relief surfaces. Surface exposures of subhorizontal joints occur at each of these outcrops, but in all cases are exposed over small lateral distances (meters to more than ten meters). These findings indicate that, where even meager indications of sheeting joints are visible on outcrop surfaces, additional sheeting joints are likely to occur up to at least 15 m below the outcrop surface. Conversely, a complete absence of evidence for sheeting joints on many other outcrop surfaces in Trollhättan, which we did not image with GPR, indicates that sheeting joints are unlikely to be located beneath these outcrops. Sheeting joints in the study areas appear limited to particular rock kernels (here defined as bodies of granitic rock that display coarser grain sizes than the surrounding granite, e.g., Thomas et al. 2004, Goodfellow et al. 2014b), which also display wide spacing of vertical joints and exceptionally flat summits. This contrasts with the ubiquitous presence of sheeting joints in some settings but is similar to their spotty presence in the Cairngorm Mountains, Scotland, where these joints occur only beneath the most convex surfaces (Goodfellow et al. 2014b). It is also illustrative that a gently convex outcrop situated 400 km southeast of Trollhättan, at Fågelmara, also in porphyritic coarse-grained granite that displays wide spacing of subvertical joints, also displays subsurface sheet jointing in GPR reflectors. We therefore consider that there is robust evidence for a relationship between spatially-extensive low convexity summits, porphyritic coarse-grained granitic rocks, meters-scale spacing of subvertical joints, and sheeting joints.

Reflectors inferred to be sheeting fractures commonly abut against subvertical fractures. We take this relationship to mean that sheeting joints commonly either nucleate at subvertical fractures or terminate against them. Reflection patterns we interpret as bifurcations of sheeting joints are also common. These patterns are common for sheeting joints (Martel 2017).

Nordkroken profiles 1 and 2 are the only ones where reflection multiples appeared, which we suspect indicate wide fracture apertures of tens of centimeters. Sheeting joints with similarly-wide apertures have been observed at Forsmark, where they have been injected with glacifluvial sediments (Carlsson 1979), and in other areas, such as Yosemite National Park in California (e.g., Matthes 1930). Perhaps the Nordkroken fractures that display multiple reflections also are filled with sediments injected by glacial processes. However, this remains to be demonstrated.

The most enigmatic outcrops in terms of testing a spatial relationship between sheeting joints and CFSs, are those located at Sandhem and Eriksroparken. At these locations, few fractures were imaged with GPR compared with the other imaged sites (Figures 5-11 to 5-14). At Sandhem, the imaged fractures are subparallel to the most convex outcrop margins, and some appear to intersect the ground surface. However, they are sparsely-distributed and the tens-of-meters long sheeting joints visible on the GPR images of other sites are absent beneath the lower convexity summits of both Sandhem and Eriksroparken. Whereas the present surface of Sandhem may be interpreted as a continuation of the imaged subsurface joints visible in Figures 5-12 and 5-13, no clear relationship emerges between the CFS at Eriksroparken and subhorizontal fractures. This does not necessarily mean subhorizontal fractures are absent. They could be present but be undetected by GPR, either because they have hair-line apertures or because they are located too deep. Furthermore, we tested only a small part of the summit area. Nonetheless, the difference in the GPR images of fractures between these three outcrop summits and the others, where subhorizontal reflectors occur, is notable. This finding has two potential key implications for the generation of CFSs. First, perhaps not all CFSs have formed through erosional exploitational of sheeting joints, as we generally suspect. Second, there may be a temporal evolution in fracturing. For example, an initially short (< 1 m) sheeting joint with a hairline aperture may propagate during glaciation, because of an increase in the magnitude of the maximum horizontal compressive stress attributable to ice sheet loading and possibly also elevated groundwater pressure. These possibilities need to be considered in a process geomorphological explanation of CFSs, whether through Precambrian weathering and erosion or through alternative processes, such as Quaternary glacial erosion.

In exploring alternative processes for the formation of the CFSs, which comprise the flattest bedrock elements of the SCP, and in light of inferred erosion rates from cosmogenic nuclides, we will consider the impact of the Fennoscandian ice sheet on these surfaces. For example, could abrasion maintain exceptional low-relief surfaces? Could subhorizontal fractures be exploited subglacially to either maintain almost-flat relief or even to create flat surfaces below antecedent convex surfaces?

6.2 Conceptual landscape evolution models

6.2.1 Model 1 – Precambrian weathering resulted in conspicuously flat landscape elements

CFSs appear to be developed exclusively in coarse-grained porphyritic granitic rocks (Figures 2-4, 2-6 and 3-2). Granitic rocks can experience rapid physio-chemical weathering to form saprolites, and this might have been even more likely before the evolution of vascular plants because the precipitation of clays, which divert water from vertical to more-horizontal flow paths in weathering rock, were seemingly slower than in modern landscapes (Kennedy et al. 2006). Coarse-grained granitic rocks can disintegrate more quickly than chemically-identical fine-grained granites because of higher connected porosity and because of longer fractures along grain boundaries at lower levels of Fe oxidation (Goodfellow et al. 2016; Figure 6-1). The latter effect occurs because oxidation of Fe in biotite and hornblende is accompanied by volumetric expansion, which increases the elastic strain energy density in the rock, leading to matrix cracking and granular disintegration. More of the Fe contained in the rock needs to oxidize to induce matrix cracking in fine-grained granite than in chemically identical coarse-grained granite. Weathering of these coarse-grained rock kernels, which are more structurally homogenous because of the sparsely spaced subvertical joints than commonly observed in granite, could perhaps have produced an almost flat surface, with potential additional structural control exerted by Precambrian sheeting joints. In this case, chemical weathering in structurally-homogenous kernels of granite to depths limited by sheeting joints could create planar bedrock surfaces beneath the zone of weathered rock. Following subsequent erosion of the overlying weathered rock, this structural control could provide for planar surfaces locally but probably not regionally because individual sheeting joints are not observed to extend for kilometers, i.e. their distribution is patchy. Marine erosive processes during the Cambrian transgression could subsequently exploit marked differences in cohesive strength either between weathered rock and bedrock or across a mechanical boundary within the weathered rock to produce an exceptional unconformity displaying only tens of centimeters of relief.

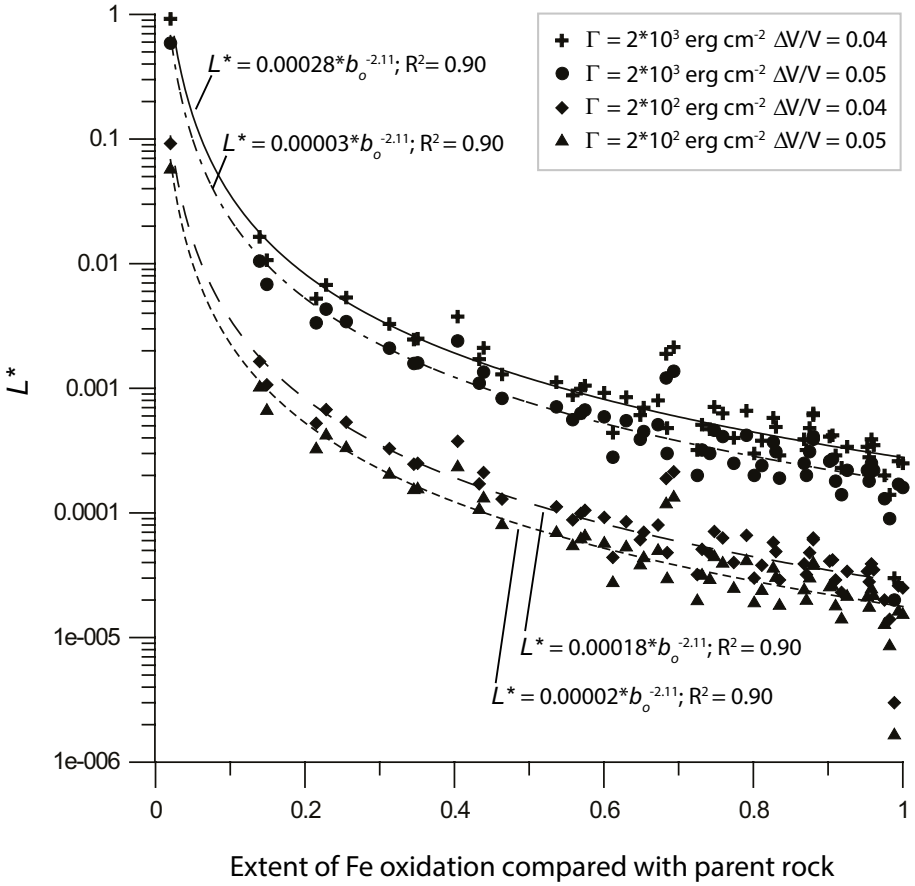

Figure 6-1. *Length-scale of cracks formed through Fe oxidation (L*) plotted against the extent of the Fe oxidation reaction (b_o). The curves constrain a range of values for L* based on empirical measurement of Fe oxidation and plausible values for the volumetric expansion associated with Fe oxidation (DV/V) and the surface energy of fractures (Γ). Matrix cracking to form grussic saprolite begins once sufficient Fe has oxidized for L* to sufficiently diminish to become equal to the dimensions of the constituent crystals of the granite. It then continues as the Fe in the granite continues to oxidize. Coarse-grained rocks will undergo grussification at lower levels of Fe oxidation compared with their chemically identical finer-grained equivalents. Figure reproduced from Goodfellow et al. (2016) with permission from John Wiley and Sons.*

While coarse-grained granites appear to more easily weather to grus than fine-grained granites, they also tend to display a wider joint spacing (Figures 6-2 and 6-3; Ehlen 1992, Moore 2000, Goodfellow et al. 2014b). The effect of the wider spacing is counteractive to high weathering rates because less of the rock matrix is exposed to fluxes of fluids and atmospheric gases that can be up to ten orders of magnitude lower than those that commonly occur in fractures (Maher 2010, Goodfellow et al. 2016). With wide fracture spacing in coarse-grained granites, weathering is more dependent upon matrix permeability and consequently slow matrix diffusion of atmospheric gases and slow fluid infiltration. Usually, joint spacing exerts more control on weathering rates than matrix characteristics, as exemplified by tors, which preferentially form in coarser-grained, but more sparely jointed granite than the surrounding granite which in more rapidly weathered to form regolith mantles (Goodfellow et al. 2014b). Weathering can therefore reasonably be expected to proceed more slowly in coarse-grained rocks that display wide joint spacing. Consequently, residual bedrock relief is normally expected on kernels of rock that display large crystal sizes and wide joint spacing. However, if the CFSs were formed by Precambrian weathering, it then seems reasonable to postulate that regolith generally tens of meters thick covered predicted convexities on these exceptional kernels of rock. In this case, only the largest convexities emerge above the regolith and so persist as bedrock hills emergent above regolith mantles at the time of the Cambrian transgression. Blå Jungfrun, and other visible hills (Figure 2-6), may provide examples of these.

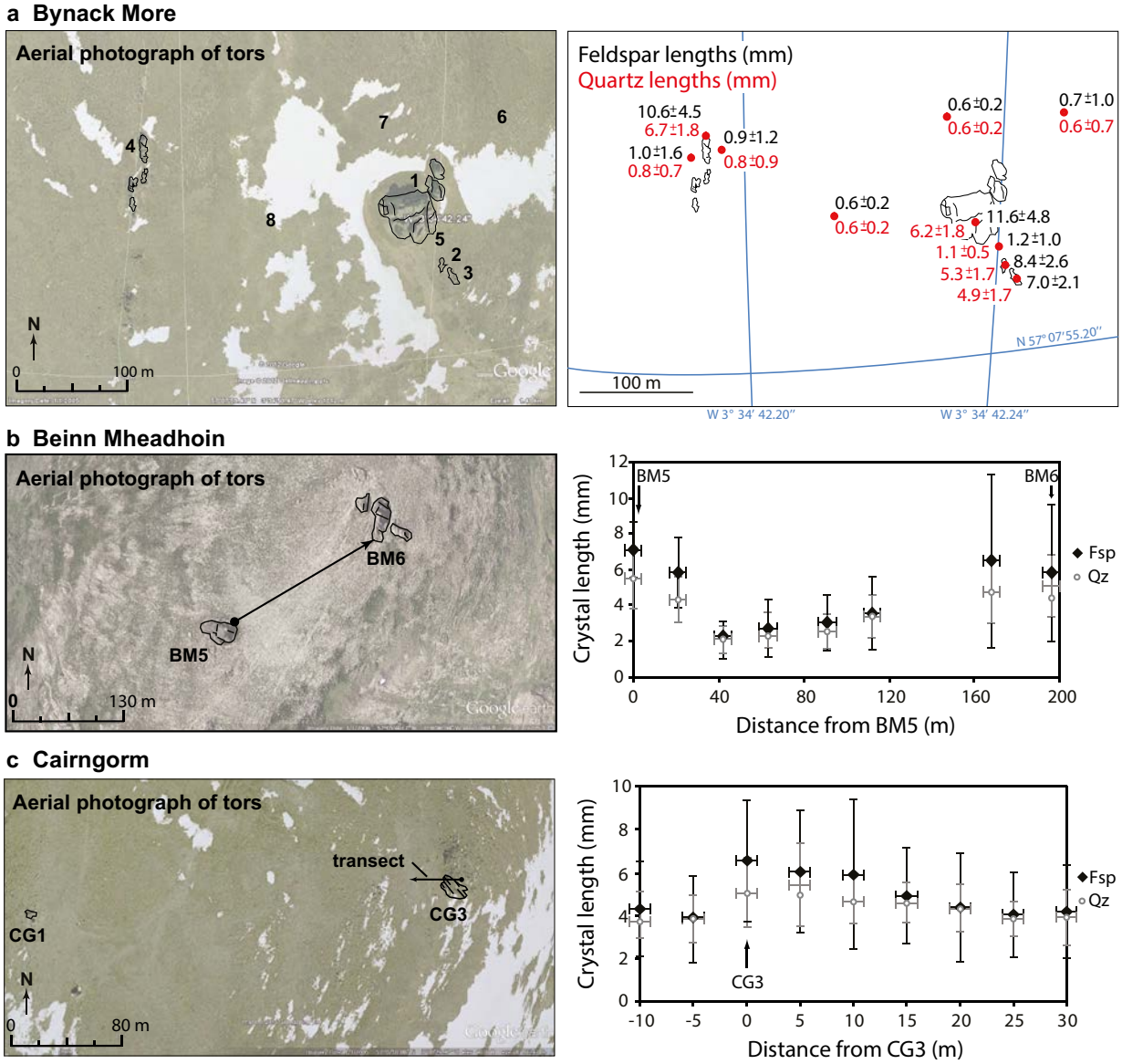

Figure 6-2. *Comparison of mean feldspar and quartz crystal lengths on tors and in surrounding autochthonous blockfields on (a) Bynack More, (b) Beinn Mheadhoin, and (c) Cairngorm, Scotland. (Goodfellow et al. 2014b). Feldspar (Fsp) and quartz (Qz) lengths are given in mm for each of the sample points in (a) and at sample points along the transects in (b) and (c). Sample points 5–8 in (a) are from boulders in autochthonous blockfields. Errors in (a) and error bars in (b) and (c) are 1 σ. Figure reproduced with permission from John Wiley and Sons.*

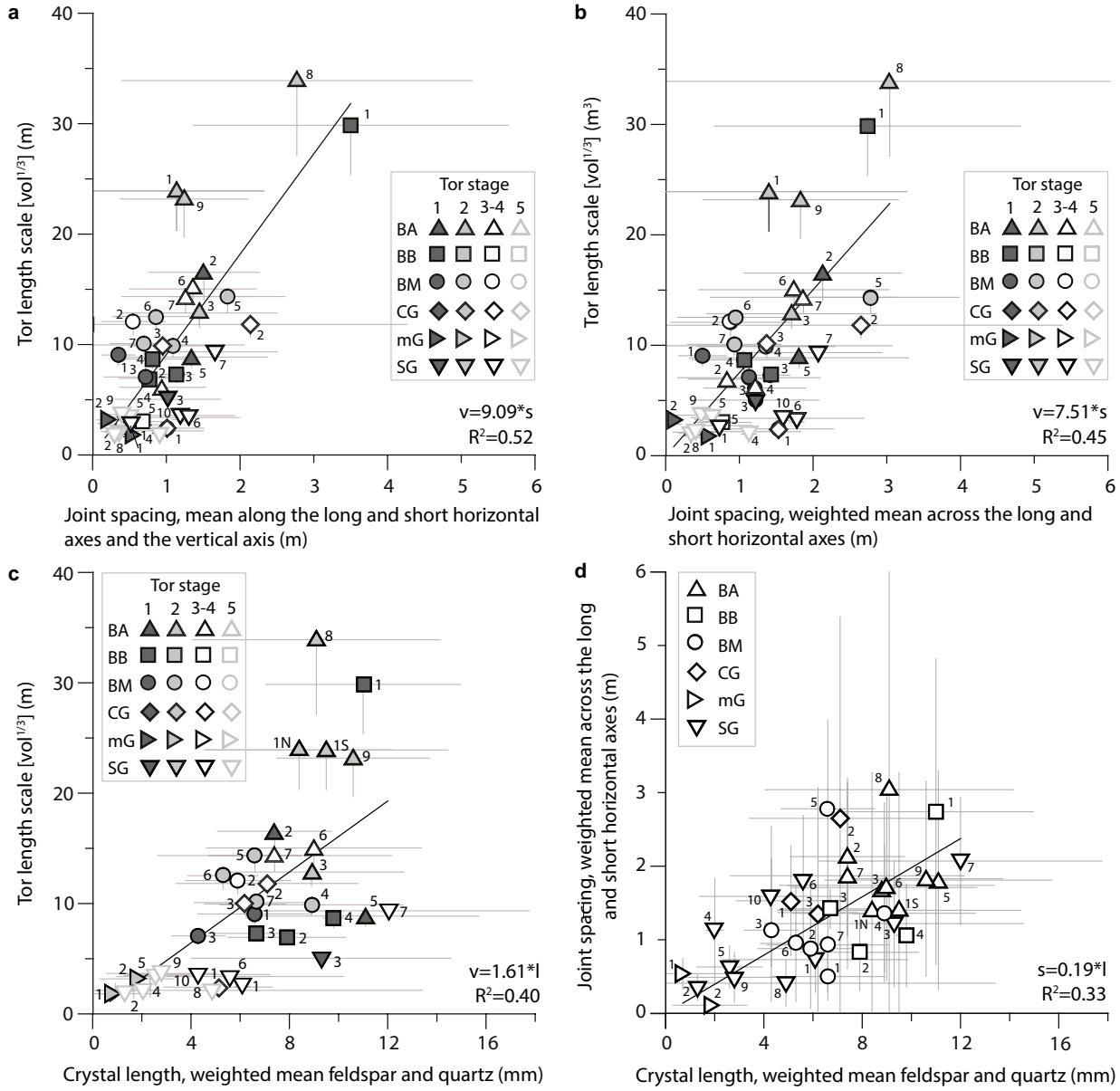

Figure 6-3. *Correlations between tor volumes, joint spacing, and crystal lengths (Goodfellow et al. 2014b). In each plot the best fit equation, R^2 value, and tor number within each group are shown. The equations assume that the tor length scale (v), which scales to the cubic root of tor volume, is given in meters, joint spacing, s (in meters), and crystal length, l (in meters). Data are grouped according to plateau (BA = Ben Avon; BB = Bynack More; BM = Beinn Mheadhoin; CG = Cairngorm; μG = microgranite; SG = Sgòr Gaoith). (a) Tor volume versus mean joint spacing across the long horizontal, short horizontal, and vertical axes. (b) Tor volume versus joint spacing across the long and short horizontal axes, weighted for axis lengths. (c) Tor volume versus mean feldspar and quartz crystal length, weighted for mineral abundances. (d) Joint spacing across the long and short horizontal axes, weighted for axis lengths, versus mean feldspar and quartz crystal length, weighted for mineral abundances. In each plot the linear regression is forced through zero and error bars indicate 1 σ. The glacial modification stage from Hall and Phillips (2006) is also indicated for each tor in (a) to (c). The tor stages range from 1, which indicates an absence of glacial modification, to 5, which indicates advanced modification through glacial erosion. Figure reproduced with permission from John Wiley and Sons.*

At least five uncertainties pertain to the model above. First, as mentioned, weathering typically follows rock structure. As such, a weathering front is not generally expected to portray an extremely flat surface over km^2 in spatially inhomogeneous crystalline rocks, even in a low-relief setting where the potential weathering depth is set by local base level and/or sheeting joints. This is particularly the case where subvertical joint spacing is of many meters (Figure 5-19). Existing residual relief is observed along parts of the unconformity developed in rocks that are likely more susceptible to weathering because of their composition and/or because of closer-spaced joints (Figure 2-5).

Second, the soil production function implies weathering rates are slow beneath thick regoliths (Figure 6-4). This could mean that spatial variations in the jointing and composition of bedrock remain important to weathering, such that chemical weathering cannot completely flatten an inhomogeneous bedrock surface. While regolith cover is crucial to lowering subregolith bedrock relief, it again seems unlikely that extremely flat surfaces would form through weathering of crystalline rocks, particularly in the absence of a structural control exerted by sheeting joints and over extensive (km^2 or larger) areas.

Third, we are unaware of modern analogues for planar surfaces forming in crystalline rocks through a combination of subaerial weathering and marine erosion. Where planar surfaces do occur on shore platforms and marine terraces, they appear to reflect structural controls, such as bedding planes in sedimentary rocks (Trenhaile 1999, Naylor and Stephenson 2010).

Fourth, the planar surfaces in question show evidence of glacial erosion. The cosmogenic nuclide data indicate a range of erosion depths during the last glacial period from about 40 cm to several meters, or more. In addition, field observations also indicate glacial erosion. These observations include striae, subhorizontal surfaces dipping in an up-ice direction to terminate on subvertical fractures, erosion of concavities, especially along subvertical fractures aligned with ice flow direction, and in the case of the surveyed surface at Fågelmara, a broad pegmatite vein that displays a smooth surface that conforms with the surrounding gently convex surface (Figures 2-4, 5-15 and 6-5).

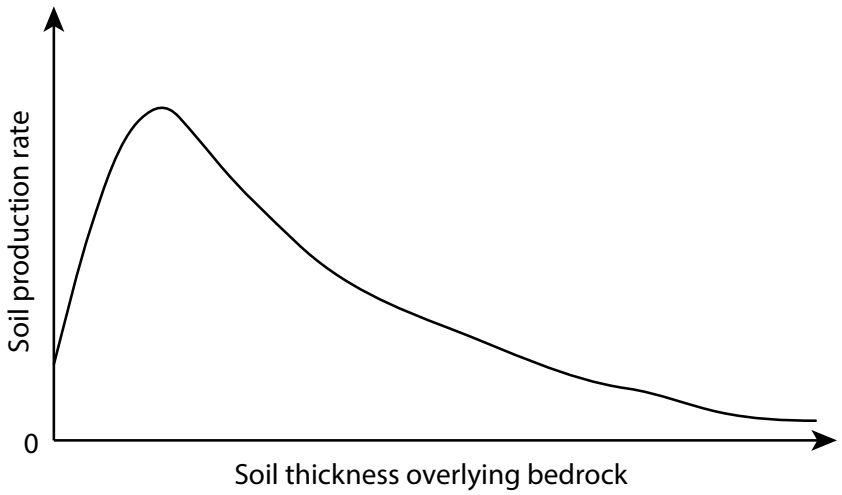

Figure 6-4. *Humped soil production curve (e.g., Humphreys and Wilkinson, 2007). The rate of soil production from underlying bedrock through chemical weathering reaches a maximum beneath a thin soil cover (mm to tens of cm depth) but declines as the thickness of soil increases or decreases. Subaerially-exposed bedrock weathers more slowly than bedrock covered by thin soil. Bedrock covered by soil is more likely to attain a low relief expression than subaerially-exposed bedrock.*

Figure 6-5. *Outcrop morphology and boulder characteristics in the Fågelmara area. (a) A 5 cm thick sheet on the surface of the Fågelmara outcrop under which sheeting joints occur, as revealed on GPR (Figure 5-15e). Even minor surface features such as this thin sheet provide an indication that longer sheeting joints dividing the bedrock into thick slabs may be present beneath the outcrop surface. (b) A series of large (axes of 2–3 m) tabular and cuboidal blocks are located adjacent to the Fågelmara GPR outcrop and (c) to (d) at other sites within 1–2 km of the Cambrian sandstone margin within 10 km north of Fågelmara.*

Fifth, we find no remnants of paleoweathering on the CFSs, including in bedrock cracks. In contrast, paleoweathering is apparent on many other, still-buried, sections of the unconformity (Angerer and Greiling 2012, Elvhage and Lidmar-Bergström 1987, Olvmo et al. 2005, Liivamägi et al. 2014, 2015, Gabrielsen et al. 2015). There are, however, visible traces of modern physio-chemical weathering, particularly on the planar surfaces at Nordkroken. It appears that granular disintegration is active there, perhaps driven by Fe-oxidation that operates at high rates because of frequent wetting and drying along the Lake Vänern shoreline. Present-day weathering is not lowering the Nordkroken surface at a constant rate but rather is increasing relief through a preferential lowering of discrete patches. Although the weathering of a subaerially exposed surface under present conditions only offers a rather poor analogue for Precambrian weathering beneath a regolith cover, it is notable that the weathering of the flat surfaces at Nordkroken is not maintaining flat surfaces.

6.2.2 Model 2. Subglacial erosion resulted in conspicuously flat landscape elements

Based on our field testing and our understanding of chemical weathering and fluvial and marine erosion, we consider Model 1 for the formation of CFSs to be incomplete. Below we compile direct evidence, from our field testing, and indirect evidence, from other partial analogue sites, that the formation of sheeting joints and Quaternary glacial erosion along these, rather than Precambrian weathering and erosional processes, may have been most important to the formation of the studied CFSs in Västra Götaland.

1. The CFSs occur in kernels of rock that display porphyritic coarse-grained granite and subvertical joint spacing of meters to tens of meters. Granitic kernels with these characteristics observed elsewhere are associated with convex landforms, such as domes and tors that emerge through regolith mantles in hilly settings and on plains (Gibbons 1981, Moore 2000). These observations also include tors in Dartmoor (Ehlen 1992) and the Cairngorm Mountains (Figures 6-2 and 6-3; Goodfellow et al. 2014b), and domes adjacent to the cover rock margin north of Fågelmara, in southeastern Sweden (Figures 2-3 and 2-6), and on the island Tjärö (Figure 2-3). So, CFSs at Trollhättan and Nordkroken occur in kernels of rock with lithological characteristics that could least likely be expected to display almost entirely flat surfaces. A similar outcrop with a near-planar summit surface at Fågelmara is also developed in coarse-grained granite with meters-wide spacing of subvertical joints, again counter to expectations and in contrast to other more convex domes located nearby and developed in rock with similarly coarse grain sizes and wide joint spacing (Figures 2-4 and 5-17).

   Convex landforms (domes/tors) occur in kernels of coarse-grained granite because the spacing of subvertical joints inhibits chemical weathering. However, wide spacing of subvertical joints also makes these kernels of rock resistant to glacial erosion (Dühnforth et al. 2010). So, explaining the flatness of these outcrops may pose a challenge regardless of which of the Precambrian weathering or Quaternary glacial erosion models is invoked. We highlight here that kernels of rock that are perhaps least likely to have weathered to completely flat surfaces are also the ones ideally suited to the formation of convex forms underlain by sheeting joints. This is because sheeting joints form best in unweathered, massive rock beneath convex surfaces (Martel 2017). Where these kernels are underlain by sheeting joints, they may become susceptible to glacial erosion.

2. The flatness of these surfaces is exceptional, rather than usual, for the SCP. Observations of the basement in Trollhättan and in the immediate vicinity of Halleberg and Hunneberg generally indicate relief in the range of meters to tens of meters (Figures 3-1, 5-21 to 5-26). Even where relief is very low elsewhere on the SCP, such as at Rockneby, Finse, and Råbäcks hamn (Figure 2-5), meter-scale relief is retained.

   While the absolute magnitudes of relief are low at all of the above listed sites (tens of meter-scale or less) the differences between the CFSs and the other surfaces span up to three orders of magnitude, which indicates that formational processes may be different. The CFSs are not representative of the SCP in general. We emphasize again that they are exceptional surfaces.

3. The CFSs are not developed in rock that is weathered through pervasive oxidation and/or kaolinization. This observation contrasts with surfaces of the SCP that remain buried beneath cover rocks and which lie adjacent to the margins of remnant Cambro–Ordovician cover rocks. Here, weathered rock is retained at many sites (Angerer and Greiling 2012, Elvhage and Lidmar-Bergström 1987, Olvmo et al. 2005, Liivamägi et al. 2014, 2015, Gabrielsen et al. 2015), in places exceeding 100 m in thickness (Liivamägi et al. 2014, 2015). In addition to these published accounts, our unpublished observations of a core taken through Kinnekulle and in millstone mines at Lugnås indicate that the basement surface beneath cover rocks is weathered at these locations. Further observations of the basement at Rockneby revealed that it too was partly weathered to a depth of a few meters. Weathering of the basement is not observed everywhere, however, such as seen by sandstones resting directly on Fe-oxide stained lumpy basement rocks at Råbäcks hamn (Figure 2-5). The CFSs may have formed through a process unrelated to weathering, or, more likely, judged from cosmogenic nuclide evidence presented here and in Stroeven et al. (2016), there has been post-exhumation erosion by the Fennoscandian ice sheet.

4. The relief of these surfaces is lower than typical for a weathering zone base but is consistent with the relief frequently observed along bedrock joints. CFSs formed through erosion along fractures can also be expressed as impressive vertical surfaces, for example Half Dome at Yosemite National Park. Here, the planar surface is clearly joint controlled, rather than relating to weathering on a peneplain.
5. Glacial erosion of sheeting joints can produce CFSs. Classical examples occur in the Cairngorm Mountains in Scotland, where subhorizontal plinths result from glacial erosion of sheeted tors. Philips et al. (2006) show this convincingly using cosmogenic nuclide inventories. We similarly propose that the Fennoscandian ice sheet has exploited sheeting joints, both pre-existing and perhaps new ones nucleated during glaciation, to produce the CFSs we see today.

   Sheeting joints can be inferred from GPR imagery and/or field observations along each outcrop we have investigated, but to variable spatial extents (Figures 5-4 to 5-15). Sheeting joints require a positive driving pressure to open (Martel 2017). The driving pressure for a prospective horizontal fracture is the difference between the water pressure in the fracture and the vertical normal stress that would exist if the fracture was absent. A positive driving pressure can arise from sufficient water pressure, a tensile vertical normal stress in the rock, or a combination of both. The vertical normal stress in rock is usually compressive, but a vertical tension can arise in dry rock if the topography is sufficiently convex and the compressive stress parallel to the ground surface is sufficiently large (Martel 2011). In many places in Sweden, however, the topography is so flat that the topographic perturbation of the regional stresses is probably a minor contributor to a positive driving stress. The water pressure in the rock thus becomes a key factor. Artesian water pressures can arise in topography of sufficient relief (e.g., Freeze and Cherry 1979) but for perfectly horizontal topography with a horizontal water table at or below the topographic surface, the pressure in the ground water will be less than vertical stress due to the overlying rock, and positive driving pressures cannot arise. How then can water pressures arise that exceed overburden pressures in gentle topography?

   Figure 6-6 shows conceptually how a positive driving pressure could arise to open sheeting joints and lift the overlying rock beneath low-relief topography. The topography is overridden by an ice sheet, of thickness h, with a supraglacial lake. This model assumes that water can flow through vertical fractures in the rock and that the horizontal regional stresses are high (~35 MPa). The high horizontal stresses would cause hydraulic fractures to open vertically. We consider two scenarios, one directly below the ice sheet, and another in front of the ice sheet.

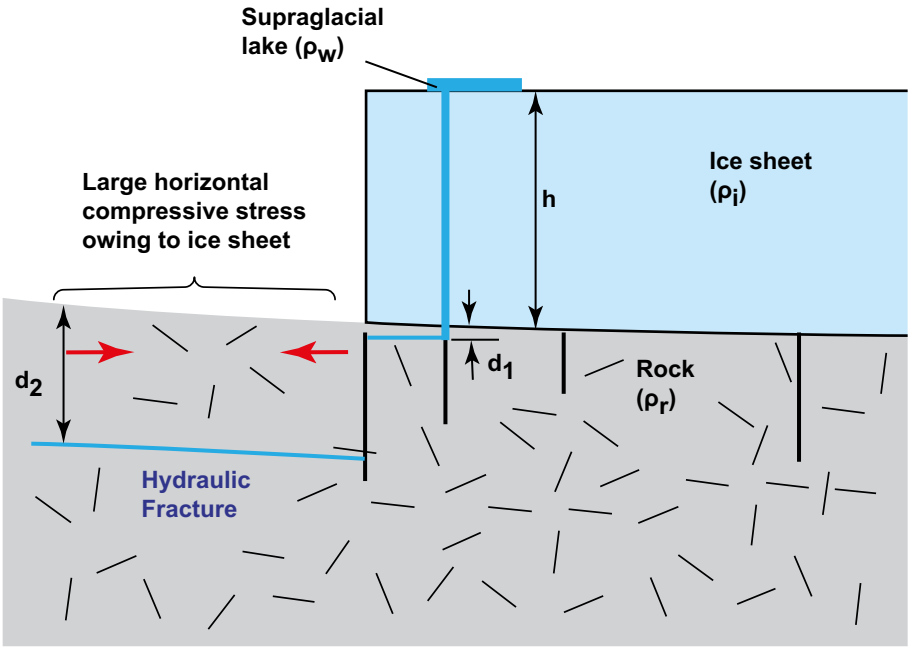

Figure 6-6. *Cartoon showing how sheet joints might arise associated with ice sheets. Pre-existing vertical fractures are shown in heavy black lines.*

First consider conditions below the ice sheet. The vertical compressive stress (S) in the rock there at a depth d_1 is $S = r_i g h + r_r g d_1$, where r_i is the density of the ice, and r_r is the density of the rock, and g is gravitational acceleration. The pressure (P) in a potential fracture, at depth d_1, is $P = r_w g(h + d_1)$, where r_w is the density of the water. Setting P equal to S, and solving for d_1, gives the maximum depth at which hydraulic fractures could open in the rock beneath the ice: $d_1 = [(r_w - r_i)/(r_r - r_w)]\ h$. Using densities for water, ice, and rock of 1×10^3, 0.9×10^3, and 2.7×10^3 kg/m^3, respectively, one obtains $d_1 = h/17$. For example, using an ice sheet thickness of 3.4 km, horizontal hydraulic fractures theoretically could open as deep as 0.2 km below the base of the ice sheet. This maximum depth greatly exceeds the depth at which sheeting joints have been detected in the study area.

Now consider conditions in front of the ice sheet. At a depth d_2, $S = r_r g d_2$. The pressure (P) in a potential fracture, at depth d_2, is $P = r_w g(h + d_2)$. Setting P equal to S, and solving for d_2, gives the maximum depth at which hydraulic fractures could open in the rock in front of the ice: $d_2 = [r_w/(r_r - r_w)]\ h$. Using the densities above, one obtains $d_2 = h/1.7$. Using an ice thickness of 3.4 km, horizontal hydraulic fractures theoretically could open as deep as 2 km below the rock surface. Hence, hydraulic fractures could extend to a far greater depth in front of the ice than they could beneath the ice. The actual depth and lateral extent of the hydraulic fractures would depend on the ice thickness, water volume, and subsurface distribution of fractures.

In addition, gently dipping CFSs display generally discordant dip angles (Figure 5-20) and subhorizontal CFSs are offset by 60 cm adjacent to the Nordkroken 4 profile (Figure 5-18j). These observations may also indicate that formation of planar to gently convex CFSs is associated with planar to gently convex fractures in the bedrock, rather than being attributable to Precambrian weathering and peneplanation.

6. We interpret tors in the Cairngorm Mountains and their glacial erosion to provide partial analogues for the CFSs in Västra Götaland and at Fågelmara. We highlight the following three observations (cf. Thomas et al. 2004, Hall and Phillips 2006, Phillips et al. 2006, Hall et al. 2013b, Goodfellow et al. 2014b):

   (i) Tors increase in size with the spacing of subvertical joints and with bedrock crystal size (Figures 6-2 and 6-3). The kernels of rock in which the tors are located also display wider joint spacing and larger crystal sizes than surrounding bedrock. Tors that remain least modified by glacial erosion are up to 20 m high. High tors occur where glacial ice was persistently cold-based during glacial periods or where the summits on which they are located were exposed as nunataks. Given that the footprints of the Cairngorm Mountains tors are smaller than the footprints of the CFSs in Västra Götaland and at Fågelmara, we infer that convex bedrock forms, resembling tors with amplitudes of meters to a few tens of meters, may have existed on the SCP where CFSs are now located, prior to cover rock removal and Quaternary glacial erosion.

   (ii) Tor morphology is highly susceptible to erosion by warm-based glacial ice, even where those conditions occur for only short periods. Under warm-based ice, tors are progressively reduced to flat plinths as the intensity of glacial erosion increases (Hall and Phillips 2006, Phillips et al. 2006). That glacial erosion can reduce tors to flat plinths while also leaving intact the large domed hills on which they are located indicate that convex bedrock outcrops which display amplitudes of meters to a few tens of meters can be highly susceptible to glacial erosion. This is particularly applicable to outcrops that either contain pre-existing sheeting joints or are predisposed to their formation during glaciation. Glacially eroded tor plinths are planar or slightly convex. They are level with, or rise as low tables up to a few meters above, their immediate surroundings.

   (iii) Tors protrude above otherwise gently convex, smooth, regolith-covered, surfaces. The regolith-covered plateaus of the Cairngorm Mountains are not a model for the sparsely distributed tors in that setting and bedrock plinths that remain after tors are not an original feature of the plateau surfaces with which they are almost level but, rather, the presence of tors in different stages of destruction reflects spatial variations in lithological properties, weathering, and erosion.

7. Cambrian sandstone fills of basement fractures highlight fracture geometries that may be most consistent with post-depositional erosion of the Precambrian basement. Such fracture fills occur on the CFSs at Sandhem, Hjortmossen, and at Nordkroken (Mattsson 1962, Rudberg et al. 1976). They also occur more widely across the Swedish landscape interpreted as SCP (Bergman 1982, Alm and Sundblad 2002, Röshoff and Cosgrove 2002, Drake and Tullborg 2009, Friese et al. 2011). At Hjortmossen, they are mapped on convex, rather than concave, locations (Rudberg et al. 1976). This spatial distribution may reflect a selection bias because the convexities are exposed, rather than concavities, which are covered by sediments and vegetation. It may also reflect a preservation gradient following greater depth of (glacial) erosion in currently concave locations. Indeed, the fracture fills have been presented as evidence for the summit surface of Hjortmossen representing an uneroded section of a peneplain. Rudberg et al. (1976) inferred that these Cambrian sands passively filled pre-existing fractures in the basement during the Cambrian transgression.

   While we agree that Cambrian sandstones fill subvertical fractures that were initiated at the unconformity surface, and therefore represent proximity to the unconformity, we disagree that their presence necessarily indicates that the outcrop surfaces upon which they are located have undergone trivial post-exhumation erosion. This is partly because these fracture fills have been observed to occur down to 100 m below the present basement surface (Drake and Tullborg 2009), because their walls are unweathered, which indicates that they were not exposed to Cambrian subaerial weathering processes, and because they display angular contacts with present bedrock surfaces, which indicates recent surface erosion. Edge rounding might be expected where recent weathering rates exceed erosion rates or if the present rock surfaces were weathered prior to Cambrian sedimentation. In addition, the subvertical fractures are described as being up to tens of meters long in the horizontal dimension (Rudberg et al. 1976, Alm and Sundblad 2002). These dimensions are significant because for cracks that extend down from a free surface, mechanical considerations favor a preferred semi-circular or semi-elliptical geometry. Hence, if a semi-circular crack had a radius of 100 m, then a depth of 50 m might be expected (Figure 6-7). Cracks that show traces on present rock surfaces of tens of meters might therefore also have extended some tens of meters below the rock surface. Hence, the present rock surface is not necessarily located close (10^{-3}–10^{0} m) to the original rock surface at the time of crack filling. Another example is provided by a 36 m long fracture filled with sandstone on the eastern edge of the flat summit of Vånga (Figure 4-2) but which displayed a depth of only 2–3 m (Mattsson 1962). Further details on how the crack is exposed are missing, but those crack dimensions might provide evidence for erosion of up to tens of meters of overlying rock from this summit. Whereas field observations can deviate from theoretical considerations, the sediment-filled cracks in the CFSs have formed in kernels of granite that are more structurally homogenous than commonly observed. Reality might therefore closely reflect theory in these locations.

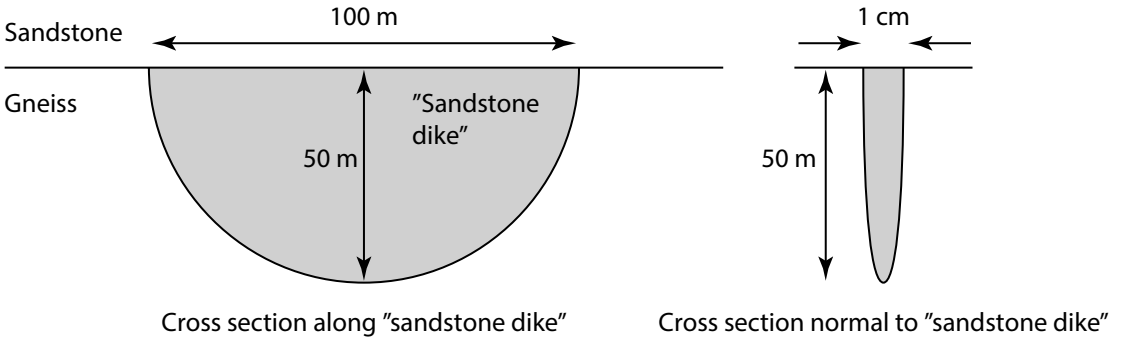

Figure 6-7. *Cartoon showing idealized dimensions for a sandstone-filled crack that extends down from a free surface. Assuming crack formation during sedimentation, mechanical considerations stipulate a semi-circular or semi-elliptical geometry for the crack. Hence, if a semi-circular fissure of 1 cm width had a radius of 100 m, then it might be expected to extend up to 50 m below the surface. Cracks containing sandstone that are observed to have horizontal dimensions of tens of meters but vertical extensions of merely a few meters can provide circumstantial evidence for erosion of overlying bedrock following coincident crack formation and sedimentation.*

There is also considerable uncertainty regarding the sedimentation processes in these subvertical fractures. On the one hand, some examples seem to represent passive fills of pre-existing fractures (Mattsson 1962). On the other hand, it seems that most fractures filled with Cambrian sandstone nucleated during or after Cambrian sedimentation and were filled with sand through active injection (Röshoff and Cosgrove 2002), for example under high hydrostatic pressures, or by a sucking mechanism during fracture propagation (Friese et al. 2011). This uncertainty also makes it more difficult to conclude that present rock surfaces displaying Cambrian sandstone fills have undergone only trivial (less than meters) erosion following basement exhumation from beneath Cambro–Ordovician cover rocks.

8. The distribution of the CFSs (Figure 3-1) appears to relate to a zone with clear signs of glacial erosion, seemingly beneath fast flowing, or streaming, ice (Figures 5-21 and 6-8). Each of the Nordkroken and Trollhättan surfaces are located 0–10 km south of the southernmost arm of Lake Vänern. This long and narrow arm has likely been deepened by glacial erosion and is oriented parallel to former ice flow direction (Figures 2-3, 3-1 and 5-21). The orientations of streamlined bedforms and glacial striae (Figures 3-1, 5-16, 5-18 and 5-23) indicate that ice flow out of this arm of the lake, over the CFSs at Nordkroken and Trollhättan, continued in a southwestern direction towards the coast. The table mountains of Halleberg and Hunneberg with their thick dolerite sills impeded ice sheet flow across them (Figure 5-23). Some of that ice was funneled around the obstacles, potentially further increasing glacial erosion of these sites.

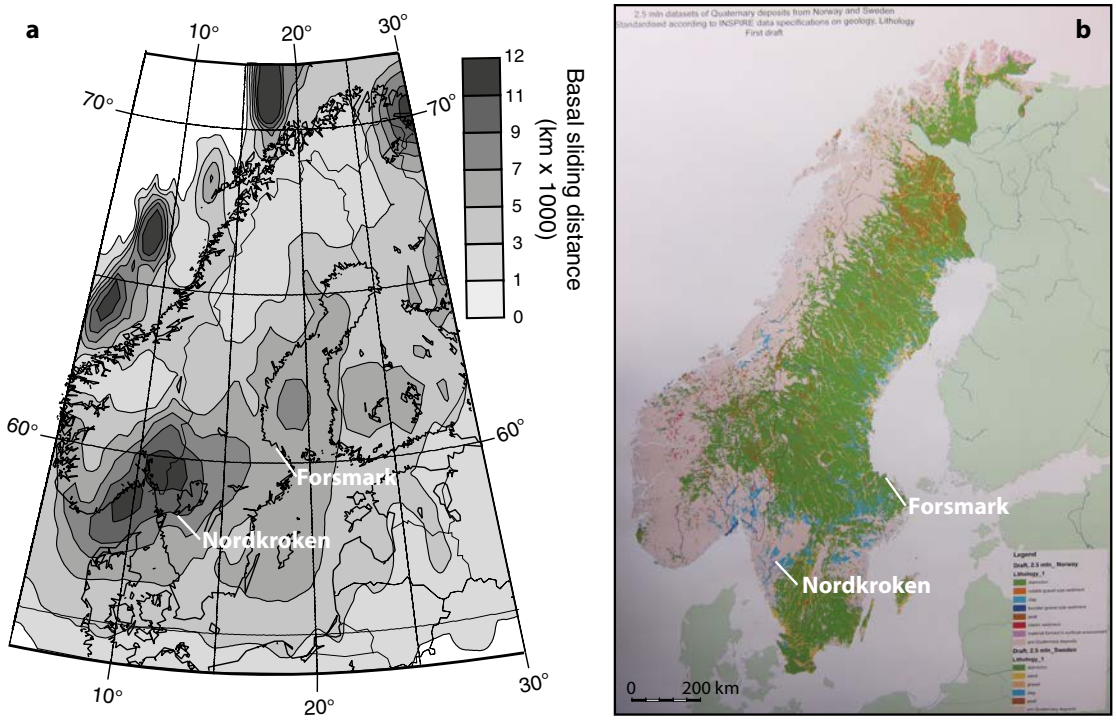

Figure 6-8. *(a) Distribution of basal sliding distance over Fennoscandia, summed up for the entire Weichselian, adapted from Näslund et al. (2003). Higher values of basal sliding distance occur over the Nordkroken–Trollhättan area than at Forsmark, implying better conditions for more intense glacial erosion at the former. (b) Distribution of Quaternary sediments across Sweden and Norway (Swedish Geological Survey). Glacial tills (green) are absent from the Nordkroken–Trollhättan area, which is characterized by bare rock and water-lain deposits. In contrast, the sediment distribution around Forsmark is dominated by glacial tills. Figure 6-8a reproduced with permission from Elsevier.*

As the ice sheet engulfed the table mountains and diverted some of the ice to flow around it, it also affected the surface morphology of the dolerite sill. Glacial erosion appears to have lowered the lee-side of Halleberg by an additional 25 m compared with its stoss side (Figure 5-23). Moreover, the 100 m high vertical wall facing up-ice, we suspect, inhibited glacial erosion of the basement in an up-ice direction by both slowing ice flow and diverting it vertically across and laterally around the obstacle (Figure 5-23). We therefore infer that the lumpy surface topography of the basement on the stoss side of the table mountains more closely represents the antecedent morphology of the unconformity than the near-planar surfaces located on their lateral-to-lee sides.

Evidence of glacial erosion lateral to the table mountains and downstream of the table mountains is ubiquitous. The coast located down-ice of Nordkroken and Trollhättan is the southernmost expanse of the sole location along the west coast of Sweden where glacial erosion created a fjord (Figures 2-3 and 6-8). During glacial periods, ice flowing over these sites appears to have removed surface regolith (Figure 6-8) and carved a fjord upflow of where it may have fed into the Norwegian channel ice stream. Similarly, glacial erosion has streamlined bedrock and carved a channel, below present lake level, along the western flank of Halleberg (Figure 5-26). This channel, which is 200–400 m wide and of uncertain depth, separates the flat-topped Nordkroken surfaces from the table mountain. Another channel, up to 61 m deep and 2 km wide, occurs along the western flank of Hunneberg. The dimensions of these channels might indicate their formation over multiple glaciations. If so, the adjacent slopes of Halleberg and Hunneberg have maintained a stable position for more than the last glaciation and cover rocks had therefore been removed from the Nordkroken surface prior to the last glaciation.

9. Our cosmogenic nuclide data indicate erosion of bedrock during the last glacial period. Even where inferred erosion rates are relatively low, such as on the summit surface of Hjortmossen, they remain higher than those on the much less massive Wave Rock, which was the sampled site that experienced least erosion at Forsmark during the last glaciation (Hall et al. 2019a). The many indications of erosion of this landscape by fast-flowing ice add further weight to the possibility that these conspicuously flat outcrops have experienced glacial erosion of sheeted bedrock, potentially under bedrock convexities.

In the above discussion we have presented nine lines of evidence that we interpret to indicate that the CFSs have a primary structural control and have undergone glacial erosion, through exploitation of that bedrock structure. We now list, and address as much as possible, nine counterarguments. Remaining uncertainties may present opportunities for further research.

1. A key outstanding question is whether the kernels of porphyritic, sparsely jointed, gneissic granite of Nordkroken are replicated under Halleberg or Hunneberg. If they are, a related question is whether the SCP developed on those kernels is also exceptionally flat beneath the table mountains. If so, it would confirm CFS formation prior to and/or during Cambrian marine transgression. If, as we infer, erosion of sheets of rock were important to the formation of these CFSs, what process during, or prior to, Cambrian marine transgression would remove bedrock sheets? Inferred broad low-relief marine shelves based on observations of low relief and low regional gradients on the SCP, may imply low shoreline wave energies. This inference is supported by the frequent presence of Precambrian saprolite remnants on the SCP and the Great Unconformity (Avigad et al. 2005, Angerer and Greiling 2012, Elvhage and Lidmar-Bergsträm 1987, Plvmo et al. 2005, Sandler et al. 2012, Gabrielsen et al. 2015, Liivamägi et al. 2015). If marine waves and currents were inefficient at entirely removing weathered rock, how would marine waves and currents remove unweathered bedrock?

   In conjunction with the hypothetical scenario of conspicuously flat basement surfaces underlying the table mountains, it is worth considering the following: (i) these exceptionally flat surfaces are developed in kernels of coarse-grained porphyritic, sparsely-jointed rock and so would remain a local, rather than a general, feature of the SCP, (ii) if sheeting joints also exist beneath the table mountains, erosional exploitation of at least one bedrock sheet by the Fennoscandian ice sheet from the Nordkroken and Trollhättan sites is not excluded, and (iii) it is questionable whether the mafic intrusions that formed the doleritic sills would occur through the centers of sparsely jointed granitic kernels, or, more likely, intruded along lithological boundaries and where more densely-jointed rock is located.

Evidence indicating that the exceptionally flat surfaces at Nordkroken do not continue under Halleberg-Hunneberg include the absence of CFSs from the eastern and southern flanks of Halleberg and Hunneberg (Figures 5-23 to 5-25). Furthermore, well logs from sediment-covered basement adjacent to the western flank of Halleberg indicate topography of meters to a few tens of meters at this location, which is also underlain by porphyritic gneissic granite (Figures 3-2 and 5-21).

2. An answer to the question above, whether Cambrian marine processes could have eroded unweathered, but fractured, bedrock, may be provided by the absence of boulders from lower Cambrian sediments (Nielsen and Shovsbo 2011). This observation is in stark contrast to the abundant, locally-derived, granitic–gneiss boulders which often display dimensions of meters, in glacial tills overlying the basement surface adjacent to the Cambrian sandstone margin in the Fågelmara area. Similarly large and abundant boulders occur in the Forsmark area, where they have been associated with the newly inferred process of glacial ripping (Hall et al. 2019a), which explicitly exploits sheeting joints.

3. Five field observations may cast doubt on Model 2. We present and, where possible, address these observations and their implications below.

   Firstly, sheeting joints do not occur in GPR imagery extending under all parts of all outcrops, and associated reflectors were largely absent from the uppermost 15 m of the summit surface of Eriksroparken (Figure 5-14b). Sheeting joints are also absent from most other outcrops distributed through Trollhättan, which are often glacially sculpted into streamlined roches moutonnées. These observations indicate that there are local controls on sheet jointing. The observed patchiness of the sheeting joints indicates that driving stresses for sheet jointing might be marginal with respect to their magnitudes, which are sufficient in only the most favorable locations. Therefore, a mechanism that provides for locally variable water pressure might be required to account for the distribution of sheeting joints near Trollhättan. The formation of sheeting joints might be limited to ideal kernels of rock, i.e. those which are massive and unweathered. The distribution of subvertical joints (Figure 5-17) could be crucial to the formation of sheeting joints because subvertical joints provide pathways for water to enter or exit the rock. In addition, the observed patchiness might simply indicate that most of the inferred sheeted domes/tors have been glacially eroded, leaving remnant sheeting joints that are perhaps too deep to be imaged on GPR. It further appears from the contrast in long, linear sheeting joints beneath the CFSs (Figures 5-4 to 5-15) and the short, hook-shaped sheeting joints visible at the ground surface on the lee side of Hjortmossen (Figure 5-17d) and in the GPR images from the lee-side of Eriksroparken (Figure 5-14c) that these contrasting joint sets formed under different bedrock stress conditions, potentially at different times. The long linear sheeting joints indicate formation under a horizontal most compressive stress that was high relative to the driving stress at the time of their formation, whereas the hook shaped joints indicate that the driving stress was locally high relative to the horizontal most compressive stress at the time of their formation (Martel 2017).

   Secondly, sheeting joints are frequently sub-parallel, rather than parallel, to the conspicuously flat outcrop summit surfaces. While sheeting joints may form a first order control on the flat morphology, additional glacial erosion processes such as the formation and erosion of new fractures (evidence for which is observed at Nordkroken; Figure 5-18e, f) and/or abrasion might be necessary. It also appears at Nordkroken and at Sandhem that parts of the present summit surfaces may represent a continuation of sheeting joints imaged by GPR under adjacent parts, and which extend up to the present outcrop surfaces (Figures 5-5 and 5-13). In these cases, the flat morphology might also result from erosional exploitation of bifurcating sheeting joints. Local perturbations of the stress field (such as might be caused by a nearby sheeting joint) can also cause the joints to not be perfectly parallel. Hook-shaped joints are evidence of such a perturbation.

   Thirdly, the long axes of the CFSs are tens to hundreds of meters, which results in the reasonable question of whether sheeting joints can be this long. The dimensions of CFSs and sheeting joints might be reconciled through the above inference that CFSs may have formed from bifurcating sheeting joints. Some vertical joints exposed on the Trollhättan and Nordkroken surfaces display straight traces of hundreds of meters, which indicates that joint lengths can be of scales comparable to those of the CFSs. Also, sheeting joints with horizontals lengths greatly exceeding 100 m have been observed at Forsmark (Carlsson 1979). However, while low-relief summit surfaces have formed in glaciated landscapes on sheeted granite, for example in Yosemite National Park, we are unaware of other examples from glaciated landscapes where exceptionally flat surfaces with dimensions of hundreds of meters are observed. We have observed close, but imprecise, analogues in roadcuts at

Ronneby (cf. Figure 2-3), where outcrops are underlain by sheeting joints with horizontal lengths of hundreds of meters and with ground surfaces that display less than meter-scale relief across similar horizontal distances. These examples occur in a landscape where summit accordance can also be inferred on 2-dimensional topographic profiles and which has not been associated with the SCP (Lidmar-Bergström 1986).

Fourthly, we invoke a similar mechanism for the formation of CFSs in Västra Götaland and at Fågelmara as we do for Forsmark. We propose that hydrofracturing, jacking, and injection of glacifluvial sediments into spectacular sheeting joints (Carlsson 1979, Leijon 2005, Hall et al. 2019a), ultimately leads to a glacial erosion of sheets. However, an important difference with the Forsmark and Fågelmara areas is the absence of extensive deposits of large locally-derived boulders, which would provide evidence for this process occurring at the termination of the most recent deglaciation. Therefore, if this process has been active in Västra Götaland and accounts for the CFSs, its timing was different. There are at least two in-principle solutions to this conundrum, one invoking the same processes, but not the same timing, the other a different set of processes involving subglacial water transport between reservoirs. The hydrofracturing (hence, preparing the bedrock for evacuation) could have occurred during a previous deglacial period, and that would remain consistent with our cosmogenic nuclide data, where they indicate more than 3 m of bedrock erosion during the last glacial period. If preparation by weakening along jointing planes occurred during an earlier glacial phase, the transport may have happened during advance to the maximum stage of the last glacial phase. Whatever erosional products were incorporated during an ice sheet advance towards its maximum stage may have been evacuated out of the local area and to ice sheet margins (e.g., Kleman et al. 2008). Alternatively, the special conditions that allowed loose overburden (regolith) to have been removed across a broad area terminating in the fjorded west coast, may have involved episodic subglacial water transport out of Lake Vänern, and into other subglacial lake basins or towards the margin off the west coast of Sweden.

Fifthly, the near-planar surfaces in Trollhättan, Nordkroken, and the similar, but less extensive and more convex, outcrops at Fågelmara are each located near Cambrian cover rock remnants. This proximity is consistent with the hypothesis that these near-planar surfaces are essentially components of the SCP, which have undergone only trivial glacial erosion because they have been recently exhumed from beneath cover rocks. Recent exhumation remains speculative at Fågelmara but is supported by the cosmogenic nuclide data for the Nordkroken surfaces (Figures 5-29 to 5-34), which indicate more than 3 m of bedrock erosion during the last glacial period.

4. Summit accordance has been inferred for the CFSs in and around the Trollhättan area (Johansson et al. 2001b), and indeed summit accordance may be the best argument for the dissected flat peneplain model. It seems fortuitous that glacial erosional processes would turn bedrock lumps into a series of accordant near- CFSs. However, these summits protrude only meters above the regional low relief surface (Figure 5-20). Furthermore, bedrock fracturing under convexities in a sinusoidal topography subject to the same strong ambient compressive regime might produce sheeting joints at closely-accordant elevations. Glacial erosion, particularly under conditions where basal sliding distances are large (Figure 6-8a) across a region of low relief (Figure 5-20), might exploit those sheeting joints to produce the observed summit accordance. Indeed, our cosmogenic nuclide data indicate erosion of these surfaces, which therefore offer support for accordance being partly attributable to glacial processes. However, the total depth of glacial erosion of these surfaces might be limited to a few meters and how streaming ice might interact with kernels of sheeted rock to perhaps produce accordant summits remains largely speculative.

   We temper the above arguments with the observation that precise summit accordance is not necessarily apparent, which may be interpreted to indicate some local control on the near-planar summit surfaces (Figure 5-20). We conclude that accordance between the Trollhättan CFSs offers supportive, but not definitive, evidence that they are remnants of a regionally extensive peneplain of similarly low relief.

5. Sheeted domes of > 100 m amplitude (and footprints of km^2) persist in otherwise low-relief areas of Sweden. These include Blå Jungfrun and Vånga (Figures 2-6 and 4-2) and hills in northern Sweden (Hall et al. 2013a), indicating that they are resistant to glacial erosion. However, glacial erosion of such sheeted domes has occurred (e.g., Johnsson 1956, pp 68–73) and they persist because of their large size. Conversely, sheeted tors with amplitudes up to a few tens of meters and footprints of tens to hundreds of m^2, were removed by glacial erosion in the Cairngorm Mountains of Scotland (Hall and Phillips 2006).

6. Cosmogenic nuclide data primarily indicate cover rock removal during the last glaciation, and so we are still looking at pristine surfaces of the SCP. This is a key consideration because our sampled conspicuously flat sites range from a few hundred meters to about 10 km from Halleberg and Hunneberg. The strongest argument for cover rock removal for the five samples that lie within 1 km of these table mountains is that none of the five samples have inheritance (Figures 5-29 and 5-30; Table 5-1). These results contrast with the eight Trollhättan samples, which all show varying degrees of inheritance (Figures 5-29 and 5-30). The 5 samples adjacent to the table mountains may primarily reflect cover rock erosion, whereas the eight Trollhättan samples might primarily reflect basement erosion.

   Accounting for the observed inheritance in samples from the flat-topped blocks at Sandhem and Hjortmossen (Figure 5-29) through cover rock erosion would imply persistence of a thin sheet (i.e. <3 m) of sandstone. Sedimentary rocks appear to be highly susceptible to glacial erosion and are removed first from convex portions of the landscape (Hall et al. 2019a). Outliers of sedimentary rock are uncommon and appear to be almost exclusively preserved in basins and on down-faulted blocks. Hence, it appears unlikely that thin cover rock remnants would have persisted up to the last glaciation either as parts of a spatially-extensive body or as outliers on the sampled CFSs in Trollhättan.

7. The bottom surface of the dolerite sill sets a maximum limit for the amplitudes of the hills that may have been located on the now planar surfaces at Nordkroken. This would seem to limit potential hills to a maximum height of c 20 m. Indeed, if they were present, hills may have been limited to some tens of meters. However, the base of the sill does not represent a robust limit for the size of hills on the Nordkroken surface because the melt from which the sill crystalized would likely follow subhorizontal sedimentary bedding planes and flow around any hills that might have protruded above this level. Based on the plan-view dimensions of individual rock blocks (Figure 3-3), with plan view dimensions of 10^2–10^3 m^2 and which are separated by linear vertical fractures, we infer that basement convexities with footprints up to hundreds of meters and with amplitudes up to tens of meters are plausible. These are maximum values and smaller, less convex forms are also plausible. We do not, based on current evidence, argue for a single dome at Nordkroken with a footprint exceeding a kilometer and an amplitude of many tens of meters, or more.
8. There is more relief through glacial erosion towards the west coast than in the Trollhättan–Nordkroken area. The latter, therefore, represents largely preserved peneplain remnants, with the CFSs representing the form of the unconformity. While we agree with observations of tens of meters, or more, of relief towards the coast, relief also reaches many tens of meters in the Trollhättan–Nordkroken area. Although the area located towards the coast may have been exhumed from beneath cover rocks sooner than the Trollhättan area, there is little evidence that relief has increased because of the inferred longer period of glacial erosion (Johansson et al. 2001a, Olvmo and Johansson 2002) except, likely, where selective linear erosion has created fjords. It appears, therefore, that, in this area of classical areal scouring, ice exploited an exhumed landscape that was already more dissected. That relief is less dramatic in the Trollhättan–Nordkroken area does not exclude glacial erosion, nor does it necessarily imply that that the lowest relief segments are the best preserved. Glacial erosion can act to maintain low relief, or even reduce it, at least locally. We suspect that many of the present bedrock valleys in the Trollhättan area have been glacially eroded from antecedent concavities present on the SCP.
9. We assign the origins of each of the CFSs to a single mechanism even though there are variations between each of them. The Nordkroken surfaces display the most overt signs of glacial erosion and display the most spectacular sheeting joints. Multiple sheeting joints, extending for up to tens of meters were imaged beneath the Hjortmossen surface but imaged joints were more restricted at Sandhem and particularly at Eriksroparken. Eriksroparken is also formed on gneissic granite that is less porphyritic than which underlies the other sites (Figure 3-2), although it remains coarse-grained and displays meters-wide joint spacing. Erosion rates, inferred from cosmogenic nuclides, also vary between the surfaces. Therefore, there is the question of equifinality and whether different processes, including Precambrian weathering, glacial erosion of sheeting joints, and glacial abrasion operating at different magnitudes can produce similar morphology on each of the surfaces.

We are attempting to infer a temporal history of these surfaces, which spans hundreds of millions of years, based on present-day spatial data and limited temporal data. This is a general problem to any model for these surfaces, including both models presented here. We infer processes of formation based on spatial data for the present landscape, on imaging of the present-day subsurface jointing, and from circumstantial evidence collected from other sites that we consider to be useful analogues. We have temporal information in the form of erosion rates inferred from the cosmogenic nuclide data, but these are biased towards the last glaciation and our arguments for the timing of cover rock removal are circumstantial. While recent advances in our understanding of bedrock fracture processes, technical advances in our ability to image subsurface jointing, and cosmogenic nuclide studies make quantitative erosion rate inferences highly valuable, our model hypothesis for these remarkably low relief surfaces are unavoidably biased towards what can be measured in the present day landscape. In this regard, our study therefore reflects some of the limitations of process geomorphology. The key links with the deep past (Permian to Precambrian) are provided by the cover rock remnants and Cambrian sandstone fissure fills. These add valuable temporal constraint on the evolution of this landscape, spatial constraint on the low relief morphology of the SCP (amplitudes of 10^0–10^1 m over wavelengths of 10^1–10^3 m) and on depths of Quaternary glacial erosion (tens of meters or less). However, our model hypothesis, based on the diverse data sources, remains largely qualitative.

In our view, Model 2 for the formation of CFSs through glacial erosion of bedrock sheets better explains the data presented here. How these surfaces are interpreted to have formed has ramifications beyond the formation of these CFSs because they are an integral part of the Subcambrian peneplain at a much larger scale. Hence, we will evaluate the implications of our findings for the traditional view of the SCP and present an updated model for the formation of the Subcambrian peneplain.

6.3 Alternative models for SCP formation

The observed morphology of the SCP as an exceptionally low-relief, but not entirely flat, unconformity requires a process geomorphological analysis: How does a low-relief surface form over such a large area? A plausible model for this is that the SCP formed beneath a regolith cover that was meters to tens of meters thick. In this model, the shape of the SCP largely reflects the interface between saprolite and bedrock. We can base this model on observations by Gilbert (1877) of soil-mantled hillslopes being convex and bare bedrock surfaces angular; observations that form the basis for a soil production function (Carson and Kirby 1972, Heimsath et al. 1997, Humphreys and Wilkinson 2007). This function relates weathering rates to soil thickness, recognizing that a weathering maximum is attained under a thin soil cover and that exposed bedrock weathers at the slowest rate (Stroeven et al. 2014; Figure 6-4). More recent observations of soil-mantled landscapes further indicate that weathering rates (the conversion of bedrock to regolith) are most strongly controlled by the regolith erosion rate (Riebe et al. 2003, Dixon et al. 2009), to which they display a positive correlation (Figure 6-9a). This is because moderate to high rates of erosion of overlying regolith maintain a moderate to high rate of supply of fresh rock minerals into a thin weathering zone where they are easily accessed by weathering fluids, atmospheric gases, and vascular plants in modern landscapes. Where regolith erosion rates are exceptionally high, such as on steep alpine slopes, bare bedrock is exposed and weathering rates decrease. Lower regolith transport rates typically occur on lower convexity hill summits and a thicker regolith cover can develop (Figure 6-9b). However, as the regolith thickens, the weathering rate again tends to decrease from its peak beneath a thin regolith cover. If the soil is sufficiently thick to form a spatially-continuous cover, bare bedrock remains unexposed even during erosional events, for example related to a high rate of surface wash during a storm. Under such conditions, the bedrock surface can weather down to a low-relief surface. This is because where regolith mantles subsurface highs it is at its thinnest and the weathering, therefore, most efficient, thus reducing sub-regolith relief.

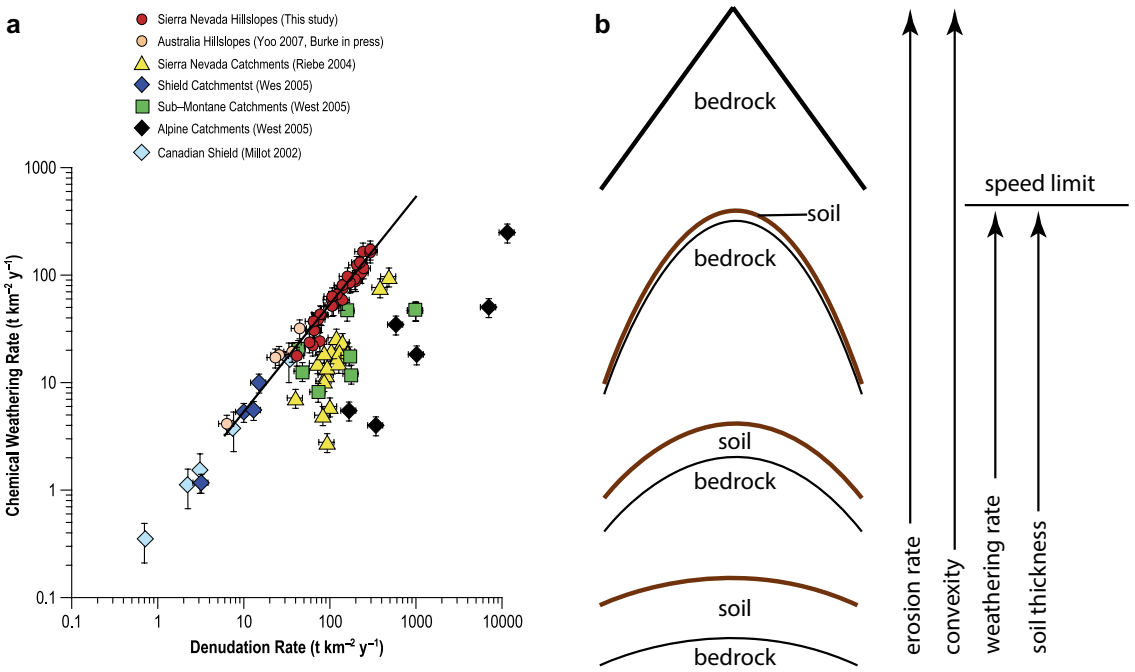

Figure 6-9. *Relationships between chemical weathering rate, denudation rate, soil thickness, and hillslope curvature. (a) Plot of empirical data showing tight coupling between chemical weathering rate and denudation rate (Dixon et al. 2009). (b) A conceptual diagram showing a sequence of hillslopes of increasing curvature, and decreasing soil depths, from bottom to top. As curvature increases, denudation rate increases, soils thin, and the chemical weathering rate increases (cf. Figure 6-4). However, as hillslopes continue to steepen, for example in an actively uplifting alpine landscape, and denudation rates continue to increase, soil thicknesses decline to zero and chemical weathering rates largely cease. A 'speed limit' is therefore imposed on chemical weathering rates (Dixon et al. 2012). Figure 6-9a reproduced with permission from John Wiley and Sons.*

If bare bedrock is exposed, then features such as tors may form. Exposed bedrock landforms typically take much longer to weather and erode, thereby promoting the formation, or maintenance, of a higher relief. This model is supported by observations of modern weathering profiles, where thick in situ regoliths develop beneath summits, with the thickness of the weathering zone relating directly to the thickness of the vadose zone, which in conditions of positive water balance (precipitation > evaporation) is controlled by stream incision (local base level) and the coincident downwards advection of mineral reaction fronts (Lebedeva et al. 2007, Brantley and White 2009, Goodfellow et al. 2014a, Anderson et al. 2019; Figures 6-10 and 6-11). A variation on the control exerted by stream incision on weathering zone thickness relates to the interaction of surface parallel compressive stresses and topography (St Clair et al. 2015). Where the ratio of horizontal compressive tectonic stresses to near-surface gravitational stresses is relatively large, the weathering zone is thickest across hills and has a convex base that mirrors the surface topography. Where the magnitude of the highest compressive stress is relatively small, the base of the weathering zone parallels the surface topography. The absence of vascular plants may have assisted the development of thick weathering profiles in the Precambrian because the formation of clay minerals seemingly occurred at much slower rates (Kennedy et al. 2006). This is because a lining and eventually plugging of pores with clay reduces regolith porosity and permeability and diverts water flow from vertical pathways to more horizontal pathways, thereby providing a negative feedback on weathering rates and on regolith thickening. Where clays precipitate slowly, the Fe oxidation front can progress unimpeded except for decreased efficiency due to the thickening of regolith (Gilbert 1877, Carson and Kirby 1972, Ahnert 1987, Heimsath et al. 1997). A scarcity of clay during thickening of regolith may also contribute to the observed differences between the low relief Subcambrian peneplain and the higher-relief bedrock surface beneath kaolinitic Mesozoic saprolite in southern Sweden (e.g., Lidmar-Bergström et al. 2017). The formation of a low-relief surface under a thick regolith cover would further imply that the landscape formed under conditions of positive water balance (Figure 6-10). However, in addition to the possible slow precipitation of clay, regolith weathering during the late Precambrian appears to have occurred under lower than present atmospheric O_2 concentrations but potentially much higher than present CO_2 concentrations (Kump 2008, Brantley et al. 2014, Liivamägi et al. 2014).

With the additional absence of vascular plants, Precambrian regolith formation appears to have proceeded under conditions different to those characterizing the Earth's surface today. These different conditions may also have been important in the formation of the geologically unique SCP and Great Unconformity.

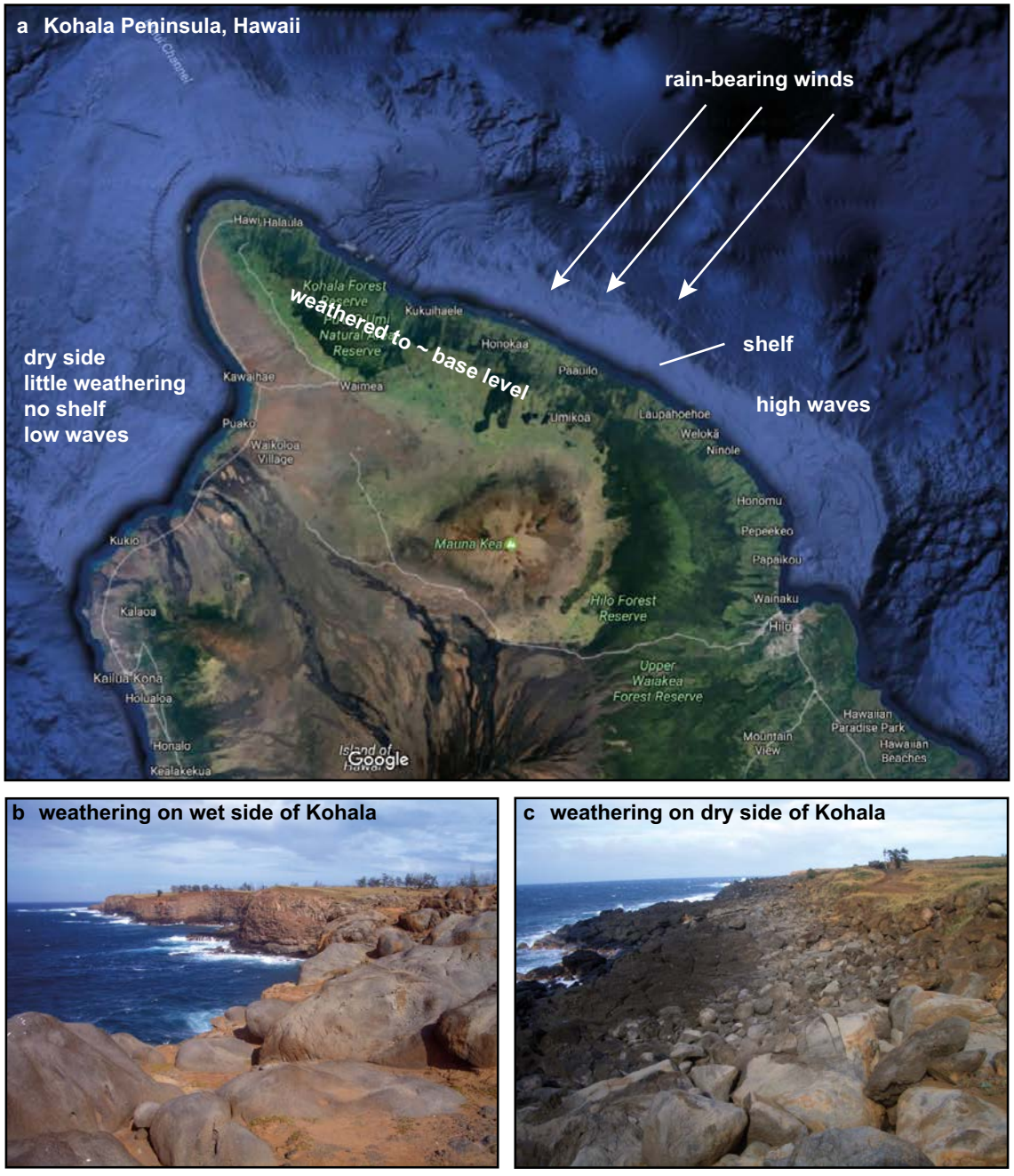

Figure 6-10. *Rock weathering on Kohala Peninsula, Hawaii, USA. (a) Google Earth image of Kohala Peninsula, also showing offshore bathymetry. Rain-bearing Trade Winds approach the 1 700 m-high mountain front from the northeast, delivering up to 4 000 mm of rainfall a year to this side of the mountain, while also attacking its flank with high waves. (b) Because of the high rainfall, the basalt has comprehensively weathered to local base level, which corresponds with stream incision level, and produced 40 m-high cliffs at the coast. As the mountain subsides, waves exploit the mechanical boundary between weathered and unweathered rock to produce a broad low relief shelf, with amplitudes of bedrock convexities limited to meters. (c) Conversely, on the dry, leeward side of Kohala Peninsula rock weathering is limited to meters and corestones remain abundant in the weathering zone, waves are low, and there is no offshore shelf. Figures 6-10b and c are from Goodfellow et al. (2014a), reproduced with permission from John Wiley and Sons.*

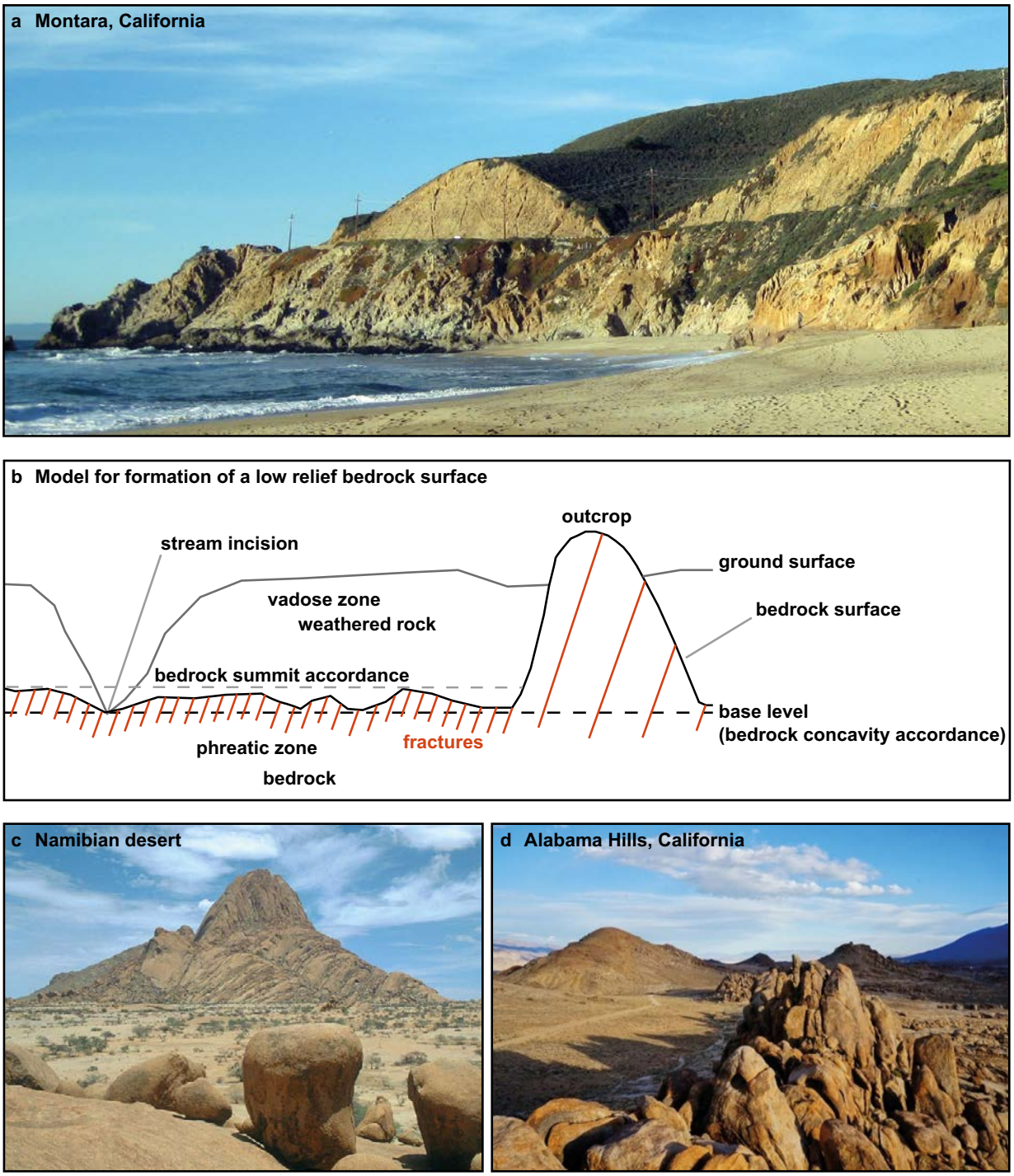

Figure 6-11. *Weathering zone developed in granite and exposed by coastal erosion at Montara, in central California, USA. (a) Weathering to grussic saprolite has occurred to local base level, set by stream incision, to produce an underlying bedrock surface with convex bumps displaying only meter-scale amplitudes. Unweathered bedrock outcrops in stream beds and on slopes and ridge crests higher up on Montara Mountain. (b) Conceptual model for the formation of a low relief bedrock surface at the base of a weathering zone. The thickness of the weathering zone corresponds with stream incision level, where stream beds occur on unweathered rock. Deepest weathering occurs beneath interfluve summits and base level is marked by the bases of concavities in bedrock rather than the apexes of convexities. Kernels of sparsely jointed rock resistant to chemical weathering might not be over-topped by weathered rock and persist as convex bedrock landforms. (c) An example from the Namibian desert of relief maintained in subaerially-exposed granite. (d) Tors occur where bedrock is subaerially exposed in the Alabama Hills, California, USA.*

The Precambrian landscape may have maintained a regolith cover of meters to tens of meters thick, which was stripped during the Cambrian transgression by nearshore currents and waves. The frequent preservation of regolith remnants inferred to have weathered in the Precambrian (Angerer and Greiling 2012, Gabrielsen et al. 2015, Liivamägi et al. 2015) indicates that stripping by marine processes occurred under low wave-energy conditions, based on the assumption that marine processes functioned then as they do now. This does not exclude marine sedimentation during Cambrian transgression from taking place during storm events, but it would imply an upper limit on the magnitude of resulting wave heights. Where a steeper landscape gradient was maintained offshore, the waves may not have fully dissipated by surfzone breaking and shore platforms may have formed, which migrated inland as the transgression progressed. It appears that on the SCP marine sedimentation during the Cambrian transgression generally occurred under storm wave conditions (Nielsen and Schovsbo 2011, Went 2013). This contrasts to the Great Unconformity across North Africa, where sedimentation is inferred to have a fluviatile component attributable to a continent-wide braided river system (Avigad et al. 2005). Where a very low gradient Subcambrian landscape occurred, at least some of the regolith stripping to form the SCP may more likely have occurred in a surfzone fringing a very shallow shelf or in slightly deeper waters where wave bases and currents interacted with the bed.

Evidence for the presence of weathering profiles preceding the Cambrian transgression is found in (i) the common remnants of oxidized weathering profiles of variable thicknesses (Angerer and Greiling 2012, Liivamägi et al. 2014, 2015, Gabrielsen et al. 2015) and, (ii) pallid weathering zones up to a few meters in thickness in, for example, Kinnekulle and Lugnås (pers. obs.). We infer that these pallid zones may represent upper phreatic zone weathering under anoxic conditions, which implies the former superposition of a vadose zone.. We also speculate that weathering profiles may have provided a source for lower Cambrian marine sedimentary deposits that varied in thicknesses from a few tens of meters to hundreds of meters (Nielsen and Schovsbo 2011). The conglomerates, which are of thicknesses limited to tens of centimeters, may have been sourced as corestones in weathering profiles, whereas grains of residual K-feldspar and, in particular, quartz, provided sediment sources for the abundant sandstones. Quartz is, for example, abundant in the tens of meters thick Precambrian weathering profiles preserved in Estonia (Liivimägi et al. 2014). Unless the lower Cambrian sediments were sourced from the regoliths on the early Cambrian landscape, it otherwise presents a challenge to understand why extensive sedimentation by sandstones coincided with a transgression across a low-relief landscape. This is because potential energy decreases as the elevation difference between high points and sea level decreases; thus, transgression is unlikely to coincide with renewed fluvial incision and stream knickpoint propagation required for sediment production. Marine wave erosion of unweathered bedrock may also have been limited if gentle offshore gradients effectively dissipated wave energy.

The absence of vascular plants provides a potential challenge to the development of thick regolith mantles because the roots of modern plants bind regolith and slow erosion. Where vegetation is sparse, such as in deserts and on beaches, regolith is most susceptible to erosion. The absence of vascular plants is a key argument for the SCP having been an inert bare bedrock platform (Rudberg et al. 1976, Calner et al. 2013, Gabrielsen et al. 2015). However, the absence of vascular plants does not preclude the existence of other life forms that could have acted to bind regolith. Indeed, microbial and algal mats, which are effective soil binding agents in some modern deserts, had evolved well before vascular plants (Simpson et al. 2013). Regolith profiles, meters to tens of meters thick, may have been maintained by these organic communities.

Because deep rooting was absent and because clay production may have been slow, stream bank stability was potentially low, resulting in broad, shallow, sandy, braided and/or anastomosing streams (Avigad et al. 2005, Gibling et al. 2014), which also provided sand for ventifacting bedrock surfaces and boulders exposed along stream channels and coastlines. Observations supporting the presence of exposed, ventifacted, bedrock on the SCP prior to marine transgression (Calner et al. 2013) may therefore be reconciled with other observations supporting a regolith cover that may have generally been meters to tens of meters thick.

We propose a model for formation of the SCP that includes mafic underplating to maintain slight positive topography over 10^8 years timescales, weathering to form thick regolith profiles that scale with relief on the SCP prior to Cambro–Ordovician marine transgression, and marine wave and current exploitation of the difference in cohesive strength at a mechanical boundary within or at the base of the weathering profile, to produce a low-relief surface over large regions. This model helps to explain

the formation of an unconformity, that largely concords with a Davisian-style peneplain with respect to relief. However, a notable difference is that the model we propose retains relief and regional gradients on the subaerial Precambrian landscape, prior to transgression. While transgression plays a key role in lowering relief to that observed on the unconformity, a residual relief of varying wavelength and amplitude and regional gradients are retained.

Our proposed model, combined with observations of the SCP close to cover rock remnants, particularly in southeastern Sweden, calls into question the practice of reconstructing the shape of the SCP from summit elevations in regions where topography is more pronounced and where cover rocks are lacking (Figure 2-2; Lidmar-Bergström et al. 2000, 2007, 2013, Bonow et al. 2003, Japsen et al. 2018, Hall et al. 2019a). According to our observations and model for formation of the unconformity, bedrock summits exist and existed above the base level of the unconformity. Former base levels were located at, or near, the bases of concave parts of the unconformity, driven by river incision rates, rather than on the summits. Care should therefore be taken to separate the construction of envelope surfaces from summits, used to estimate erosion volumes, from the Eulerian inference that real peneplains are being reconstructed. Only in exceptional cases might the two correlate. This is because unknown amounts of summit erosion, in addition to an unknown signature of the antecedent topography, will lead to erosion volumes being under- or overestimated from summit envelopes. In the case of the glacially eroded Subordovician unconformity at Forsmark (Hall et al. 2019a), total integrated summit erosion of as much as tens of meters, estimated from cosmogenic nuclides, implies, for that location, that erosion volumes across the landscape are likely underestimated from the summit envelope. However, given that the topographic amplitudes in Forsmark of c 60 m are similar to those observed on the basement along the Cambrian sandstone margin in southeastern Sweden, there is even a chance that erosion volumes might conversely be overestimated. Uncertainties remain, therefore, significant. Erosion volume estimates of meters to tens of meters have uncertainty ranges of meters to tens of meters.

We further highlight that using the SCP/Great Unconformity, which displays low residual relief of a magnitude and extent that appears to be unique in the geologic record, as a general interpretative model for landscape evolution is likely to be flawed. Specifically, inferring remnants of former peneplains in accordant summits is frequently questionable (e.g., Japsen et al. 2018), particularly in the face of alternative process-based explanations for their formation (Egholm et al. 2015, Andersen et al. 2018, Braun 2018) and in the absence of cover rock constraints. In addition, making arguments for the temporal evolution of a landscape, in this case the SCP, from spatial data on what remains at the end of that evolution is untenable in the absence of data on processes and erosion rates.

The logical argument against using a unique geologic feature as the foundation of a general model for landscape evolution, however, also poses a challenge to the converse; i.e., using modern analogues and process-based arguments derived from modern landscapes to explain a 0.5 billion-year-old geologically-unique feature. We recognize that unavoidable challenge to inferring processes of formation for the SCP/Great Unconformity, which we attempt to meet through use of observations, measurements, and process-based arguments from modern partial analogues to propose a formational model, which also recognizes how the differences between the modern Earth and the Precambrian might influence Precambrian landscape evolution. Those differences in the Precambrian landscape include the absence of vascular vegetation, lower and higher atmospheric partial pressures of O_2 and CO_2, respectively, and mafic underplating to form thick dense cratonic crust. While clear uncertainties remain, this approach differs from using a single, geologically unique, feature as the general governing model for landscape interpretation.

Given that we are making arguments for how a surface may have formed ~0.5 billion years ago, which is also seemingly unique in the geologic record, there is speculation and uncertainty. We therefore highlight that the model we propose is not the only possible model for the formation of the SCP. We note that continental glaciation during Precambrian Snowball Earth has also been invoked as a potential mechanism for formation of the low relief of the Great Unconformity (Keller et al. 2019). This model is based on the salient observations of global oxygen and hafnium isotope excursions in magmatic zircon and the globally low volumes of preserved Precambrian sediments. This model is difficult to reconcile with the weathering and erosion model we present here, unless glacial erosion left a residual relief that was later weathered and from which evidence of glacial landforms was removed by the inferred subsequent weathering and erosion. We do not, however, dismiss this model or the salient observations which support it. Rather, we acknowledge the importance of diverse hypotheses as a key component to advancing our knowledge on an old, enigmatic landscape.

7 Conclusions

7.1 In brief

- We propose a hypothesis for the formation of an areally-extensive low-relief Subcambrian unconformity (Subordovician at Forsmark) incorporating the need for crustal underplating, the maintenance of a regolith cover on the Precambrian landscape through weathering to local and regional base levels, and finally marine erosion at, or near, the base of the vadose zone to produce an unconformity surface with relief amplitudes generally constrained to 10^0–10^2 meters over wavelengths of 10^1–10^3 m.
- The Subcambrian unconformity and Precambrian land surface are not the same feature. The unconformity formed during the Cambro–Ordovician marine transgression(s) through erosion of weathered rock by marine processes rather than representing the Precambrian land surface, which we argue had a regolith cover and higher relief. The landform identified in the modern landscape as the Subcambrian peneplain has evolved from the Subcambrian unconformity through lowering and topographic modification by erosion processes, including ice sheet erosion, following exhumation from beneath Cambro–Ordovician cover rocks.
- We suggest some pathways to resolve differences between historical- and process geomorphology following advice by Rhoads and Thorn (1996), especially concerning their notion in Table 2-1 on page 28 that "Observations that are undertaken to evaluate a comprehensive theory presuppose that very theory in a way that prevents an objective test of that theory".
- We propose three methodological approaches for future attempts to reconcile contrasting observations and conceptualizations of relief on the SCP; these include (i) the application of a least-squares best-fit plane to each of the CFSs to test if the strike, dip, and misfit values of the best-fit planes are statistically compatible with being from the same population; (ii) the use of the concepts of absolute and relative relief; and (iii) the application of a conceptual separation of the bedrock surface at the time of Cambrian transgression from the surface that was formed by the transgression.
- We offer six general recommendations for landscape interpretation based on our considerations of SCP relief; these include (i) migrate from subjective, qualitative and semi quantitative assessments to quantitative assessments of relief; (ii) defocus the emphasis on flatness and summit accordance, and refocus on the importance of higher relief parts of the inferred SCP and dissected parts of the Swedish landscape that are not classified as SCP; (iii) increase focus on process rather than morphology; (iv) make a conceptual adjustment from peneplains, graded to base level, being generally preserved on summits to summits being located above the general base level during formation of the 'peneplain'; (v) apply caution when inferring that exceptionally low relief summits represent the general relief of the Subcambrian unconformity; and (vi) avoid using the exceptionally-low relief of what appears to be a geologically unique landform (the SCP/Great Unconformity) as a general, or sole, model to assess the evolution of other, younger, landscapes.
- We advance interpretations of the SCP relief and its glacial modification at Rockneby and Fågelmara, southeastern Sweden, and at Trollhättan and Nordkroken in southwestern Sweden. At the sites in southeastern Sweden, the ice sheet lowered the landscape a few meters by eroding partly weathered bedrock that may include lowering and flattening of, at least some, convexities. At the latter site, ice sheet erosion appears to be in the meters to tens of meters range, and has been strongly guided by landscape physiography, especially the influence of Halleberg and Hunneberg. We cite cosmogenic nuclide evidence of bedrock erosion rates and depths, the ubiquitous streamlining of bedrock and/or formation of roche moutonnées on and around studied outcrops, ice sheet model inferences of streaming through this area, and the location of this landscape between a lake basin (Lake Vänern) and the only fjords along the Swedish west coast as direct and indirect evidence for glacial erosion.

- The conspicuously flat surfaces (CFSs) at Trollhättan and Nordkroken reflect a primary structural control exerted by subhorizontal sheeting joints, revealed on GPR images. These joints may have been exploited by Quaternary glacial erosion or even been formed by hydrofracturing related to high proglacial or subglacial water pressures to initiate the erosion of overlying slabs of rocks to produce the CFSs. Glacial abrasion may have contributed to further flattening of the SFSs.
- The relief that we see at Forsmark may approximate the antecedent SCP relief. It is, for example, similar to that seen on the SCP adjacent to, and under, the cover rock margin in the Fågelmara area. One implication of that is that we cannot necessarily assign all of the relief now present, independent of block movements, to Quaternary glacial erosion.

7.2 Hypothesis for the formation of an exceptionally low relief unconformity

We propose a hypothesis for the formation of an aerially-extensive low-relief unconformity incorporating the need for underplating, weathering to local and regional base level, and finally marine erosion at, or near, the base of the vadose zone to produce a surface with relief amplitudes generally constrained to 1–20 m over wavelengths of 10–1 000 m. This model is based on observations of the Subcambrian peneplain (SCP) in southern Sweden and of weathering zones in locations as diverse as those developed in Californian granite and Hawaiian basalt. While no single observation provides a precise analogue, observations from such diverse locations are valuable to constructing a plausible model for how an exceptionally low relief unconformity might develop across regional spatial scales.

The SCP, and its continuation as the Great Unconformity, in terms of being a uniquely low relief, low elevation unconformity that covers vast areas, may conform with the Davisian concept of a peneplain. However, timescales of formation from initial orogenesis are in the order of 1–2 billion years (Stephens et al. 2010). These exceptionally long periods of underplating, weathering, and denudation might explain why peneplains are not more generally observed in younger landscapes.

Our proposed model of formation of the SCP does not require that the Precambrian subaerial landscape to have been of very low relief. To the contrary, the maintenance of relief (tens to even some hundreds of meters over different wavelengths) on the land surface and associated thick mantles of weathered rock (tens of meters, and more in some places) are explicitly required to produce a bedrock surface with only up to ~20 m relief at the vadose–phreatic zone interface. From observations of modern landscapes, a thin weathering zone (up to meters thick), where bedrock crops out in many places, is likely to produce a bedrock surface that retains more relief than generally observed on the SCP. If our model is correct, the SCP does not, from a geomorphic process-based perspective, strictly conform to the Davisian conceptualization of peneplanation. Areally-extensive, rather than patchy, regolith mantles are also required to source extensive Cambrian offshore deposits, particularly during transgressions when potential energies driving fluvial erosive processes are further lowered.

Our model does not produce a surface that is everywhere entirely flat. Residual relief is expected for the base of the weathering zone and is observed across different wavelengths. We agree with previous interpretations of the SCP that relief amplitudes are generally meters to a few tens of meters but recognize that higher amplitude examples also occur. Although the presence of higher relief frequently appears attributable to block movements associated with faulting, in the Öland–Kalmar area, for example, it appears also to be related to other controls, such as lithological variations. The presence of locally flat surfaces is also not excluded where lithological controls such as spacings of sub-vertical joints of tens of centimeters occur. However, we emphasize that residual relief comprised of short wavelength (10^1–10^2 meters) convexities superimposed on long wavelength (10^3–10^5 meters) regional gradients is the general condition.

7.3 Reconciling contrasting observations and conceptualizations of relief on the SCP

Contrasting observations of relief on the SCP, and models of relief generation, can be, at least partly, reconciled through:

1. At Nordkroken–Trollhättan fit a least-squares best-fit plane to each of the CFSs to test if the strike, dip, and misfit values of the best-fit planes are statistically compatible with being from the same population. Since the SCP is visible as a contact (a contour) but not as a uniformly sampled surface, whereas the Nordkroken and Trollhättan CFSs are visible, take random contours of the CFSs and then extract the 1D spectrum (amplitude vs. wavelength) of the SCP and CFS contours by taking a Fast Fourier Transformation (FFT) to test if the spectra are statistically compatible with being from the same population. The using the 2D spectral method from Perron et al. (2008), compare the spectra of the SCP and CFSs. However, because the density of data points would be different between the SCP (beneath cover rocks and visible adjacent to its margins), this latter method might be the least sound.
2. Use of the concepts of absolute and relative relief, which are defined by Martel (2017) using amplitude/wavelength ratios. Whereas absolute relief may be low (for example, where amplitudes might be tens of meters measured over wavelengths of kilometers), relative relief may be high (for example where 10 m amplitudes occur over wavelengths of 100 m superimposed on the long wavelength topography).
3. Conceptual separation of the bedrock surface at the time of Cambrian transgression from the surface that was formed by the transgression. The usual location of the Cambrian bedrock surface was likely below a zone of weathered rock. Exceptionally flat surfaces may have formed in locations where marine waves and currents cut into the weathered rock to a specific level, rather than down to unweathered bedrock. This level may have been defined by the location where the cohesive strength of the weathered rock equaled the tractive forces imposed by waves, currents, and bedload, i.e. whatever clastic sediments were being transported across the actively evolving subhorizontal surface.

7.4 General recommendations for landscape interpretation based on our considerations of SCP relief

1. Migrate from subjective, qualitative and semi quantitative assessments to quantitative assessments of relief, as described above.
2. Defocus the emphasis on flatness and summit accordance and refocus more on the importance of higher relief parts of the inferred SCP and dissected parts of the Swedish landscape that are not classified as SCP.
3. Increase focus on process rather than morphology. We argue that the morphology cannot be fully interpreted unless we understand how the morphology formed. Past qualitative descriptions of morphology have provided important background but the tools are now available to use that accumulated information to constrain quantitative studies and guide development of process-based models.
4. Make a conceptual adjustment from peneplains, graded to base level, being generally preserved on summits to summits being located above the general base level during formation of the ‘peneplain’. Convexities are present on the SCP rather than present summits being ‘the’ remnants of the SCP.
5. Apply caution when inferring that exceptionally low relief summits represent the general relief of the Subcambrian unconformity. In particular, outcrop summits at Nordkroken and Trollhättan display exceptionally low relief and are developed in kernels of rock displaying exceptionally wide spacing (i.e., tens of meters) of vertical joints. At best, they are low endmember examples of relief of the Subcambrian unconformity and, if our interpretations are correct, they are surfaces that have been exposed following lowering and perhaps also flattening of inferred overlying bedrock through erosion along sheeting joints by Quaternary ice sheet flow around the table mountains.
6. Avoid using the exceptionally low relief of what appears to be a geologically unique landform (the SCP/Great Unconformity) as a general, or sole, model to assess the evolution of other, younger, landscapes.

7.5 Suggestions for pathways to resolve differences between historical- and process geomorphology

We identify the following form of theory-laden observation as defined by Rhoads and Thorn (1996) as particularly problematic to the study of pre-Quaternary landscape evolution: "Observations that are undertaken to evaluate a comprehensive theory presuppose that very theory in a way that prevents an objective test of that theory" (Rhoads and Thorn 1996, p 28). To address this issue, we advocate the use of working hypotheses, genuine testing that invokes falsification, acknowledgements of uncertainty, and the opportunity to evolve our theoretical models as new information comes to light. In particular, we regard the following paradigms, that are sometimes explicitly stated, but are often implicitly assumed, as problematic and should undergo either reformulation as working hypotheses and subjected to genuine testing, or be abandoned.

(i) The assignment of the genetic term 'peneplain' to a low-relief erosional surface. This includes elevating model surfaces constructed from summit envelopes to the status of 'reconstructed peneplains';

(ii) That the Subcambrian unconformity is conceptualized as totally flat over all wavelengths in all places to justify strict Eulerian interpretations of subsequent landscape evolution, including through Quaternary glacial erosion;

(iii) That where peneplains are inferred they are universally preserved in summits;

(iv) That summits, including those that are accordant, do not erode or only undergo trivial erosion;

(v) That summit accordance necessarily indicates peneplains and only peneplains;

(vi) That glacial erosion only increases relief; and;

(vii) That glacial erosion can only produce summit discordance. On the other hand, developing models for the formation of the Subcambrian unconformity also provides a challenge for process geomorphologists. They, instead, struggle with the difficulty of inferring a temporal history from merely those fragmented spatial data that remain of the conclusion of its formation. To raise the challenge to process geomorphologists further, Precambrian environments display marked differences to those that exist today. It is therefore crucial that knowledge of contemporary processes, founded in laws of physics and chemistry, is applied to reconstructed environmental characteristics of the Cambrian and Precambrian to understand the landscape evolution that ultimately led to the formation of the Subcambrian unconformity. We see in the identification of Snowball Earth periods during the late Precambrian an outstanding parallel example of how knowledge of contemporary geologic processes has been used to reconstruct geologic events in deep time. Whereas Snowball Earth periods do not conform to uniformitarian principles, their identification in the sedimentary record and understanding of their potential causes was based on an understanding of diverse geologic processes that characterize modern environments and the recent past (Hoffman et al. 1998).

7.6 Interpretation of the SCP relief and its glacial modification at Rockneby and Fågelmara, southeastern Sweden

The contribution of glacial erosion to the relief expressed on the SCP is difficult to ascertain precisely because modification commenced immediately following cover rock removal. This is clearly displayed at Rockneby, southeastern Sweden (Figure 2-3), where glacial ice initially flattens the landscape and lowers it a few meters by eroding partly weathered bedrock (Figures 2-3 and 2-5a). The basement further South at Fågelmara appears to emerge from beneath Cambrian sandstone with relief amplitudes of a few meters to more than ten meters over wavelengths of hundreds of meters (Figures 2-3 and 2-6). This includes convex domes with visible relief of meters. Quaternary tills comprised of abundant, large, angular blocks are also a feature of this area (Figure 6-5b–d). Similar to Forsmark (Hall et al. 2019a), numerous blocks have dimensions of meters. The domes being exhumed from beneath cover rocks might be key sources of these large blocks because the domes seem like prime candidates for the development of sheeting joints, and they display vertical joint spacings of meters. Some of them show surface indications of sheeting joints (Figure 6-5a) and the only one we have subjected to GPR measurements, which is also the lowest-relief example of which we are aware (Figure 2-4e), showed reflectors that we interpret as subsurface sheeting joints (Figure 5-15). Where these domes are underlain

by sheeting joints, they may be susceptible to glacial erosion to produce tills comprised of large boulders and leaving bedrock plinths that have previously been identified as SCP. Sheeted bedrock convexities of comparable amplitudes have elsewhere been demonstrated to be highly susceptible to glacial erosion and to produce gently convex plinths when eroded, while also leaving surrounding areas largely intact (Phillips et al. 2006).

The basement at the Cambrian sandstone margin in southeastern Sweden provides an excellent opportunity to better constrain relative relief on the SCP and how it has been altered by glacial erosion, potentially including through excavation of antecedent concavities and through lowering and flattening of, at least some, convexities. It forms a valuable analogue to Forsmark because relief amplitudes are similar, it is located in an area of similar basal sliding distances (Figure 6-8a) and therefore similar intensity of glacial erosion, it displays similar blocky till characteristics, and because the emergent basement can be observed along a more than 100 km margin of Cambrian sandstone.

7.7 Interpretation of the SCP relief, with a focus on conspicuously flat surfaces (CFSs), and its glacial modification at Trollhättan and Nordkroken

Glacial erosion in the Trollhättan and Nordkroken area is strongly guided by landscape physiography. For example, in contrast to a considerable amount of glacial erosion that we infer off the west flank of Halleberg, glacial erosion may have been much less effective off its east flank. This is because the 100 m-high vertical wall of Halleberg forms a marked topographic barrier to ice flow, therefore potentially limiting the ability for ice to erode the basement rock east of Halleberg. Indeed, on the east side of Halleberg, we cannot exclude the possibility that most convexities in this area largely reflect the original character of the unconformity.

We infer that the exceptionally flat surfaces west of Halleberg and Hunneberg at Nordkroken and to the SW in Trollhättan, which often form summits, have experienced glacial erosion and cite cosmogenic nuclide evidence of bedrock erosion, the ubiquitous streamlining of bedrock and/or formation of roche moutonnées on and around these outcrops, ice sheet model inferences of streaming through this area, and the location of this landscape between a lake basin (Lake Vänern) and the only fjords along the Swedish west coast as evidence for this. Although our data offer no precision on how much these summits have been lowered, it nevertheless appears to be in the meters to tens of meters range.

We consider the Nordkroken surfaces to be the clearest candidates for erosion through exploitation of sheeting joints. These surfaces are formed in kernels of coarse-grained granitic-gneiss with vertical joints spacing of meters to tens of meters, which are usually associated with convex landforms. Here, it is plausible that former convexities, with amplitudes perhaps up to few tens of meters, have been glacially eroded along sheeting joints to yield a reduction in relief and a lower bedrock surface. One potential process responsible for this erosion, through the propagation of existing fractures and the formation of new ones, is subglacial hydrofracturing.

The similarly low relief surfaces at Sandhem, Hjortmossen, and Eriksroparken are more enigmatic. As with Nordkroken, they are formed in kernels of coarse-grained rock with vertical joints spacing of meters to tens of meters. From this we again infer that these surfaces may have existed as convex forms above the surrounding low relief unconformity. We consider that their exceptionally low relief surfaces could well reflect a first order structural control, specifically through erosion of bedrock sheets. However, on the basis of close accordances of large parts of the summit areas of each of these outcrops, we cannot exclude the possibility that these remarkable surfaces reflect the original local forms of the SCP and have undergone only a few meters of glacial erosion in total. Glacial erosion might involve hydrofracturing or plucking, both of which would remove sheets, and/or abrasion. They are resistant to vertical dissection during glaciations because of the exceptionally wide spacing of vertical joints, particularly those oriented parallel to the direction of ice flow (Figure 5-19). However, the same jointing pattern might make them susceptible to erosion along pre-existing, or newly formed, subhorizontal sheeting joints during glaciation. The possibility that these surfaces closely approximate the original form of the overlying unconformity and are located within a few meters of it can be accommodated in our model. This occurs if surrounding areas, which are presently lower and frequently concave, were developed in intensely fractured and/or weathered rock and displayed an unconformity surface with

meter-scale relief at about the same elevation at the modern day almost-flat summits. Sheeting joints would preferentially form in the sparsely jointed rock kernels that now form these near flat-topped domes and the surrounding rock would be more easily eroded by Quaternary glacial ice. If this model, which broadly conforms to the traditional interpretation of these surfaces, is correct, how these types of rock kernels could weather to such low relief surfaces remains an outstanding unresolved question. If large thicknesses of rock sheets have been glacially eroded, these summits might still approximate the former general level and form of the SCP, but in an unexpected way.

We caution against using the exceptionally low relief surfaces developed in the kernels of rock displaying exceptionally large crystal sizes and broad joint spacing, as the analogue for the Subordovician unconformity at Forsmark. We apply further caution to their utility as analogue surfaces because they are located in a landscape that also contains two vertical-sided 100 m high table mountains, and which has undergone higher rates of glacial erosion than at Forsmark, based on the cosmogenic nuclide data (Figures 5-29 to 5-34; Table 5-1), more efficient transport of erosional products away from this area, based on mapping of Quaternary sediments (Figure 6-8b), and model inferences of longer basal sliding distances of glacial ice (Figure 6-8a). The possibility that they represent surfaces that have been lowered, and even further flattened, by Quaternary glacial erosion cannot be excluded based on the evidence we have accumulated. However, given their proximity to Cambro–Ordovician cover rock remnants, and that similar, but not as flat or areally-extensive, examples also occur in the Fågelmara area, they may alternatively provide a low end-member example of relief on the SCP, as has been previously inferred for the surfaces. As such, they would appear to be special cases, rather than providing for a general analogue.

7.8 Implications for Forsmark

The relief that we see now at Forsmark may approximate the antecedent SCP relief. It is, for example, similar to that seen on the SCP adjacent to, and under, the cover rock margin in the Fågelmara area. One implication of that is that we cannot necessarily assign all of the relief now present, independent of block movements, to Quaternary glacial erosion.

We emphasize our use of ‘approximate’ to indicate other implications. From our Lagrangian perspective, Quaternary glacial erosion exploits pre-existing topography and bedrock structure to excavate valleys in some locations, thereby increasing relief. However, it may also maintain low relief where rock structure, such as closely spaced joints, favours that. The Ironworks Block site (Hall et al. 2019a) might be an example of this. Initial investigations indicate closely-spaced vertical joints over a broad area. This may have predisposed formation on this block of a Subordovician uniformity displaying only meter-scale relief. However, that same rock structure is also anticipated to favor roughly even rates of glacial erosion over that block, thereby maintaining low relief. Indeed, a key component of our cosmogenic nuclide data from the Forsmark area (Hall et al. 2019a), including samples from the Ironworks Block, is that they are well clustered and generally indicate 1–3 meters of erosion during the last glacial cycle. Only one sample indicated more than 3 meters of erosion and there were only a few outliers indicating less than 1 meter of erosion during the last glaciation. If, alternatively, the Ironworks Block has not undergone much glacial erosion and it essentially represents the unconformity surface, how this interpretation might be explained remains unresolved. This is because the present Cambro–Ordovician cover rock margin lies 50–60 km away in basins to the north and southeast. While the cover rock margin has retreated by 50–60 km from the Ironworks Block to its present locations, it is stated that the Ironworks Block has been lowered by less than ten meters over the same period. This implies that erosion of the fractured basement of the Ironworks Block has occurred at 1/10 000 of the rate of cover rock recession. While sedimentary rocks are more susceptible to glacial erosion than crystalline basement, a four orders of magnitude difference should be questioned and tested. Because the Ironworks Block forms a topographic high it seems a most unlikely location to maintain a cover rock outlier and the formation of persistent cold-based ice also seems most unlikely in this low elevation, low relief landscape. We do not dismiss the possibility that this surface closely approximates the Ordovician unconformity in elevation, but also note that there is quantitative evidence in uranium mobilization (Hall et al. 2019a) and from our cosmogenic nuclide depth profile (Hall et al. 2019a) that cover rocks may have been removed around 1 million years ago. Based also on our cosmogenic nuclide data, this would imply lowering of the Ironworks Block and the wider Forsmark-Uppland area by a few tens of meters through Quaternary glacial erosion.

It is also possible that Quaternary glacial erosion has diminished relief, at least locally, in the Forsmark area. This is evidenced in the extensive deposits of locally derived blocky tills, in which blocks with dimensions of meters are abundant (Lagerbäck et al. 2005, Hall et al. 2019a). As described above, similar deposits are also present in the Fågelmara area. Whether these blocky deposits have formed through plucking and/or ripping, as described in Hall et al. (2019a), it appears that their formation is at least partly attributable to erosion of summits, in agreement with Lagerbäck et al. (2005). Sheeting joints may also be important for inferred hydraulic fracturing and jacking and may therefore set erosional depths, inferred to be some meters per glaciation. Glacial lowering of summits and relief is also evidenced along the uplifted margins of blocks (Grigull et al. 2019, Hall et al. 2019a). Rather than solely exploiting the low parts of the downfaulted blocks to increase relief, the adjacent uplifted block margins have been ubiquitously eroded by glacial ice to lower summit elevations and decrease the local relief.

The bedrock blocks at Nordkroken, which display exceptionally low surface relief, may provide an analogue for the spectacularly sheeted rock masses observed at Forsmark (Carlsson 1979). This includes how they might be exploited by high pressure groundwater related to glaciations to jack them, inject sediments, propagate new joints, and ultimately erode them. Sheeting joints were observed on GPR under parts of these Nordkroken blocks, including the only location we surveyed where multiple reflectors were imaged from a single sheeting joint. This observation might indicate an exceptionally wide, sediment filled joint, similar to those observed at Forsmark (Carlsson 1979). In addition, we infer streaming ice flow over the Nordkroken blocks, which has been further enhanced by diversion around a topographic obstacle provided by Halleberg-Hunneberg. Basal ice sheet conditions may therefore be conducive to intense glacial erosion, including along sheeting joints. The location of both the Nordkroken and Forsmark sites on northwards-dipping blocks adjacent to the southern margins of basins presently filled with water might also be important and this similarity in topographic setting might be worthy of further exploration. It is further noted that sheeting joints extend for hundreds of meters in both locations under surfaces that display meter-scale relief, or lower. It may be that both locations reflect glacial erosion involving sheeting joints, including the potential further flattening of surface topography in some locations.

In Hall et al. (2019a) it is concluded on the grounds of the low relief bedrock morphology of the Forsmark area that glacial erosion has lowered the landscape on average by less than 10 meters. We agree that the low relief is consistent with that expected for the SCP. However, in our view we cannot exclude that erosion of some tens of meters has occurred. There remain key outstanding questions regarding how relief is developing through glacial erosion over time, including whether valley incision is confined to certain zones, the balance between processes that increase relief versus those that decrease relief, and whether a steady state is ultimately reached. The pervasive production of large blocks in the Forsmark and Fågelmara areas may reflect proximity to the Cambro–Ordovician unconformity. However, given that the basement bedrock is pervasively fractured to depths of tens, to even hundreds, of meters in places at Forsmark (Martin 2007), ‘proximity’ can at present only be loosely constrained to tens of meters.

8 Acknowledgements

We thank our Forsmark research team members Adrian Hall, Karin Ebert, Clas Hättestrand, and Maarten Krabbendam for stimulating arguments which have motivated us to sharpen the arguments and ideas presented in this paper. We also thank Jens-Ove Näslund (SKB) for supporting this research, and particularly for its publication. Sample preparation for AMS measurement of cosmogenic nuclides was completed by Tom Clifton and Greg Chmiel. SKB is thanked for their financial support. We thank Derek Fabel (SUERC, Glasgow) and Magnus Johansson (Karlstad University) for sampling assistance in Trollhättan in 2000.

References

SKB's (Svensk Kärnbränslehantering AB) publications can be found at www.skb.com/publications.

Ahnert F, 1987. Approaches to dynamic equilibrium in theoretical simulations of slope development. Earth Surface Processes and Landforms 12, 3–15.

Alinaghi A, Bock G, Kind R, Hanka W, Wylegalla K, TOR and Svekalapko Working Groups. 2003. Receiver function analysis of the crust and upper mantle from the North German Basin to the Archean Baltic Shield. Geophysical Journal International 155, 641–652.

Alm E, Sundblad K, 2002. Fluorite-calcite-galena-bearing fractures in the counties of Kalmar and Blekinge, Sweden. SKB R-02-42, Svensk Kärnbränslehantering AB.

Andersen J L, Egholm D L, Knudsen M F, Linge H, Jansen J D, Goodfellow B W, Pedersen V K, Tikhomirov D, Olsen J, Fredin O, 2018. Pleistocene evolution of a Scandinavian plateau landscape. Journal of Geophysical Research: Earth Surface 123, 3370–3387.

Anderson R S, Rajaram H, Anderson S P, 2019. Climate driven coevolution of weathering profiles and hillslope topography generates dramatic differences in critical zone architecture. Hydrological Processes 33, 4–19.

André M-F, 1996. Rock weathering rates in arctic and subarctic environments (Abisko Mts., Swedish Lappland). Zeitschrift für Geomorphologie 40, 499–517.

André M-F, 2002. Rates of Postglacial rock weathering on glacially scoured outcrops (Abisko–Riksgränsen area, 68°N). Geografiska Annaler 84A, 139–150.

Angerer T, Greiling R O, 2012. Fabric evolution at basement-cover interfaces in a fold-and-thrust belt and implications for décollement tectonics (Autochthon, Lower Allochthon, central Scandinavian Caledonides). International Journal of Earth Sciences 101, 1763–1788.

Anjar J, Larsen N K, Håkansson L, Möller P, Linge H, Fabel D, Xu S, 2014. A ^{10}Be-based reconstruction of the last deglaciation in southern Sweden. Boreas 43, 132–148.

Avigad D, Sandler A, Kolodner K, Stern R J, McWilliams M, Miller N, Beyth M, 2005. Mass-production of Cambro–Ordovician quartz-rich sandstone as a consequence of chemical weathering of Pan-African terranes: Environmental implications. Earth and Planetary Science Letters 240, 818–826.

Balco G, 2011. Contributions and unrealized potential contributions of cosmogenic-nuclide exposure dating to glacier chronology, 1990–2010. Quaternary Science Reviews 30, 3–27.

Balco G, 2017. Production rate calculations for cosmic-ray-muon-produced ^{10}Be and ^{26}Al benchmarked against geological calibration data. Quaternary Geochronology 39, 150–173.

Balco G, Stone J O, Lifton N A, Dunai T J, 2008. A complete and easily accessible means of calculating surface exposure ages or erosion rates from ^{10}Be and ^{26}Al measurements. Quaternary Geochronology 3, 174–195.

Bastani M, Persson L, Erlström M, Dahlqvist P, Jørgensen F, Lundh Gulbrandsen M, 2018. Improved geological information by modelling airborne TEM data over the island of Öland, Sweden. 7th International Workshop on Airborne Electromagnetics (AEM2018), Kolding, Denmark, 17–20 June 2018.

Bergman L, 1982. Clastic dykes in the Åland islands, SW Finland and their origin. Geological Survey of Finland, Bulletin 317, 7–33.

Bishop P, 1980. Popper's principle of falsifiability and the irrefutability of the Davisian cycle. The Professional Geographer 32, 310–315.

Bishop P, 2011. Landscape evolution and tectonics. In Gregory K J, Goudie A S (eds). The SAGE handbook of geomorphology. London: SAGE Publications, 489–512.

Bishop P, Brown R, 1992. Denudational isostatic rebound of intraplate highlands: The Lachlan River valley, Australia. Earth Surface Processes and Landforms 17, 345–360.

Björck S, Digerfeldt G, 1982. Late Weichselian shore displacement at Hunneberg, southern Sweden, indicating complex uplift. Geologiska Föreningens i Stockholm Förhandlingar 104, 131–155.

Blackburn T, Ferrier K L, Perron J T, 2018. Coupled feedbacks between mountain erosion rate, elevation, crustal temperature, and density. Earth and Planetary Science Letters 498, 377–386.

Blomdin R, Fu P, Goodfellow B W, Gribenski N, Heyman J, Newall J C, Stroeven A P (eds), 2015. Third Nordic Workshop on cosmogenic nuclide techniques: Celebrating 30 years of counting cosmogenic atoms. Stockholm: Svensk Kärnbränslehantering AB.

Bonow J M, Lidmar-Bergström K, Näslund J-O, 2003. Palaeosurfaces and major valleys in the area of the Kjølen Mountains, southern Norway – consequences of uplift and climatic change. Norsk Geografisk Tidsskrift 57, 83–101.

Borchers B, Marrero S, Balco G, Caffee M, Goehring B, Lifton N, Nishiizumi K, Phillips F, Schaefer J, Stone J, 2016. Geological calibration of spallation production rates in the CRONUS-Earth project. Quaternary Geochronology 31, 188–198.

Brantley S L, White A F, 2009. Approaches to modeling weathered regolith. Reviews in Mineralogy and Geochemistry 70, 435–484.

Brantley S L, Lebedeva M, Bazilevskaya E, 2014. Relating weathering fronts for acid neutralization and oxidation to pCO_2 and pO_2. In Holland H D, Turekian K K (eds). Treatise on geochemistry. 2nd ed. Oxford: Elsevier, 327–352.

Braun J, 2018. A review of numerical modeling studies of passive margin escarpments leading to a new analytical expression for the rate of escarpment migration velocity. Gondwana Research 53, 209–224.

Brook E J, Nesje A, Lehman S, Raisbeck G, Yiou F, 1996. Cosmogenic nuclide exposure ages along a vertical transect in western Norway: implications for the height of the Fennoscandian ice sheet. Geology 24, 207–210.

Calner M, Ahlberg P, Lehnert O, Erlström M, 2013 (eds). The lower Palaeozoic of southern Sweden and the Oslo Region, Norway: field guide for the 3rd Annual Meeting of the IGCP project 591. Uppsala: Geological Survey of Sweden. (Rapporter och meddelanden 133)

Carlsson A, 1979. Characteristic features of a superficial rock mass in southern central Sweden: horizontal and subhorizontal fractures and filling material. Uppsala : Societas Upsaliensis pro geologia quaternaria. (Striae 11)

Carson M A, Kirby M J, 1972. Hillslope form and process. Cambridge: Cambridge University Press. (Cambridge geographical studies 3)

Chmeleff J, von Blanckenburg F, Kossert K, Jakob D, 2010. Determination of the ^{10}Be half-life by multicollector ICP-MS and liquid scintillation counting. Nuclear Instruments and Methods in Physics Research Section B: Beam Interactions with Materials and Atoms 268, 192–199.

Cocks L R M, Torsvik T H, 2005. Baltica from the Late Precambrian to mid-Palaeozoic times: the gain and loss of a terrene's identity. Earth-Science Reviews 72, 39–66.

Cowton T, Nienow P, Bartholomew I, Sole A, Mair D, 2012. Rapid erosion beneath the Greenland ice sheet. Geology 40, 343–346.

Cuffey K M, Paterson W S B, 2010. The physics of glaciers. 4th ed. Amsterdam: Butterworth-Heinemann.

Davis W M, 1899. The geographical cycle. The Geographical Journal 14, 481–504.

Dixon J L, Heimsath A M, Amundson R, 2009. The critical role of climate and saprolite weathering in landscape evolution. Earth Surface Processes and Landforms 34, 1507–1521.

Dixon J L, Hartshorn A S, Heimsath A M, DiBiase R A, Whipple K X, 2012. Chemical weathering response to tectonic forcing: a soils perspective from the San Gabriel Mountains, California. Earth and Planetary Science Letters 323–324, 40–49.

Drake H, Tullborg E-L, 2009. Fracture mineralogy Laxemar. Site descriptive modelling SDM-Site Laxemar. SKB R-08-99, Svensk Kärnbränslehantering AB.

Drotz M K, Wängberg A-Å, Jakobsson E, Gustavsson E, 2014. Lake Vänern: historical outline. Aquatic Ecosystems Health and Management 17, 323–330.

Dunai T J, 2010. Cosmogenic nuclides: principles, concepts and applications in the earth surface sciences. Cambridge: Cambridge University Press.

Dunne J, Elmore D, Muzikar P, 1999. Scaling factors for the rates of production of cosmogenic nuclides for geometric shielding and attenuation at depth on sloped surfaces. Geomorphology 27, 3–11.

Dühnforth M, Anderson R S, Ward D, Stock G M, 2010. Bedrock fracture control of glacial erosion processes and rates. Geology 38, 423–426.

Ebert K, Hättestrand C, Hall A M, Alm G, 2011. DEM identification of macroscale stepped relief in arctic northern Sweden. Geomorphology 132, 339–350.

Ebert K, Hall A M, Hättestrand C, 2012. Pre-glacial landforms on a glaciated shield: the inselberg plains of northern Sweden. Norwegian Journal of Geology 92, 1–17.

Egholm D L, Andersen J L, Knudsen M F, Jansen J D, Nielsen S B, 2015. The periglacial engine of mountain erosion – Part 2: Modelling large-scale landscape evolution. Earth Surface Dynamics 3, 463–482.

Egholm D L, Jansen J D, Brædstrup C F, Pedersen V K, Andersen J L, Ugelvig S V, Larsen N K, Knudsen M F, 2017. Formation of plateau landscapes on glaciated continental margins. Nature Geoscience 10, 592–597.

Ehlen J, 1992. Analysis of spatial relationships among geomorphic, petrographic and structural characteristics of the Dartmoor tors. Earth Surface Processes and Landforms 17, 53–67.

Elvhage C, Lidmar-Bergström K, 1987. Some working hypotheses on the geomorphology of Sweden in the light of a new relief map. Geografika Annaler, Series A 69, 343–358.

Fabel D, Stroeven A P, Harbor J, Kleman J, Elmore D, Fink D, 2002. Landscape preservation under Fennoscandian ice sheets determined from in situ produced ^{10}Be and ^{26}Al. Earth and Planetary Science Letters 201, 397–406.

Flodén T, 1977. Tectonic lineaments in the Baltic from Gävle to Simrishamn. KBS TR 59, Kärnbränslesäkerhet (KBS).

Freeze R A , Cherry J A, 1979. Groundwater. Englewood Cliffs, NJ: Prentice Hall.

Friese N, Vollbrecht A, Leiss B, Jacke O, 2011. Cambrian sedimentary dykes in the Proterozoic basement of the Västervik area (southeast Sweden): episodic formation inferred from macro- and microfabrics. International Journal of Earth Sciences 100, 741–752.

Fu P, Stroeven A P, Harbor J M, Heyman J, Hättestrand C, Caffee M W, 2019. Ice cap erosion patterns from bedrock ^{10}Be and ^{26}Al, southeastern Tibetan Plateau. Earth Surface Processes and Landforms 44, 918–932.

Gabrielsen R H, Nystuen J P, Jarsve E M, Lundmark A M, 2015. The Sub-Cambrian Peneplain in southern Norway: its geological significance and its implications for post-Caledonian faulting, uplift and denudation. Journal of the Geological Society 172, 777–791.

Geopark, 2019. Platåbergens Geopark. Available at: https://www.platabergensgeopark.se/. [24 April 2019]. (In Swedish.)

Gibbons C L M H, 1981. Tors in Swaziland. Geographical Journal 147, 72–78.

Gibling M R, Davies N S, Falcon-Lang H J, Bashforth A R, DiMichelle W A, Rygel M C, Ielpi A, 2014. Palaeozoic co-evolution of rivers and vegetation: a synthesis of current knowledge. Proceedings of the Geologists' Association 125, 524–533.

Gilbert G K, 1877. Geology of the Henry Mountains. U.S. Geological Survey.

Goodfellow B W, Chadwick O A, Hilley G E, 2014a. Depth and character of rock weathering across a basaltic-hosted climosequence on Hawai'i. Earth Surface Processes and Landforms 39, 381–398.

Goodfellow B W, Skelton A, Martel S J, Stroeven A P, Jansson K N, Hättestrand C, 2014b. Controls of tor formation, Cairngorm Mountains, Scotland. Journal of Geophysical Research: Earth Surface 119, 225–246.

Goodfellow B W, Hilley G E, Webb S M, Sklar L S, Moon S, Olson C A, 2016. The chemical, mechanical, and hydrological evolution of weathering granitoid. Journal of Geophysical Research: Earth Surface 121, 1410–1435.

Gosse J C, Phillips F M, 2001. Terrestrial in situ cosmogenic nuclides: theory and application. Quaternary Science Reviews 20, 1475–1560.

Grad M, Tiira T, ESC Working Group, 2009. The Moho depth map of the European Plate. Geophysics Journal International 176, 279–292.

Granger D E, Caffee M W, Woodruff T E, 2014. A tenfold increase in ^{26}Al currents at PRIME Lab: Revisiting old ideas and exploring new possibilities with a gas-filled-magnet. GSA Annual Meeting, Vancouver, Canada.

Grigull S, Peterson G, Nyberg J, Öhrling C, 2019. Phanerozoic faulting of Precambrian basement in Uppland. SKB R-19-22, Svensk Kärnbränslehantering AB**.**

Hack J T, 1975. Dynamic equilibrium and landscape evolution. In Melhorn W N, Flemal R C (eds.) Theories of landform development: proceedings of the Sixth Annual Geomorphology Symposium, Binghamton, New York, 26–27 September 1975. London: Allen & Unwin, 87–102.

Hagenfeldt S E, Söderberg P, 1994. Lower Cambrian sandstone erratics and geophysical indications of sedimentary rock in the Stockholm area, Sweden. Geologiska Föreningens Förhandlingar 116, 185–190.

Hall A M, Phillips W M, 2006. Weathering pits as indicators of the relative age of granite surfaces in the Cairngorm Mountains, Scotland. Geografiska Annaler: Series A, Physical Geography, 135–150.

Hall A M, Ebert K, Hättestrand C, 2013a. Pre-glacial landform inheritance in a glaciated shield landscape. Geografiska Annaler: Series A, Physical Geography 95, 33–49.

Hall A M, Ebert K, Kleman J, Nesje A, Ottesen D, 2013b. Selective glacial erosion on the Norwegian passive margin. Geology 41, 1203–1206.

Hall A M, Ebert K, Goodfellow B W, Hättestrand C, Heyman J, Krabbendam M, Moon S, Stroeven A P, 2019a. Past and future impact of glacial erosion in Forsmark and Uppland. Final report. SKB TR-19-07, Svensk Kärnbränslehantering AB.

Hall A M, Krabbendam M, van Boeckel M, Ebert K, Hättestrand C, Heyman J, 2019b. The sub-Cambrian unconformity in Västergötland, Sweden: Reference surface for Pleistocene glacial erosion of basement. SKB TR-19-21, Svensk Kärnbränslehantering AB.

Harbor J, Stroeven A P, Fabel D, Clarhall A, Kleman J, Li Y, Elmore D, Fink D, 2006. Cosmogenic nuclide evidence for minimal erosion across two subglacial sliding boundaries of the late glacial Fennoscandian ice sheet. Geomorphology 75, 90–99.

Heimsath A M, Dietrich W E, Nishiizumi K, Finkel R C, 1997. The soil production function and landscape equilibrium. Nature 388, 358–361.

Heyman J, Stroeven A P, Harbor J M, Caffee M W, 2011. Too young or too old: Evaluating cosmogenic exposure dating based on an analysis of compiled boulder exposure ages. Earth and Planetary Science Letters 302, 71–80.

Hilley G E, Arrowsmith J R, 2008. Geomorphic response to uplift along the Dragon's back pressure ridge, Carrizo Plain, California. Geology 36, 367–370.

Hjulström F, 1935. Studies of the morphological activity of rivers as illustrated by the River Fyris. Bulletin of the Geological Institute, University of Uppsala 25, 221–527**.**

Hoffman P F, Kaufman A J, Halverson G P, Schrag D P, 1998. A Neoproterozoic Snowball Earth. Science 281, 1342-1346.

Hooke R LeB, Calla P, Holmlund P, Nilsson M, Stroeven A 1989. A 3 year record of seasonal variations in surface velocity, Storglaciären, Sweden. Journal of Glaciology 35, 235–247.

Humphreys G S, Wilkinson M T, 2007. The soil production function: A brief history and its rediscovery. Geoderma 139, 73–78.

Högbom A G, Ahlström N G, 1924. Über die subkambrische Landflache am Fusse vom Kinnekulle. Bulletin of the Geological Institution of Uppsala 19, 55–88.

Jahns R H, 1943. Sheet structure in granites: Its origin and use as a measure of glacial erosion in New England. The Journal of Geology 51, 71–98.

Jansen J D, Knudsen M F, Andersen J L, Heyman J, Egholm D L, 2019. Erosion rates in Fennoscandia during the past million years. Quaternary Science Reviews 207, 37–48.

Japsen P, Green P F, Bonow J M, Erlström M, 2016. Episodic burial and exhumation of the southern Baltic Shield: Epeirogenic uplifts during and after break-up of Pangaea. Gondwana Research 35, 357–377.

Japsen P, Green P F, Chalmers J A, Bonow J M, 2018. Mountains of southernmost Norway: uplifted Miocene peneplains and re-exposed Mesozoic surfaces. Journal of the Geological Society 175, 721–741.

Johansson M, Migon P, Olvmo M, 2001a. Development of joint-controlled rock basins in Bohus granite, SW Sweden. Geomorphology 40, 145–161.

Johansson M, Olmo M, Lidmar-Bergström K, 2001b. Inherited landforms and glacial impact of different palaeosurfaces in southwest Sweden. Geografiska Annaler: Series A, Physical Geography, 67–89.

Johnsson G, 1956. Glacialmorfologiska Studier i Södra Sverige: med särskild hänsyn till glaciala riktningselement och periglaciala frostfenomen (Glacial Morphology in Southern Sweden). Meddelanden från Lunds universitets Geografiska institution, avhandlingar 30. (In Swedish.)

Keller C B, Husson J M, Mitchell R N, Bottke W F, Gernon T M, Boehnke P, Bell E A, Swanson-Hysell N L, Peters S E, 2019. Neoproterozoic glacial origin of the Great Unconformity. PNAS 116, 1136–1145.

Kennedy M, Droser M, Mayer L M, Pevear D, Mrofka D, 2006. Precambrian oxygenation: inception of the clay mineral factory. Science 311, 1446–1449.

King L C, 1953. Canons of landscape evolution. Geological Society of America Bulletin 64, 721–752.

Kleman J, 1992. The palimpsest glacial landscape in northwestern Sweden: Late Weichselian deglaciation landforms and traces of older west-centered ice sheets. Geografiska Annaler: Series A, Physical Geography 74, 305–325.

Kleman J, Borgström I, 1996. Reconstruction of palaeo-ice sheets: the use of geomorphological data. Earth Surface Processes and Landforms 21, 893–909.

Kleman J, Hättestrand C, 1999. Frozen-based Fennoscandian and Laurentide ice sheets during the last glacial maximum. Nature 402, 63–66.

Kleman J, Hättestrand C, Borgström I, Stroeven A, 1997. Fennoscandian palaeoglaciology reconstructed using a glacial geological inversion model. Journal of Glaciology 43, 283–299.

Kleman J, Stroeven A P, Lundqvist J, 2008. Patterns of Quaternary ice sheet erosion and deposition in Fennoscandia and a theoretical framework for explanation. Geomorphology 97, 73–90.

Kohl C, Nishiizumi K, 1992. Chemical isolation of quartz for measurement of in situ-produced cosmogenic nuclides. Geochimica et Cosmochimica Acta 56, 3583–3587.

Korja A, Heikkinen P, Aaro S, 2001. Crustal structure of the northern Baltic Sea palaeorift. Tectonophysics 331, 341–358.

Korschinek G, Bergmaier A, Faestermann T, Gerstmann U, Knie K, Rugel G, Wallner A, Dillmann I, Dollinger G, Von Gostomski C L, 2010. A new value for the half-life of ^{10}Be by heavy-ion elastic recoil detection and liquid scintillation counting. Nuclear Instruments and Methods in Physics Research Section B: Beam Interactions with Materials and Atoms 268, 187–191.

Kump L R, 2008. The rise of atmospheric oxygen. Nature 451, 277–278.

Lagerbäck R, Sundh M, Svedlund J-O, Johansson H, 2005. Forsmark site investigation. Searching for evidence of late-or post-glacial faulting in the Forsmark region. SKB R-05-51, Svensk Kärnbränslehantering AB**.**

Lal D, 1991. Cosmic ray labeling of erosion surfaces: in situ nuclide production rates and erosion models. Earth and Planetary Science Letters 104, 424–439.

Lassen A, Thybo H, 2012. Neoproterozoic and Palaeozoic evolution of SW Scandinavia based on integrated seismic interpretation. Precambrian Research 204–205, 75–104.

Lebedeva M I, Fletcher R C, Balashov V N, Brantley S L, 2007. A reactive diffusion model describing transformation of bedrock to saprolite. Chemical Geology 244, 624–645.

Leijon B (ed), 2005. Forsmark site investigation: Investigations of superficial fracturing and block displacements at drill site 5. SKB P-05-199, Svensk Kärnbränslehantering AB.

Lidmar-Bergström K, 1986. Berggrundsformer i Blekinge. Blekinges natur 1986, 15–31. (In Swedish.)

Lidmar-Bergström K, 1995. Relief and saprolites through time on the Baltic Shield. Geomorphology 12, 45–61.

Lidmar-Bergström K, 1996. Long term morphotectonic evolution in Sweden. Geomorphology 16, 33–59.

Lidmar-Bergström K, Olvmo M, 2015. Plains, steps, hilly relief and valleys in northern Sweden – review, interpretations and implications for conclusions on Phanerozoic tectonics. Uppsala: Geological Survey of Sweden. SGU Research Paper C838.

Lidmar-Bergström K, Ollier C D, Sulebak J R, 2000. Landforms and uplift history of southern Norway. Global and Planetary Change 24, 211–231.

Lidmar-Bergström K, Näslund J-O, Ebert K, Neubeck T, Bonow J M, 2007. Cenozoic landscape development in northern Scandinavia. Norwegian Journal of Geology 87, 181–196.

Lidmar-Bergström K, Bonow J M, Japsen P, 2013. Stratigraphic Landscape Analysis and geomorphological paradigms: Scandinavia as an example of Phanerozoic uplift and subsidence. Global and Planetary Change 100, 153–171.

Lidmar-Bergström K, Olvmo M, Bonow J M, 2017. The South Swedish Dome: a key structure for identification of peneplains and conclusions on Phanerozoic tectonics of an ancient shield. Geologiska Föreningens Förhandlingar 139, 244–259.

Lifton N, Sato T, Dunai T J, 2014. Scaling in situ cosmogenic nuclide production rates using analytical approximations to atmospheric cosmic-ray fluxes. Earth and Planetary Science Letters 386, 149–160.

Liivamägi S, Mahaney W C, Somelar P, Kirs J, Vircava I, Kirsimäe K, 2014. Late Neoproterozoic Baltic paleosol: Intense weathering at high latitude? Geology 42, 323–326 .

Liivamägi S, Somelar P, Vircava I, Mahaney W C, Kirs J, Kirsimäe K, 2015. Petrology, mineralogy and geochemical climofunctions of the Neoproterozoic Baltic paleosol. Precambrian Research 256, 170–188.

Lisiecki L E, Raymo M E, 2005. A Pliocene-Pleistocene stack of 57 globally distributed benthic $\delta^{18}O$ records. Paleoceanography 20, PA1003. doi:10.1029/2004PA001071

Lundqvist J, Lundqvist T, Lindström M, Calner M, Sivhed U, 2011. Sveriges geologi från urtid till nutid. 3rd ed. Lund: Studentlitteratur. (In Swedish.)

Lönnqvist M, Hökmark H, 2013. Approach estimating the maximum depth for glacially induced hydraulic jacking in fractured crystalline rock at Forsmark, Sweden. Journal of Geophysical Research: Earth Surface 118, 1777–1791.

Mansour W B, England R W, Fishwick S, Moorkamp M, 2018. Crustal properties of the northern Scandinavian mountains and Fennoscandian shield from analysis of teleseismic receiver functions. Geophysical Journal International 214, 386–401.

Marrero S M, Phillips F M, Borchers B, Lifton N, Aumer R, Balco G, 2016. Cosmogenic nuclide systematics and the CRONUScalc program. Quaternary Geochronology 31, 160–187.

Maher K, 2010. The dependence of chemical weathering rates on fluid residence time. Earth and Planetary Science Letters 294, 101–110.

Martel S J, 2011. Mechanics of curved surfaces, with application to surface-parallel cracks. Geophysical Research Letters 38, L20303. doi:10.1029/2011GL049354

Martel S J, 2017. Progress in understanding sheeting joints over the past two centuries. Journal of Structural Geology 94, 68–86.

Martin C D, 2007. Quantifying in situ stress magnitudes and orientations for Forsmark; Forsmark stage 2.2. SKB R-07-26, Svensk Kärnbränslehantering AB.

Matthes F E, 1930. Geologic history of the Yosemite Valley. U. S. Geological Survey. (Professional Paper 160)

Mattsson Å, 1962. Morphologische Studien in Südschweden und auf Bornholm über die nichtglaziale Formenwelt der Felsenskulptur. PhD thesis. Lund University, Sweden.

Mckenzie D, 1984. A possible mechanism for epeirogenic uplift. Nature 307, 616–618.

Mitchell S G, Montgomery D R, 2006. Influence of a glacial buzzsaw on the height and morphology of the Cascade Range in central Washington State, USA. Quaternary Research 65, 96–107.

Moon, S, Perron, J T, Martel, S J, Goodfellow, B W, Mas Ivars, D, Simeonov, A, Munier, R, Näslund, J-O, Hall, A M, Stroeven, A P, Ebert K, Heyman J, 2019. Landscape features influence bedrock fracture openness in the deep subsurface. GSA Abstracts with Programs 51. doi:10.1130/abs/2019AM-336309

Moore J G, 2000. Exploring the Highest Sierra. Stanford, CA: Stanford University Press.

Munier R, Talbot C J, 1993. Segmentation, fragmentation, and jostling of cratonic basement in and near Äspö, southeast Sweden. Tectonics 12, 713–727.

Naylor L A, Stephenson W J, 2010. On the role of discontinuities in mediating shore platform erosion. Geomorphology 114, 89–100.

Neubeck T, 2000. Hällformer inom två olika paleoytor i södra Sverige. Degree project. Stockholm University. (In Swedish.)

Nielsen A T, Schovsbo N H, 2011. The Lower Cambrian of Scandinavia: Depositional environment, sequence stratigraphy and palaeogeography. Earth-Science Reviews 107, 207–310.

Nishiizumi K, 2004. Preparation of ^{26}Al AMS standards. Nuclear Instruments and Methods in Physics Research Section B: Beam Interactions with Materials and Atoms 223, 388–392.

Nishiizumi K, Winterer E L, Kohl C P, Klein J, Middleton R, Lal D, Arnold J R, 1989. Cosmic ray production rates of ^{10}Be and ^{26}Al in quartz from glacially polished rocks. Journal of Geophysical Research 94, 17907–17915.

Nishiizumi K, Imamura M, Caffee M W, Southon J R, Finkel R C, McAninch J, 2007. Absolute calibration of ^{10}Be AMS standards. Nuclear Instruments and Methods in Physics Research Section B: Beam Interactions with Materials and Atoms 258, 403–413.

Näslund J-O, Rodhe L, Fastook J L, Holmlund P, 2003. New ways of studying ice sheet flow directions and glacial erosion by computer modelling – examples from Fennoscandia. Quaternary Science Reviews 22, 245–258.

Olvmo M, Johansson M, 2002. The significance of rock structure, lithology and pre-glacial deep weathering for the shape of intermediate-scale glacial erosional landforms. Earth Surface Processes and Landforms 27, 251–268.

Olvmo M, Ronnert L, Ekman S R, Olsson S, 1996. A weathered diamicton beneath Upper Weichselian sediments at Silvereke, southeastern Sweden. GFF 118, 65–71.

Olvmo M, Lidmar-Bergström K, Ericson K, Bonow J M, 2005. Saprolite remnants as indicators of pre-glacial landform genesis in southeast Sweden. Geografiska Annaler, Series A 87, 447–460.

Påsse T, Daniels J, 2015. Past shore-level and sea-level displacements: Uppsala: Geological Survey of Sweden. Rapporter och meddelanden 137.

Pedersen V K, Huismans, R S, Moucha R, 2016. Isostatic and dynamic support of high topography on a North Atlantic passive margin. Earth and Planetary Science Letters 446, 1–9.

Penck W, 1924. Die morphologische Analyse: ein Kapitel der physikalischen Geologie. Stuttgart: Engelhorn. (In German.)

Perron J T, Dietrich W E, Kirchner J W, 2008. Controls on the spacing of first-order valleys. Journal of Geophysical Research 113, F04016. doi:10.1029/2007JF000977

Phillips J D, 2002. Erosion, isostatic response, and the missing peneplains. Geomorphology 45, 225–241.

Phillips W M, Hall A M, Mottram R, Fifield L K, Sugden D E, 2006. Cosmogenic ^{10}Be and ^{26}Al exposure ages of tors and erratics, Cairngorm Mountains, Scotland: Timescales for the development of a classic landscape of selective linear glacial erosion. Geomorphology 73, 222–245.

Phillips F M, Argento D C, Balco G, Caffee M W, Clem J, Dunai T J, Finkel R, Goehring B, Gosse J C, Hudson A M, 2016. The CRONUS-Earth project: a synthesis. Quaternary Geochronology 31, 119–154.

Peters S E, Gaines R, 2012. Formation of the `Great Unconformity' as a trigger for the Cambrian explosion. Nature 484, 363–366 .

Porter S C, 1989. Some geological implications of average Quaternary conditions. Quaternary Research 32, 245–261.

Putkonen J, Swanson T, 2003. Accuracy of cosmogenic ages for moraines. Quaternary Research 59, 255–261.

Rhoads B L, Thorn C E, 1996. Observations in geomorphology. In Rhoads B L, Thorn C E (eds). The scientific nature of geomorphology. Chichester: Wiley, 21–56.

Riebe C S, Kirchner, J W, Finkel R C, 2003. Long-term rates of chemical weathering and physical erosion from cosmogenic nuclides and geochemical mass balance. Geochimica et Cosmochimica Acta 67, 4411–4427.

Rudberg S, 1954. Västerbottens bergggrundsmorfologi: ett försök till rekonstruktion av preglaciala erosionsgenerationer i Sverige. Uppsala. Geographica 25.

Rudberg S, 1960. Geology and Geomorphology. In Sømme A C Z (ed). A geography of Norden: Denmark, Finland, Iceland, Norway, Sweden. J.W. Capellens förlag, 27–40.

Rudberg S, Eriksson E, Krathmann R, Sandquist A, Wejedal J, 1976. Halle- and Hunneberg: Inventory of geo-objects with a geomorphological map. GUNI Report 9, University of Gothenburg .

Röshoff K, Cosgrove J, 2002. Sedimentary dykes in the Oskarshamn–Västervik area A study of the mechanism of formation. SKB R-02-37, Svensk Kärnbränslehantering AB.

Sandler A, Teutsch N, Avigad D, 2012. Sub-Cambrian pedogenesis recorded in weathering profiles of the Arabian–Nubian Shield. Sedimentology 59, 1305–1320.

Schumm S A, Lichty R W, 1965. Time, space, and causality in geomorphology. American Journal of Science 263, 110–119.

Simpson E L, Heness E, Bumby A, Eriksson P G, Eriksson K A, Hilbert-Wolf H L, Linnevelt S, Fitzgerald Malenda H, Modungwa T, Okafor O J, 2013. Evidence for 2.0 Ga continental microbial mats in a paleodesert setting. Precambrian Research 237, 36–50.

SKB, 2010. Climate and climate-related issues for the safety assessment SR-Site. SKB TR-10-49, Svensk Kärnbränslehantering AB.

Small E, Anderson R S, Repka J L, Finkel R, 1997. Erosion rates of alpine bedrock summit surfaces deduced from in situ ^{10}Be and ^{26}Al. Earth and Planetary Science Letters 50, 413–425.

St Clair J, Moon S, Holbrook W, Perron J, Riebe C, Martel S, Carr B, Harman C, Singha K, 2015. Geophysical imaging reveals topographic stress control of bedrock weathering. Science 350, 534–538.

Stephens M B, 2010. Forsmark site investigation. Bedrock geology – overview and excursion guide. SKB R-10-04, Svensk Kärnbränslehantering AB.

Stephens M B, Fox A, La Pointe P, Simeonov A, Isaksson H, Hermanson J, Öhman J, 2007. Geology Forsmark. Site descriptive modelling Forsmark-stage 2.2. SKB R-07-45, Svensk Kärnbränslehantering AB.

Stroeven A P, Kleman J, 1999. Age of Sirius Group on Mount Feather, McMurdo Dry Valleys, Antarctica, based on glaciological inferences from the overridden mountain range of Scandinavia. Global and Planetary Change 23, 231–247.

Stroeven A P, Fabel D, Harbor J, Hättestrand C, Kleman J, 2002a. Quantifying the erosional impact of the Fennoscandian ice sheet in the Torneträsk–Narvik corridor, northern Sweden, based on cosmogenic radionuclide data. Geografiska Annaler: Series A, Physical Geography 84, 275–287.

Stroeven A P, Fabel D, Hättestrand C, Harbor J, 2002b. A relict landscape in the centre of Fennoscandian glaciation: cosmogenic radionuclide evidence of tors preserved through multiple glacial cycles. Geomorphology 44, 145–154.

Stroeven A P, Harbor J, Fabel D, Kleman J, Hättestrand C, Elmore D, Fink D, Fredin O, 2006. Slow, patchy landscape evolution in northern Sweden despite repeated ice-sheet glaciation. In Willett S D, Hovius N, Brandon M T, Fisher D M (eds). Tectonics, climate and landscape evolution. Boulder, CO: Geological Society of America. (GSA Special Paper 398), 387–396.

Stroeven A P, Fabel D, Margold M, Clague J, Xu S, 2014. Investigating absolute chronologies of glacial advances in the NW sector of the Cordilleran Ice Sheet with terrestrial in situ cosmogenic nuclides. Quaternary Science Reviews 92, 429–443.

Stroeven A P, Heyman J, Fabel D, Björck S, Caffee M W, Fredin O, Harbor J M, 2015. A new Scandinavian reference ^{10}Be production rate. Quaternary Geochronology 29, 104–115.

Stroeven A P, Hättestrand C, Kleman J, Heyman J, Fabel D, Fredin O, Goodfellow B W, Harbor J M, Jansen J D, Olsen L, Caffee M W, Fink D, Lundqvist J, Rosqvist G C, Strömberg B, Jansson K N, 2016. Deglaciation of Fennoscandia. Quaternary Science Reviews 147, 91–121.

Sugden D E, Hall A M, Phillips W M, Stewart M, 2019. Plucking enhanced beneath ice sheet margins: evidence from the Grampian Mountains, Scotland. Geografiska Annaler: Series A, Physical Geography 101, 34–44.

Sundborg Å, 1956. The river Klarälven a study of fluvial processes. Geografiska Annaler 38, 125–316.

Söderberg P, Hagenfeldt S E, 1995. Upper Proterozoic and Ordovician submarine outliers in the archipelago northeast of Stockholm, Sweden. Geologiska Föreningens Förhandlingar 117, 153–161.

Tarr R S, 1898. The peneplain. American Geologist 21, 351–370.

Thomas C W, Gillespie M R, Cordan C J, Hall A M, 2004. Geological structure and landscape of the Cairngorms. Commissioned Report 64, Scottish Natural Heritage.

Trenhaile A S, 1999. The width of shore platforms in Britain, Canada, and Japan. Journal of Coastal Research 15, 355–364.

Tuuling I, Flodén T, 2001. The structure and relief of the bedrock sequence in the Gotland–Hiiumaa area, northern Baltic Sea. Geologiska Föreningens Förhandlingar 123, 35–49.

Tuuling I, Flodén T, Sjöberg J, 1997. Seismic correlation of the Cambrian sequence between Gotland and Hiiumaa in the Baltic Sea. Geologiska Föreningens Förhandlingar 119, 45–54.

Went D J, 2013. Quartzite development in early Palaeozoic nearshore marine environments. Sedimentology 60, 1036–1058.

Westergård A H, 1939. Den kambro–ordoviciska lagerserien. In Sandegren R, Asklund B, Westergård A H. Beskrivning till Kartbladet Gävle. Stockholm. (Sveriges geologiska undersökning Aa 178), 39–63. (In Swedish.)

Wolman M G, Miller J P, 1960. Magnitude and frequency of forces in geomorphic processes. Journal of Geology 68, 54–74.

Øvretveit K, 2016. Depositional and structural relationships along the basement-Cambrian contact in the Hardangervidda area. Master thesis in Geodynamics. University of Bergen.

Arkitektkopia AB, Bromma, 2020

SKB is responsible for managing spent nuclear fuel and radioactive waste produced by the Swedish nuclear power plants such that man and the environment are protected in the near and distant future.

skb.se